

1979

PREDICTION AND MEASUREMENT OF  
TURBULENCE IN THE DEVELOPING  
REGION OF AXISYMMETRIC  
ISOTHERMAL FREE JETS.

S. M. NAZRUL ISLAM

*University of Windsor*

Follow this and additional works at: <http://scholar.uwindsor.ca/etd>

---

Recommended Citation

ISLAM, S. M. NAZRUL., "PREDICTION AND MEASUREMENT OF TURBULENCE IN THE DEVELOPING REGION OF AXISYMMETRIC ISOTHERMAL FREE JETS." (1979). *Electronic Theses and Dissertations*. Paper 3160.

This online database contains the full-text of PhD dissertations and Masters' theses of University of Windsor students from 1954 forward. These documents are made available for personal study and research purposes only, in accordance with the Canadian Copyright Act and the Creative Commons license—CC BY-NC-ND (Attribution, Non-Commercial, No Derivative Works). Under this license, works must always be attributed to the copyright holder (original author), cannot be used for any commercial purposes, and may not be altered. Any other use would require the permission of the copyright holder. Students may inquire about withdrawing their dissertation and/or thesis from this database. For additional inquiries, please contact the repository administrator via email ([scholarship@uwindsor.ca](mailto:scholarship@uwindsor.ca)) or by telephone at 519-253-3000ext. 3208.





National Library of Canada  
Collections Development Branch

Canadian Theses on  
Microfiche Service

Bibliothèque nationale du Canada  
Direction du développement des collections

Service des thèses canadiennes  
sur microfiche

## NOTICE

The quality of this microfiche is heavily dependent upon the quality of the original thesis submitted for microfilming. Every effort has been made to ensure the highest quality of reproduction possible.

If pages are missing, contact the university which granted the degree.

Some pages may have indistinct print especially if the original pages were typed with a poor typewriter ribbon or if the university sent us a poor photocopy.

Previously copyrighted materials (journal articles, published tests, etc.) are not filmed.

Reproduction in full or in part of this film is governed by the Canadian Copyright Act, R.S.C. 1970, c. C-30. Please read the authorization forms which accompany this thesis.

THIS DISSERTATION  
HAS BEEN MICROFILMED  
EXACTLY AS RECEIVED

## AVIS

La qualité de cette microfiche dépend grandement de la qualité de la thèse soumise au microfilmage. Nous avons tout fait pour assurer une qualité supérieure de reproduction.

S'il manque des pages, veuillez communiquer avec l'université qui a conféré le grade.

La qualité d'impression de certaines pages peut laisser à désirer, surtout si les pages originales ont été dactylographiées à l'aide d'un ruban usé ou si l'université nous a fait parvenir une photocopie de mauvaise qualité.

Les documents qui font déjà l'objet d'un droit d'auteur (articles de revue, examens publiés, etc.) ne sont pas microfilmés.

La reproduction, même partielle, de ce microfilm est soumise à la Loi canadienne sur le droit d'auteur, SRC 1970, c. C-30. Veuillez prendre connaissance des formules d'autorisation qui accompagnent cette thèse.

LA THÈSE A ÉTÉ  
MICROFILMÉE TELLE QUE  
NOUS L'AVONS REÇUE

PREDICTION AND MEASUREMENT OF TURBULENCE IN THE  
DEVELOPING REGION OF AXISYMMETRIC ISOTHERMAL FREE JETS

by

S.M. Nazrul Islam

A Dissertation  
submitted to the Faculty of Graduate Studies  
through the Department of Mechanical Engineering  
in partial fulfilment of the requirements for  
the Degree of Doctor of Philosophy at the  
University of Windsor

Windsor, Ontario, Canada

1979

© S.M. Nazrul Islam 1979  
All Rights Reserved

727636 -

## ABSTRACT

Flow in the developing region of axisymmetric turbulent jets in still air has been studied both theoretically and experimentally.

Jets produced by three nozzles having three different turbulent boundary layer velocity profiles at the nozzle exit were investigated to determine the influence of the initial conditions on the flow. The displacement thicknesses at the exit of the nozzles were  $\delta_a^*/r_0 = 0.0064, 0.0179$  and  $0.0628$ , and for all three nozzles, the Reynolds number based on the outlet diameter and the average velocity was  $Re_D = 1.53 \times 10^5$ .

For each case, the mean velocities, the turbulent intensities in  $x, r$  and  $\theta$ -direction and the shear stresses were measured by the hot-wire anemometer. They were found to be self-preserving in the initial region except close to the nozzle, but not in the transition region. The increased boundary layer thickness at the nozzle exit moves the self-preserving point downstream, although the potential core length remains the same.

Numerical solutions of the differential momentum, continuity and turbulent kinetic energy equations together with an empirical length scale were performed by using a finite-difference method to predict the mean and turbulent quantities in the initial region for any arbitrary initial condition. Prandtl's mixing length model of shear stress

was used for calculation and other shear stress models were examined. Prandtl's model is not applicable to the transition region and an empirical model of turbulent diffusivity was used to calculate the mean flow quantities from the continuity and momentum equations. The calculated results are in satisfactory agreement with the experimental measurements.

For the thin boundary layer at the nozzle exit, the measured mean velocities are shown to fit a polynomial form velocity profile which is used to determine the jet boundaries in the initial region by solving the integral momentum and mean kinetic energy equations in conjunction with the Prandtl's model of shear stress. Agreement with the measurements and numerical solution is shown.

The turbulence level in the core of the jets was high near 5% intensity. The effect of this turbulence on the shear layer was not investigated, but might be important.

Dedicated to

Prophet Muhammad (Peace Be Upon Him)



## ACKNOWLEDGEMENTS

With deep sincerity, the author acknowledges profound indebtedness to Dr. H.J. Tucker, without whose constant and unparallel guidance and invaluable suggestions, this work would not have been possible.

The author is highly grateful to Dr. K. Sridhar for his deep interest and unceasing encouragement for this work. He thanks Dr. R.H. Pletcher of Iowa State University, Dr. B.G. Newman, McGill University, Dr. A.C. Smith, Prof. W.G. Colborne and Dr. T.W. McDonald for their suggestions and help.

The author thanks the Canadian Commonwealth Scholarship and Fellowship Committee for offering him a scholarship, and financial support to his family. He thanks the authority of Bangladesh University of Engineering and Technology, Decca, for granting leave on deputation.

Thanks are also due to Messrs. R. Tattersal and late C. Cada for their technical assistance in fabricating the experimental set up; and Mrs. Barbara L. Denomey for typing the Dissertation.

His final expression of gratitude are offered to his parents and wife as their encouragement and continued support have led him to this point.

TABLE OF CONTENTS

	<u>Page</u>
ABSTRACT.....	iii
DEDICATION.....	v
ACKNOWLEDGEMENTS.....	vi
TABLE OF CONTENTS.....	vii
LIST OF FIGURES.....	x
LIST OF TABLES.....	xiv
LIST OF APPENDICES.....	xv
NOMENCLATURE.....	xvi
CHAPTER I INTRODUCTION.....	1
1.1 General.....	1
1.2 Axisymmetric Jets in Still-Surroundings.....	3
1.2.1 Turbulent Jet Formation.....	3
1.2.2 Flow in Axisymmetric Turbulent Jets.....	4
1.3 Energy Transfer in Turbulent Jets.....	6
1.4 Statement of the Problem.....	8
CHAPTER II LITERATURE SURVEY.....	10
2.1 General.....	10
2.2 Mean Velocity.....	11
2.2.1 Developed Region.....	11
2.2.2 Initial and Transition Regions.....	16
2.3 Differential Transport Equations.....	24
2.4 Turbulence.....	33
CHAPTER III THEORY.....	36
3.1 General.....	36
3.2 Governing Equations.....	37
3.2.1 Mean Flow Equations.....	37
3.2.2 General Turbulent Kinetic Energy Equation.....	40
3.3 Formation of Empirical Turbulent Energy Equation.....	41

	<u>Page</u>
3.3.1	Production..... 41
3.3.2	Dissipation..... 42
3.3.3	Diffusion..... 43
3.3.4	Empirical Turbulent Energy Equation..... 44
3.4	Differential Method..... 45
3.4.1	Equations and Boundary Conditions..... 45
3.4.2	Calculation Technique..... 46
3.5	Integral Method..... 48
3.5.1	Integral Equations..... 48
3.5.2	Empirical Mean Velocity Profile..... 48
3.5.3	Jet Boundaries..... 49
CHAPTER IV	EXPERIMENTS AND UNCERTAINTIES..... 52
4.1	General..... 52
4.2	Experimental Facilities..... 52
4.3	Hot-Wire Calibration..... 54
4.4	Measurements..... 55
4.5	Uncertainty Statement..... 56
CHAPTER V	RESULTS AND DISCUSSION..... 59
5.1	General..... 59
5.2	Nozzle Exit Conditions..... 59
5.3	Mean Motion in the Initial Region..... 61
5.3.1	Thin Exit Boundary Layer..... 61
5.3.2	Intermediate and Thick Exit Boundary Layers..... 66
5.4	Mean Motion in the Transition Region... 69
5.5	Turbulent Motion in the Initial Region..... 72
5.5.1	Thin Exit Boundary Layer..... 72
5.5.2	Intermediate and Thick Exit Boundary Layers..... 77
5.6	Turbulent Motion in the Transition Region..... 78
CHAPTER VI	CONCLUSION..... 79
REFERENCES	..... 82

	<u>Page</u>
FIGURES.....	90
APPENDICES.....	138
VITA AUCTORIS.....	205

LIST OF FIGURES

<u>Figure</u>		<u>Page</u>
1.1	Jet Geometry and Nomenclature.....	91
1.2	Representation of Energy Transfer With Wave Numbers.....	91
3.1	Co-ordinate System and Finite-Difference Grid.....	92
4.1	Schematic Diagram of Experimental Set-Up and Round Axisymmetric Nozzles.....	93
5.1	Measured Axial Velocity and Turbulent Kinetic Energy Distribution at Exit Plane, Thin Boundary Layer.....	94
5.2	Measured Velocity and Turbulent Kinetic Energy Distributions at Exit Plane, Inter- mediate Boundary Layer.....	95
5.3	Measured Velocity and Turbulent Kinetic Energy Distributions at Exit Plane, Thick Boundary Layer.....	96
5.4	Calculated and Experimental Self-Preserving Velocity Profiles in the Initial Region for Thin Boundary Layer.....	97
5.5	Calculated and Experimental Mean Axial Velocity Distribution, Thin Boundary Layer.	98
5.6	Length Scale, $b/r_0$ , and Prandtl's Mixing Length, $L/r_0$ , for Thin, Intermediate and Thick Boundary Layers.....	99
5.7	Calculated and Experimental Iso-Velocity Lines, Thin Boundary Layers.....	100
5.8	Calculated Mean Velocity at $r/r_0=1$ and Its Comparisons with Hatta's Model and Experi- ments, Thin Boundary Layer.....	101
5.9	Mean Radial Velocity Distribution in the Initial Region, Thin Boundary Layer....	102
5:10	Experimental Values of the Ratio $L/b$ , Thin Boundary Layer.....	103
5.11	Velocity Profiles in the Initial Region, Intermediate Boundary Layer.....	104
5.12	Velocity Profiles in the Initial Region, Thick Boundary Layer.....	105
5.13	Calculated and Experimental Mean Axial Velocity Distribution, Intermediate Boundary Layer.....	106

<u>Figure</u>		<u>Page</u>
5.14	Calculated and Experimental Mean Axial Velocity Distribution, Thick Boundary Layer.....	107
5.15	Calculated and Experimental Iso-Velocity Lines Thin, Intermediate and Thick Boundary Layers.....	108
5.16	Experimental Values of the Ratio, L/b, Thick Boundary Layer.....	109
5.17	Calculated and Experimental Mean Velocity Distributions in $u/u_c$ vs. $\eta$ Plane for the Transition Region.....	110
5.18	Comparison of Experimental Mean Axial Velocity with Tollmien's and Schlichting's Model for Developed Region.....	111
5.19	Prandtl's Mixing Length in Transition Region.....	112
5.20	Eddy Viscosity vs. Radial Distance in the Transition Region.....	113
5.21	Calculated and Experimental Mean Velocity Distributions in the Transition Region.....	114
5.22	Comparison of Shear Stress Models and Measurements, Thin Boundary Layer, $x/r_0=2..$	115
5.23	Comparison of Shear Stress Models and Measurements, Thin Boundary Layer, $x/r_0=4..$	116
5.24	Comparison of Shear Stress Models and Measurements, Thin Boundary Layer, $x/r_0=6..$	117
5.25	Comparison of Shear Stress Models and Measurements, Thin Boundary Layer, $x/r_0=8..$	118
5.26	Experimental Values of $\overline{u'^2}/2k$ , $\overline{v'^2}/2k$ and $\overline{u'v'}/k$ in the Initial Region.....	119
5.27	Calculated and Experimental Turbulent Kinetic Energy Distributions, Thin Boundary Layer.....	120
5.28	Calculated and Experimental Turbulent Axial Intensity Distribution, Thin Boundary Layer.....	121
5.29	Calculated and Experimental Turbulent Radial Intensity Distributions, Thin Boundary Layer.....	122
5.30	Calculated and Experimental Production and Dissipation of Turbulent Energy Distributions, Thin Boundary Layer.....	123

<u>Figure</u>		<u>Page</u>
5.31	Calculated and Experimental Diffusion of Turbulent Energy Distribution, Thin Boundary Layer.....	124
5.32	Calculated and Experimental Convective Transportation of Turbulent Energy Distribution, Thin Boundary Layer.....	125
5.33	Calculated and Experimental Shear Stress Distributions, Intermediate Boundary Layer.....	126
5.34	Calculated and Experimental Shear Stress Distributions, Thick Boundary Layer.....	127
5.35	Calculated and Experimental Turbulent Kinetic Energy Distributions, Intermediate Boundary Layer.....	128
5.36	Calculated and Experimental Turbulent Kinetic Energy Distributions, Thick Boundary Layer.....	129
5.37	Calculated and Experimental Turbulent Axial Intensity Distributions, Intermediate Boundary Layer.....	130
5.38	Calculated and Experimental Turbulent Radial Intensity Distributions, Intermediate Boundary Layer.....	131
5.39	Calculated and Experimental Turbulent Axial Intensity Distributions, Thick Boundary Layer.....	132
5.40	Calculated and Experimental Turbulent Radial Intensity Distribution, Thick Boundary Layer.....	133
5.41	Experimental Turbulent Shear Stress Distributions in the Transition Region.....	134
5.42	Experimental Turbulent x-Intensity Distributions in the Transition Region.....	135
5.43	Experimental Turbulent r-Intensity Distributions in the Transition Region.....	136
5.44	Experimental Turbulent $\theta$ -Intensity Distributions in the Transition Region.....	137
C.1	Wire Configuration in 3-Dimensional Velocity Field.....	173
C.2	Hot-Wire Configuration for Measurements of $\overline{u'^2}$ , $\overline{v'^2}$ and $\overline{u'v'}$ .....	173
C.3	Calibration of Pitot Tube Against a Micro-manometer.....	174

<u>Figure</u>		<u>Page</u>
C.4	A Typical Calibration Curve for a Normal Wire Without a Linearizer.....	175
C.5	Typical Calibration Curves for a Slanting Wire Without a Linearizer.....	176
C.6	Typical Calibration Curves for Normal and Slanting Wires With a Linearizer.....	177
C.7	Typical Calibration Curve for Normal Wire at Low Velocity.....	178
C.8	Distributions of Turbulent Intensities in a Fully Developed Pipe Flow.....	179
C.9	Reynold's Shear Stress Distribution in a Fully Developed Pipe Flow.....	180



LIST OF TABLES

<u>Table</u>		<u>Page</u>
2.1	Relevant Experimental Work.....	12
2.2	Relevant Theoretical Work.....	14
2.3	Two-Equation Models.....	29
5.1	A Comparison of Mean Velocity RMS Deviations.....	63
5.2	Constant of Energy Transport Equation...	75
C.1	Best Values of Exponent $c$ in Hot-Wire Equation.....	171

LIST OF APPENDICES

<u>APPENDIX</u>		<u>Page</u>
A	DERIVATION OF EQUATIONS.....	139
B	CALCULATIONS BY THE INTEGRAL METHOD.....	149
C	HOT-WIRE EQUATIONS AND CALIBRATIONS.....	165
D	THE FINITE-DIFFERENCE FORMULATION.....	181
E	STABILITY ANALYSIS OF MOMENTUM EQUATION...	189
F	COMPUTER PROGRAMMES.....	193

## NOMENCLATURE

$A, B, B_L$	Constants
$a_1$	Constant in Energy Equation (3.13)
$a_2$	Constant in Harsha's Model
$a_p$	Constant in Rotta's Model
$a_t$	Tollmien Constant for the Similarity Variable
$b$	Length Scale for the Similarity Variable $\eta$
$b_l$	Width of the Shear Layer
$b_m$	Mean Width of the Shear Layer
$c$	Exponent of the Hot-Wire Equation
$c_r, c_L$	Constants in Rotta's Transport Model
$c_1$	Constant in the Energy Model of Shear Stress
$c_2, c_3, c_D, c_\mu$	Constants in Launder's Transport Model
$c_4$	Proportionality Constant of Length Scale and Width of the Shear Layer
$c_a, c_K, c_s, c_t$	Constants for Different Mean Velocity Models for the Developed Region
$\frac{D}{Dt}$	Material Derivative of a Dependent Variable
$d$	Hot-Wire Diameter
$\bar{E}$	Mean Voltage of the Hot-Wire Anemometer Without Linearizer.
$E'$	Fictitious Voltage
$\bar{E}_L$	Mean Voltage with Linearizer
$e, e_L$	Fluctuating Voltages
$f$	Characteristic Frequency
$H$	Shape Factor
$k$	Turbulent kinetic Energy
$k_2$	Hot-Wire Constant
$K^* = K/u_0^2$	Non-Dimensional Kinetic Energy

$k_q, k_{qL}, k_{qt}$	Constants in Rotta's Transport Model
$L$	Prandtl's Mixing Length
$L^0$	Integral Length Scale
$L^1$	Characteristic Length Scale for the Transport Model
$L^* = Lu_0/\nu$	Non-Dimensional Length Scale
$l$	Hot-Wire Length
$n_1, n_2$	Slopes of the Normal and Slanting Wires
$P$	Production of the Turbulent Energy
$p$	Mean Static Pressure
$p'$	Fluctuating Pressure
$p^0$	Instantaneous Pressure
$Pr$	Prandtl's number in Harsha's Model
$R = ru_0/\nu$	Non-Dimensional Radial Distance
$r_0$	Radius of Nozzle
$r_{1/2}$	Radial Distance at Half-Velocity ( $u/u_c = 0.5$ )
$r_1$	Radius of the Potential Core
$r_2$	Outer Radius of the Jet
$r_m$	Mean Jet Radius
$Re_D$	Reynolds Number Based on the Exit Diameter and Average Velocity
$Re\delta^*$	Reynolds Number Based on the Exit Displacement Thickness and the Average Velocity
$S$	Secondary source Term in Launder's Model
SPL	Sound Pressure Level
$s_1, s_2$	Hot-Wire Constants
$U = u/u_0$	Non-Dimensional Mean Velocity
$u$	Axial Mean Velocity
$u_c$	Centre Line Mean Velocity
$u_0$	Area Average Velocity at Exit

$u_T = \tau_{\max} / \rho$	Shear Velocity
$U_C$	Convection Velocity
$U_E$	Cooling Velocity
$U_{T^*}$	Tangential Cooling Velocity
$U_N$	Normal Cooling Velocity
$V = v / u_0$	Non-Dimensional Radial Mean Velocity
$v$	Radial Mean Velocity (See note at end of nomenclature)
$v_e$	Effective Velocity in Bradshaw's Model
$u^0, v^0, w^0$	Instantaneous Velocities in x, r and $\theta$ -Directions
$u', v', w'$	Fluctuating Velocities in x, r and $\theta$ -Directions
$X = x u_0 / \nu$	Non-Dimensional Axial Distance
$X_t$	Laminar Transition Length
$x, y, z$	A Coordinate System
$x, r, \theta$	An Axisymmetric Coordinate System
$z$	A Dummy Variable for Launder's Model
$\alpha$	Angle of Hot-Wire Inclination
$\alpha_L$	Constant in Rotta's Length Scale Model
$\beta$	A Constant in the Intermittency Equation
$\gamma$	Intermittency Factor
$\delta$	Error in Velocity in Stability Analysis
$\delta_0$	Boundary Layer Thickness at the Exit
$\Delta$	Difference
$\delta^*$	Displacement Thickness
$\theta_0$	Momentum Thickness at the Exit
$\sigma$	Standard Deviation
$\sigma_k, \sigma_z$	Constants in Launder's Transport Model

$\nu_{eff}$	Effective Viscosity
$\nu$	Molecular Diffusivity
$\nu_t$	Turbulent or Eddy Diffusivity
$\eta$	Self-Preserving Variable
$\eta_t, \eta_H$	Tollmien's and Hatta's Similarity Variable
$\rho$	Density
$\epsilon$	Dissipation of Turbulent Energy
$\xi$	A Constant in Rotta's Length Scale Equation
$\tau = \tau_{rx}$	Shear Stress

Subscripts

0	Exit Condition
RMS	Root Mean Square
i	Axial Direction
j	Radial Direction
Max	Maximum Value
Min	Minimum Value

Note: the symbol,  $\nu$ , was inadvertently used in place of the usual symbol,  $v$ , during typing throughout the Dissertation. Because of extensive changes, the symbol,  $\nu$  was retained, and the author apologizes for any inconvenience this may cause to the reader.

## CHAPTER I

### INTRODUCTION

#### 1.1 General

A jet is formed when a fluid discharges through an opening or nozzle from a container under higher pressure into a region of lower pressure. The neighbouring fluid surrounding the jet may itself be in motion or at rest. The formation of a boundary layer within the nozzle and its separation at the outlet is the initiation of a shear layer in the free jet flow. Turbulence originates as an instability in the laminar flow, and the flow becomes turbulent when the Reynold's number exceeds some critical value.

Jets are of three kinds: 1) bounded, 2) wall, and 3) free jets. In bounded jets, the flow is confined by solid boundaries; wall jets flow over solid surfaces. Free jets flow without contacting solid surfaces and are axisymmetric when formed by discharging through a circular nozzle or orifice.

A detailed knowledge of the mean and turbulent quantities within a jet is essential to many problems of diffusion, aerodynamic noise and airplane design. The diffusion phenomena in free jets is associated with flows in the exhaust of rocket engines, atomized fuel injection systems, sprays, waste disposal plumes and jets in numerous cleaning devices.

Wall and bounded jets also have a number of physical applications. In airplanes, jets may be blown along aerofoil surfaces to energise the boundary layer and prevent separation. This is usually used to reduce the take-off and landing speed of the airplane. It has been applied with success to carrier-based naval aircraft; for example, the Blackburn NA39 has blowing applied to the leading edge of the wing, the flaps and the leading edge of the tail plane which reduces landing and take-off speeds by tens of knots [1]<sup>1</sup>. Directly related, although restricted by boundaries (i.e., free surfaces), is the diffusion of plunging nappes from spillways or of submerged jets from sluice gates. Bounded jets are applied to the relatively new technology of fluidics which include switches and proportional amplifiers.

Free jets in the exhausts of rocket engines create aerodynamic noise which in many cases is objectionable and should be controlled. The aerodynamic noise is generated by Reynolds stresses associated with either subsonic or supersonic flows. It is necessary to know the turbulence structure within such jets for better design related to noise reduction.

Recently, research on free jets has received considerable attention. One kind of jet, the axisymmetric, isothermal jet is a practical flow which embodies many of

---

<sup>1</sup> Numbers in brackets designate references.



the essential features of shear flow turbulence, and it remains a fertile ground for investigation.

## 1.2 Axisymmetric Jets in Still Surroundings

### 1.2.1 Turbulent Jet Formation

The turbulence in jet flow is caused by the generation of vortices and their breakdown due to interaction. Using flow visualisation technique [2], it has been shown that waves starting from the nozzle outlet grow with unstable amplitude within two-to-three wave lengths from the exit. The wave crest in contact with the stationary ambient air folds back into the following trough. This folding engulfs the surrounding fluid and forms a ring vortex core which rolls downstream. After one or two revolutions, the vortices interact strongly with the waves behind and break down into turbulent eddies [2]. The interactions (like vortex pairing) of turbulent eddies cause large scale vortical motions; small scale vortical motions also evolve through breakdown of the large eddies. When the initial boundary layer is laminar, the initial vortical structure results from the instability and rollup of the free shear layer, and the initial size and spacing of vortices can be determined by the unstable eigenmode of the profile. For this case, the laminar-turbulent transition length from the outlet depends on Reynolds number,  $R_{eD}$ . The higher the Reynolds number, the smaller the laminar-turbulent

transition length.

A free shear layer resulting from an initially turbulent boundary layer can also roll up into an organized vortical structure from which evolve large and small scale motions not unlike the initially laminar case. This kind of jet flow is shown in Figure 1.1, with three distinguishable layers: 1) shear, 2) ambient, and 3) potential core. For convenient analysis, the turbulent jet flow is divided into three principal regions: 1) initial region, 2) transition region, and 3) developed region, shown in Figure 1.1. The initial region applied to jets with an initial core of uniform velocity or potential core and extends until the core disappears. The transition region starts after the initial region. Further downstream, there exists a developed region where the flow variables, i.e., mean velocity, turbulent intensity, etc. become approximately self-preserving. The combined initial and transition regions is called the developing region of the jet.

### 1.2.2 Flow in Axisymmetric Turbulent Jets

A continuous transfer of momentum and energy takes place from the jet fluid to the surrounding fluid. A difference in velocity between a jet and the region into which it is discharged forms a pronounced degree of instability due to the intensive shearing of the peripheral jet fluid with the ambient fluid. The shearing action initially occurs over a small lateral region; but, the fluid near

the axis remains unsheared. For turbulent jets, the shearing phenomenon steadily converts kinetic energy of the oncoming mean flow into kinetic energy of turbulence, and the latter decays through viscous shear. Such a conversion of energy occurs throughout the jet flow. On the other hand, the reduction of kinetic energy of the mean flow represents a decrease in the flow velocity. The elementary consideration of continuity indicates that the area of flow section must increase as the flow velocity decreases. Newton's principle of action and reaction would suggest that deceleration of the fluid in the jet can occur only through a simultaneous acceleration of the surrounding fluid, so that the total rate of flow past successive sections of the jet increases with distance from the outlet. This phenomena flattens the velocity profile in the shear layer and reduces centre line velocity after the potential core region.

The initial and boundary conditions play an important role and influence the flow and mixing process in the initial region. The boundary conditions are related to the shape of the nozzle and the space surrounding the shear layer. The initial conditions for steady jets are the flow properties at the exit plane of the nozzle which depend on the boundary layer thickness inside the nozzle. The flow variables in the initial region are dominated by the large scale structure which can be expected to achieve independence

of the initial conditions in a finite flow length and the flow may become self-preserving depending on the boundary conditions.

### 1.3 Energy Transfer in Turbulent Jets

Turbulent flow represents a continuous interaction, mixing or superposition of turbulent eddies of various sizes which cause fluctuation of flow variables (velocity, pressure, etc.) about their mean values. Energy transfer in a turbulent flow field depends on the interaction of eddies, and correlations between various quantities of the turbulence and the mean motion. For simplicity, turbulence may be considered to consist mainly of eddies of two kinds, depending on scale: 1) large eddies, and 2) small eddies. The large eddies are energy containing eddies, and they are strained by both the mean and turbulent stresses present in the flow field. The small eddies contain less energy and they are invariant to mean and turbulent stresses in the flow field. The small scale eddies exist in the field of large scale eddies and dissipate turbulent energy to heat. The kinetic energy related to small eddies in the field of the big eddies may be called the internal energy of big eddies.

Forms of energy in a turbulent shear flow are:

- 1) turbulent kinetic energy (for both large or small eddies);
- 2) mean kinetic energy;

- 3) energy due to pressure.

These forms of energy transform from one form to another in the following processes:

- 1) energy transfer from mean motion to turbulence;
- 2) turbulent energy dissipation to heat;
- 3) energy transfer due to interaction, between eddies of different size.

The relative magnitude of energy transfer with respect to wave number is shown in Figure 1.2.

The major portion of turbulent energy production takes place at relatively low wave numbers which correspond to the larger scale eddies of the turbulence. The large eddies are stretched by the mean motion which performs work on them and this causes turbulence production. Tucker [3] interpreted turbulence production through vortex stretching for an irrotational flow field. Experimentally and analytically, he has shown that the vortex stretching increases turbulent kinetic energy which comes from the mean motion. Though this analysis is not applicable to jet flow, it gives an insight of energy transfer from the mean motion to turbulence.

Dissipation means the decay of turbulence which occurs through the transfer of energy from the large eddies to the small eddies. This kind of energy transformation is large at high wave numbers which represent the small scale eddies, Figure 1.2.

The energy transfer due to eddy interaction depends on the size of eddies, the correlation of pressure and velocity fluctuations and the triple correlations of the fluctuating velocity components. This transformation is called the diffusion of turbulent energy and its magnitude is high at intermediate wave numbers, Figure 1.2. A detailed discussion of energy transformation related to axisymmetric jets will be presented later.

#### 1.4 Statement of the Problem

The flow in the developing region of axisymmetric incompressible turbulent jets will be studied, both theoretically and experimentally. Jets produced by three different nozzles having different boundary layer velocity profiles at the nozzle exit will be investigated. The exit Reynolds number based on the average velocity and the outlet diameter will be  $1.53 \times 10^5$  for all three cases.

The mean velocity and turbulent intensity at the nozzle exit will be measured to identify the initial conditions of the jet. The mean velocity, the turbulent intensities in x, r and  $\theta$ -direction, and the shear stress will be measured in the initial and transition regions.

A differential method will be used to determine mean flow properties by solving the differential momentum and continuity equations for the initial and transition regions with an arbitrary initial condition. This method will be extended with a differential transport equation for

turbulent kinetic energy together with an algebraic equation for length scale to determine turbulent properties in the initial region.

An integral method will be used as a special case to determine jet boundaries in the initial region for a thin boundary layer at the nozzle exit.

CHAPTER II  
LITERATURE SURVEY

2.1 General

Turbulent flows can be expressed mathematically by the conservation of mass equation and the Navier-Stokes equations. Since the Navier-Stokes equations are non-linear, each individual flow pattern has certain unique characteristics that are associated with its initial and boundary conditions. The equations have been analysed by researchers for various flow patterns, but it is still not possible to make quantitative predictions concerning turbulent quantities without relying greatly on empirical data because, in the time averaged turbulent equations, there are more unknown dependent variables than there are equations. In order to obtain a useful set of closed equations, it is necessary to make crucial assumptions concerning the flow, with physical concepts based on experimental data and experience. In this way, many authors have developed empirical and semi-empirical equations to obtain a set of closed equations. Progress in this line of research, as related to axisymmetric jets, is presented in this chapter.

The developed region of axisymmetric jets, sufficiently far downstream, is not affected by the initial conditions. Much work has been done both theoretically and experimentally in this region by Wygnanski [4], Heskestad



[5], Newman [6], Townsend [7], Rotta [8], Launder [9], Roshko [83] and others. On the other hand, much less work has been done in the initial and transition regions except lately in relation to noise by Bradshaw et al [10], Ko and Davies [11], Lau [12] and others. Some relevant experimental work in these regions of turbulent jets is presented in chronological order in Table 2.1, with information on jet size, exit conditions, Reynolds numbers and the variables measured. Relevant theoretical work with information on the equations used is shown in Table 2.2.

## 2.2 Mean Velocity

### 2.2.1 Developed Region

In 1925, Prandtl [13] published the concept of mixing length for free turbulent shear flow and it was used by Tollmien [14] in 1926 to calculate mean velocities in an axisymmetric jet without any special consideration of the region of the jet close to the nozzle. The investigation was based on the assumptions that: (a) the effective force was the tangential shear expressed in terms of the lateral momentum transport and mixing length, (b) the mixing length varies as the first power of the axial distance from the efflux section, (c) turbulence velocity was proportional to the mixing length and mean velocity gradient. Tollmien [14] established a series solution for mean velocity with variable,  $\eta_t = r/(a_t x)$ , and the Prandtl's mixing length,  $L = c_t x$  where  $a_t$  and  $c_t$  are empirical con-

TABLE 2.1: Relevant Experimental Work

	Authors	Nozzle Size And Jet	Reynolds No.	Exit Conditions	Variables Measured	Model	Initial Region	Transition Region
1	Trupel (1915) [27]	45cm Air jet	$5 \times 10^6$	Not Identified	u	---	X	X
2	Kuethe (1935) [16]	10cm Air jet	$1.75 \times 10^4$	"	$u, \sqrt{u'^2}$	u	X	
3	Albertson et al (1948) [18]	2.54, 1.27 & 0.64cm Air jet	$9.17 \times 10^4$	"	$u, \sqrt{u'^2}$	u	X	X
4	Abramovich (1948) [27]	10cm Air jet	$1.64 \times 10^4$	"	u	u	X	X
5	Laurence (1954) [31]	8.89cm Air jet	1.92, 3.0, 5.0 and $7.5 \times 10^4$	"	$u, \sqrt{u'^2}, L^0, \frac{u' u''}{u' u'}$	---	X	X
6	Davies et al (1963) [30]	2.54cm Air jet	$1.92 \times 10^5$	"	$u, \sqrt{u'^2}, L^0, \frac{u' u''}{u' u'}, U_c$ SPL	$L^0, SPL$	X	X
7	Bradshaw (1964) [10]	5.08cm Air jet	$3 \times 10^5$	$\delta_0 = 0.0008$ in $H_0 = 2.2$	$u, \sqrt{u'^2}, \sqrt{u''^2}, \frac{u' u''}{u' u'}, \sqrt{u'^2}$	---	X	X
8	Kolpin (1964) [33]	2.54, 1.25cm Air jet	$1.82 \times 10^5$ and more	Not Identified	$u, \sqrt{u'^2}, \sqrt{u''^2}$	---	X	X
9	Bradshaw (1966) [36]	5.08cm Air jet	$3 \times 10^5$	Various $\theta_0$	$u, \sqrt{u'^2}, \sqrt{u''^2}, \frac{u' u''}{u' u'}, SPL$	---	X	X

TABLE 2.1 (Cont'd)

	Authors	Nozzle Size And Jet	Reynolds No.	Exit Conditions	Variables Measured	Model	Initial Region	Transition Region
10	Sami et al [24] (1967)	30.48cm Air jet	$2.2 \times 10^5$	Not Identified	$u, \sqrt{u'^2}, \sqrt{u''^2}$ $\overline{u'u'}, \sqrt{\overline{p'^2}}$	---	X	X
11	Von Frank [25] (1970)	30.48cm Air jet	$5 \times 10^5$	"	$u, \sqrt{u'^2}, \sqrt{u''^2}$	---	X	X
12	Nilsen [71] (1970)	30.48cm Air jet	$6.25 \times 10^5$	"	$u, \sqrt{u'^2}, \sqrt{p'^2}$	---	X	X
13	Crow [37] (1971)	2.54cm Air jet	$1.05 \times 10^4$ to $5.14 \times 10^4$	Various $\delta_0$	$u, \sqrt{u'^2}$ , spectra	---	X	X
14	Ko [11] (1971)	2.54cm Air jet	$2 \times 10^5$ $10^5$	Not Identified	$u, \sqrt{u'^2}, \overline{u'u'}$ $U_c, SPL$	---	X	
15	Hatta [23] (1975)	3.6 cm Air jet		"	u	u	X	X
16	Yule [38] (1977)	5.08cm Air jet	$9 \times 10^3$ to $2 \times 10^5$	"	$u, \sqrt{u'^2}, \sqrt{u''^2}$ , $\sqrt{w'^2}, \overline{u'u'}$	---	X	
17	Yuu [34] (1978)	0.8 cm Air jet	$2.2 \times 10^5$	"	u	u	X	

TABLE 2.2: Relevant Theoretical Work

	Authors	Equations	Shear Stress Model	Initial Region	Transition Region	Comment
1	Squire [17] (1944)	Integral Form a) Mass b) Momentum	$L^2 (\partial u / \partial r)^2$ $L = c_4 b_1$	X	X	Assumed a cosine velocity profile and determined jet boundaries. Shear layer width, $b_1$ , was assumed between $u/u_c=0$ and $u/u_c=1$
2	Kuethe [16] (1935)	Integral Form a) Mass b) Momentum	$L^2 (\partial u / \partial r)^2$ $L = c_4 b_1$	X		Assumed a velocity profile and improved by iteration. The width of shear layer was defined between $u/u_c=0$ and $u/u_c=1$ .
3	Kirshner [20] (1968)	Integral Form a) Mass b) Momentum	$v_t (\partial u / \partial r)$ $v_t = \text{const.}$		X	Similar to that of laminar flow case. The solution is not applicable to the initial region.
4	Peters [66] (1972)	Integral Form a) Mass b) Momentum c) Turbulent K.E.	$c_1 k$ $c_1 = \text{const.}$	X	X	Assumed a cosine velocity profile for the initial region, and solved for kinetic energy, velocity in the transition region. Width of shear layer is the length scale.

TABLE 2.2 (Cont'd)

Authors	Equations	Shear Stress Model	Initial Region	Transition Region	Comment
5 Harsha [44] (1972)	Diff. Form a) Mass b) Momentum c) Turbulent K.E.	$c_1 k$		X  X	Calculation was performed for the transition and developed region.
6 Madni [26] (1975)	Diff. Form a) Mass b) Momentum	$L^2 (\partial u / \partial r)^2$ $L = c_4 b_1$	X	X With Different Shear Stress Model	Flat mean velocity profile at the nozzle exit. Sufficient data were not reported.
7 Hatta [23] (1975)	Diff. Form a) Mass b) Momentum c) Energy	$\nu_t (\partial u / \partial r)$ $\nu_t \sim (r_m - r_1) u_c$	X	X	Obtained a polynomial form velocity profile. Linear jet boundaries were calculated. Length scale is $b_1$ .
8 Rotta [8] (1972) [41] (1975)	Diff. Form a) Mass b) Momentum c) Turbulent K.E. d) L'k-Equation	$K_0 \sqrt{kL} (\partial u / \partial r)$			For developed region of jets and other shear flows
9 Launder [9] (1974) [59] (1977)	Diff. Form a) Mass b) Momentum c) Turbulent K.E. d) Dissipation	$k^2 / \mu \epsilon (\partial u / \partial r)$	X	X	Used two-equation model.

stants. The series solution agreed fairly well with measurements [14] for the developed region of jets. In 1930, Schlichting [15] used Prandtl's hypothesis to express turbulent shear stress,  $\tau/\rho = c_s b_1 (U_{\max} - U_{\min}) (\partial u/\partial r)$  where  $c_s$  is an empirical constant and  $b_1$  is the width of shear layer, and solved the same problem as Tollmien [14] did in 1926 using similar assumptions. The solution shows satisfactory agreement with measurements except in the region of low velocity near the jet boundary.

### 2.2.2 Initial and Transition Regions

The solutions given by Tollmien [14] and Schlichting [15] do not apply to the initial region of a jet issuing from a nozzle because of the presence of the potential core and the effects of the initial conditions, although Prandtl's mixing length is approximately linear for this region.

Kuete [16], in 1935, applied Prandtl's mixing length to the initial and transition regions and worked out an approximate method for computing the mean velocity for a round jet. He assumed Prandtl's mixing length to be proportional to the width of shear layer and performed successive approximations introducing a profile for the first approximation of the form:

$$(u)_{1st.app.} = \left[ 1 - \left( \frac{r - r_1}{b_1} \right)^{\frac{3}{2}} \right]^2 \quad (2.1)$$

where  $b_1$ , the width of shear layer and  $r_1$ , the radius of potential core were calculated by successive approximations.

In this analysis, shear stress was expressed as:

$$\overline{u'u'} = L^2 \left| \frac{\partial u}{\partial r} \right| \frac{\partial u}{\partial r} \quad (2.2)$$

where  $L = c_4 b_1$ ;  $c_4$  is an empirical constant determined by experiment.

The theoretical calculations of the mean velocity for both initial and transition regions showed agreement with experimental results from pitot tube measurements.

In 1944, Squire and Truncer [17] developed a mean velocity model for the initial and transition regions of co-flowing jets with assumptions similar to those that Kuethe [16] used for jets in still air. The Reynolds shear stress was expressed by Prandtl's mixing length hypothesis given by Equation (2.2). The empirical constant,  $c_4$ , used to determine the mixing length was found to be different from that predicted by Kuethe [16]. As a special case, the length of the potential core was calculated to be  $x/r_0 = 7.75$  for jets in still air. This value does not agree with that of Kuethe [16].

Albertson et al [18], in 1948, measured mean axial velocities for both axisymmetric and two-dimensional jets, and their measurements of mean velocity in the initial and transition regions were found to follow the normal probability function:

$$\frac{u}{u_0} = e^{-(r^2/2\sigma^2)} \quad (2.3)$$

where  $o = c_a x$ ;  $c_a$  is an empirical constant which has two values, one for the initial region and the other for the transition region. This model of mean axial velocity showed satisfactory agreement for the two-dimensional case, but it was not wholly satisfactory for the axisymmetric case. The experimental value of the potential core length was found to be  $x/r_o = 12$ , but the authors, using  $x/r_o = 9$  achieved agreement with measurements of the velocity in the downstream sections. The measurements were carried out by using a hypodermic needle as a stagnation tube connected directly to a manometer.

In 1957, Miller and Comings [19] used Brandt's mixing length hypothesis for a two-dimensional jet flow and developed a self-preserving empirical model for mean axial velocity in the transition region after  $x/r_o = 10$ :

$$\frac{u}{u_c} = \exp \left[ - \frac{\pi}{8} \left( \frac{r}{b_m} \right)^2 \right] \quad (2.4)$$

where  $b_m$  was defined by:  $b_m = \int_0^{\infty} (u/u_c) dr$ .

The measured values of  $b_m$  showed a linear relationship with axial distance. Experimentally, it was shown that the axial component of Reynolds shear stress was balanced by the static pressure. They applied similar assumptions to those of Kuethe [16] for the theoretical analysis. Reynolds shear stress was expressed by Equation (2.2). This model does not apply to the initial region.

Kirshner [20] used a constant viscosity model for



the transition region and solved the momentum integral equation in the same way as for laminar flow. The expression for the mean axial velocity of the turbulent jet was the same as that for the laminar jet with the molecular diffusivity replaced by constant eddy diffusivity. The constant eddy diffusivity was defined by:  $v_t = c_k b_1 u_c$ , where  $c_k$  is an empirical constant. The results of this solution agreed with the measurements of Kirshner [20] for the transition region. Though this model is simple to use, the turbulent diffusivity is not constant throughout the jet flow, specially in intermittent regions [21, 22].

Hatta and Nozaki [23], in 1975, developed a model for axial mean velocity by an approximate solution of the axial momentum integral equation for the initial and transition regions. Turbulent diffusivity,  $v_t$  was defined by:

$$v_t \propto (r_m - r_1) u_c$$

where  $r_m$  is the mean radius of the jet expressed by:

$$u_o r_m^2 = r_1^2 u_o + 2 \int_{r_1}^{r_m} u r dr$$

Neglecting the pressure gradient in the momentum equation, a model for the axial mean velocity was established:

$$\frac{u}{u_o} = (1 - \eta_H)^4 (1 + 4\eta_H) \quad (2.5)$$

where  $\eta_H = r/b_1$ .

This investigation also derived expressions for  $b_m$ ,  $b_1$ , and  $r_1$  as linear functions of axial distance. Though this approximate model showed agreement with Hatta and Nozaki's [23] measurements, it does not agree wholly with the measurements of Bradshaw et al [10], Sami et al [24] and Von-Frank [25]. This discrepancy likely comes from the initial conditions which were not documented by the authors.

Madni and Pletcher [26] calculated the mean velocity by an explicit finite-difference method from the differential forms of mass and momentum conservation equations derived by using the boundary layer approximations. Reynolds shear stress was defined by Equation (2.2) for the initial region, and for the transition region by:

$$\overline{u'u'} = \nu_t \frac{\partial u}{\partial r} \quad (2.6)$$

where,

$$\nu_t = \frac{0.03}{r_0} \int_r^\infty u r dr \quad (2.7)$$

The calculation started with uniform exit velocity and showed satisfactory agreement with measurements for the main portion of the shear layer. This model underpredicts the mean velocity of the outer region where velocity is low.

Many experimental investigations, without identifying initial conditions, showed self-preservation of the mean velocity in the initial and transition regions of the turbulent jets. Some empirical equations for the

U

initial region are:

$$\left. \begin{aligned}
 \text{Abramovich [27]: } \frac{u}{u_c} &= (1 - \eta^{3/2})^2 \\
 \text{Simson [28] : } \frac{u}{u_c} &= (1 - \eta^{7/4})^2 \\
 \text{Kimura [23] : } \frac{u}{u_c} &= 1 - 3\eta^2 + 2\eta^3
 \end{aligned} \right\} (2.8a)$$

where,

$$\eta = r/b_1$$

and for the transition region is:

$$\text{Nayer et al [29]: } \frac{u}{u_c} = e^{-1.415(\eta + 0.7)} \quad (2.8b)$$

where,

$$\eta = (r - r_{\frac{1}{2}})/b_1$$

In the first three models, the shear layer width,  $b_1$ , was chosen between  $u/u_c = 1$  and  $u/u_c = 0$ , and Nayer measured the width,  $b_1$  between  $u/u_c = 0.99$  and  $u/u_c = 0.01$ . Nayer's definition is realistic, but this model does not apply to the initial region. Though these models are developed from similar experimental data, they do not agree with each other, probably because of different initial conditions.

Davies et al [30] measured the axial mean velocity and showed self-preservation against the independent variable  $(r - r_0)/x$  in the initial and transition regions. Measurements of Bradshaw et al [10], Von-Frank [25], Sami et al [24], Laurence [31], Lau [32], Kolpin [33] and others

show that the axial mean velocity is self-preserving when it is plotted against the variable  $(r - r_1)/b_1$ . These measurements do not show wholly self-preservation against the variable  $(r - r_0)/x$ . Yuu et al [34] used a polynomial form as an empirical model for the axial velocity in the initial and transition regions with independent variable  $(r - r_1)/x$ , where  $r_1$  is potential core radius. This model does not show satisfactory agreement with measurements in the initial region, but it is fairly applicable to the developed region. It is interesting to note here that measurements of Heskestad [5], Wagnanski [4], Gortler [15], Reed [35], and others show self-preservation of axial mean velocity when it is plotted against the variable  $r/x$  for the developed region.

Recently, Bradshaw [36], Crow and Champagne [37], Yule [38] and Hussain and Zedan [39,40] published some experimental results for jet flow, identifying the initial conditions. Bradshaw [36] studied the effects of exit boundary layer on turbulence with boundary layer untripped or tripped by concentric rings. Experimental results have shown that the shear layer becomes fully turbulent at an approximate distance  $x_t = 7 \times 10^5 (\frac{v}{u_0})$  from the exit for any boundary layer thickness used in the experiment. The investigation was carried out with maximum momentum thickness 0.15 mm. at the nozzle exit. He also noticed a significant change of virtual origin and an increase of noise emission with boundary layer thickness. Yule [38]

studied the jet flow for a wide range of Reynolds numbers ( $9 \times 10^3 - 10^5$ ) by using flow visualisation and hot-wire techniques. He found the shear layer fully turbulent at an approximate distance  $x_t = 1.2 \times 10^5 \left(\frac{u}{u_0}\right)$  from the nozzle exit which is different from Bradshaw's [36] results. This work did not mention the exit boundary layer thickness and turbulence level.

Hussain and Zedan [39,40] measured mean velocity and determined the jet boundaries, varying both the laminar and turbulent boundary layer thicknesses, and controlling the turbulence at the nozzle exit. Experimental results showed the mean velocity to be self-preserving at a distance from the exit which varies with the initial turbulence level and boundary layer thickness. For a turbulent boundary layer at the nozzle exit, the virtual origin was found to be very close to the geometric origin at the nozzle exit. This investigation was carried out over a range of Reynolds numbers ( $6 \times 10^4 - 1.4 \times 10^5$ ) with maximum momentum thickness  $\theta_0/r_0 = 0.011$  at the exit plane.

All the theoretical work referenced to the above, used the width of the shear layer,  $b_1$ , as the scale for the similarity variable  $\eta$ . In most cases,  $b_1$  is the width between iso-velocity lines  $u/u_c = 1$  and  $u/u_c = 0$ . Physically it is impossible to determine iso-velocity line  $u/u_c = 0$ .

Numerical calculations of the differential momentum

equation together with the semi-empirical transport equations presented later, were performed by Rotta [8,41] Biringen [42], Launder and Morse [43], Launder and Spalding [9], Harsha [44] and others for mean velocity and turbulence quantities. This approach will be described in the following sections in some detail.

### 2.3 Differential Transport Equations

Turbulent shear flows can be expressed mathematically by the continuity equation, the momentum equation, and a set of semi-empirical transport equations for one or more dependent variables, such as turbulent kinetic energy, length scale, dissipation energy, etc. If the set of empirical constants are known, these differential equations may be solved by numerical methods to simulate the behaviour of turbulent quantities in the shear flow. Kolmogorov [45], in 1940, first proposed the semi-empirical transport equations for the turbulent kinetic energy,  $k$ , and the characteristic frequency,  $f$ . These equations describe how the dependent variables are influenced by basic forms of energy transfer, i.e., production, dissipation, diffusion and convection. The length scale of turbulence was defined by:  $L^1 = \sqrt{k}/f$  in this model. These equations were difficult to use because of their complexity.

A few years after Kolmogorov's [45] work, Prandtl [46] independently suggested a similar differential transport equation for the turbulent kinetic energy,  $k$ , but he

used a linear algebraic equation for the length scale of turbulence which was different from Kolmogorov's equation. Glushko [47] applied this model to turbulent boundary layer calculations.

Recently, Rotta [8], Launder and Spalding [9], Rodi and Spalding [48], Bradshaw [49], Daly and Harlow [50], Kovaszny [51], Launder et al [52] and others have developed independently a number of useable differential transport equations. The equations have been applied to a variety of flows, including the developed region of turbulent jets, by Rotta [8], Launder and Spalding [9] and others. These mathematical models can be described as one-equation, two-equation, three-equation models, etc., depending on the number of semi-empirical transport equations used. Usually, increasing the number of equations means longer computer time and greater effort in determining a larger number of empirical constants. On the other hand, the model having the large number of equations can usually be applied to a wider variety of flows, although the accuracy of the calculated values may not be superior.

Bradshaw, Ferriss and Atwell [53] calculated turbulent quantities in a turbulent boundary layer using a differential transport equation for turbulent kinetic energy which was similar to that of Kolmogorov and Prandtl. The equation is:

$$\underbrace{\rho(u \frac{\partial k}{\partial x} + v \frac{\partial k}{\partial y})}_{\text{Transportation}} - \underbrace{\tau \frac{\partial u}{\partial y}}_{\text{Pro-duction}} + \underbrace{\frac{\partial}{\partial y}(\overline{p'u'} + \overline{\rho k v'})}_{\text{Diffusion}} + \underbrace{\rho \epsilon}_{\text{Dissipation}} = 0 \quad (2.9)$$

where  $\tau = \overline{\rho u'v'}$  and  $\epsilon = \overline{\nu \left( \frac{\partial u_i}{\partial x_j} \right)^2}$

The Reynolds shear stress,  $\overline{\rho u'v'}$  was expressed by:

$$-\overline{\rho u'v'} = c_1 \rho k \quad (2.10)$$

and the diffusion term was simplified to:

$$\overline{\rho'v'} + \overline{\rho k v'} = \overline{\rho k v_e} \quad (2.11)$$

where  $c_1$  is supposedly a universal constant and  $v_e$  is the effective velocity at which turbulent energy is transported in the transverse direction by the large eddies. The effective velocity,  $v_e$ , was expressed in terms of shear stress and an unknown function,  $G$ :

$$v_e = \left( \frac{\tau_{\max}}{\rho} \right)^{1/2} G\left(\frac{y}{\delta}\right) \quad (2.12)$$

where  $\delta$  is boundary layer thickness and  $\tau_{\max}$  is wall shear stress. The dissipation term was expressed as:

$$\epsilon = L^1 (\overline{u'v'})^{3/2} \quad (2.13)$$

The length scale  $L^1$  was assumed to be a universal function of  $y/\delta$ . This function was similar to that employed by Glushko [47] for developing Prandtl's model. Bradshaw, Ferriss and Atwell [53] calculated turbulence quantities from the continuity equation and a momentum equation and a differential transport equation for turbulent kinetic energy together with an empirical length scale model.

Lauder and Spalding [9], Rodi and Spalding [48], Ng



and Spalding [54], Jones and Launder [55] and Spalding [56] have developed two-equation transport models for turbulence and applied these to a variety of flows. In all models, one dependent variable in the transport equations is the turbulent kinetic energy,  $k$ . The second dependent variable is the length scale itself. However, since an equation for  $k$  is prescribed, its simultaneous solution with an equation for a variable,  $Z$  of the form  $k^m L^{lh}$  has been used to find the length scale,  $L^l$ . The above authors have developed three principal models of this type, which resemble each other. The differential transport equation for  $Z$  for two dimensional flow is:

$$\rho \frac{DZ}{Dt} = \frac{\partial}{\partial y} \left( \frac{\mu_{eff}}{\sigma_z} \frac{\partial Z}{\partial y} \right) + Z \left[ \frac{c_2 \mu_{eff}}{k} \left( \frac{\partial u}{\partial y} \right)^2 - c_3 \rho^2 k / \mu_{eff} \right] + S \quad (2.14)$$

where the term,  $S$  represents a secondary source term; its form is included in Table 2.3.

The equation for turbulent kinetic energy,  $k$ , which is the same for all the models of Launder-Spalding et al, may be written in a form:

$$\rho \frac{Dk}{Dt} = \frac{\partial}{\partial y} \left( \frac{\mu_{eff}}{\sigma_k} \frac{\partial k}{\partial y} \right) + k \left[ \frac{\mu_{eff}}{k} \left( \frac{\partial u}{\partial y} \right)^2 - c_D \rho^2 k / \mu_{eff} \right] \quad (2.15)$$

Equations (2.14) and (2.15) express the supposition that convective changes in  $Z$  and  $k$  may occur through three agencies:

- i) Spatial gradients in turbulent quantities which

give rise to diffusive transfer.

- ii) interactions between the turbulence and the mean velocity field.
- iii) direct action by turbulent motion itself.

The differential equations for  $Z$  and  $k$  contain the terms  $c_2$ ,  $c_3$ ,  $c_D$ ,  $\sigma_z$  and  $\sigma_k$  which are assumed to be a set of empirical constants. The expressions for  $Z$  and  $S$ , and the values of constants are presented in Table 2.3.

All these models use the same expression for turbulent shear stress,  $\overline{\rho u'v'}$ .

$$-\overline{\rho u'v'} = \mu_{\text{eff}} \frac{\partial u}{\partial y} \quad (2.16)$$

where the effective viscosity  $\mu_{\text{eff}}$  is:

$$\mu_{\text{eff}} = \rho c_D \sqrt{k} L^1 \quad (2.17)$$

These models were applied to turbulent boundary layers, internal flows and many other flows including the developed region of turbulent jets and satisfactory results have been shown in Refs. [9,43,57,58,59].

Rotta [8] also developed two-equation transport models for turbulence. One equation has been formed with the dependent variable either the turbulent kinetic energy or the shear stress, and the other equation with the variable,  $kL^1$ . In these equations, it is assumed that the convective changes in dependent variables are balanced by production, dissipation, and diffusion of turbulence. The differential equations are:

TABLE 2: Two-Equation Models

Reference	Z	Physical Meaning	$c_2$	$c_3$	$c_D$	$\sigma_k$	$\sigma_\epsilon$	s
Rodi & Spalding [48] Ng & Spalding [54]	$kL^1$	Energy And Length Scale Product	0.98	0.059	0.09	1.0	1.0	$(\frac{L^1}{\bar{y}})^5 k^{3/2} (-702)$
Spalding [56]	$k/(L^1)^2$	Square of Ch. Frequency	1.04	0.17	0.09	0.9	0.9	$3.5\mu_{eff} (\frac{\partial u}{\partial y^2})^2$
Jones & Launder [55] Launder & Spalding [9]	$k^{3/2}/L^1$	Dissipation Energy	1.45	0.14	0.09	1.0	1.1	---

the K.E. equation,

$$\frac{Dk}{Dt} = \overline{u'u'} \frac{\partial u}{\partial y} - c_r \frac{k^{3/2}}{L} + \frac{1}{y^j} \frac{\partial}{\partial y} \left( y^j k_q \sqrt{k} L \frac{\partial k}{\partial y} \right) \quad (2.18)$$

the length scale equation,

$$\begin{aligned} \frac{DkL}{Dt} = \overline{u'u'} \xi L \frac{\partial u}{\partial y} - c_L c_r k^{3/2} \\ + \frac{1}{y^j} \frac{\partial}{\partial y} \left( y^j k_{qL} \sqrt{k} L (L \frac{\partial k}{\partial y} + \alpha_L k \frac{\partial k}{\partial y}) \right) \end{aligned} \quad (2.19)$$

where  $j = 1$  for axisymmetric flow and  $j = 0$  for two dimensional flow. These equations contain the terms  $c_r$ ,  $k_q$ ,  $\xi$ ,  $c_L$ ,  $k_{qL}$  and  $\alpha_L$  which are assumed to be empirical constants. Rotta [8] determined these constants for the developed region of turbulent jets to be:

$$\begin{aligned} c_r = 0.165 ; \quad c_L = 0.8 ; \quad k_q = 0.6 \\ \xi = 0.99 ; \quad k_{qL} = 0.6 ; \quad \alpha_L = 0.5 \end{aligned}$$

Rotta [8] further used this model replacing the kinetic energy equation by the turbulent shear stress equation in the form:

$$\begin{aligned} \frac{D}{Dt} (\overline{\rho u'u'}) = \rho k a_p \frac{\partial u}{\partial y} - k_p c_r \frac{\sqrt{k}}{L} (\overline{\rho u'u'}) \\ + k_{qt} \frac{\partial}{\partial y} \left( \sqrt{k} L^2 a_p \frac{\partial \overline{u'u'}}{\partial y} \right) \end{aligned} \quad (2.20)$$

The terms  $a_p$ ,  $k_p$  and  $k_{qt}$  are empirical constants and the values of these constants for developed region of jets are:

$$a_p = 0.09, \quad k_p = 1 \quad \text{and} \quad k_{q\tau} = k_q$$

For these models, the relationship between turbulent kinetic energy and shear stress is the same as that of Launder and Spalding [9] shown in Equations (2.16) and (2.17). These differential transport equations together with the mass continuity equation and momentum equation were solved numerically for many cases of shear flows [8], including the developed region of turbulent jets.

Harsha [44] formed a one-equation transport model for calculating shear flow turbulence. He used a differential transport equation for the turbulent kinetic energy and an algebraic expression for the length scale. The energy equation is:

$$\rho \frac{Dk}{Dt} = \frac{1}{y^j} \frac{\partial}{\partial y} \left( \frac{\mu_{\text{eff}} y^j}{p_r} \frac{\partial k}{\partial y} \right) + \overline{\rho u'v'} \frac{\partial u}{\partial y} - a_2 \frac{\rho k^{3/2}}{L^1} \quad (2.21)$$

for axisymmetric flow  $j = 1$ .

The length scale  $L^1$  was chosen to be twice the half-velocity width,  $r_x$ , for axisymmetric flow, and the effective viscosity was expressed as:

$$\mu_{\text{eff}} = 0.0125 L^1 (u_{\text{max}} - u_{\text{min}}) \quad (2.22)$$

The empirical constants  $p_r$  and  $a_2$  were determined for axisymmetric flows:

$$p_r = 0.70; \quad a_2 = 1.69$$

Harsha [44] used Equation (2.10) for relating turbu-

lent shear stress and kinetic energy in the same way as that of Bradshaw et al [53]; and Harsha and Lee [60] established the constant,  $c_1 = 0.3$  experimentally. Harsha's [44] calculation of the differential transport equation together with the differential form of mass and momentum conservation equations showed satisfactory results everywhere in jet flow except the initial region.

At the Los Alamos laboratory of The University of California, Harlow and co-workers have developed transport models for turbulence which are similar to that of Kolmogorov [45]. They have formed the differential transport equations with two (or more) turbulent quantities as dependent variables. All models developed by this research group used the turbulent kinetic energy as one dependent variable for a transport equation. The other dependent variable was chosen to be the length scale by Harlow and Nakayama [61] and local dissipation rate by Harlow and Nakayama [62] to form another differential transport equation. Recently, Harlow and Hirt [63] and Harlow and Daly [64] have employed differential equations for turbulent shear stresses and normal stresses in the three individual directions of the co-ordinate system. Each model contains a set of empirical constants, and the shear stresses were expressed by similar expressions to those given in Equations (2.16) and (2.17). These models have been applied to a variety of turbulent flows, but their application to axisymmetric jets in still surroundings has not been reported.

The calculation of turbulence by using the differential transport equations has become routine for many turbulent flows. Recently, Heck and Smith [65], Peters and Phares [66], Biringen [42], McGuirk and Rodi [67], Launder et al [52,59,98] and others applied the transport models described above to a variety of flows and obtained satisfactory results. Each worker used a different numerical method of solution and a different set of empirical constants, yet each achieved satisfactory results.

From a survey of the literature, it is apparent that not much theoretical work has been done in the initial and transition regions of axisymmetric jets. This dissertation presents some theoretical work for these regions using a single transport equation together with the continuity and momentum equations.

#### 2.4 Turbulence

Jet shear flows are anisotropic in character and a continuous transfer of energy takes place from mean motion to the turbulence due to the interaction of the Reynolds stresses and the mean velocity gradients. This kind of flow has high Reynolds stresses which are the major cause of jet noise [68]. The turbulence in shear flows is determined either by measurements or by empirical/semi-empirical relations.

Bradshaw et al [10], Davies et al [30,69], Ko and Davies [11], Lau [12,32], Laurence [31], Lau and Fisher [70], Arndt and Nilsen [71] and others measured turbulence in

different jet geometries and at different Reynolds numbers, as shown in Table 2.1. Though most of the measurements were made under similar conditions using the hot-wire anemometer, the results do not wholly agree with each other in the initial region. The agreement of different measurements is satisfactory in the transition and developed regions. The disagreement of measurements in the initial region may be due to different initial conditions which were unspecified.

Rotta [8], Launder et al [9], Harsha [44] and others applied transport models for calculating turbulence in the developed and transition regions of jets. Rotta [8] and Launder et al [9] calculated turbulent kinetic energy and length scale from a two-equation transport model and determined the shear stress by Equations (2.16) and (2.17). Harsha [44] calculated turbulent kinetic energy from a one-equation transport model and determined the shear stress by Equation (2.10). Harsha [44] also applied the following model for shear stress in jet flow:

$$\overline{\rho u'v'} = c_1 \rho \left[ \frac{(\frac{\partial u}{\partial r})}{(\frac{\partial u}{\partial r})_{\max}} \right] k \quad (2.23)$$

This model of shear stress does not show satisfactory agreement with measurements for the initial region.

Rudy and Bushnell [72] calculated Prandtl's mixing length for many shear flows, and twenty-two out of twenty-four cases in Langley Workshop conference were tested by Prandtl's mixing length. The present research examines the Prandtl's mixing length model of shear stress in addition to



that given in Equations (2.10) and (2.16) for the initial region.

The authors referred to in Section 2.1 above did not report relationship between individual components of Reynolds normal stresses and turbulent kinetic energy. Townsend [7] and Csanady [73] approximated the normal stresses in  $r$  and  $\theta$  directions as  $v'^2 = w'^2$ , and in  $x$  direction as  $\overline{u'^2} = k$ . Measurements of Bradshaw et al [10], Sami et al [24], Von-Frank [25] and others do not agree with the assumption,  $v'^2 = w'^2$  in the developing region of jets. The present research develops semi-empirical relations between the individual components of Reynolds normal stresses and the turbulent kinetic energy.

## CHAPTER III

### THEORY

#### 3.1 General

Turbulent motion is governed by the Navier-Stokes differential equations. The general solution of the non-linear Navier-Stokes equations is not available. In order to apply Navier-Stokes equations to practical cases, hypothesis and empirical assumptions have to be introduced in order to obtain a closed set of equations with time average dependent variables. The early theoretical work uses Boussinesq's eddy viscosity hypothesis and Prandtl's mixing length equation to calculate mean velocities with the eddy viscosity and the mixing length as empirical quantities. The assumptions, necessary to build the empirical relations depend on the boundary conditions of the flow field and have to be readjusted for each particular flow case.

Theoretical work on turbulence can be developed in any of the four levels:

- 1) Empirical algebraic formulae connecting the turbulent and mean flow quantities. The most common example is eddy viscosity formulae.

- 2) Empirical differential equations (transport equations) for one-point turbulent quantities. Examples are the Reynolds stress transport equations, length scale transport equation, etc.

- 3) Empirical differential equations for two-point correlations or spectrum tensor. Examples are Kraichnan

"Direct Interaction" model [74] and Deissler's Linearized models [75].

4) Direct numerical solution of the time-dependent Navier-Stokes equations. Examples are Deardorff [76] and Schumann [77].

Studies at level 3 refer mainly to isotropic turbulence. The mathematical treatment to the shear flow equations simplifies level 3 almost to level 2. Progress at level 4 is possible for low Reynolds no. flows, but consumes much computer time producing results inferior to that of level 3, even for the small scale motion. Therefore, engineering calculations of turbulent flows are confined to levels 1 and 2 for the immediate future.

Theoretical analyses at levels 1 and 2 are most simply explained as attempts to 'close' the exact Reynolds stress transport equations for  $-\rho \overline{u_i u_j}$  which are derived by manipulating the Navier-Stokes equation and time averaging as shown in Appendix A. Up to the present, the most successful method of closure has been to obtain an empirical turbulent energy transport equation and relate the Reynolds stresses to energy equation by using physical concepts.

### 3.2 Governing Equation

#### 3.2.1 Mean Flow Equations

Assuming steady, incompressible flow without contacting any solid surface and constant fluid properties and zero pressure gradient, the equations for mean motion are derived in Appendix A.

the mass conservation equation is:

$$\frac{\partial(ur)}{\partial x} + \frac{\partial(ur)}{\partial r} = 0 \quad (3.1)$$

the momentum conservation equation is:

$$u \frac{\partial u}{\partial x} + v \frac{\partial u}{\partial r} = \frac{1}{r} \frac{\partial}{\partial r} (r \frac{\tau}{\rho}) \quad (3.2)$$

where  $\tau$  is the shear stress and  $\rho$  is the density of the fluid. The co-ordinate system is shown in Figure 1.1

The shear stress,  $\tau$ , includes both viscous and turbulent contributions, and it was written as:

$$\frac{\tau}{\rho} = \nu \frac{\partial u}{\partial r} - \overline{u'v'} \quad (3.3)$$

where  $\nu$  is the molecular diffusivity. The turbulent part of shear stress is  $-\overline{\rho u'v'}$  and it is usually expressed by Boussinesq's hypothesis:

$$-\overline{\rho u'v'} = \rho \nu_t \frac{\partial u}{\partial r} \quad (3.4)$$

$\nu_t$  is the turbulent diffusivity. For the initial region of turbulent jets, the diffusivity,  $\nu_t$  is expressed in terms of Prandtl's mixing length,  $L$  and mean velocity gradient,  $\partial u / \partial r$ .

for the initial region:

$$\nu_t = L^2 \left| \frac{\partial u}{\partial r} \right| \quad (3.5)$$

where  $L$  is Prandtl's mixing length. This model is not applicable to the transition region. Schetz's [21] and Madni-Pletcher's [26] models are combined for calculating

mean flow properties in the transition region.

Madni-Pletcher's model is:

$$v_t = \frac{0.03}{r_0} \int_r^\infty ur \partial r \quad (3.6)$$

Schetz's model is:

$$v_t = \frac{0.024\gamma}{r_0} \int_0^\infty ur \partial r \quad (3.7)$$

where  $\gamma$  is an intermittency factor. An expression was developed by the author for  $\gamma$  as follows:

$$\left. \begin{aligned} \gamma &= 1.0 && ; 0 \leq r/r_{1/2} \leq 0.8 \\ \gamma &= (0.5)^\beta && ; r/r_{1/2} > 0.8 \end{aligned} \right\} \quad (3.7a)$$

where,

$$\beta = (r/r_{1/2} - 0.8)^{2.5}$$

This gives a distribution for  $\gamma$  which agrees well with the experimentally determined curve in ref. [87].

A variable  $\eta = (r - r_{1/2})/b$  is defined to be a self-preserving variable for the initial region, where the scale,  $b$ , is defined as:

$$b/r_0 = \frac{-1}{\left[ \frac{\partial(u/u_c)}{\partial(r/r_0)} \right]_{r=r_{1/2}}} \quad (3.8)$$

where  $r_0$  is the jet exit radius,  $r_{1/2}$  is the radial distance for  $u/u_c = 0.5$  and  $u_c$  is the centre line velocity. The coordinate at  $r_{1/2}$  and the scale,  $b$ , were chosen as the most convenient for establishing self-preserving qualities of the jet in the initial region.

### 3.2.2 General Turbulent Kinetic Energy Equations

The general turbulent kinetic energy equation derived in Appendix A is:

$$\begin{aligned}
 \underbrace{u \frac{\partial k}{\partial x} + v \frac{\partial k}{\partial r}}_{\text{Transport}} &= - \underbrace{\left[ \overline{u'^2} \frac{\partial u}{\partial x} + \overline{u'v'} \left( \frac{\partial u}{\partial r} + \frac{\partial v}{\partial x} \right) + \frac{\overline{u'w'}}{r} \frac{\partial u}{\partial \theta} \right.}_{\text{Production}} \\
 &+ \underbrace{\left. \frac{\overline{w'u'}}{r} \frac{\partial v}{\partial \theta} + \overline{w'^2} \frac{v}{r} \right]}_{\text{Production}} - \nu \underbrace{\left[ \left( \frac{\partial u'}{\partial x} \right)^2 + \left( \frac{\partial v'}{\partial x} \right)^2 + \left( \frac{\partial w'}{\partial x} \right)^2 \right.}_{\text{Dissipation}} \\
 &+ \underbrace{\left. \left( \frac{\partial u'}{\partial r} \right)^2 + \left( \frac{\partial v'}{\partial r} \right)^2 + \left( \frac{\partial w'}{\partial r} \right)^2 + \left( \frac{1}{r} \frac{\partial u'}{\partial \theta} \right)^2 + \left( \frac{1}{r} \frac{\partial v'}{\partial \theta} - \frac{w'}{r} \right)^2 \right.}_{\text{Dissipation}} \\
 &+ \underbrace{\left. \left( \frac{1}{r} \frac{\partial w'}{\partial \theta} + \frac{v'}{r} \right)^2 \right]}_{\text{Dissipation}} - \underbrace{\left[ \frac{\partial}{\partial x} \{ u' (p'/\rho + k) \} \right]}_{\text{Diffusion}} \\
 &+ \underbrace{\left[ \frac{1}{r} \frac{\partial}{\partial r} \{ u' r (p'/\rho + k) \} + \frac{1}{r} \frac{\partial}{\partial \theta} \{ w' (p'/\rho + k) \} \right]}_{\text{Diffusion}} \\
 &- \underbrace{\left[ \nu \left\{ \frac{\partial^2 k}{\partial x^2} + \frac{1}{r} \frac{\partial}{\partial r} \left( r \frac{\partial k}{\partial r} \right) + \frac{1}{r^2} \frac{\partial^2 k}{\partial \theta^2} \right\} \right]}_{\text{Diffusion}} \quad (3.9)
 \end{aligned}$$

where  $k = (\overline{u'^2} + \overline{v'^2} + \overline{w'^2})/2$ . From physical concepts, this equation contains four basic terms: 1) convective transport, 2) production, 3) dissipation and 4) diffusion transport.

A correct interpretation of the terms in the transport equation (3.9) is important. For practical purposes, Equation (3.9) is simplified by introducing empirical assumptions. This means that the terms are approximated by algebraic relations.

### 3.3 Formation of Empirical Turbulent Energy Equation

#### 3.3.1 Production

The main source of turbulence is the production term. Production means transfer of energy from mean motion to turbulence. This occurs through interaction of turbulent motion with mean flow. In other words, it can be defined as the work done by Reynolds stresses due to the deformation caused by mean flow. It may be seen from Equation (3.9), that the production term is the product of the Reynolds stresses and the rate of deformation caused by mean flow. Mathematically, the production term is:

$$\text{Production} = -\overline{u'_i u'_j} S_{i,j}$$

where  $u'_i = (u', v', w')$  and  $S_{i,j} = \frac{1}{2} \left( \frac{\partial u_i}{\partial x_j} + \frac{\partial u_j}{\partial x_i} \right)$ ,  $u_i = (u, v, w)$  and  $x_i = (x, y, z)$ .  $S_{i,j}$  is the deformation tensor due to mean velocity, and  $\overline{u'_i u'_j}$  is Reynolds stress tensor.

Production of turbulence causes the flow to be anisotropic. A vortical motion exists in the flow; the mean motion stretches the vortices and performs work on them which causes the generation of turbulence.

For axisymmetric flow, the azimuthal gradient of any property is zero; hence,  $\partial u / \partial \theta$ ,  $\partial v / \partial \theta$  and  $\partial k / \partial \theta$  are equal to zero in Equation (3.9). From the order of magnitude principle, the transverse gradient of any property is very high compared to the longitudinal gradient for a thin shear flow. The production by the transverse mean velocity gradient,  $\overline{u'v'} \frac{\partial u}{\partial r}$ , in Equation (3.9) dominates the whole turbulence

generation except near the centre of the transition region. Therefore, the production term in Equation (3.9) is expressed as,

$$\text{Production} = a_1 \overline{u'v'} \frac{\partial u}{\partial r} \quad (3.10)$$

where  $a_1$  is an empirical constant which accounts for the contribution of all the mean velocity gradients to the production term.

### 3.3.2 Dissipation

Turbulent dissipation means the transfer of turbulent energy to molecular motion. It is the rate at which the viscous stresses perform deformation work against the fluctuating strain rate. This term given in Equation (3.9) is the product of the molecular diffusivity and the quadratic fluctuating deformation. It can be simplified by restricting the flow to high Reynolds numbers and assuming that the dissipation is independent of the viscosity, and hence the Reynolds number. The idea behind this assumption is that for high Reynolds numbers, the turbulent spectra extend over a very wide range of wave numbers, and that the contribution to dissipation comes mainly from the small eddies or large wave number spectra. The motion of the large wave number components is statistically independent of the energy containing part of the spectra. Although the small eddies are mainly responsible for dissipation, and independent of the behaviour of the large eddies, the viscous dissipation is governed by the rate of energy transfer from large to small eddies and not by the viscosity,



i.e., the rate of energy dissipation is independent of viscosity. The magnitude may be expressed empirically [78]:

$$\text{Dissipation} = c_r \frac{k^{3/2}}{L^1} \quad (3.11)$$

where  $L^1$  is a length scale for energy containing eddies and  $c_r$  is an empirical constant. Although this simplification is made for high Reynolds number flows, its extension to low Reynolds number flows is also found to be valid [55] except for the laminar-turbulent transition.

### 3.3.3 Diffusion

Turbulent diffusion is a method of energy transport caused by turbulent mixing or interaction of eddies. It is high for the lower wave numbers corresponding to the eddies which contain the major portion of the turbulent energy. The diffusion term has two parts: (1) inertia, and (2) viscous diffusion. Viscous diffusion is the second part of diffusion term in Equation (3.9), and it is negligible in high Reynolds number flows. Inertia diffusion is the first part of diffusion term in Equation (3.9) and is triple correlations of the fluctuating velocities and correlations between fluctuating pressures and fluctuating velocities.

In general, the flow field is less affected by the diffusion transport than by the other terms, although diffusion may predominate in certain parts of the flow field. Therefore, some crude assumptions are admissible. Launder [9], Rotta [8] and others have used the simple gradient type diffusion as suggested by Prandtl [46], and expressed

diffusion in the transverse direction by:

$$\overline{(p'/\rho + k)u'} = -k_q \sqrt{k} L^1 \frac{\partial k}{\partial r} \quad (3.12)$$

where  $k_q$  is an empirical constant. By the order of magnitude principle, the longitudinal rate of diffusion is negligible compared to that in the transverse direction for thin shear layers.

### 3.3.4 Empirical Turbulent Energy Equation

Using the above interpretations and Equations (3.10), (3.11) and (3.12) for the production, dissipation and diffusion terms respectively, together with axisymmetry and thin shear layer conditions, Equation (3.9) becomes:

$$u \frac{\partial k}{\partial x} + u' \frac{\partial k}{\partial r} = a_1 \overline{u'u'} \frac{\partial u}{\partial r} - c_r \frac{k^{3/2}}{L^1} + \frac{1}{r} \frac{\partial}{\partial r} \{ k_q L^1 \sqrt{k} r \frac{\partial k}{\partial r} \} \quad (3.13)$$

The closure of the equations are achieved relating the turbulent shear stress and the kinetic energy in any of the following forms:

$$-\overline{u'u'} = c_1 k \quad (3.14)$$

$$-\overline{u'u'} = c_D \sqrt{k} L^1 \frac{\partial u}{\partial r} = c_{\mu \epsilon} \frac{k^2}{\mu \epsilon} \frac{\partial u}{\partial r} \quad (3.15)$$

Besides these two models, Equation (2.2) may be used for closure.

### 3.4 Differential Method

#### 3.4.1 Equations and Boundary Conditions

For mean flow properties, Equation (3.1) and Equation (3.2) were solved numerically using the shear stress Equation (3.4). The turbulent diffusivity,  $v_t$ , was expressed by Equation (3.5), for the initial region and by a combination of Equations (3.6) and (3.7), for the transition region. The appropriate boundary conditions applicable to Equations (3.1) and (3.2) are:

$$\frac{\partial u(x,0)}{\partial r} = 0 ; v(x,0) = 0 ; \lim_{r \rightarrow \infty} u(x,r) = 0 \quad (3.16)$$

In addition, the measured initial distribution for  $u(x,r)$  was used:

$$u(x_0, r) = f(r) \quad (3.17)$$

where  $x_0$  is the exit section of the jet.

This calculation was extended with turbulent kinetic energy Equation (3.13) in addition to Equation (3.1), and Equation (3.2) to calculate turbulent properties in the initial region. Equation (3.13) is subject to boundary conditions.:

$$\frac{k(x,0)}{\partial r} = 0 ; \lim_{r \rightarrow \infty} k(x,r) = 0 \quad (3.18)$$

and the measured initial distribution:

$$k(x_0, r) = g(r) \quad (3.19)$$

All calculations use an empirical equation for length scale given by:

$$L^1/b = L/b = 0.10625$$

Here  $L^1$  is made equal to  $L$  by adjusting the constants in the shear stress and dissipation equations. Experimental determination of  $L/b$  will be presented later. The fluid properties  $\rho$  and  $\nu$  are assumed constant.

#### 3.4.2 Calculation Technique

An explicit finite difference technique of the Dufort-Frankel [94] type was applied here to the momentum Equation (3.2) the continuity Equation (3.1) and the transport Equation (3.13) associated with boundary conditions (3.16), (3.17), (3.18) and (3.19) to calculate the turbulent kinetic energy and the mean velocities. How the derivatives are approximated for this method and their truncation errors are given in Appendix D. The finite difference grid used for the calculation are shown in Figure 3.1. The computer programme developed for this purpose had the capability of handling non-uniform grid spacings in both  $r$ - and  $x$ -direction.

Von Neuman's method of stability analysis [79] with first order error was applied to the momentum equation and found to generate a mild stability constraint given in Appendix E. For calculating the mean flow properties from the continuity and momentum equations, non-uniform grid spacings were used in  $x$ -direction which was restricted by the stability constraint. The grid spacings in the  $r$ -direction were chosen to be uniform, dividing the discharge radius  $r_0$  into 30 equal divisions to attain convergence of the solution. The calculation with uniform grid spacings ( $\Delta x/\Delta r < 0.5$ ) in both directions also attains convergence but consumes more computer time.

Von-Neuman's method of stability analysis [79] was found to be ineffective with the finite difference equation of the turbulent kinetic energy. For calculating turbulence in addition to mean flow properties from the continuity, momentum and turbulent energy equations, small uniform grid spacings in both directions were used with  $\Delta x/\Delta r < 0.5$  which satisfies the stability constraint generated with the momentum equation. All calculations reported here for turbulence use  $\Delta x/\Delta r = 0.5$  dividing the discharge radius  $r_0$  into 50 equal divisions to attain convergence of the solution in the initial region. Convergence was not obtained in the transition region, and hence, no turbulence predictions are presented for the region.

The Dufort-Frankel technique requires information from two previous stations for the calculations to proceed in the streamwise direction. The associated boundary conditions give information at one station and information for the second station is calculated by a simple finite difference technique that requires only the previous step values. Switching of the calculations from the initial to the transition region takes place when the centre line velocity in the initial region decreases by 1%.

The finite difference equations for the continuity, momentum and turbulent kinetic energy are shown in Appendix D for both the Dufort-Frankel scheme and the simple finite-difference scheme.

Any calculation reported here did not require more than 1.5 minutes of computation time on IBM 370 computer.

### 3.5 Integral Method

The integral method is an alternative to the differential method for solving a set of differential equations by assuming an empirical mean velocity profile. Mass, momentum and energy are conserved over an integrated finite length to develop the governing equations. This is an approximate method, preferable for ease of calculation.

It was possible to establish an empirical self-preserving velocity profile for the initial region of a jet having a thin boundary layer at the nozzle exit. This velocity profile was used in the integral equations to determine jet geometry.

#### 3.5.1 Integral Equations

The integral momentum and energy equations for the mean flow are derived in Appendix A. The momentum integral equation is:

$$\frac{\partial}{\partial x} \int_0^{\infty} u^2 r \, dr = 0 \quad (3.21)$$

The energy integral equation is:

$$\frac{1}{2} \frac{\partial}{\partial x} \int_0^{\infty} u^3 r \, dr = - \int_0^{\infty} v_t r \left( \frac{\partial u}{\partial r} \right)^2 \, dr \quad (3.22)$$

The eddy diffusivity,  $v_t$  is given by Equation (3.5).

#### 3.5.2 Empirical Mean Velocity Profile

Using the present mean velocity measurements for the initial region, which will be presented in Chapter V, in a third order polynomial for the main portion of the mixing layer and superimposing Townsend's [7] hyperbolic

tangent velocity profile at the outer layer side, the following velocity profile was established:

$$\left. \begin{aligned} \frac{u}{u_c} &= 1.0 ; & \eta < -0.736 \\ \frac{u}{u_c} &= 0.5 - \eta + 0.05\eta^2 + 0.66\eta^3 ; & -0.736 < \eta < 0.5 \\ \frac{u}{u_c} &= A [1 - \tanh B(\eta - 0.5)] ; & \eta < 0.5 \end{aligned} \right\} (3.23)$$

where  $\eta = (r - r_{\frac{1}{2}})/b$ .

The constants  $A = 0.095$  and  $B = 4.79$  were determined by using continuity of velocity and matching the slope of the velocity profile at  $\eta = 0.5$ . This composite velocity profile behaves asymptotically at the outer part of the jet with RMS deviation of  $(\Delta u/u_c)_{\text{RMS}} = 0.0112$ .

### 3.5.3 Jet Boundaries

Equation (3.23) shows that the inner radius,  $r_1$  corresponds to  $\eta = -0.736$  where  $u/u_c = 1.0$ , and the outer radius is defined here as corresponding to  $\eta = 0.8$  where  $u/u_c = 0.01$ . So, the inner and outer radii of the jet in terms of  $r_{\frac{1}{2}}$  and  $b$  are:

$$r_1 = r_{\frac{1}{2}} - 0.736b \quad (3.24)$$

$$r_2 = r_{\frac{1}{2}} + 0.8b \quad (3.25)$$

The width of the shear layer  $b_1$  can be obtained by subtracting  $r_1$  from  $r_2$ :

$$b_1 = 1.536b \quad (3.26)$$

Introducing Equation (3.5) into Equation (3.22), transforming variable  $r$  to  $\eta$ , and using empirical velocity Equation (3.23) in the fundamental integral equations (3.21) and (3.22), and integrating, the following two ordinary differential equations are obtained (details are shown in Appendix B):

$$\frac{\partial}{\partial x} \left[ \frac{r_1^2}{2} + 0.547578 r_{1/2} b - 0.215408 b^2 \right] = 0 \quad (3.27)$$

$$\begin{aligned} \frac{1}{2} \frac{\partial}{\partial x} \left[ \frac{r_1^2}{2} + 0.45101941 r_{1/2} b - 0.20326464 b^2 \right] \\ = \frac{L^2}{b^2} \left[ -0.65829521 r_{1/2} + 0.01311954 b \right] \end{aligned} \quad (3.28)$$

For thin boundary layer at the nozzle exit, these equations are subject to the approximate boundary conditions:

$$\text{at } x = 0, \quad b = 0, \quad r_1 = r_0$$

Physically, these boundary conditions mean that the potential core fills the nozzle and there is no boundary layer at the nozzle exit. Integrating Equation (3.27) with the boundary conditions at  $x = 0$ , and using Equation (3.24), the following relation is obtained:

$$\frac{r_{1/2}}{r_0} = 0.18842198 b/r_0 + \sqrt{1.0 - 0.075377 (b/r_0)^2} \quad (3.29)$$

Equation (3.27) and Equation (3.29) are used in Equation (3.28) to obtain:



$$\begin{aligned}
\frac{d(b/r_0)}{d(x/r_0)} &= 2(L/b)^2 \left[ 0.658296 - 0.049620(b/r_0)^2 \right. \\
&\quad \left. + 0.1109177 b/r_0 \sqrt{1 - 0.075377(b/r_0)^2} \right] / \\
&\quad \left[ 0.0965586 - 0.0145566(b/r_0)^2 \right. \\
&\quad \left. + 0.01210 b/r_0 \sqrt{1 - 0.075377(b/r_0)^2} \right] \quad (3.30)
\end{aligned}$$

The ratio  $L/b$  was determined experimentally by measuring the shear stresses and velocity gradients, and using the following relation:

$$\overline{u'v'} = L^2 \left| \frac{\partial u}{\partial r} \right| \frac{\partial u}{\partial r} \quad (3.31)$$

Transforming the variable  $r$  into  $\eta$ , Equation (3.31) is written as:

$$(L/b)^2 = \frac{\overline{u'v'}}{\left| \frac{du}{d\eta} \right| \frac{\partial u}{\partial \eta}} \quad (3.32)$$

The experimental values of  $L/b$  presented in Chapter V, lie within the range 0.099 to 0.109 with an average,  $L/b=0.10625$  given by Equation (3.20). Using Equation (3.20); Equation (3.30) can be integrated numerically with the starting conditions at  $x = 0$ , to obtain  $b$ , and hence,  $r_1$ ,  $r_2$  and  $b_1$  from Equations (3.24), (3.25) and (3.26) respectively, as functions of  $x$ .

## CHAPTER IV

### EXPERIMENTS AND UNCERTAINTIES

#### 4.1 General

Of many experimental investigations on jet flows that have been published, only a very few have identified the nozzle exit conditions.

The aim of the present investigation was to provide information on turbulence and mean flow quantities in the initial and transition regions of jets with varying flow conditions at the nozzle exit. Of the many flow quantities, only the boundary layer thickness and the turbulent intensity were considered as identifying the exit conditions. In all the experiments, the boundary layers were turbulent at the nozzle exit, being considered turbulent when the following two conditions were satisfied simultaneously:

i) the exit fluctuation intensity profile showed characteristic peak intensity near the wall with  $\sqrt{u'^2}/u_c$  near 10%, a value typical of turbulent boundary layers.

ii) the shape factor was close to 1.40.

The shape factor,  $H_0$ , is defined as the ratio of the displacement thickness to the momentum thickness of the mean velocity profile.

#### 4.2 Experimental Facilities

Axisymmetric turbulent jets were produced by discharging air through a series of circular nozzles from a large settling chamber as shown in the schematic diagram

of the experimental set-up and nozzles in Figure 4.1.

Air from the compressed air facility in the laboratory was passed through a 3-micron filter, pressure regulator and needle valve before entering the large settling chamber which contained a set of flow straighteners followed by 3 screens. Figure 4.1a shows a short circular nozzle fitted to the large settling chamber. The displacement thickness near the outlet of this nozzle ( $x = -1.0$  mm) was  $\delta_o^*/r_o = 0.0064$ , for  $R_{eD} = 1.53 \times 10^5$ . The jet exit conditions were changed by using nozzles with extensions shown in Figures 4.1b and 4.1c and tripping the boundary layer by projections of 0.397 mm and 1.59 mm. The displacement thicknesses for these cases were  $\delta_o^*/r_o = 0.0179$  and  $\delta_o^*/r_o = 0.0628$  respectively, for  $R_{eD} = 1.53 \times 10^5$ . The turbulent intensity profiles at the exit were different for each case. Each jet contained a core of uniform velocity at the exit, which was found to be axisymmetric from measurements of the axial mean velocity and turbulent intensity at  $x/r_o = 1.0$  in both the vertical and the horizontal central planes, as shown in Figures 5.1, 5.2, 5.3. The mean velocity profile within the nozzle was also found to be symmetric about its axis.

Turbulence and mean flow quantities were measured by using a DISA constant temperature hot-wire anemometer (type 55M10) with a linearizer (type 55D10), signal conditioner (type 55D31). A DISA miniature probe (55P11) with a 5 $\mu$  tungsten normal wire was used for the mean axial velocity and the axial turbulent intensity. The shear stress and

the turbulent intensities in  $r$ - and  $\theta$ -directions were measured using the same normal wire and a single  $5\mu$  tungsten slanting wire with a DISA miniature probe (55P12).

#### 4.3 Hot-Wire Calibration

Calibration of the hot wires was performed by making simultaneous measurements of the voltage with the hot wire connected to the anemometer, and the velocity with a pitot tube connected to a Lambrecht inclined tube manometer. The hot wire and the pitot tube were set up side-by-side in the uniform velocity of the potential core and the velocity was varied in steps over a range of values 2.5 m/s to 100 m/s. The inclined tube manometer was calibrated against a Meriam Micromanometer having a precision of 0.0254 mm; the results are shown in Figure C.3 of Appendix C. The hot-wire equations and the typical calibration curves for both normal and slanting wires without linearizer are shown in Figures C.4 and C.5 of Appendix C. Figure C.6 of Appendix C is a typical calibration curve of the hot wires with linearizer for high velocities (above 6 m/s), and Figure C.7 shows its calibration for low velocities (below 6 m/s). The low velocity calibration was performed as outlined in Ref. [80]. The calibration constants were determined by simple curve fitting principles [86] and their values are given in Appendix C.

The calibration curve was checked at the beginning and end of each series of transverses. If the curve had changed then the whole series of transverses were repeated.

The hot-wire was traversed in the radial and axial directions by a motor operated traversing mechanism with a scale having precision of 0.0254 mm.

#### 4.4 Measurements

All measurements were performed for a Reynolds number,  $R_{eD} = 1.53 \times 10^5$  based on the exit diameter and the average velocity. The main air supply was adjusted until the required value of the nozzle exit velocity, as measured by pitot tube, was obtained.

The velocity profile, about 1 mm inside the exit was measured by using a normal hot wire and recording the anemometer output voltage. The hot wire was traversed over a scale with precision 0.0254 mm, and a large number of readings were taken where the velocity began to deviate from the centre line velocity. At each station, at least five readings were taken within a time interval of 2 minutes. For higher fluctuating values, ten observations were taken at a station. The mean velocity and axial turbulence were calculated by using Equations (C.17) and (C.20) of Appendix C.

For the axial mean velocity and the turbulent intensity within the jet, a normal hot wire was positioned on the centre line of the nozzle, and the output from the linearizer was recorded. The hot wire was traversed vertically through the jet, with a large number of readings being taken where the velocity began to deviate from the jet centre line velocity. Within the turbulent shear layer

which corresponded to high fluctuating values, ten observations were noted for a station within a time interval of 2 minutes. After the upper half of the jet had been completely traversed, the hot wire was returned to jet centre line. The linearizer output was compared with the value obtained at this location before traversing upwards through the jet; this provided a check on whether the linearizer output had drifted or the main flow rate had varied. If the two values were the same, then the hot wire was traversed vertically through the lower portion of the jet, and its axisymmetry was checked. This procedure was followed at the downstream locations:

$$x/r_0 = 2, 4, 6, 8, 10, 12, 15 \text{ and } 18$$

Traversing and taking readings, similar to those described above were followed to measure the shear stress and radial turbulent intensity using the same normal wire and a slanting wire. The mean velocity and turbulence were calculated by using the calibration constants and Equations (C.17) and (C.20) derived in Appendix C.

#### 4.5 Uncertainty Statement

The variation of the slopes of any calibration curve was found to lie within  $\pm 1\%$  for at least 4 calibrations. The angle of inclination of the slanting wire was measured by positioning the probe in a slide projector and projecting the wire image on a paper screen. To minimize image distortion, the wire was located near the centre of the lens and the screen was positioned perpendicular to the projector. Twenty values of the angle of the slanting

wire fell within the range  $45^{\circ} \pm 36'$ .

The uncertainty of the measurements of mean velocity, turbulent intensity and shear stress are influenced by variations of the ambient temperature, characteristics of the linearized circuit, contamination of the hot wires, the accuracy of the angle of inclination of the hot wire to the mean flow direction and the accuracy of the calibration equipment. All uncertainties presented here were calculated by using the standard procedure given in Ref. [81,82]. In the calibration unit, the uncertainty of mean velocity,  $u/u_c$  was estimated to be less than  $\pm 0.3\%$ \*. The mean velocities which were obtained by using a linearized circuit showed uncertainty of  $\pm 1.5\%$  in the main portion of shear layer and  $\pm 4\%$  in the outer layer where velocity is near 6 m/s. The uncertainty of  $\sqrt{u'^2}/u_c$  was found to be less than  $\pm 5.5\%$  for the major portion of the shear layer where the mean velocity is greater than 6 m/s. The uncertainty of the shear stress was estimated to be less than  $\pm 4.5\%$  neglecting the wire angle uncertainty which could cause an additional  $\pm 3\%$  bringing total uncertainty less than  $\pm 7.5\%$  for the major portion of the shear layer where the mean velocity is greater than 6 m/s. The uncertainties of  $\sqrt{u'^2}/u_c$  and  $\sqrt{w'^2}/u_c$  for the major portion of shear layer are less than  $\pm 7\%$ . These values are exceeded at the outer layer side where mean velocities are low. All uncertainties reported here exclude the error in the hot-wire equations by assuming

---

\* All uncertainties and repeatabilities were calculated assuming 20:1 odds.

weak turbulence. Estimated from Ref. [22], this could cause additional uncertainty in the shear and intensity values of 15% in the main portion of the shear layer and  $\pm 8\%$  near the outer boundary.

The repeatability of the mean velocity, turbulent intensities and shear stresses were tested by taking 300 readings at each of 18 locations in the mixing layer at planes normal to the axis of the jet and at distances  $x/r_0 = 4, 6, 8, 12$  and 18 from the nozzle exit. Repeatability of the measurements was estimated to be  $\pm 5\%$ .

The uncertainty in measuring the linear distance was negligible. Temperature variation during the experiments was within  $0.3^\circ\text{C}$ .



CHAPTER V  
RESULTS AND DISCUSSION

5.1 General

Properties of the flow in the initial and transition regions of jets were determined both theoretically and experimentally. Three different nozzles were used to produce jets with three different exit conditions. For all three cases, the momentum and continuity equations were solved by a finite difference method for the mean flow quantities. In addition, a simple integral method was applied to the initial region to determine the jet properties for the first case, the very thin exit boundary layer. Turbulent quantities in the initial region were calculated by solving one differential transport equation for the turbulent kinetic energy in conjunction with the momentum and continuity equations. All calculations for the initial region use an empirical equation for turbulent length scale.

This chapter presents comparisons of experimental and theoretical results of the mean and turbulent motions in the developing region of the jets.

5.2 Nozzle Exit Conditions

The present limited measurements of mean velocity within the boundary layer shown in Figure 5.1 give the displacement thickness  $\delta_o^*/r_o = 0.0064$  at the nozzle exit,  $x/r_o = -0.08$ , the boundary layer was assumed turbulent.

The measured velocity distribution, as shown in Figure 5.1 fits to the following velocity profile inside the boundary layer:

$$\text{thin boundary layer: } u/u_c = \left[ \frac{r_o - r}{\delta_o} \right]^{1/6.66} \quad \text{for } \delta_o^*/r_o = 0.0064$$

The shape factor and the Reynolds number based on the displacement thickness at the exit were calculated to be  $H_o = 1.31$  and  $R_{e\delta}^* = 503$  for thin boundary layer. Similar measurements at the nozzle exit were performed for the two other nozzles having intermediate and thick boundary layers of displacement thicknesses  $\delta_o^*/r_o = 0.0179$  and  $0.0628$ , respectively. The velocity distributions for these two cases are shown in Figures 5.2 and 5.3, and they fit the following boundary layer velocity profiles:

intermediate boundary layer:

$$u/u_c = \left[ \frac{r_o - r}{\delta_o} \right]^{1/5.38} \quad \text{for } \delta_o^*/r_o = 0.0179$$

thick boundary layer:

$$u/u_c = \left[ \frac{r_o - r}{\delta_o} \right]^{1/5.29} \quad \text{for } \delta_o^*/r_o = 0.0628$$

The shape factors and the Reynolds numbers based on the displacement thicknesses at the nozzle exits were calculated to be  $H_o = 1.372$ ,  $R_{e\delta}^* = 1387$  for intermediate boundary layer and  $H_o = 1.378$ ,  $R_{e\delta}^* = 4824$  for thick boundary layer. In all the three cases, the distributions of turbulent intensity showed peaks close to the wall with values of  $\sqrt{u'^2}/u_c$  close to 10%, typical of turbulent boundary layers.

The velocity distributions in Figures 5.1, 5.2 and 5.3 were used to start the finite difference calculations with the momentum and continuity equations for mean flow properties.

The turbulence in the jet core was not controlled, but did not vary widely for the three nozzles; the intensity of turbulence in the core was near 5% which is high when compared to that existing near shear layers investigated in low turbulence wind tunnels.

### 5.3 Mean Motion in the Initial Region

#### 5.3.1 Thin Exit Boundary Layer

Figure 5.4 shows that the measurements of the axial mean velocity in the initial region has an approximate self-preserving distribution when plotted against the similarity variable,  $\eta = (r - r_x)/b$ . It is also shown that the empirical velocity profile as expressed by the composite Equation (3.23) is in good agreement with the measurements. The empirical velocity profile given by Equation (3.23) was obtained by curve fitting based on least squares. The overall RMS deviation of the combined experimental data at sections,  $x/r_0 = 2, 4, 6$  and 8 from the empirical velocity profile was calculated to be  $(\Delta u/u_c)_{RMS} = 0.0112$ . The axial mean velocity obtained from the finite difference solution is approximately self-preserving in the  $u/u_c$  vs.  $\eta$  plane. The results of the finite difference solutions at sections,  $x/r_0 = 2$  and 8 are plotted in Figure 5.4 to show a comparison with the empirical model. The RMS deviation of the empirical model and the finite difference solution from the experimental data are shown in Table 5.1. The similarity variable,  $\eta$  was chosen to force agreement with experimental

measurements and self-preservation in the central region of the mixing layer. It is not surprising that the slight disagreement of the measurements with the model shows up in the outer and inner parts of the mixing layer, and the major part of the RMS deviation shown in Table 5.1 comes from the outer part of the mixing layer. The comparison shows that Equation (3.23) describes the axial mean velocity in the initial region with deviation from the experimental values of not more than  $\pm 1.5\%$ . It is interesting to note that the conventional similarity variable  $(r - r_0)/x$  does not produce satisfactory self-preservation of the axial mean velocity in the present experimental measurements or in those of Bradshaw et al [10] and Sami et al [24].

The axial mean velocity calculated by finite difference technique is plotted against the radial distance  $r/r_0$  in Figure 5.5 for comparison with the measurements of Bradshaw et al [10], Sami et al [24] and the present measurements. Satisfactory agreement is shown. Simpson's integration rule [84] is used to calculate the scale  $b/r_0$  from the first order differential Equation (3.30) with starting condition at  $x = 0$ . The scale,  $b/r_0$ , may be considered as a measure of the width of the shear layer. These results together with measurements and those obtained from the finite difference solution are shown in Figure 5.6. The root mean square deviation of the result of Equation (3.30) from those of the finite difference solution was calculated using values of 100 points of equally spaced intervals in the axial direction. Similarly

TABLE 5.1: A Comparison of  $\bar{u}$  Mean Velocity RMS Deviations

Axial Distance $x/r_0$	Finite Difference Solution ( $\Delta \bar{u}/u_c$ ) RMS			Empirical Solution ( $\Delta u/u_c$ ) RMS
	Thin	Intermediate	Thick	
2	0.0067	0.0088	0.0110	0.0154
4	0.0119	0.0103	0.0128	0.0137
6	0.0150	0.0131	0.0166	0.0101
8	0.0180	0.0210	0.0229	0.0098

the RMS deviation of the radial distance,  $r_{1/2}$ , for the half velocity,  $u/u_c = 0.5$  was also calculated. The resulting values are:

$$(\Delta b/r_o)_{\text{RMS}} = 0.001285 \text{ and } (\Delta r_{1/2}/r_o)_{\text{RMS}} = 0.000953$$

Figure 5.6 shows that the scale,  $b$ , is only approximately a linear function of  $x$ . The nonlinearity of the scale,  $b$ , would generate the width of the shear layer,  $b_1$ , and the Prandtl's mixing length,  $L$ , as nonlinear functions of  $x$ . The linear approximation of Prandtl's mixing length given by Rotta [8] has also been compared with the present results and measurements in Figure 5.6. The non-self-preservation of the mean axial velocity, and hence, the nonlinearity of  $b$  arises when using the variable,  $\eta = (r - r_o)/x$  as already noted.

The radii  $r_{1/2}$ ,  $r_1$  and  $r_2$  for  $u/u_c = 0.5$ ,  $u/u_c = 0.99$  and  $u/u_c = 0.01$  respectively were calculated by using Equations (3.29), (3.24) and (3.25), and plotted in Figure 5.7 to show a comparison with the measurement and the results of the finite difference solution. The iso-velocity lines  $u/u_c = 0.99$  and  $u/u_c = 0.5$  obtained from the results of the finite difference solution are in good agreement with the measurement and the deviation from that of the integral method is insignificant for the major part of the shear layer. The deviation that is observed in the outer and inner boundaries shown in Figure 5.7 may be expressed in terms of the RMS difference which was calculated by choosing 100 points at equally spaced intervals in the axial

direction and found to be  $(\Delta r_2/r_0)_{\text{RMS}} = 0.0193$  for the outer boundary and  $(\Delta r_1/r_0)_{\text{RMS}} = 0.00215$  for the inner boundary. Here it is to be noted that the jet boundaries are not quite linear with the axial distance,  $x$ . Laurence's [31] approximation of outer boundary is also drawn in Figure 5.7 to show a comparison with the present outer boundary for  $u/u_c = 0.01$ . The major contribution to uncertainty in the velocity measurement occurred in the outer boundary. If one wishes to compare theoretical results with experimental values, it is preferable not to formulate in terms of the outer radius and the width of the mixing layer as Abramovich [27] and others have done. Hatta and Nazaki [23] approximated  $r_1$  and  $r_2$  to be linear functions of  $x$ , and developed a self-preserving model of axial mean velocity in terms of  $r_1$  and  $r_2$  which predicts constant axial mean velocity at  $r/r_0 = 1.0$  for any axial distance in this region. Figure 5.8 shows the shortcoming of Hatta and Nazaki's [23] model and the agreement of present calculations and measurements with the experimental measurements of Bradshaw et al [10] and Von Frank [25].

Using the empirical model of the axial mean velocity in the mass conservation equation and integrating by Simpson's rule [34], the radial mean velocity was calculated. The RMS deviation of these results from the results obtained by the finite difference technique was calculated by using 100 points at equally spaced intervals in the radial direction at sections,  $x/r_0 = 4, 6$  and  $8$ ; its value was found to

be  $(\Delta u/u_c)_{RMS} = 0.0196$ . A comparison of the present calculations and the measurements of Sami et al, [24] for the radial mean velocity is presented in Figure 5.9 with the results of the finite difference method and shows good agreement.

The length of the initial region calculated by the finite difference method was close to  $x/r_o = 9.0$ , which agrees with the prediction of Madni and Pletcher [26]. It was calculated here to be  $x/r_o = 8.8$  by the integral method. Albertson et al [18] measured its value to be less than 10.0 and Davies et al [30] found it to be 9.0.

The experimental measurements of the turbulent shear stresses, presented in Figures 5.22 to 5.25 were used to calculate the  $L/b$  ratio from Equation (3.32) for axial distances  $x/r_o = 2, 4, 6, 8$  and their variations with the radial direction are shown in Figure 5.10. It may be observed that the ratio  $L/b$  lies in the range of 0.099 to 0.109 for the initial region of the jet. The calculations used  $L/b = 0.10625$  as an average of all observations obtained for  $x/r_o = 2, 4, 6$  and 8.

### 5.3.2 Intermediate and Thick Exit Boundary Layers

The mean velocities obtained by experimental measurements and by finite difference calculations are shown in Figures 5.11 and 5.12 in the plane  $u/u_c$  vs.  $\eta$  for the intermediate ( $\delta_o^*/r_o = 0.0179$ ) and the thick ( $\delta_o^*/r_o = 0.0628$ ) boundary layer velocity profiles at the nozzle exits. Figure 5.11, for the intermediate boundary layer, shows that the



mean axial velocity profiles are approximately self-preserving in the initial region starting from  $x/r_0 = 2.5$  with an RMS deviation less than 2% from the measured values at  $x/r_0 = 2.5, 4, 6$  and  $8$ . In comparison, Figure 5.4, for the thin exit boundary layer, shows satisfactory self-preservation starting from  $x/r_0 = 2$  with an RMS deviation of 1.12% from the measured values at  $x/r_0 = 2, 4, 6$  and  $8$ . The mean velocity profiles for the thick exit boundary layer, in Figure 5.12, also show an approach to self-preservation to the initial region at an increased distance downstream,  $x/r_0 = 3.5$  and the RMS deviation of the results of finite difference solution from the measured values at  $x/r_0 = 3.5, 4, 6$  and  $8$  was found to be less than 1.5%.

Mean velocities obtained by the finite difference method are plotted in Figure 5.13, for  $\delta_0^*/r_0 = 0.0179$  and in Figure 5.14, for  $\delta_0^*/r_0 = 0.0628$  and show that the radial distribution of  $u/u_c$  and the present measurements are in satisfactory agreement. The RMS deviation of the calculated and experimental results at sections,  $x/r_0 = 2, 4, 6$  and  $8$  are given in Table 5.1 for the intermediate and thick boundary layers.

Iso-velocity lines  $u/u_c = 0.01$ ,  $u/u_c = 0.5$  and  $u/u_c = 0.99$  obtained by the finite difference solution are plotted in Figure 5.15, and satisfactory agreement is shown with the experimental measurements for  $u/u_c = 0.5$  and  $0.99$ . The experimental values on line,  $u/u_c = 0.99$  where intermittency occurs, were approximated by taking several readings near the inner boundary of the shear layer. Figure

5.15 also shows that the radial distances  $r_2$  and  $r_{1/2}$ , for  $u/u_c = 0.01$  and  $u/u_c = 0.5$  respectively, decrease with the increase of the exit boundary layer thickness. The value of the potential core radius,  $r_1$ , decreases with the increase of the thickness of the exit boundary layer at the beginning of the shear layer growth and becomes independent of the exit boundary layer thickness after some axial distance,  $x/r_0$ . For the intermediate boundary layer, the radius of the potential core,  $r_1$ , becomes equal to that of the thin exit boundary layer at  $x/r_0 = 4.5$ , and for the thick boundary layer ( $\delta_0^*/r_0 = 0.0628$ ) at  $x/r_0 = 6$ . It may be observed from Figure 5.15 that the jet boundaries are not exactly linear for any exit conditions and the results of the integral method for the thin exit boundary layer shown in Figure 5.7 also agree with this finding.

The scale,  $b$ , for the jets with the intermediate and thick exit boundary layers are plotted in Figure 5.6 and compared with the experimental results. Figure 5.6 shows that the scale,  $b$ , is nonlinear in  $x$  and its value is higher than that of the thin exit boundary layer at the beginning of the shear layer and becomes smaller after some axial distance,  $x/r_0$ .

The values of  $L/b$  for the jet with the intermediate boundary layer ( $\delta_0^*/r_0 = 0.0179$ ) were calculated by using shear stresses given in Figure 5.33. All the calculated values of  $L/b$  at sections  $x/r_0 = 2, 4, 6$  and  $8$  fall within the range  $0.099$  to  $0.109$  which is the same as shown in Figure

5.10 for the thin boundary layer. Though the values for  $L/b$  lie within the same range, the average of all calculated values in this case is found to be 0.1076 which is slightly higher than the value, 0.10625 for the case given in Figure 5.10. The finite difference calculation for this case was performed with  $L/b = 0.10625$ .

The experimental values of shear stresses are shown in Figure 5.34, for the jet with thick boundary layer ( $\delta_o^*/r_o = 0.0628$ ). These experimental values were used to calculate the ratio,  $L/b$  at sections  $x/r_o = 2, 4, 6$  and  $8$ , and all the calculated values lie between 0.102 and 0.12, having an average value of 0.1135, as shown in Figure 5.16. This value differs significantly from those obtained in the cases of thin and intermediate boundary layers with the displacement thicknesses,  $\delta_o^*/r_o = 0.0064$  and  $0.0179$  respectively. The finite difference calculation for this jet was performed by using  $L/b = 0.1135$ .

#### 5.4 Mean Motion in the Transition Region

The jet flow is approximately self-preserving in the initial region, but does not remain self-preserving in the transition region which starts from the end of potential core. This is probably due to the interaction of the shear layers along the centre line of the jet. The experimental values of the mean velocities at sections,  $x/r_o = 10, 12, 15$  and  $18$  are plotted in Figure 5.17 in the  $u/u_c$  vs.  $\eta$  plane. The flow maintains its self-preservation in the central part of the shear layer as required by the scales chosen, but becomes non-self-preserving near the centre line and

the outer boundary of the jet. The results of finite difference calculations at sections,  $x/r_0 = 10$  and  $18$  are also presented in Figure 5.17 and show agreement with the experimental values.

The flow develops towards a new mean velocity profile and again becomes self-preserving in the developed region far downstream according to the findings in Figures 5.4, 5.17 and 5.18. The length of the transition region was determined by measuring the mean velocity at different axial distances until the experimental values fitted the velocity profile given by Tollmien [14] for the developed region. The experimental values of the mean axial velocities of various workers at axial distances,  $x/r_0 = 18, 24, 32, 40, 64, 80$  and  $100$  are compared with Tollmien's [14] and Schlichting's [15] velocity profiles in Figure 5.18. It is observed from Figure 5.18 that the mean axial velocity achieves approximate self-preservation at  $x/r_0 = 24$  which may be considered to be the beginning of the developed region. Therefore, the transition region extends from  $x/r_0 = 9$  to  $x/r_0 = 24$  as determined from the mean axial velocity. The turbulent quantities may not achieve self-preservation at  $x/r_0 = 24$ .

The experimental results of shear stress are plotted in Figure 5.41 for the transition region. These experimental values were used to calculate the ratio of Prandtl's length scale,  $L$ , and the length scale,  $b$ , for the transition region. The ratio,  $L/b$ , is plotted against the variable,  $\eta = (r-r_x)/b$  in Figure 5.19 and shows that the values

of  $L/b$  do not lie within as narrow a range as that shown in Figure 5.10 for the initial region. Therefore, the ratio,  $L/b$ , cannot be treated as a constant for the transition region, but must be considered as a function of the axial and the radial distances, and can no longer be expressed by a simple algebraic relation. Rotta [8] determined the length scale of turbulence by solving a differential transport equation for the developed region and he found it to be self-preserving as shown in Figure 5.19. Rotta's [8] calculation agrees with experimental observations that the length scale of turbulence is a function of both axial and radial distances in the developed region, though Townsend [7] and others used it as a function of  $x$  only which gives,  $L/b = \text{constant}$ , as in Figure 5.19.

The present finite-difference method replaces the turbulent diffusivity,  $\nu_t$ , by combining the turbulent diffusivity models of Madni-Pletcher [26] and Schetz [21], given by Equations (3.6) and (3.7). This approach is not based on any valid physical grounds, but only on empirical agreement. The calculated results of the mean velocity obtained by using the Madni-Pletcher's [26] model of turbulent diffusivity gives values less than the experimental values near the outer boundary. The RMS deviation of these results from the experimental values at sections,  $x/r_0 = 10, 12, 15$  and  $18$  was calculated to be about 12%. The application of Schetz's [21] model of turbulent diffusivity to the momentum equation and the finite difference calculation predicted

the mean axial velocity to be higher than that of the experimental values near the outer boundary with RMS deviation at  $x/r_0 = 10, 12, 15$  and  $18$  to be about 9%. The present calculation used Madni-Pletcher's [26] model of turbulent diffusivity from the centre line to the half-radius line and continued by using constant turbulent diffusivity until it became equal to that of Schetz's [21] model and then followed the latter. Both Madni-Pletcher's model and Schetz's model together with the present combination are presented in Figure 5.20. The present results of the mean velocity are plotted in Figure 5.21 and show satisfactory agreement with experimental measurements. The RMS deviation between the experimental and calculated results at sections,  $x/r_0 = 10, 12, 15$  and  $18$  was calculated to be about 2%.

## 5.5 Turbulent Motion in the Initial Region

### 5.5.1 Thin Exit Boundary Layer

The momentum equation, the continuity equation and the differential transport equation for the turbulent kinetic energy were solved for turbulent kinetic energy by the finite difference method. The length scale and the Reynolds shear stress were expressed by Equations (3.20) and (3.31). The measured velocity and turbulent kinetic energy distributions for the thin boundary layer at the nozzle exit, in Figure 5.1 was used to start the finite difference solution from  $x/r_0 = 0$ .

The shear stresses obtained from Prandtl's mixing length model, Equation (3.31), are in good agreement with the measurements of Bradshaw et al [10], Sami et al [24] and the

present measurements for  $x/r_0 = 2, 4$  and  $6$  as shown in Figures 5.22, 5.23 and 5.24, respectively. In Figure 5.25, the model for  $x/r_0 = 8$  shows somewhat less agreement than the agreement shown for  $x/r_0 = 2, 4$  and  $6$ .

Although the Prandtl's mixing length model adequately represents the turbulent shear stress in the initial region of the jet, it is interesting to examine an energy model for the shear stress given by Equation (3.14), based on the assumption that the ratio of the turbulent shear stress and the kinetic energy in the flow remains constant, i.e.,

$$\frac{-\overline{u'u'}}{k} = c_1 \quad (3.14)$$

This energy model has been used for boundary layers by Bradshaw et al [53] and for the developed region of jets by Harsha and Lee [60]. In the latter flow, the value of  $c_1$  was reported to be 0.3.

The present measurements in Figure 5.26 show that  $-\overline{u'u'}/k$  remains constant at a value near 0.375 in the central portion of the mixing layer, but decreases near both boundaries. The shear stresses, based on the energy model,  $-\overline{u'u'}/k = 0.375$ , are shown in Figures 5.22, 5.23, 5.24 and 5.25. As expected, agreement with measurements are good in the central region of the mixing layer with less agreement near the boundaries. It may be noted in passing that the energy model may be improved by using the form  $\overline{u'u'}/k = 0.375\gamma$ , where  $\gamma$  is an intermittency factor. However, this introduces another empirical quantity into the model which is a disadvantage when compared with Prandtl's mixing length

model.

The empirical model of shear stress used by Launder and Spalding [9] and Rotta [8] has already been mentioned in Chapter III and it is rewritten here in the form:

$$-\overline{u'v'} = c_{\mu} \frac{k^2}{\epsilon} \frac{\partial u}{\partial r} \quad (3.15)$$

where  $k$  is the turbulent kinetic energy, and  $L^1$  is a length scale which is the dependent variable in an empirical differential transport equation.  $\epsilon$  is the rate of dissipation of turbulent energy. The two equations,  $k$ - $\epsilon$ , transport model of Launder and Spalding [8] was solved by using the above empirical model of shear stress and satisfactory results were found by them for the developed region of jets and also for other turbulent flows. Figures 5.22, 5.23, 5.24 and 5.25 show this model is in reasonable agreement with measurements when  $k$  and  $\epsilon$  are obtained from a single transport Equation (3.13) for the turbulent kinetic energy and an algebraic Equation (3.11) for the dissipation of energy together with the length scale Equation (3.20). The value of the constant  $c_{\mu}$  is 0.09 as proposed by Launder and Spalding [9]. The empirical constants  $a_1=1.09$ ,  $c_r=0.211$ , and  $k_q=0.86$  which were used in Equation (3.13) were obtained from the experimental values of Sami [85]. This will be discussed later.

The calculated values of turbulent kinetic energy are plotted in Figure 5.27 and show satisfactory agreement with measurements. The experimental values of  $\overline{u'^2}/2k$  and  $\overline{v'^2}/2k$  are plotted in Figure 5.26 and show that these ratios remain approximately constant throughout the shear layer. The values of  $\overline{u'^2}/2k$  lie between 0.42 and 0.45 and those of  $\overline{v'^2}/2k$  between 0.27 and 0.30. Values of  $\overline{w'^2}/2k$  were very



close to those of  $\overline{u'^2}/2k$  and are not shown. The ratios of the normal stresses to the turbulent kinetic energy were estimated experimentally by taking 300 readings at each of the nine stations at distances  $x/r_0 = 4, 6$  and  $8$ . By drawing frequency distributions and using 20:1 odds, the ratios are selected to be:

$$\begin{aligned} \overline{u'^2}/2k &= 0.44 \\ \overline{v'^2}/2k &= 0.29 \end{aligned} \quad (5.1)$$

These ratios together with the calculated values of the kinetic energy were used to determine turbulent intensities. Figures 5.28 and 5.29 show comparisons of the calculated intensities with the measurements of Sami et al [24], Bradshaw et al [10], Laurence [31] and the present measurements. These show reasonable agreement between the calculated intensities and the measurements.

Rotta [8] estimated the constants  $a_1$ ,  $c_r$  and  $k_q$  in Table 5.2, associated with turbulent energy Equation (3.13) and obtained good agreement with the measurements of Wygnanski and Fiedler [4] for the developed region of jets.

TABLE 5.2 Constant of Energy Transport Equation

	$a_1$	$c_r$	$k_q$	$c_1$
Rotta [8]	1.0	0.165	0.60	---
Present	1.09	0.211	0.86	0.375

The calculated values using these constants do not show satisfactory agreement with measured diffusion energy, transport energy, etc. of Sami [85] for the initial region. To achieve satisfactory agreement with Sami's measurements, the constants  $a_1$ ,  $c_r$  and  $k_q$  are adjusted to the values shown in Table 5.2. This agreement is shown in Figures 5.30, 5.31 and 5.32. The constants are chosen on the basis of minimum RMS deviation of the calculated values from the measured values of Sami [85].

The choice of constant  $a_1 = 1$  used by Rotta [8] ignores the contribution of the other velocity gradients to the production term. Figure 5.31 shows the energy production term obtained by using  $a_1 = 1.09$  is in good agreement with the measurement of Sami [85]. This indicates that the contribution of other velocity gradients to the production term is about 9% of  $\overline{u'u'} \partial u / \partial r$  for this region.

The comparisons show that one transport equation for turbulent kinetic energy associated with an algebraic length scale used here is adequate to simulate turbulent flow in the initial region of jets. The term by term energy balance indicates useful performance of this model. This calculation saves computer time necessary for simultaneous solution of two transport equations and shows satisfactory agreement with experimental measurements.

The results of the turbulent quantities presented here for the initial region show that these are approximately self-preserving, starting from  $x/r_0 = 2$  for the jet

with the exit displacement thickness  $\delta_o^*/r_o = 0.0064$ .

### 5.5.2 Intermediate and Thick Exit Boundary Layers

The turbulent kinetic energy equation (3.13), the momentum equation (3.2) and the continuity equation (3.1) together with an empirical length scale model were solved for the turbulent kinetic energy. The measured velocity and kinetic energy distributions at the nozzle exit, in Figure 5.2, for  $\delta_o^*/r_o = 0.0179$  and, in Figure 5.3, for  $\delta_o^*/r_o = 0.0628$  were used to start the solutions from the exit section of the nozzles. The length scale models used in this calculation were:  $L/b = 0.10625$ , for  $\delta_o^*/r_o = 0.0179$  and  $L/b = 0.113$ , for  $\delta_o^*/r_o = 0.0628$ . The shear stress was related in terms of the length scale,  $L$ , and the mean velocity gradient given by Equation (3.31). The empirical constants associated with the energy equation already determined for the thin boundary layer were used for the intermediate and thick boundary layers.

The turbulent shear stresses calculated by using Prandtl's mixing length and the present experimental measurements are shown in Figures 5.33 and 5.34 for the intermediate and thick boundary layers with displacement thicknesses at exit of  $\delta_o^*/r_o = 0.0179$  and  $0.0628$  respectively. An approximate self-preservation is also achieved in the initial region for the intermediate and thick exit boundary layer velocity profiles after  $x/r_o = 4$ . The energy model of shear stress is also presented in Figures 5.33 and 5.34 and shows a reasonable agreement with the

experimental measurement except near the boundaries.

The calculated values of turbulent kinetic energy are plotted in Figures 5.35 and 5.36 and show good agreement with measurements. The turbulent intensities,  $\sqrt{u'^2}/u_c$  and  $\sqrt{v'^2}/u_c$  were calculated as for the case with the thin boundary layer. The calculated results of  $\sqrt{u'^2}/u_c$  and  $\sqrt{v'^2}/u_c$  plotted in Figures 5.37 and 5.38, for  $\delta_o^*/r_o = 0.0179$  and in Figures 5.39 and 5.40 for  $\delta_o/r_o = 0.0628$ , and the experimental results show satisfactory agreement with the calculated results. Figures 5.37 to 5.40 show the turbulent intensities are approximately self-preserving in the initial region at  $x/r_o = 4$ , for the intermediate and thick boundary layers.

#### 5.6 Turbulent Motion in the Transition Region

As already mentioned, the mean velocity is not self-preserving in the transition region of axisymmetric jets. The turbulent quantities were measured in this region, for the thin boundary layer at the nozzle exit, to examine whether they possess self-preservation. The experimental values of shear stress,  $-\overline{u'v'}/u_o^2$ , and the intensities  $\sqrt{u'^2}/u_o$ ,  $\sqrt{v'^2}/u_o$  and  $\sqrt{w'^2}/u_o$  are plotted in Figures 5.41, 5.42, 5.43 and 5.44 respectively. Figures 5.41 to 5.44 show turbulent quantities are not self-preserving in this region. Similar plots for the intermediate and thick boundary layers, not included here, show that the turbulent quantities for these jets are also not self-preserving in the transition region.

## CHAPTER VI

### CONCLUSION

Numerical calculations were performed for the mean and turbulent properties in the initial and transition regions of axisymmetric turbulent jets, and the results were compared with experimental measurements. Jets produced by three different nozzles having displacement thicknesses at the nozzle exit of  $\delta_o^*/r_o = 0.0064, 0.0179$  and  $0.0628$ , and Reynolds number,  $Re_D = 1.53 \times 10^5$  were investigated.

Prandtl's mixing length model with a simple algebraic equation for length scale,  $L$ , adequately represents the shear stress in the initial region. The length scale,  $L$ , is found to be a nonlinear function of  $x$  and its dependency on radial distance is negligible.

Both the mean and turbulent properties are approximately self-preserving in the initial region except close to the outlet for all three nozzles. The increase of the displacement thickness and the turbulent intensity at the exit of the nozzle cause the self-preserving point to move downstream. Self-preservation of mean axial velocity starts from the axial distances,  $x/r_o = 2, 2.5$  and  $3.5$  for the displacement thicknesses,  $\delta_o^*/r_o = 0.0064, 0.0179$  and  $0.0628$ , respectively, with the length of potential core the same for all three nozzles.

The width of the shear layer obtained by defining outer and inner boundaries is not the most suitable as a length scale for developing the self-preserving model

because the highest experimental uncertainty occurs near the outer boundary where the mean velocity is low. Therefore, in developing the self-preserving model it is found convenient to define the length scale on the basis of the measurements along the half-radius ( $u/u_c = 0.5$ ) where experimental uncertainty is the lowest. The length scale,  $b$ , was chosen as inversely proportional to the mean velocity gradient at half-radial line.

Calculations using the one-equation transport model together with an empirical length scale gives satisfactory results for the mean and turbulent properties in the initial region and consumes less computer time than that required when using the two-equation model.

The ratios of the turbulent intensities to turbulent kinetic energy remain constant at values close to  $\overline{u'^2}/2k = 0.44$  and  $\overline{v'^2}/2k = 0.29$  throughout the whole initial region shear layer. The ratio of the shear stress to turbulent kinetic energy  $\overline{u'v'}/k$  remains constant at 0.375 in the central portion of the shear layer, but decreases near the boundaries where intermittency also occurs. It is concluded that the structure of turbulence is uniform in the central region of the shear layer.

For the thin boundary layer at the nozzle exit, a polynomial form mean velocity profile fits the experimental measurements in the initial region. A simple integral method is applied to determine jet boundaries which agree with the results of the finite difference solution and measurements.

The length scale model used for the initial region is not applicable to the transition region because the shear layers interact along the centre line causing a change in the boundary conditions and the length scale. A simple algebraic equation cannot be adopted for the length scale. So, Boussinesq's model, with an empirical equation for turbulent diffusivity, is preferred for the shear stress. The mean and turbulent properties are not self-preserving in the transition region which starts near  $x/r_0 = 9$ .

## REFERENCES

1. Newman, B.G., "The Prediction of Turbulent Jets and Wall Jets," Canadian Aeronautics and Space Journal, Vol. 15, No. 8, October, pp. 287-305.
2. Beavers, G.S. and Wilson, T.A., "Vortex Growth in Jets," Journal of Fluid Mechanics, Vol. 44, Part 1, April 1970, pp. 97-112.
3. Tucker, H.J., "The Distortion of Turbulence by Irrational Strain," Techn. Report No. 70-7, Mechanical Engineering Research Laboratories, McGill University, Montreal, Dec. 1970.
4. Wagnanski, I. and Fiedler, H., "Some Measurements in the Self-Preserving Jets," Journal of Fluid Mechanics, Vol. 38, Part 3, March 1969, pp. 577-612.
5. Heskestad, G., "Hot-wire Measurements in a Radial Turbulent Jet," ASME Journal of Applied Mechanics, Vol. 33, Series E, June 1966, pp. 417-424.
6. Newman, B.G., "Turbulent Jets and Wakes in a Pressure Gradient," Fluid Mechanics of Internal Flow, G. Sovran, ed., Elsevier, 1967, pp. 170-201.
7. Townsend, A.A., The Structure of Turbulent Shear Flow, Cambridge University Press, 1956.
8. Rotta, J.C., "Prediction of Turbulent Shear Flow Using the Transport Equations for Turbulence Energy and Turbulence Length Scale," Lecture Presented at Von Karman Inst., Belgium, No. VKILS 76, March 1975.
9. Launder, B.E. and Spalding, D.B., "The Numerical Calculation of Turbulent Flow," Comp. Methods in Appl. Mech. and Eng., Vol. 3, 1974, p. 269.
10. Bradshaw, P., Ferriss, D.H. and Johnson, R.F., "Turbulence in the Noise-Producing Region of a Circular Jet," Journal of Fluid Mechanics; Vol. 19, 1964, pp. 591-624.
11. Ko, N.W.M. and Davies, P.O.A.L., "The Near Field Within the Potential Cone of Subsonic Cold Jets," Journal of Fluid Mechanics, Vol. 50, Part 1, 1971, pp. 49-78.



12. Lau, J.C., "The Contraction of Vortex Rings in Turbulent Round Jets," Engineering Journal of Singapore, Vol. 2, 1975, pp. 62-73.
13. Prandtl, L., "Bericht Uber Untersuchungen Zur Ausgebildeten Turbulenz," ZAMM, Vol. 5, 1925, p. 136.
14. Tollmien, W., "Berechnung Turbulenter Ausbreitungsvorgange," ZAMM, Vol. 6, Part 6, 1926, p. 468.
15. Schlichting, H., "Boundary Layer Theory," 6th Ed., McGraw-Hill, New York, N.Y., 1968.
16. Kuethe, A., "Investigation of the Turbulent Mixing Regions Formed by Jets," Journal of Applied Mechanics, Vol. 3, Series A., 1935, p. 87.
17. Squire, H.B. and Truncer, J., "Round Jets in a General Stream," ARC Report No. 1974, January 1944.
18. Albertson, M.L., Dai, Y.B., Jensen, R.A. and Rouse, H., "Diffusion of Submerged Jets," Proc. Am. Soc. Civil Engrs., Vol. 74, 1948, p. 1751.
19. Miller, D.E. and Comings, E.W., "Static Pressure Distribution in the Free Turbulent Jet," Journal of Fluid Mechanics, Vol. 3, Part 1, Oct. 1957, pp. 1-15.
20. Kirshner, J.M., "Jet Flows," Fluidics Quarterly, Vol. 1, No. 3, April 1968, pp. 33-46.
21. Schetz, J.A., "Turbulent Mixing of a Jet in a Co-Flowing Stream," AIAA Journal, Vol. 6, 1968, pp. 2008-2010.
22. Hinze, J.O., Turbulence: An Introduction to its Mechanism and Theory, McGraw-Hill Book Co., Inc., 1959.
23. Hatta, K. and Nozaki, T., "Two-dimensional and Axisymmetric Jet Flows With Finite Initial Cross Sections," Bull. of the J.S.M.E., Vol. 18, No. 118, 1975, pp. 349-357.
24. Sami, S., Carmady, T. and Rouse, H., "Jet Diffusion in the Region of Flow Establishment," Journal of Fluid Mechanics, Vol. 27, Part 2, 1967, pp. 231-252.
25. Von Frank, E., "Turbulence Characteristics in the Mixing Region of a Perturbed and Unperturbed Round Free Jet," M.S. Thesis, Dept. of Aero. Engineering, Penn. State University, 1970.

26. Madni, I.K. and Pletcher, R.H., "Prediction of Turbulent Jets in Coflowing and Quiescent Ambients," ASME Journal of Fluids Engineering, Vol. 97, Dec. 1975, pp. 558-567.
27. Abramovich, G.N., Theory of Turbulent Jets, Translation by Scripts Technica, MIT Press, 1963.
28. Simson, A.K., "Measurement of Velocity in the Establishment Region of a Two-Dimensional Jet," ASME Paper, No. 64-WA/Aut-2, 1964.
29. Nayer, B.M., Siddon, T.E. and Chu, W.T., "Properties of the Turbulence in the Transition Region of a Round Jet," Technical Note No. 131, IAS, University of Toronto, January, 1969.
30. Davies, P.O.A.L., Fisher, M.H. and Barrat, M.H., "The Characteristics of Turbulence in the Mixing Region of a Round Jet," Journal of Fluid Mechanics, Vol. 15, 1963, pp. 337-367.
31. Laurence, J.C., "Intensity, Scale and Spectra of Turbulence in the Mixing Region of Free Subsonic Jet," NACA, Rep. No. 1292, April 1956.
32. Lau, J.C., "The Jet Vortex Street," Proceedings of Thermo-Fluid Conference, Inst. of Engineering, Australia, Melbourne, 1974, pp. 96-100.
33. Kolpin, M.A., "The Flow in the Mixing Region of a Jet," Journal of Fluid Mechanics, Vol. 18, 1964, pp. 529-548.
34. Yuu, S., Yasukouchi, N., Hiyosawa, Y. and Jotaki, T., "Particle Turbulent Diffusion in a Dust Laden Round Jet," AICHE Journal, Vol. 24, No. 3, May 1978, pp. 509-519.
35. Reed, B., Spiegel, L. and Hartland, S., "Some Measurements of Spatial Correlations in an Axisymmetric Turbulent Jet," Proceedings of Symposium on Turbulent Shear Flows, University Park, Penn., April 1977.
36. Bradshaw, P., "The Effect of Initial Conditions on the Development of a Free Shear Layer," Journal of Fluid Mechanics, Vol. 26, Part 2, 1966, pp. 225-236.
37. Crow, S.C. and Champagne, F.H., "Orderly Structure of Jet Turbulence," Journal of Fluid Mechanics, Vol. 48, Part 3, 1971, pp. 547-591.


38. Yule, A.J., "Observations of Late Transitional and Turbulent Flow in Round Jets," Proceedings of Symposium on Turbulent Shear Flows, University Park, Penn., April 1977.
39. Hussain, A.K.M.F. and Zedan, M.F., "Effects of the Initial Condition on the Axisymmetric Free Shear Layer: Effects of the Initial Momentum Thickness," Physics of Fluids, Vol. 21, No. 7, July 1978, pp. 1100-1112.
40. Hussain, A.K.M.F. and Zedan, M.F., "Effects of the Initial Condition on the Axisymmetric Free Shear Layer: Effect of the Initial Fluctuation Level," Physics of Fluids, Vol. 21, No. 9, Sept. 1978, pp. 1475-1481.
41. Rotta, J.C., "Turbulent Shear Layer Prediction on the Basis of the Transport Equations for the Reynold's Stresses," Proceedings 13th Congr. Theor. Appl. Mech., Moscow, 1972, pp. 295-308.
42. Biringen, S., "Calculation of Axisymmetric Jets and Wakes with Three-Equations Model of Turbulence," Journal of Fluid Mechanics, Vol. 86, Part 4, 1978, pp. 745-759.
43. Launder, B.E., Morse, A.P., Rodi, W. and Spalding, D.B., "The Prediction of Free Shear Flows - A Comparison of the Performance of Six Turbulence Models," Proceedings Langely Free Shear Flows Conference, NASA SP. 321, Vol. 1, July 1972, pp. 361-422.
44. Harsha, P.T., "Prediction of Free Turbulent Mixing Using Turbulent Kinetic-Energy Method," Proceedings of Langley Free Shear Flows Conference, NASA SP. 321, Vol. 1, July 1972, p. 463.
45. Kolmogorov, A.N., "Equations of Turbulent Motions of an Incompressible Turbulent Fluid," Izv. Akad. Nank SSSR Ser Phys., VI no. 1-2, 1942, p. 56.
46. Prandtl, L., "Uber ein neues Formelsystem fur die ausgebildete Turbulenz," Nachrichten Von der Akad der Wissenschaft in Gottingen, 1945.
47. Glushko, G., "Turbulent Boundary Layer on a Flat Plate in an Incompressible Fluid," Izv. Acad. Nank SSR Mekh., No. 4, 1965, p. 13.
48. Rodi, W. and Spalding, D.B., "A Two-Parameter Model of Turbulence and its Application to Free Jets," Warme-und-Stoffubertragung, Bd. 3, 1970, p. 85.

49. Bradshaw, P., "The Understanding and Prediction of Turbulent Flow," Aeronautical Journal, Vol. 76, July 1972, pp. 403-413.
50. Daly, B.J. and Harlow, F.H., "Transport Equations in Turbulence," Physics of Fluids, Vol. 13, 1970, p. 2634.
51. Nee, V.W. and Kovaszny, L.S.G., "The Calculation of the Incompressible Turbulent Boundary Layer by a Simple Theory," Conf. on Computation of Turbulent Boundary Layers, Vol. 1, Stanford University, 1968.
52. Launder, B.E., Reece, G.J. and Rodi, W., "Progress in the Development of a Reynolds Stress Turbulence Closure," Journal of Fluid Mechanics, Vol. 68, Part 2, 1975, p. 537.
53. Bradshaw, P. Ferriss, D.H. and Atwell, N.P., "Calculation of Boundary Layer Development Using the Turbulent Energy Equation," Journal of Fluid Mechanics, Vol. 28, 1967, p. 593.
54. Ng, K.H. and Spalding, D.B., "Turbulence Model for Boundary Layer Near Walls," Physics of Fluids, Vol. 15, 1972, p. 20.
55. Jones, W.P. and Launder, B.E., "The Calculation of Low Reynold's Number Phenomena With a Two-Equation Model of Turbulence," Int. Journal Heat and Mass Transfer, Vol. 16, 1973, p. 1189.
56. Spalding, D.B., "The Prediction of Two-Dimensional, Steady Turbulent Flows," Imperial College, Mech. Engineering Department Report EF/TN/A/16, 1969.
57. Launder, B.E. and Spalding, D.B., "Turbulence Models And Their Application to the Prediction of Internal Flows," Heat and Fluid Flow, Vol. 2, 1972.
58. Launder, B.E., "Progress in Modelling of Turbulent Transport," Lecture Presented at Von Karman Inst., Belgium, No. VKILS 76, March 1975.
59. Launder, B.E. and Morse, A., "Numerical Prediction of Axisymmetric Free Shear Flows with a Second Order Reynold's Stress Closure," Proceedings of Symposium on Turbulent Shear Flows, Penn. State University, University Park, April 1977.

60. Harsha, P. and Lee, S.C., "Correlation Between Turbulent Shear Stress and Turbulent Energy," AIAA Journal, Vol. 8, No. 8, 1970, pp. 1508-1510.
61. Harlow, F.H. and Nakayama, P.I., "Turbulent Transport Equations," Physics of Fluids, Vol. 10, No. 11, 1967, p. 2323.
62. Harlow, F.H. and Nakayama, P.I., "Transport of Turbulence Energy Decay Rate," Los Alamos Sci. Lab., University of California, Rep. LA-3854, 1968.
63. Harlow, F.H. and Hirt, C.W., "Generalised Transport Equations of Anisotropic Turbulence," Los Alamos Sci. Lab., Univ. California Rep. LA-4086, 1969.
64. Harlow, F.H. and Daly, B.J., "Transport Theory of Turbulence," Los Alamos Sci. Lab., University California Rep. LA-DC-11304, 1970.
65. Heck, P.H. and Smith, M.A., "Turbulent Kinetic Energy Equation and Free Mixing," Proceedings Langley Shear Flows Conference. NASA SP. 321, Vol. 1, July 1972, p. 523.
66. Peters, C.E. and W.J. Phares, "An Integral Turbulent Kinetic Energy Analysis of Free Shear Flows," Proceedings Langley Shear Flows Conference, NASA SP. 321, Vol. 1, July 1972, p. 523.
67. McGuirk, J.J. and Rodi, W., "The Calculation of Three-Dimensional Turbulent Free Jets," Proceedings of Symposium on Turbulent Shear Flows, Penn. State University, University Park, April 1977.
68. Lighthill, M.H., "On Sound Generated Aerodynamically II. Turbulence As a Source of Sound," Proc. Roy. Soc., Vol. A222, 1954, pp. 1-32.
69. Davies, P.O.A.L., Ko, N.W.M. and Bose, B., "The Local Pressure Field of Turbulent Jets," Aero. Research Council, London, Current Paper, No. 989, 1968.
70. Lau, J.C. and Fisher, M.H., "The Vortex-Street Structure of Turbulent Jets. Part 1," Journal of Fluid Mechanics, Vol. 67, Part 2, 1975, pp. 299-337.
71. Arndt, R.E.A. and Nilsen, A.W., "On the Measurement of Fluctuating Pressure in the Mixing Zone of a Round Jet," ASME Paper 71-FE-31, 1971.

72. Rudy, D.H. and Bushnell, D.M., "A Rational Approach to the Use of Prandtl's Mixing Length Model in Free Turbulent Shear Flow Calculations," Proceedings Langley Free Shear Flows Conference, NASA SP. 321, Vol. 1, July 1972, p. 67.
73. Csanady, G.T., "On the Energy Balance of a Turbulent Mixing Layer," Journal of Fluid Mechanics, Vol. 15, 1963, pp. 545-552.
74. Leslie, D.C., Developments in the Theory of Turbulence, Clarendon Press, Oxford, 1973.
75. Deissler, R.L., "Remarks on the Decay of Homogeneous Turbulence From a Given State," Physics Fluids, Vol. 17, 1974, p. 652.
76. Deardorff, J.W., "Numerical Investigation of Neutral and Unstable Planetary Boundary Layers," Journal Atmos. Sci., Vol. 29, 1972, p. 91.
77. Schumann, U., "Results of a Numerical Simulation of Turbulent Channel Flows," Paper Presented at ANS International Meeting on Reactor Heat Transfer, Karlsruhe, 1973.
78. Tennekes, H. and Lumley, J.L., A First Course in Turbulence, The MIT Press, 1972.
79. O'Brien, G.G., Hyman, M.A. and Kaplan, S., "A Study of the Numerical Solution of Partial Differential Equations," Journal of Mathematical Physics, Vol. 29, 1951, p. 223.
80. Instruction Manual for DISA 55D10 Linearizer, by DISA Elektronik A/S, Herlev, Denmark, Oct. 1966.
81. Kline, S.J. and McClintock, F.A., "Describing Uncertainties in Single-Sample Experiments," ASME Mechanical Engineering, Vol. 75, Jan. 1953, pp. 3-8.
82. Thrasher, L.W. and Binder, R.C., "A Practical Application of Uncertainty Calculations to Measured Data," Transaction of the ASME, Feb. 1957, pp. 373-376.
83. Roshko, A., "Structure of Turbulent Shear Flows: A New Look," AIAA Journal, Vol. 14, No. 10, October 1976, pp. 1349-1357.
84. Salvadori, M.G. and McCormick, J.M., Numerical Methods in Fortran, Prentice-Hall, Inc., New Jersey, 1964.
85. Sami, S., "Balance of Turbulence Energy in the Region of Jet Flow Establishment," Journal of Fluid Mechanics, Vol. 29, Part 1, 1967, pp. 81-92.

86. Stoecker, W.F., Design of Thermal Systems, McGraw-Hill Book Company, 1971.
87. Schubauer, G.B. and Tchen, C.M., "Turbulent Flow," Turbulent Flow and Heat Transfer, Vol. 5 of High Speed Aerodynamics of Jet Propulsion, Princeton Press, 1959, p. 165.
88. Rotta, J.C., and Vollmers, H., "Ahnliche Losungen der Differentialgleichungen fur gemittelte Geschwindigkeiten, Turbulenzenenergie und Turbulenzlänge," DFVLR Report, DLR-FB 76-24, Gottingen 1976.
89. Bird, R.B., Stewart, W.E. and Lightfoot, E.N., Transport Phenomena, Wiley, New York, 1960.
90. Webster, C.A.G., "A Note on the Sensitivity of Yaw of a Hot-Wire Anemometer," Journal of Fluid Mechanics, Vol. 13, 1962, pp. 307-312.
91. Champagne, F.H., "Turbulence Measurements with Inclined Hot-Wires," Boeing Scientific Research Laboratories Document DL-82-0491, 1965.
92. Laufer, J., "The Structure of Turbulence in a Fully Developed Pipe Flow," NACA Report 1174, 1954.
93. Pletcher, R.H., "On the Finite-Difference Solution for the Constant-Property Turbulent Boundary Layer," AIAA Journal, Vol. 7, No. 2, February 1969, pp. 305-311.
94. DuFort, E.C. and Frankel, S.P., "Stability Conditions in the Numerical Treatment of Parabolic Differential Equations," Mathematical Tables Aids Computation, Vol. 7, 1953, pp. 135-152.
95. Roache, P.J., Computational Fluid Dynamics, Hermosa Publishers, 1976.
96. Forsythe, G.E. and Wasow, W.R., Finite-Difference Methods for Partial Differential Equations, Wiley, New York, 1960, pp. 88-139.
97. Richtmyer, R.D. and Morton, K.W., Difference Methods for Initial Value Problems, 2nd ed. Interscience, New York, 1967, pp. 3-24.
98. Hanjalic, K. and Launder, B.E., "A Reynolds Stress Model of Turbulence and its Application to Thin Shear Flows," Journal of Fluid Mechanics, Vol. 52, Part 4, 1972, pp. 609-638.



FIGURES



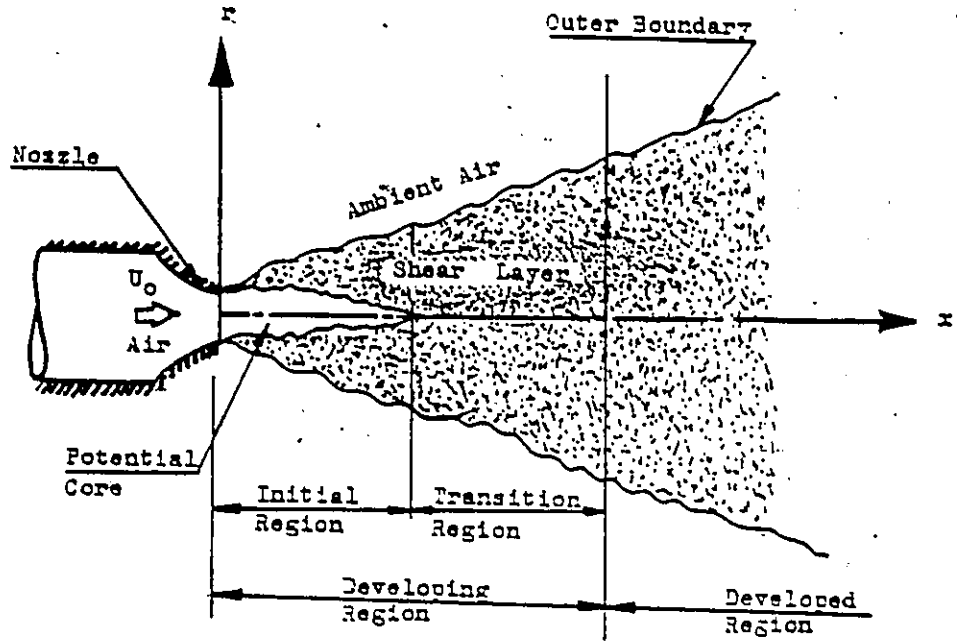


Fig.1.1

Jet Geometry and Nomenclature.

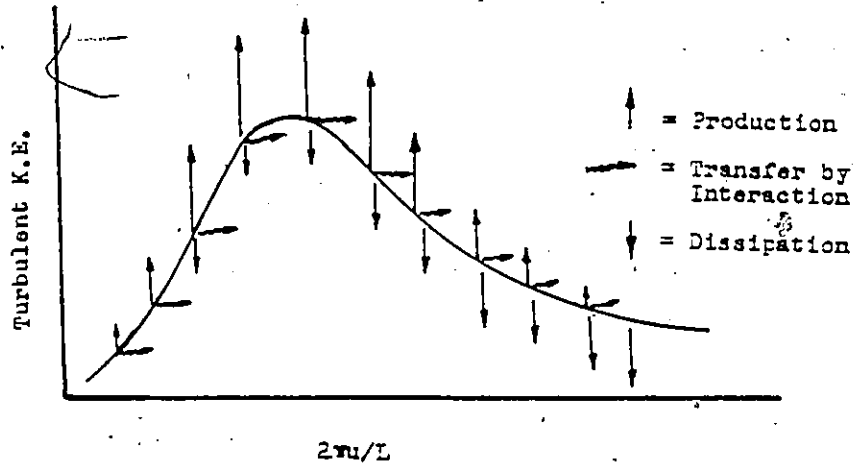


Fig.1.2

Representation of Energy Transfer with Wave Numbers.

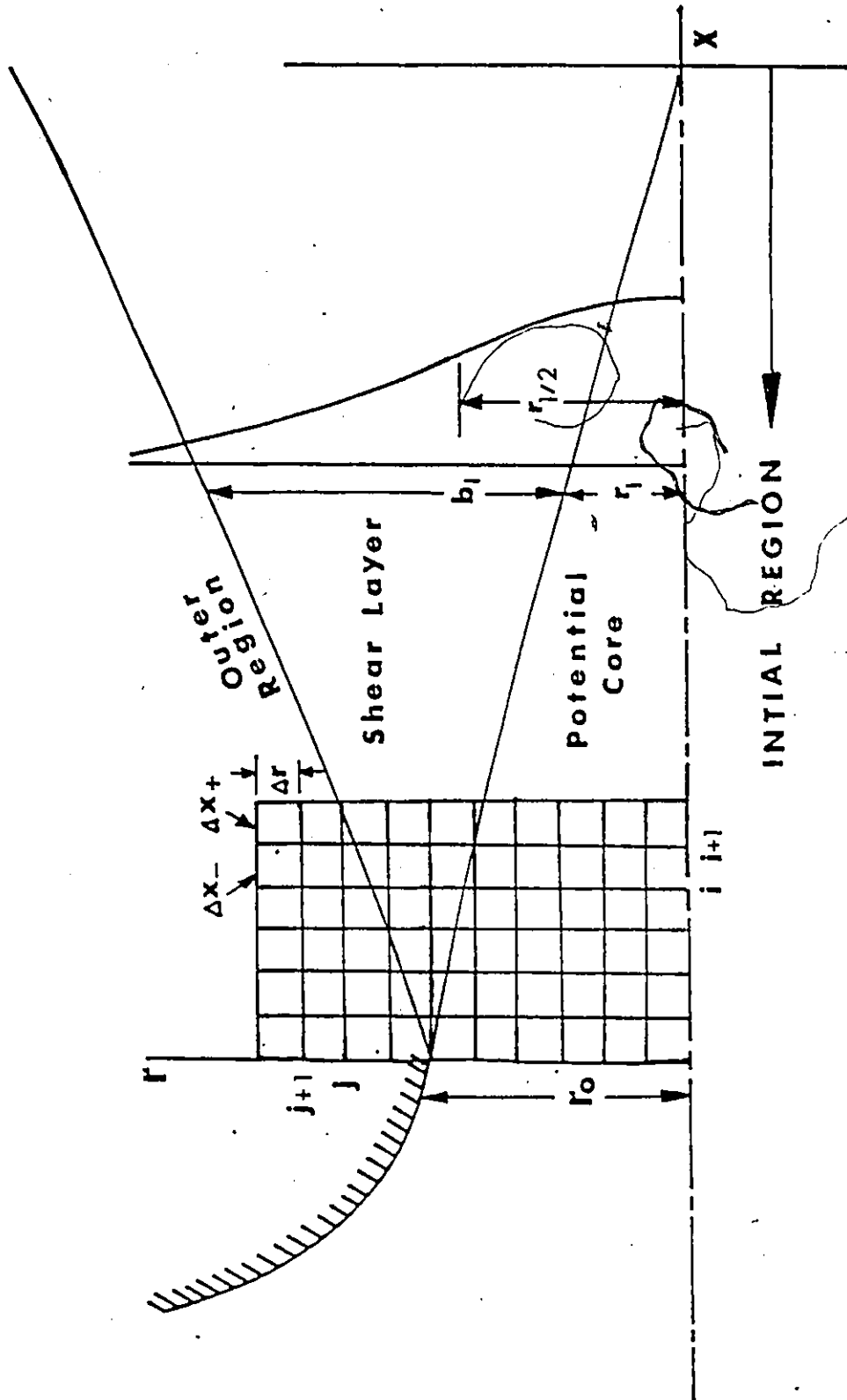


Fig.3.1.

Co-ordinate System and Finite-Difference Grid.

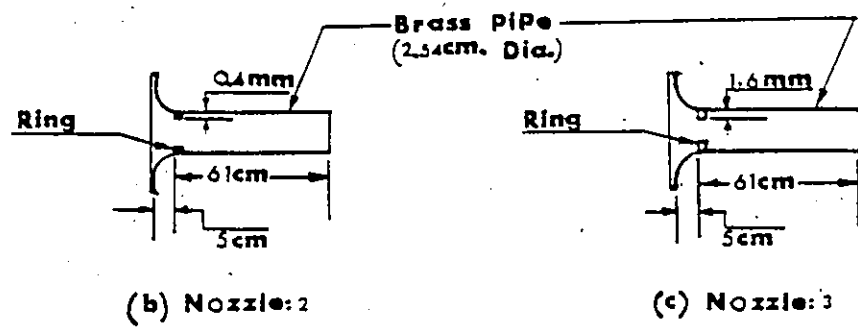
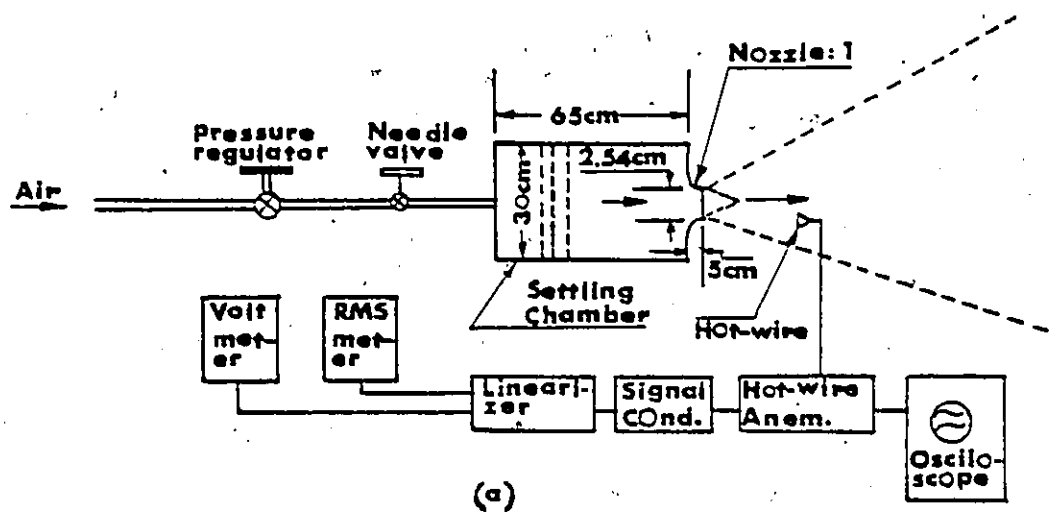


Fig.4.1

Schematic Diagrams of Experimental Set-up and Round Axisymmetric Nozzles.

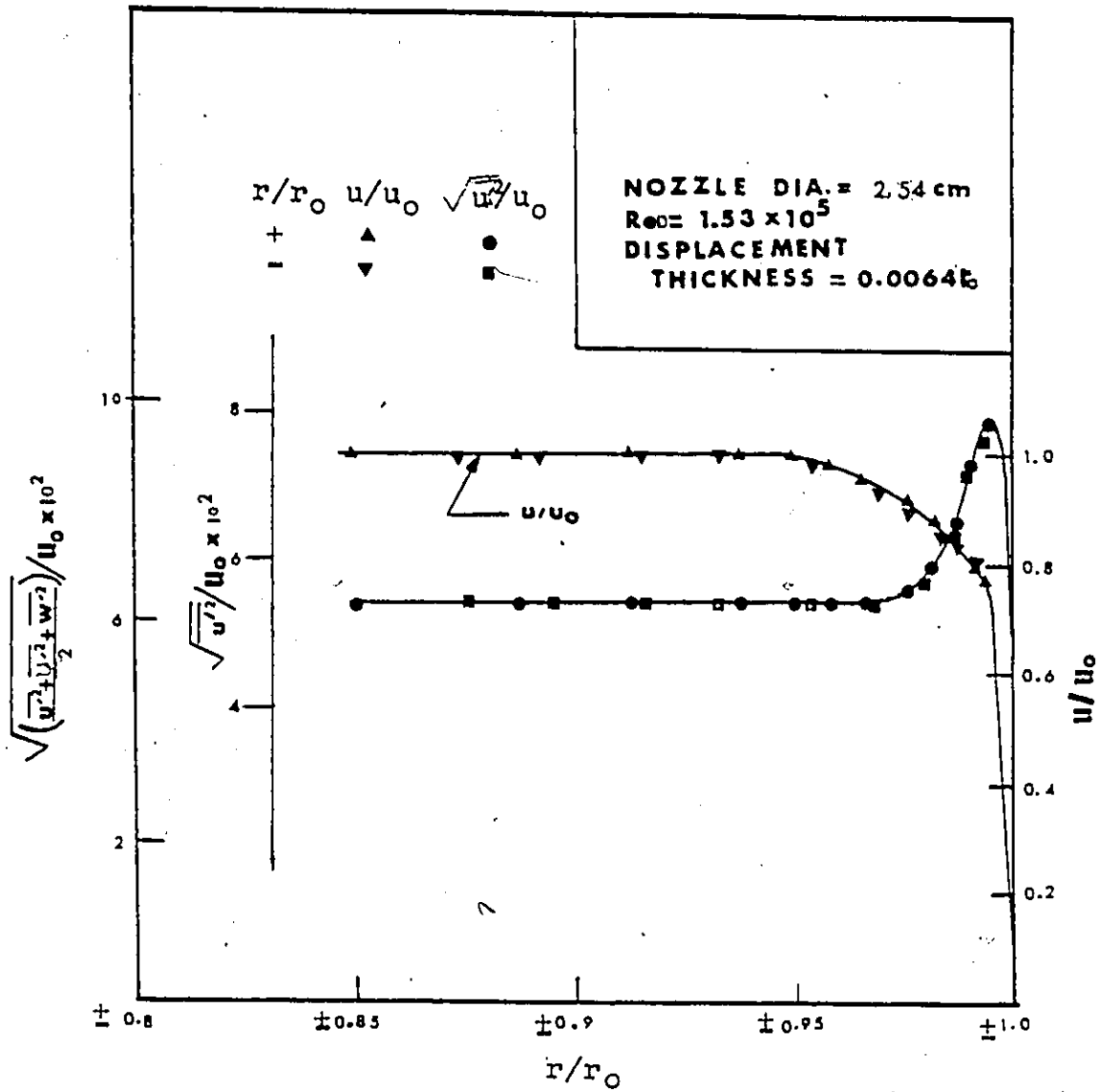


Fig.5.1

Measured Axial Velocity and Turbulent Kinetic Energy Distributions at exit Plane, Thin Boundary Layer.

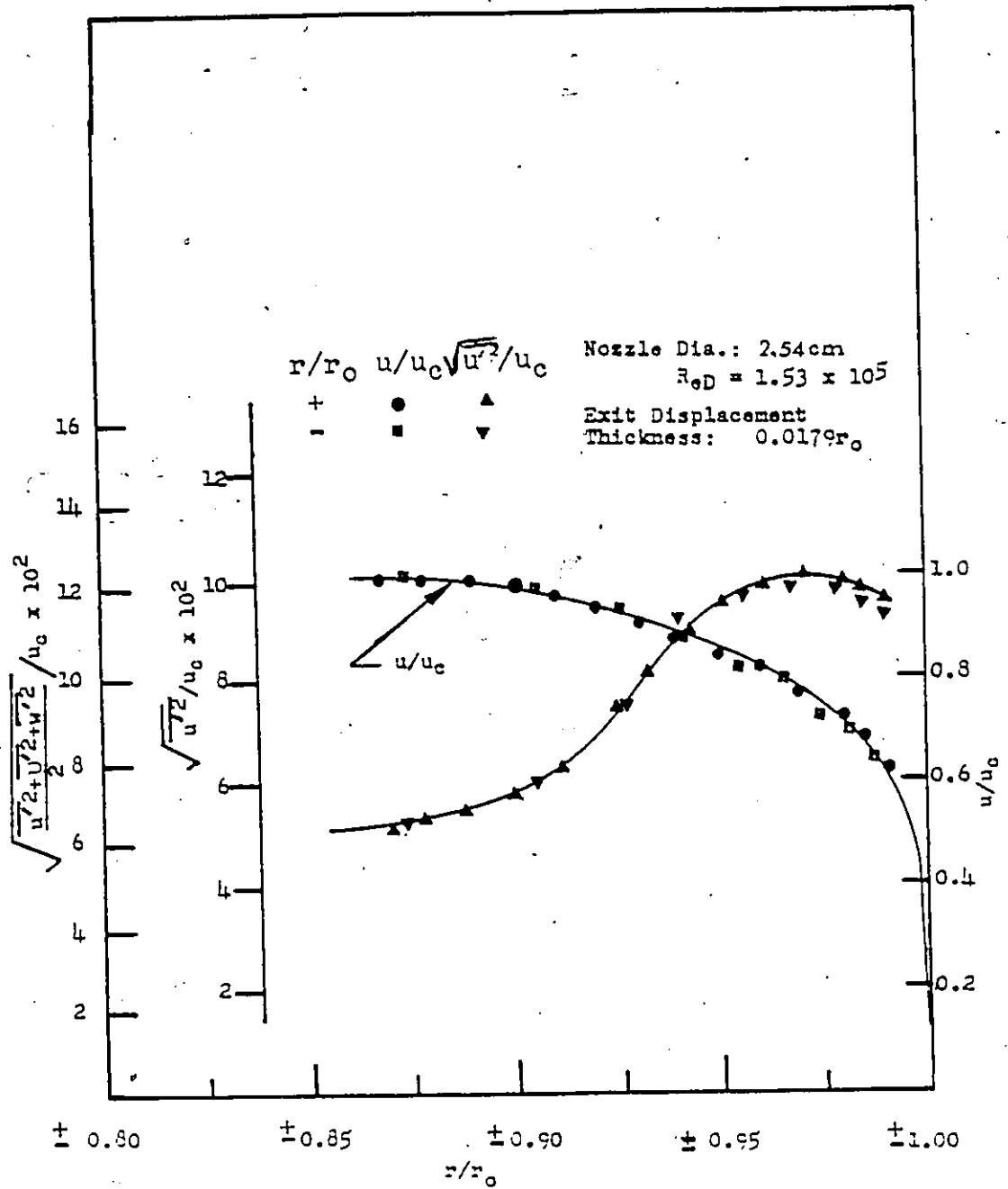


Fig.5.2

Measured Velocity and Turbulent Kinetic Energy Distributions at Exit Plane, Intermediate Boundary Layer.

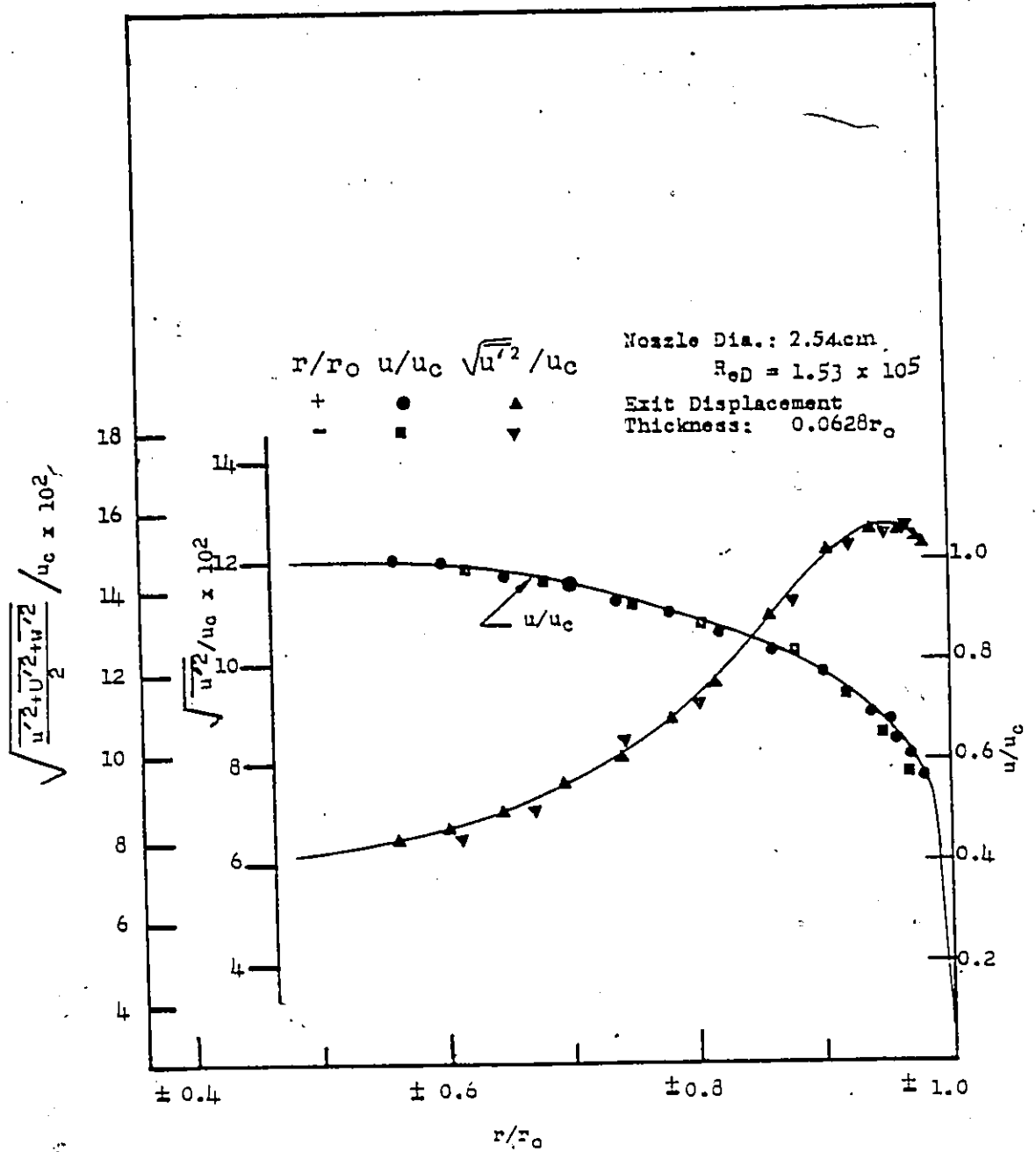


Fig.5.3

Measured Velocity and Turbulent Kinetic Energy

Distributions at exit Plane, Thick Boundary Layer.

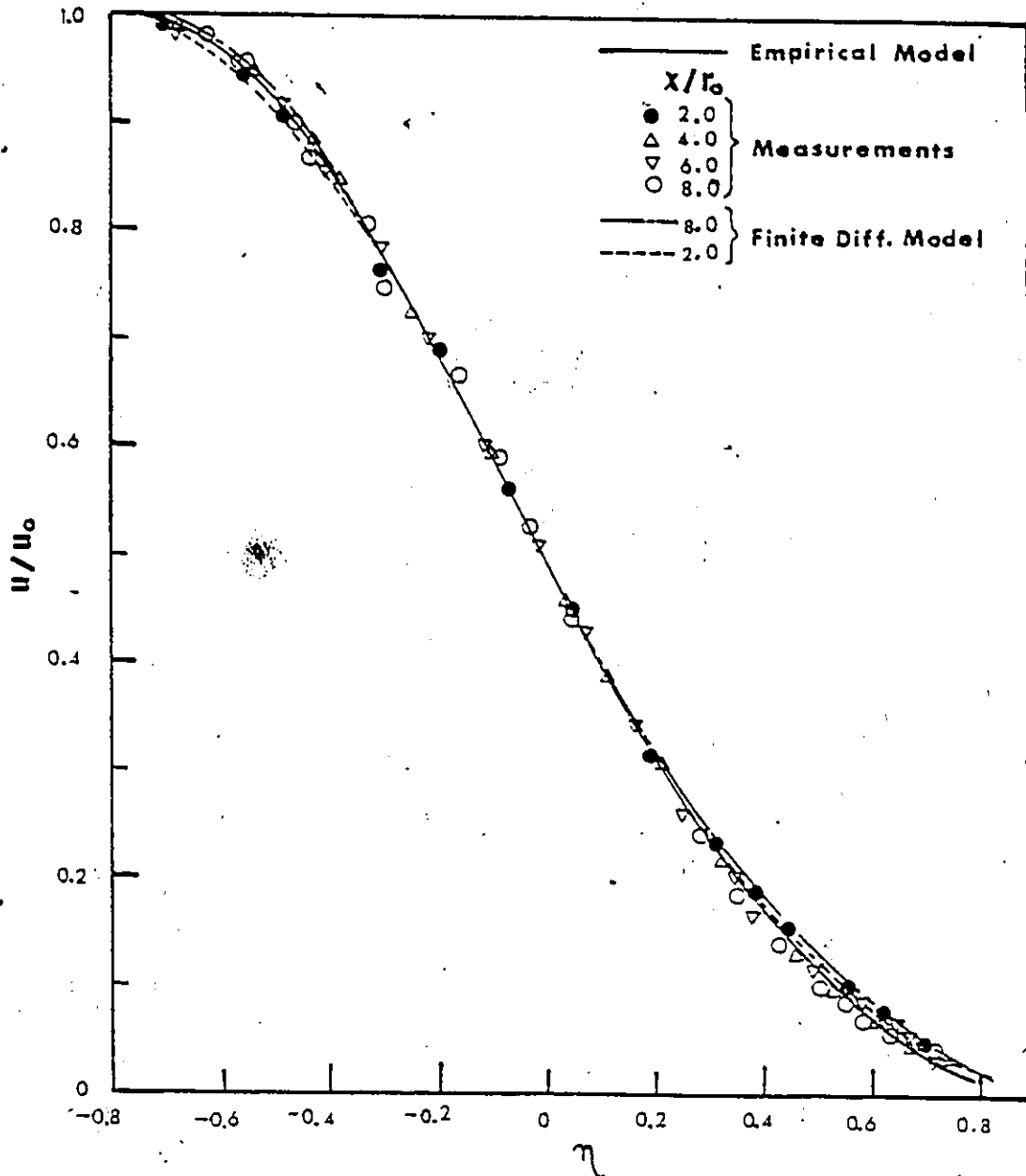


Fig.5.4.

Calculated and Experimental Self-Preserving Velocity Profiles in the Initial Region for Thin Boundary Layer.

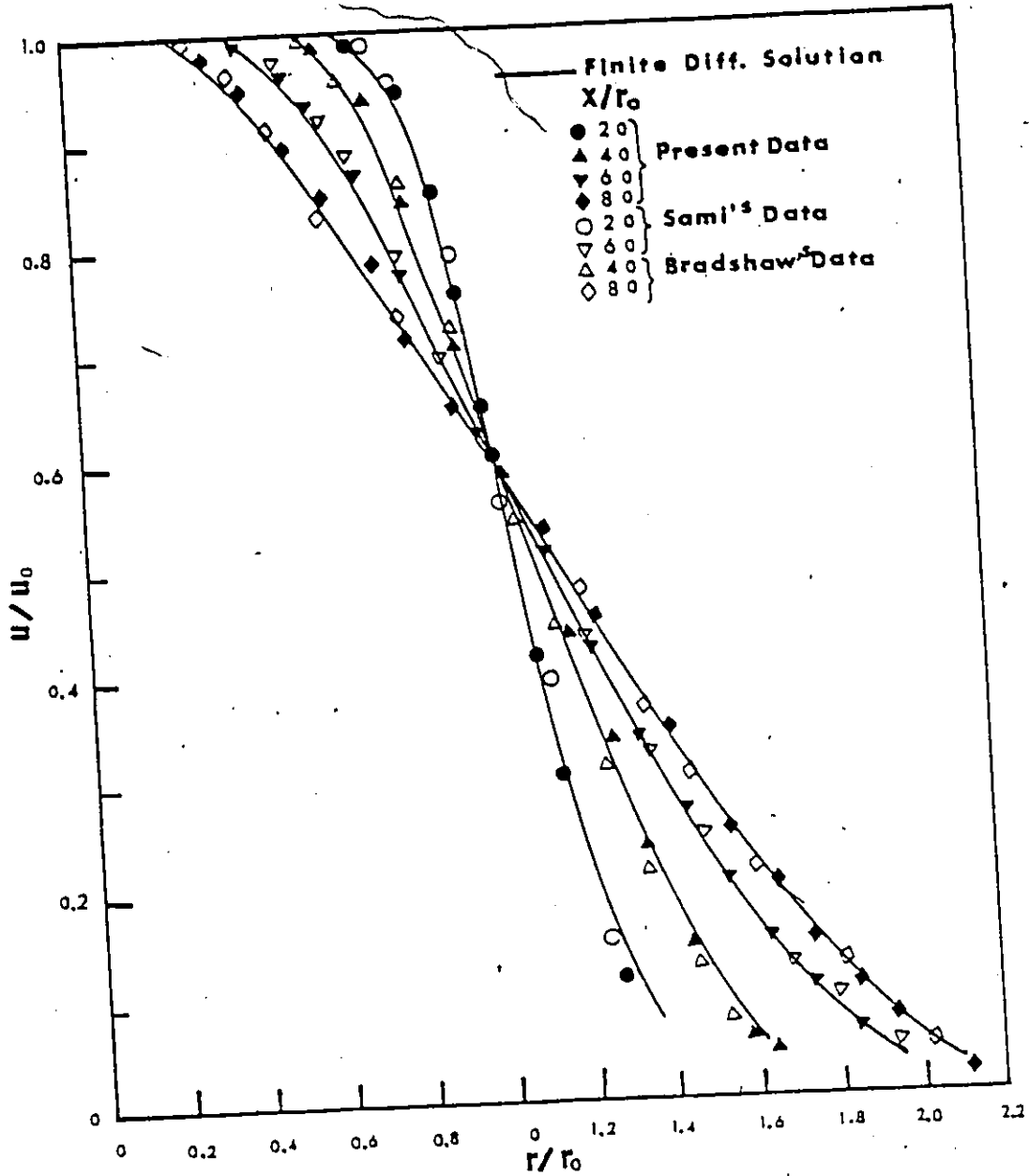


Fig. 5.5.

Calculated and Experimental Mean Axial Velocity  
Distribution, Thin Boundary Layer.



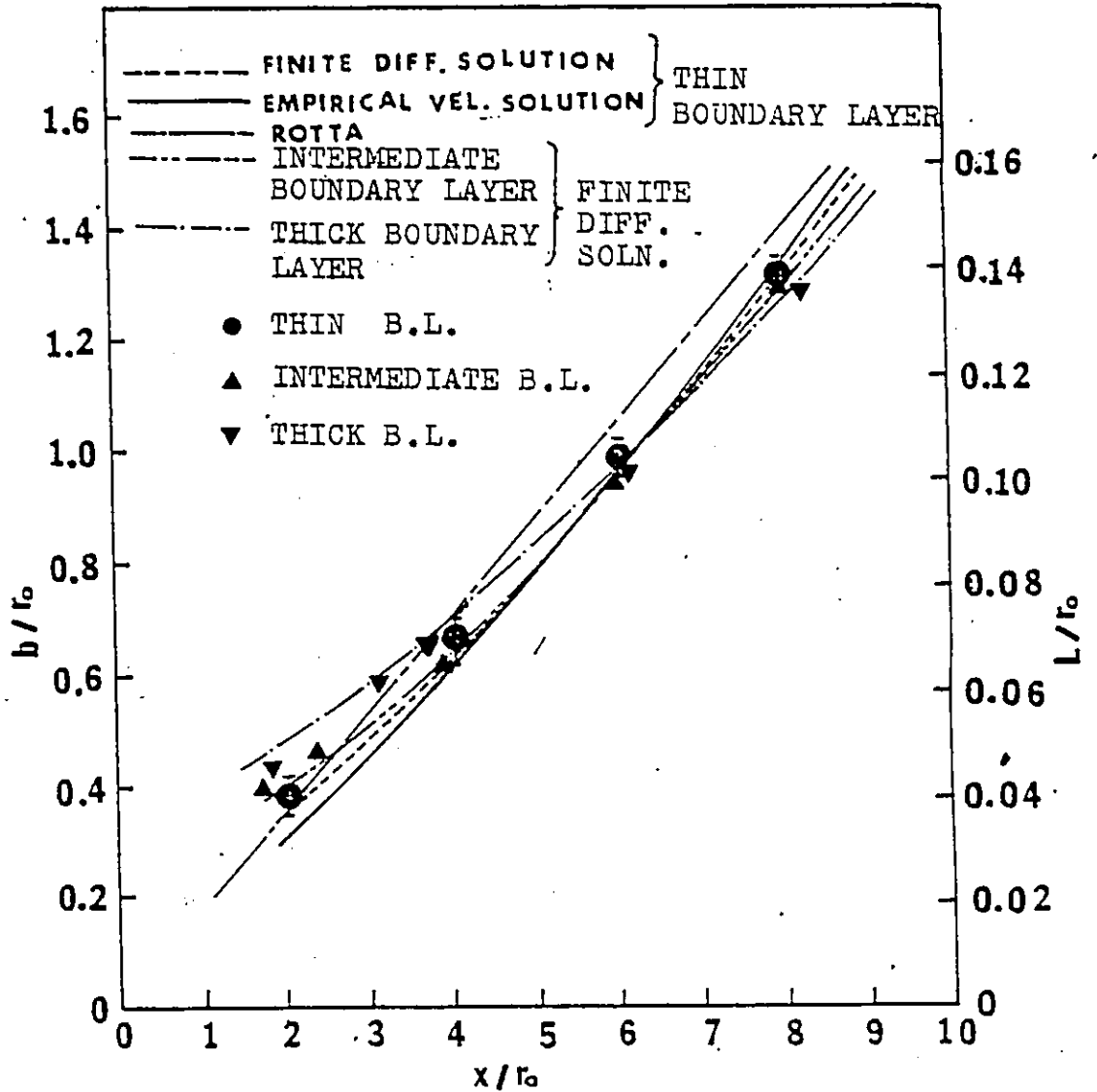


Fig.5.6

Length Scale,  $b/r_0$  and Prandtl's Mixing Length,  $L/r_0$  for Thin, Intermediate and Thick Boundary Layers.

2

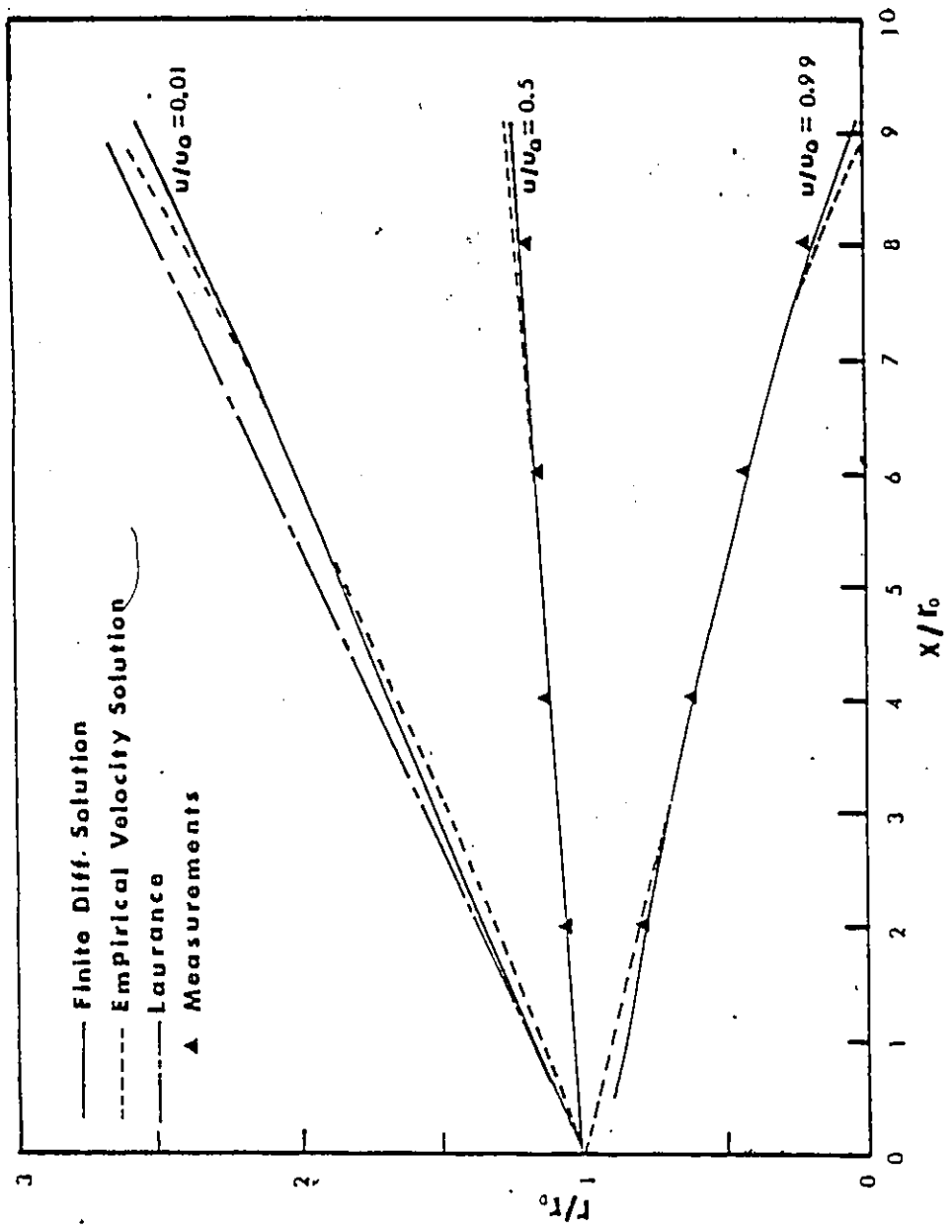


Fig. 5.7

Calculated and Experimental Iso-Velocity Lines, Thin Boundary Layer.

R

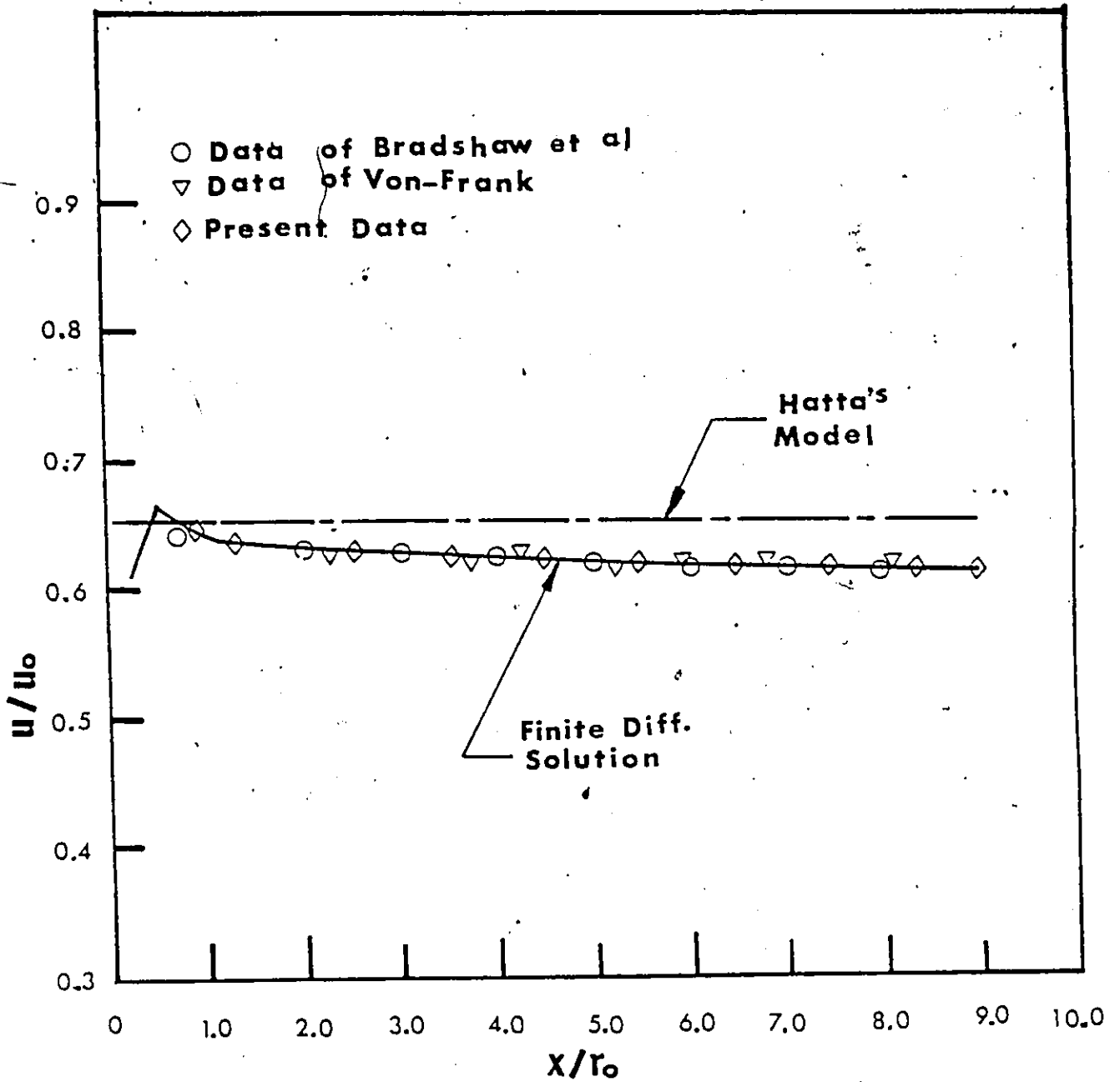


Fig.5.8.

Calculated Mean Velocity at  $r/r_0 = 1$  and Its Comparisons with Hatta's Model and Experiments, Thin Boundary Layer.

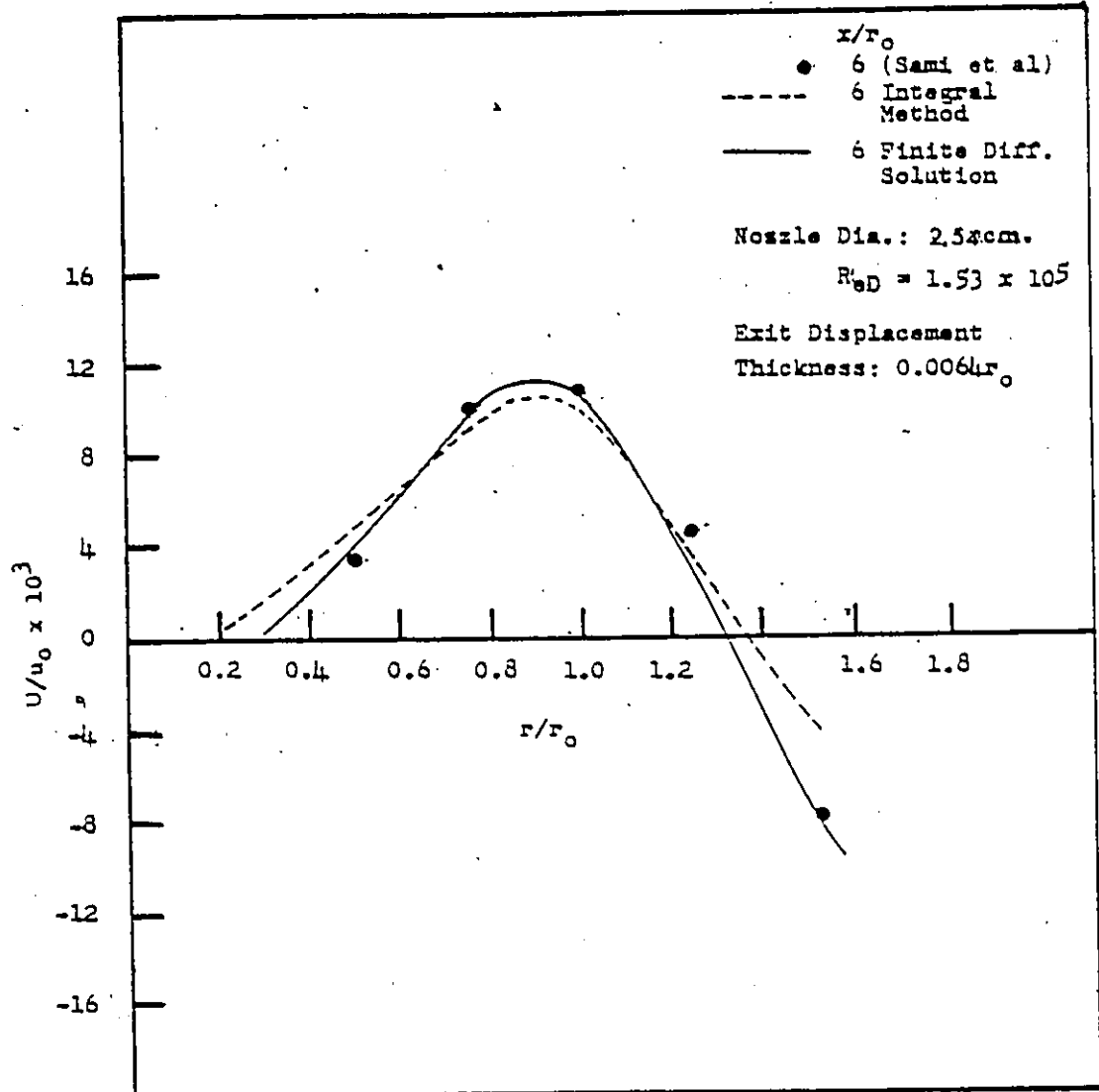


Fig.5.9

Mean Radial Velocity Distribution in the Initial Region, Thin Boundary Layer.

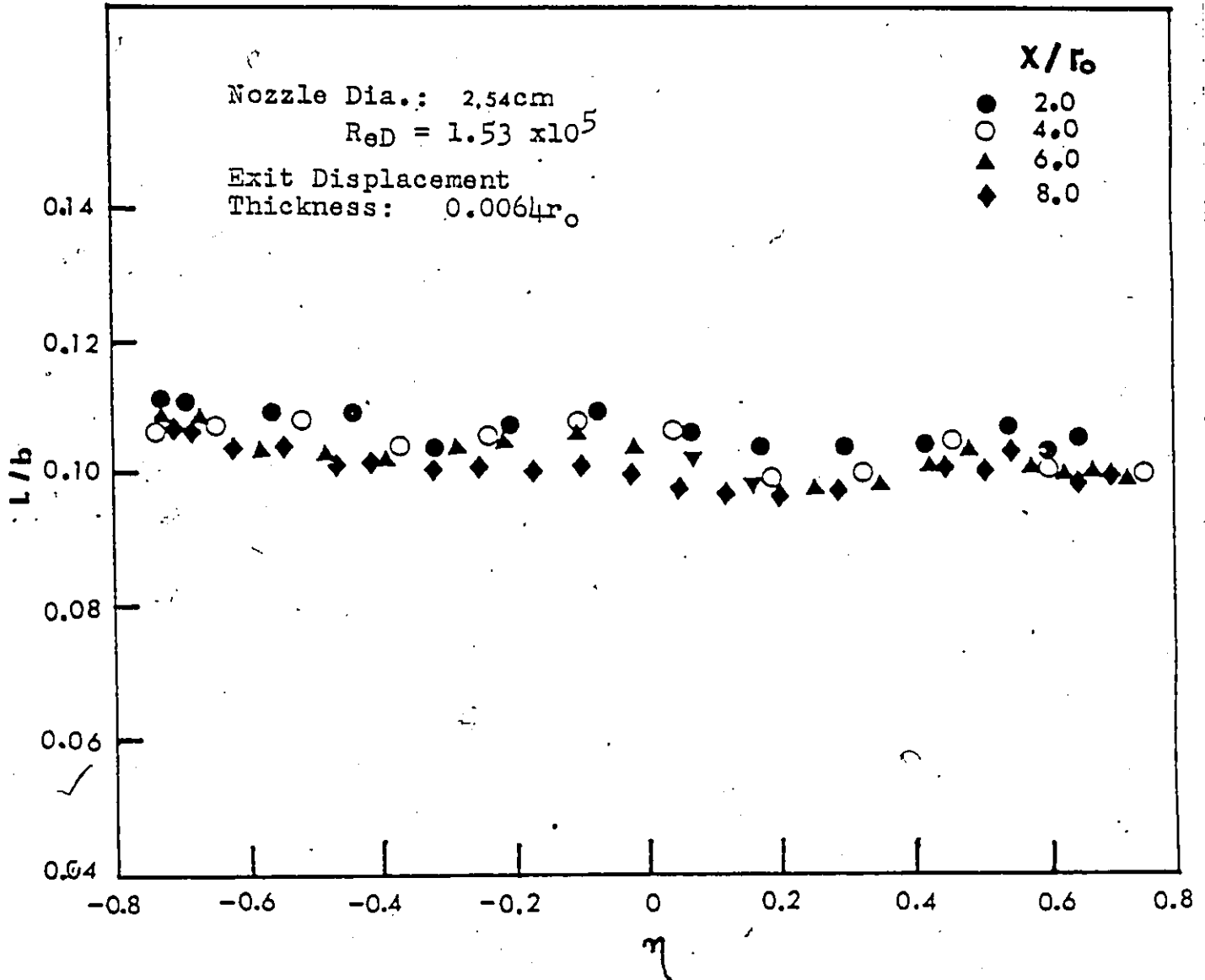


Fig.5.10

Experimental Values of the Ratio,  $L/b$ , Thin Boundary Layer.

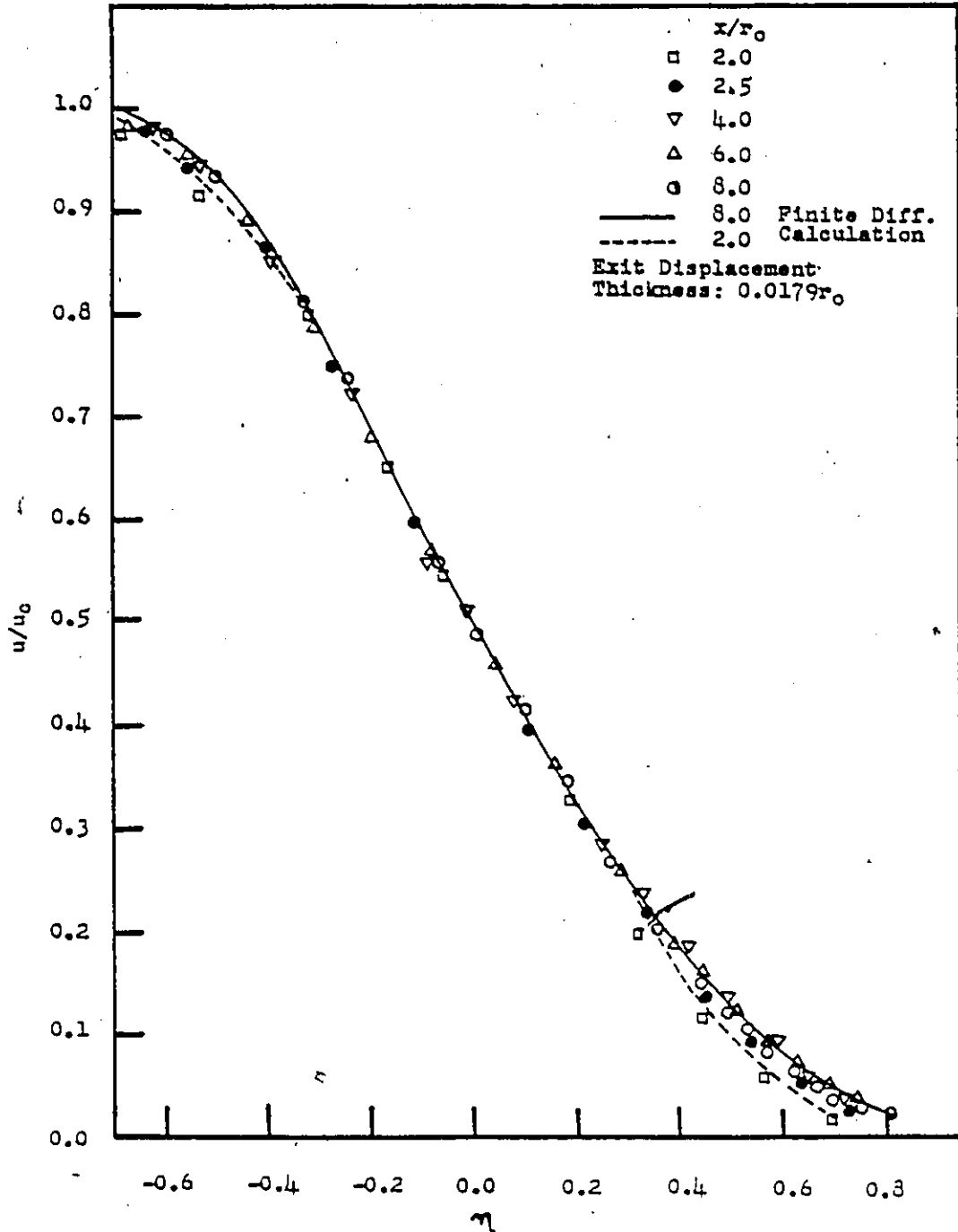


Fig.5.11

Velocity Profiles in the Initial Region, Intermediate  
 Boundary Layer.

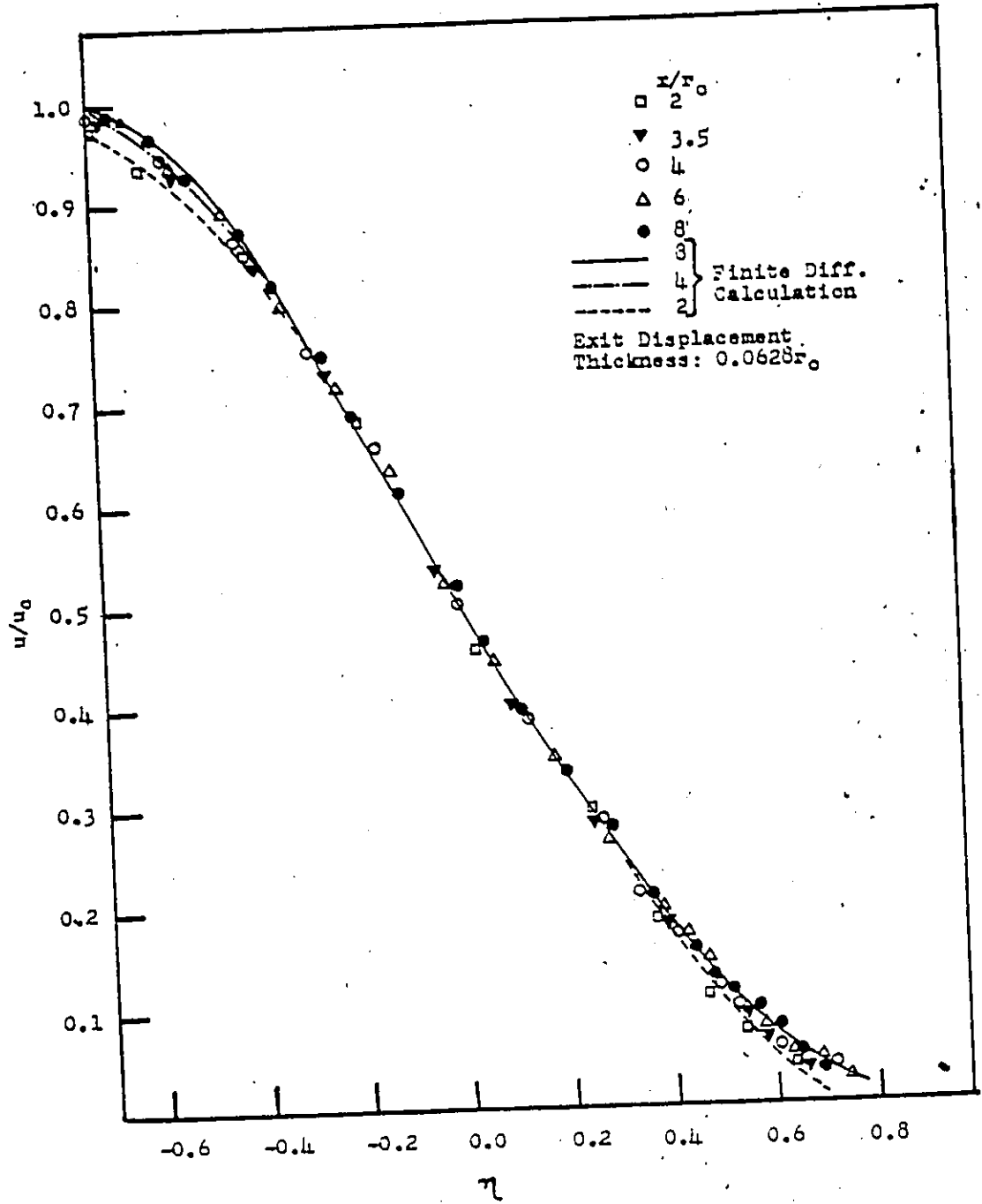


Fig.5.12

Velocity Profiles in the Initial Region, Thick Boundary Layer.

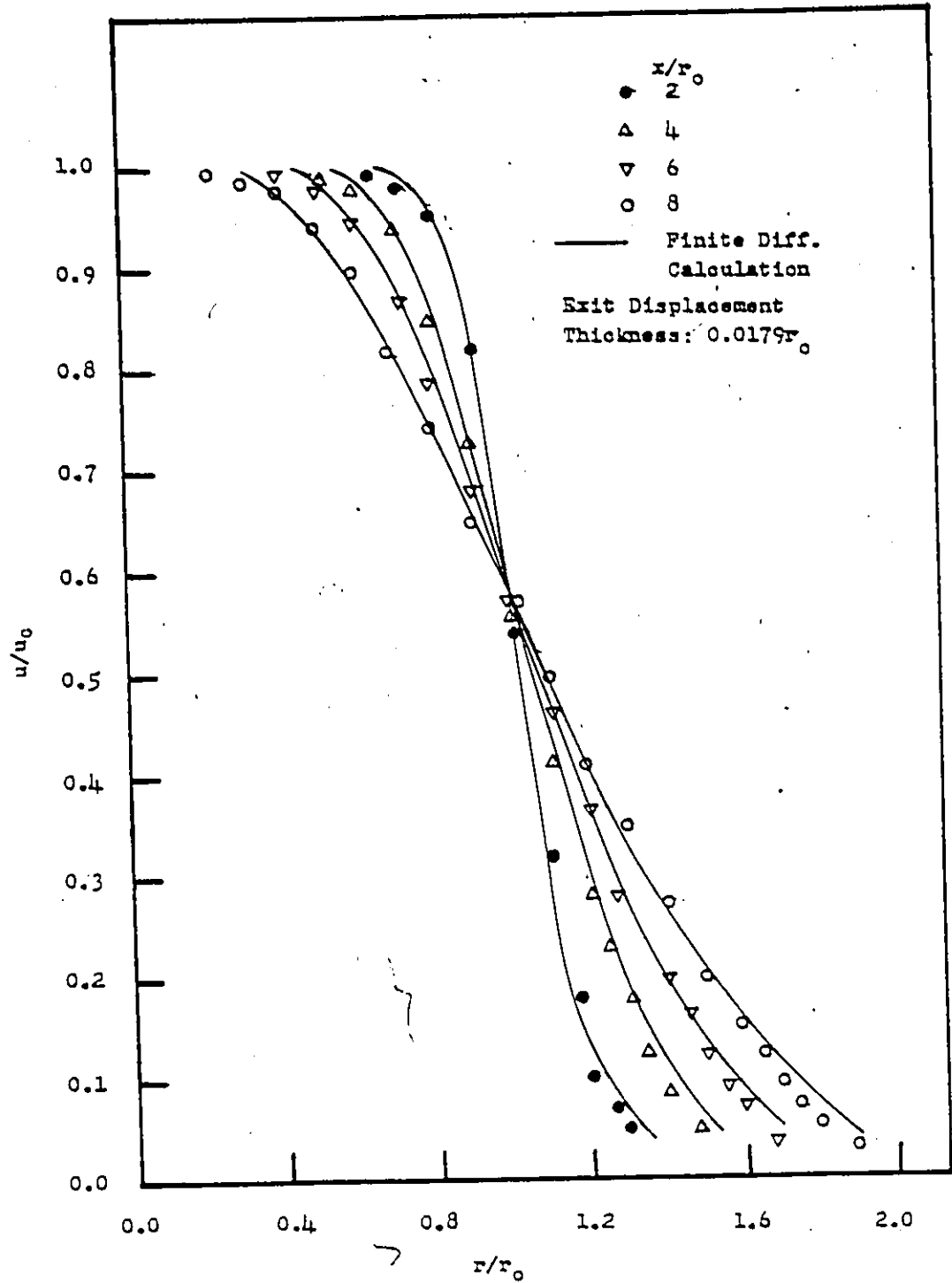


Fig.5.13

Calculated and Experimental Mean Axial Velocity  
Distribution, Intermediate Boundary Layer.



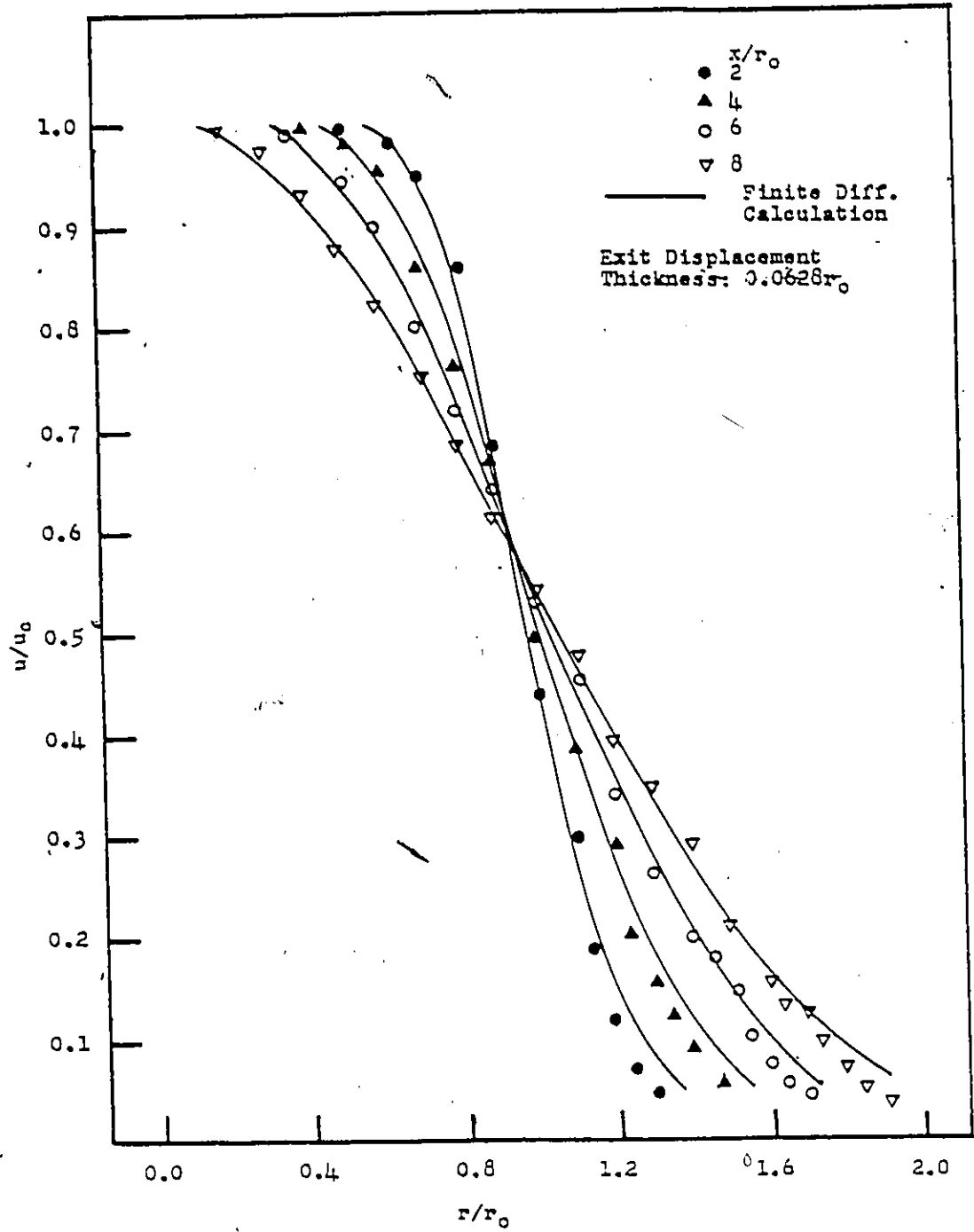


Fig.5.14

Calculated and Experimental Mean Axial Velocity  
 Distribution, Thick Boundary Layer.

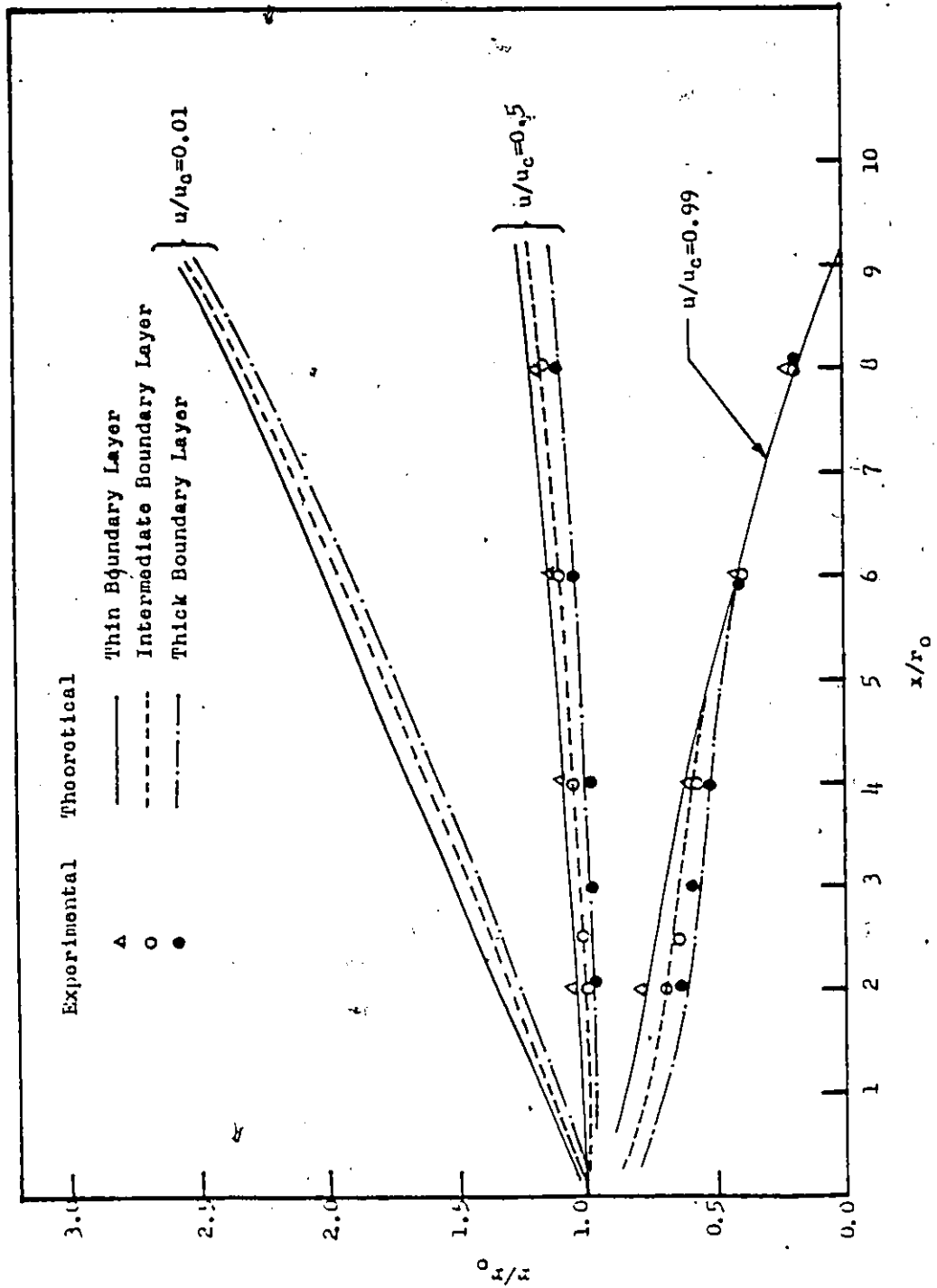


Fig. 5.15

Calculated and Experimental Iso-Velocity Lines, Thin, Intermediate and Thick Boundary Layers.

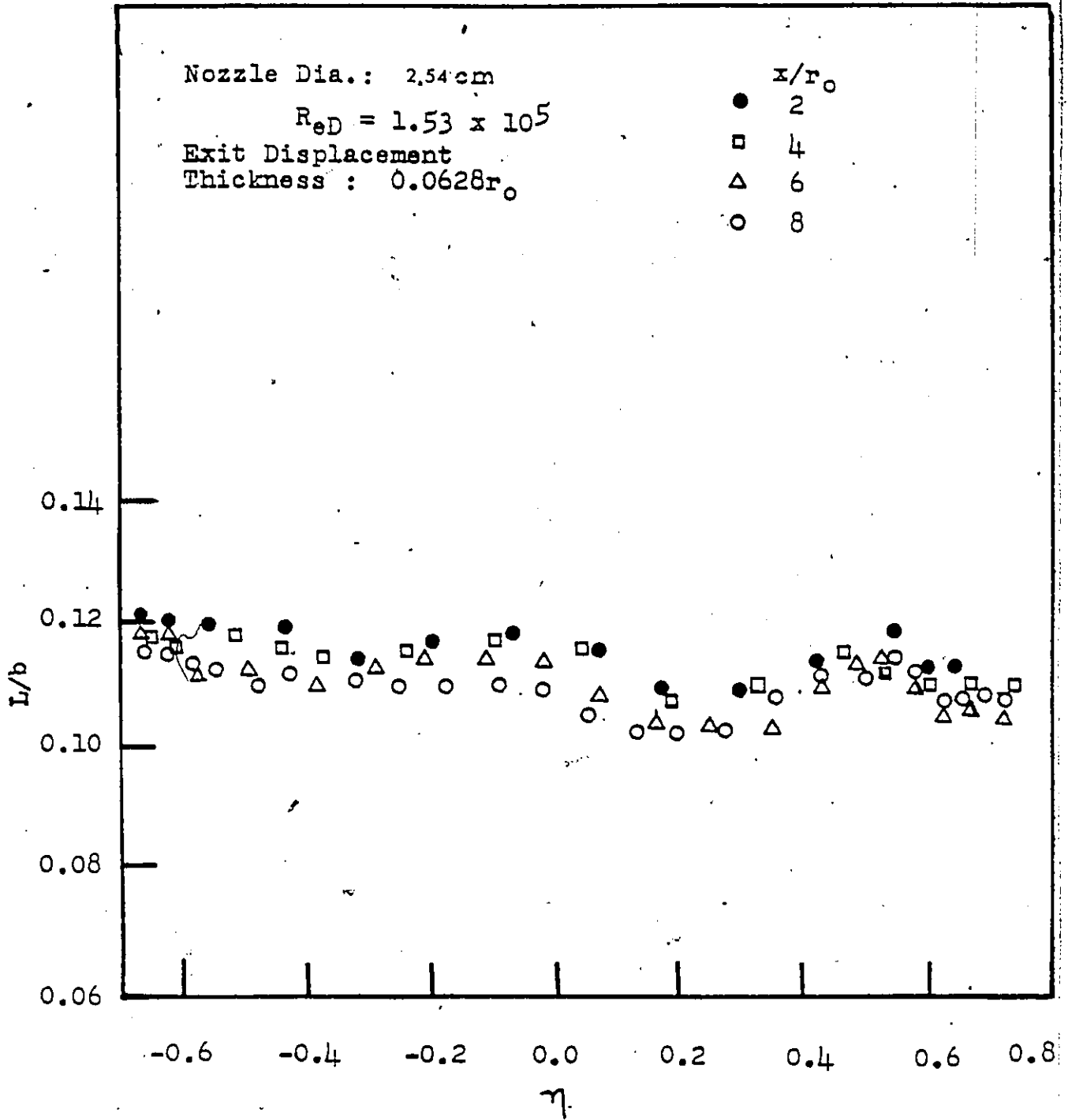


Fig.5.16

Experimental Values of the Ratio,  $L/b$ , Thick Boundary Layer.

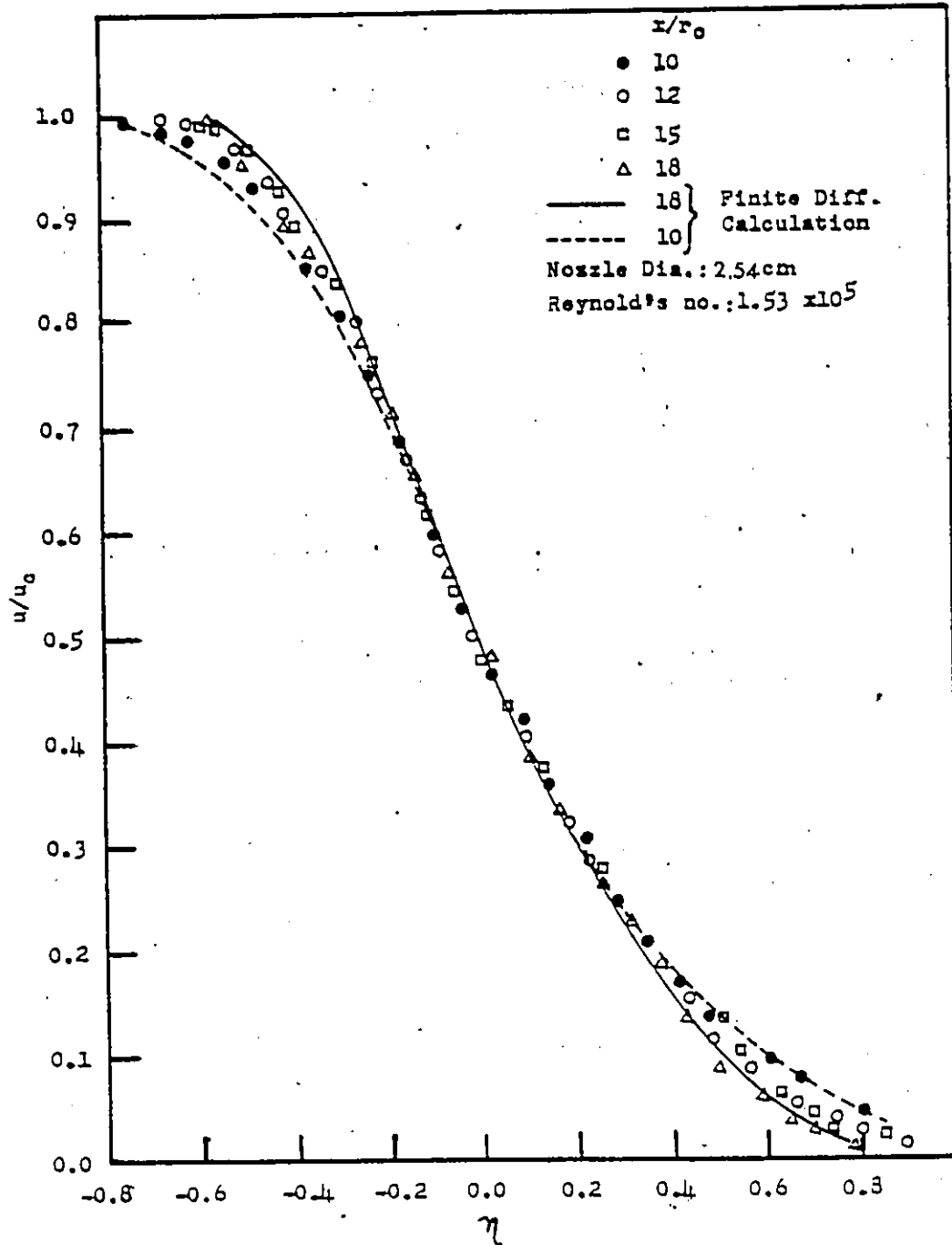


Fig.5.17

Calculated and Experimental Mean Axial Velocity  
 Distributions in  $u/u_c$  vs  $\eta$  Plane for the,  
 Transition Region.

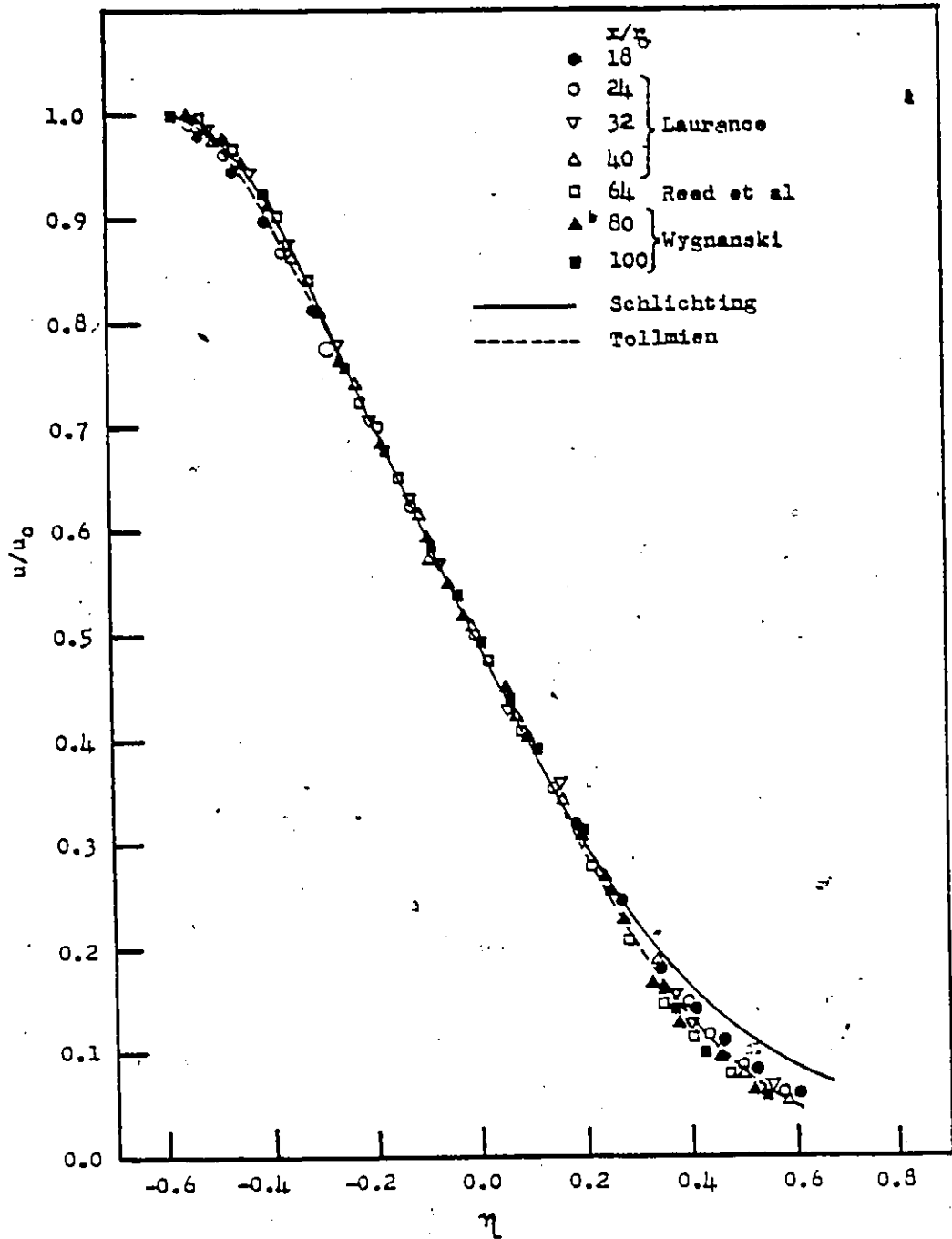


Fig.5.18

Comparison of Experimental Mean Axial Velocity with Tollmien's and Schlichting's Models for the Developed Region.

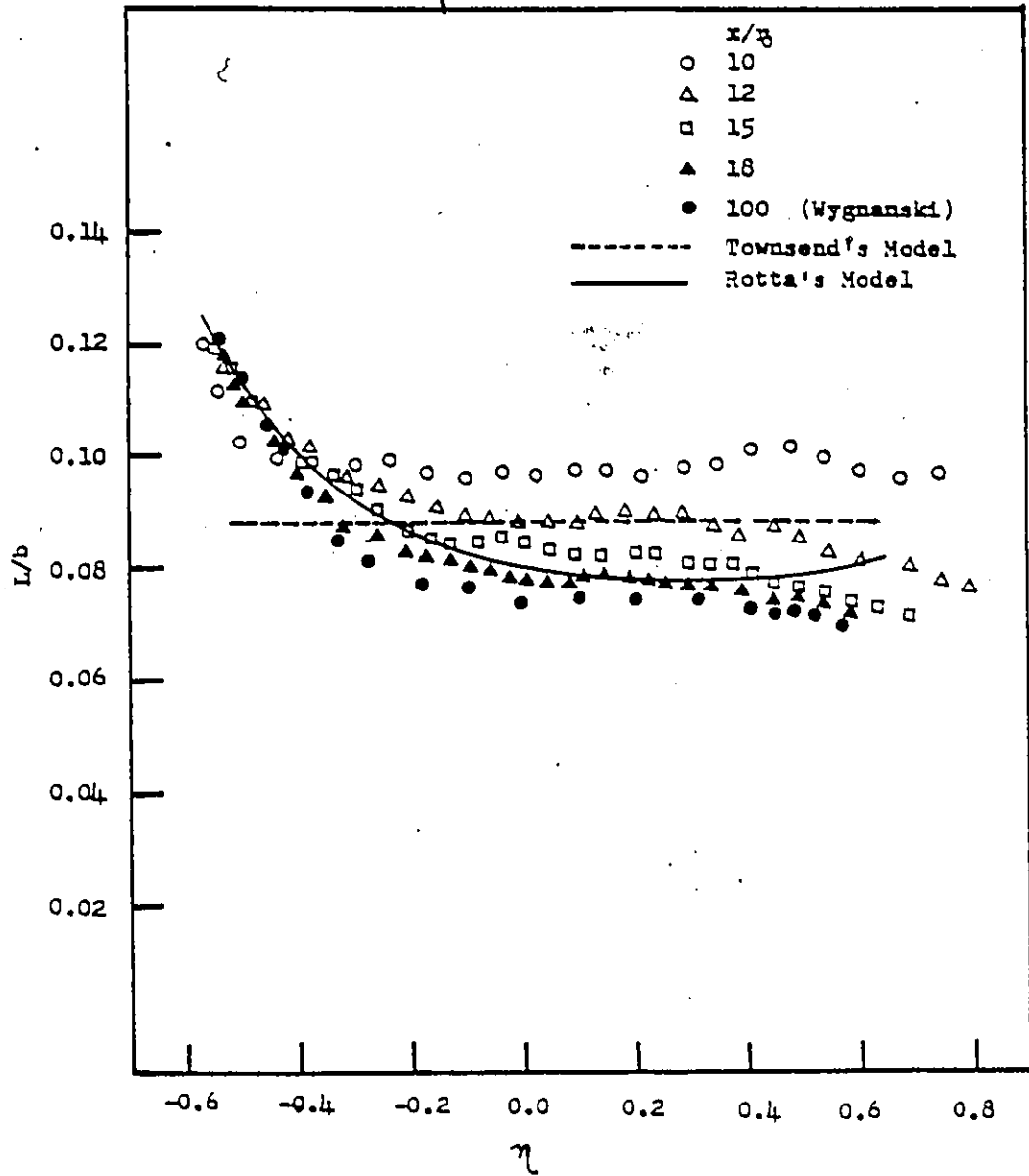


Fig.5.19

Prandtl's Mixing Length in the Transition Region.

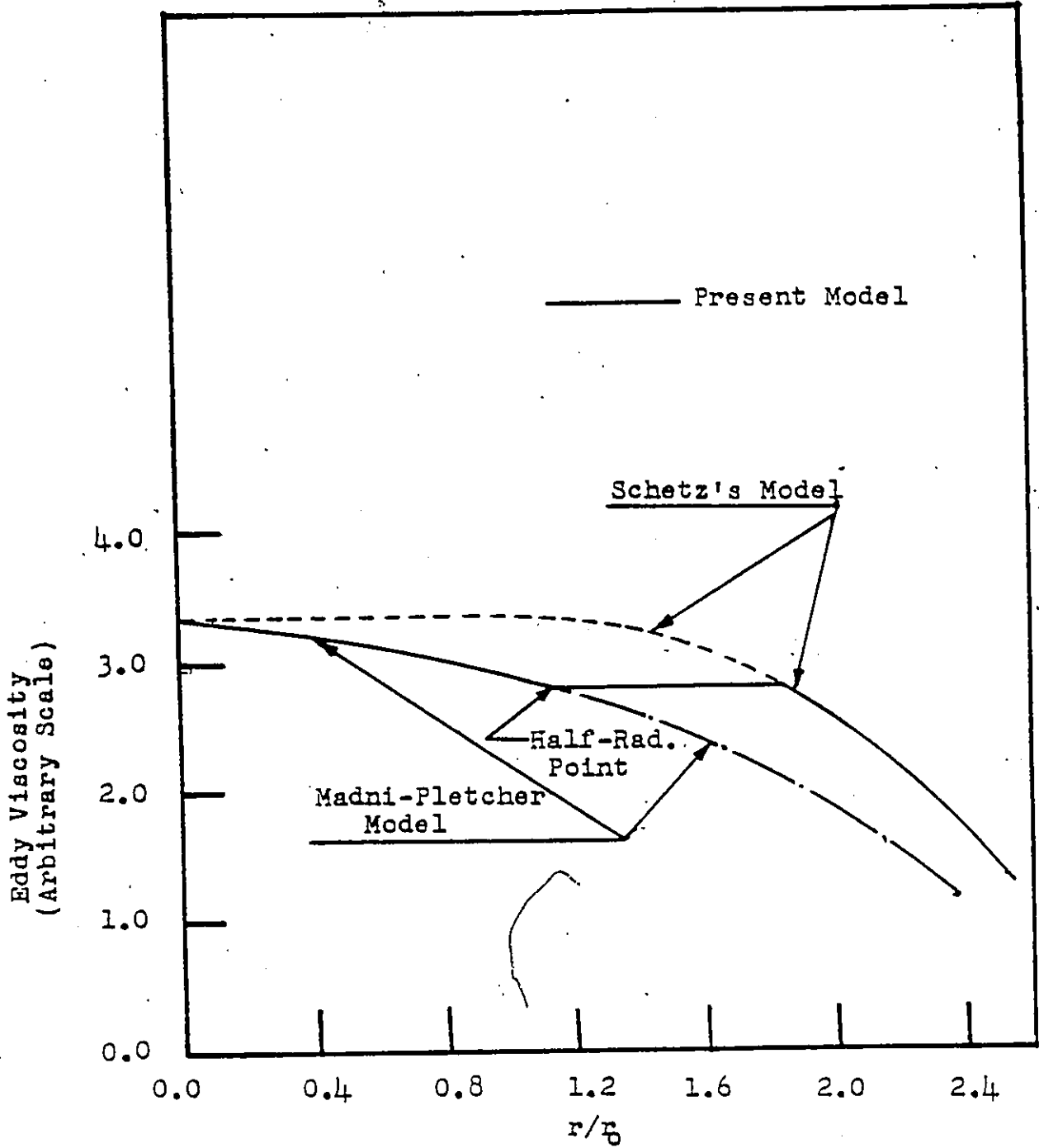


Fig.5.20

Eddy Viscosity vs Radial Distance in the Transition Region.

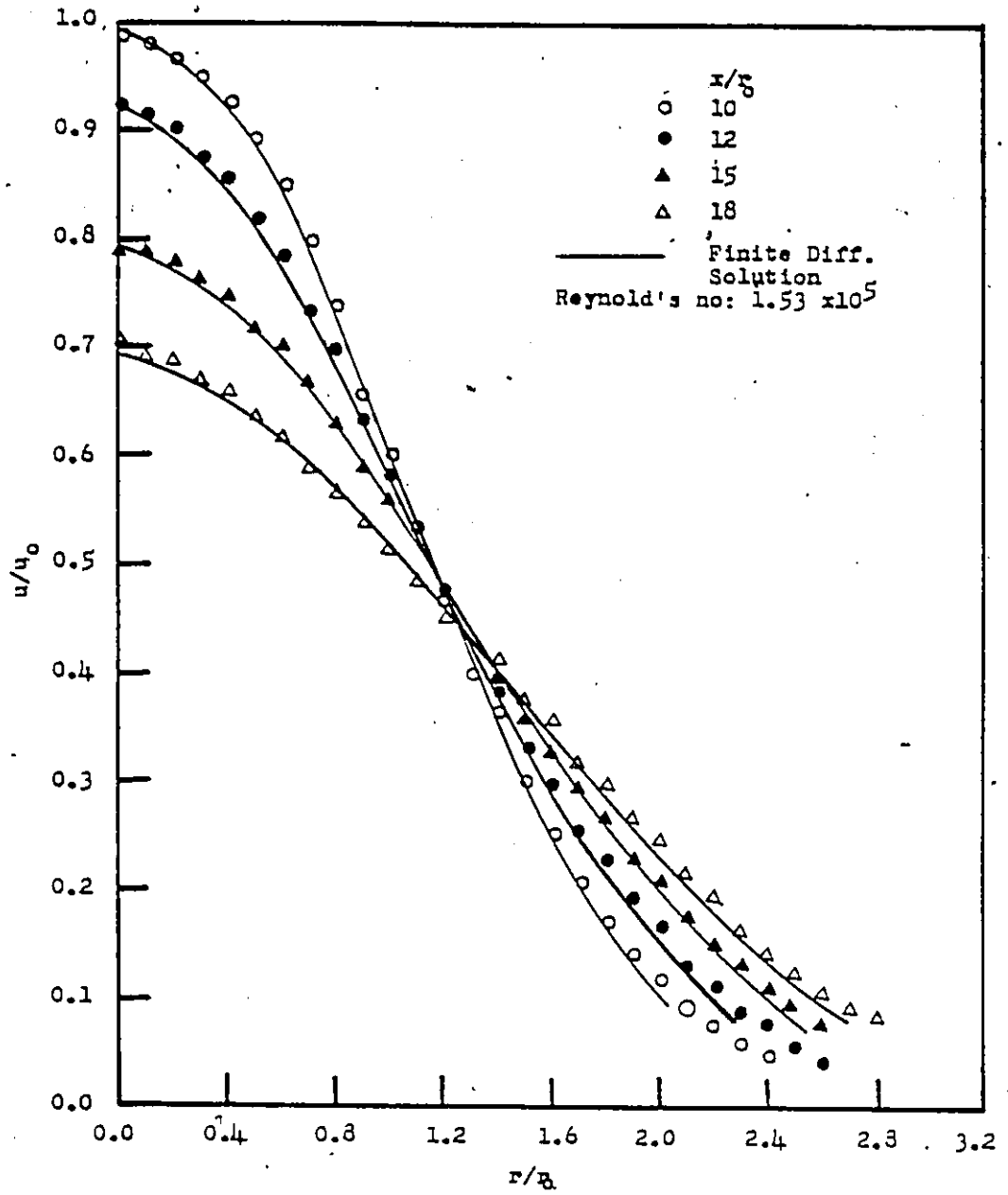


Fig.5.21

Calculated and Experimental Mean Axial Velocity Distributions in the Transition Region.



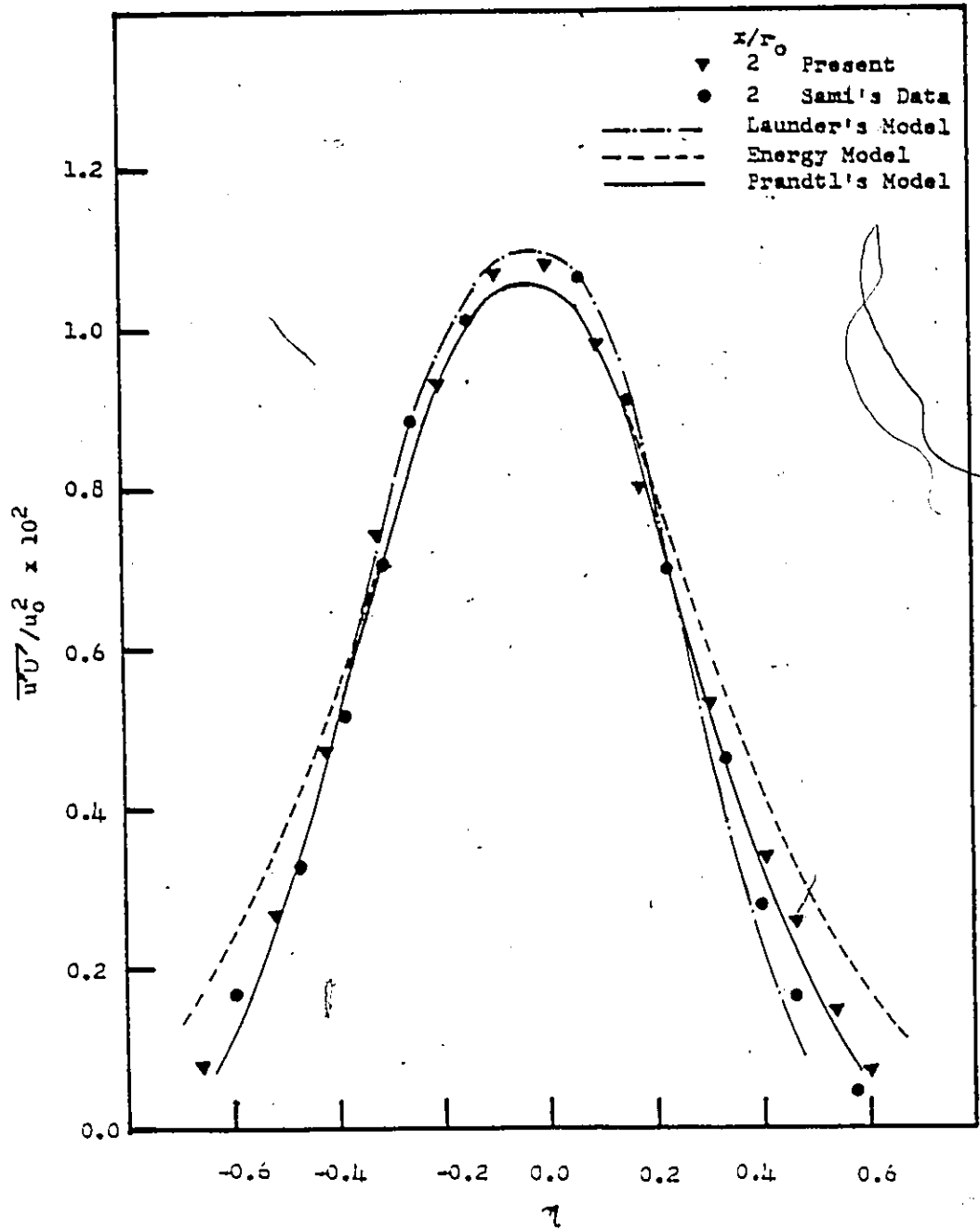


Fig.5.22

Comparison of Shear Stress Models and Measurements,

Thin Boundary Layer,  $x/r_0 = 2.$

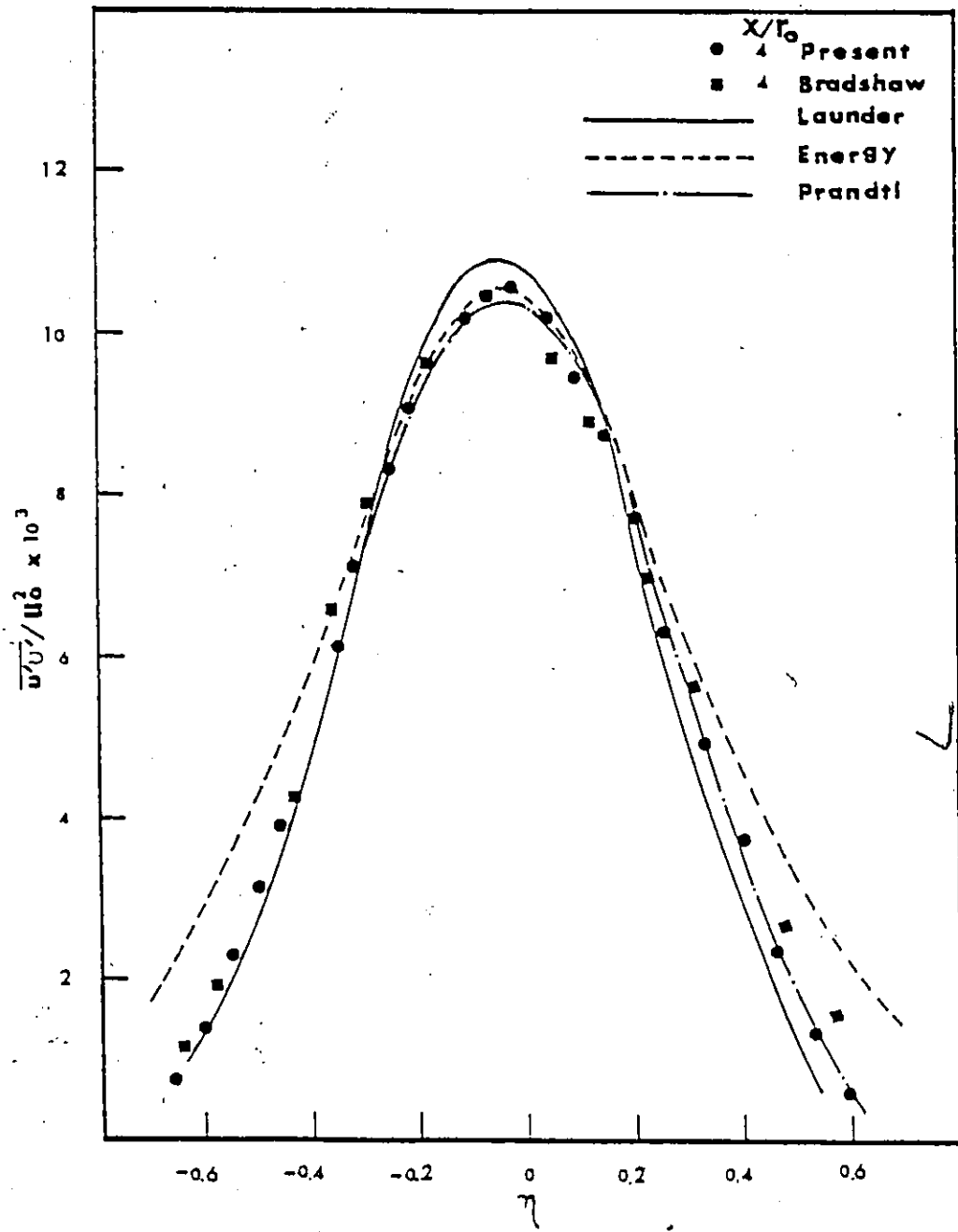


Fig.5.23.

Comparison of Shear Stress Models and Measurements, Thin Boundary Layer,  $x/r_0 = 4$ .

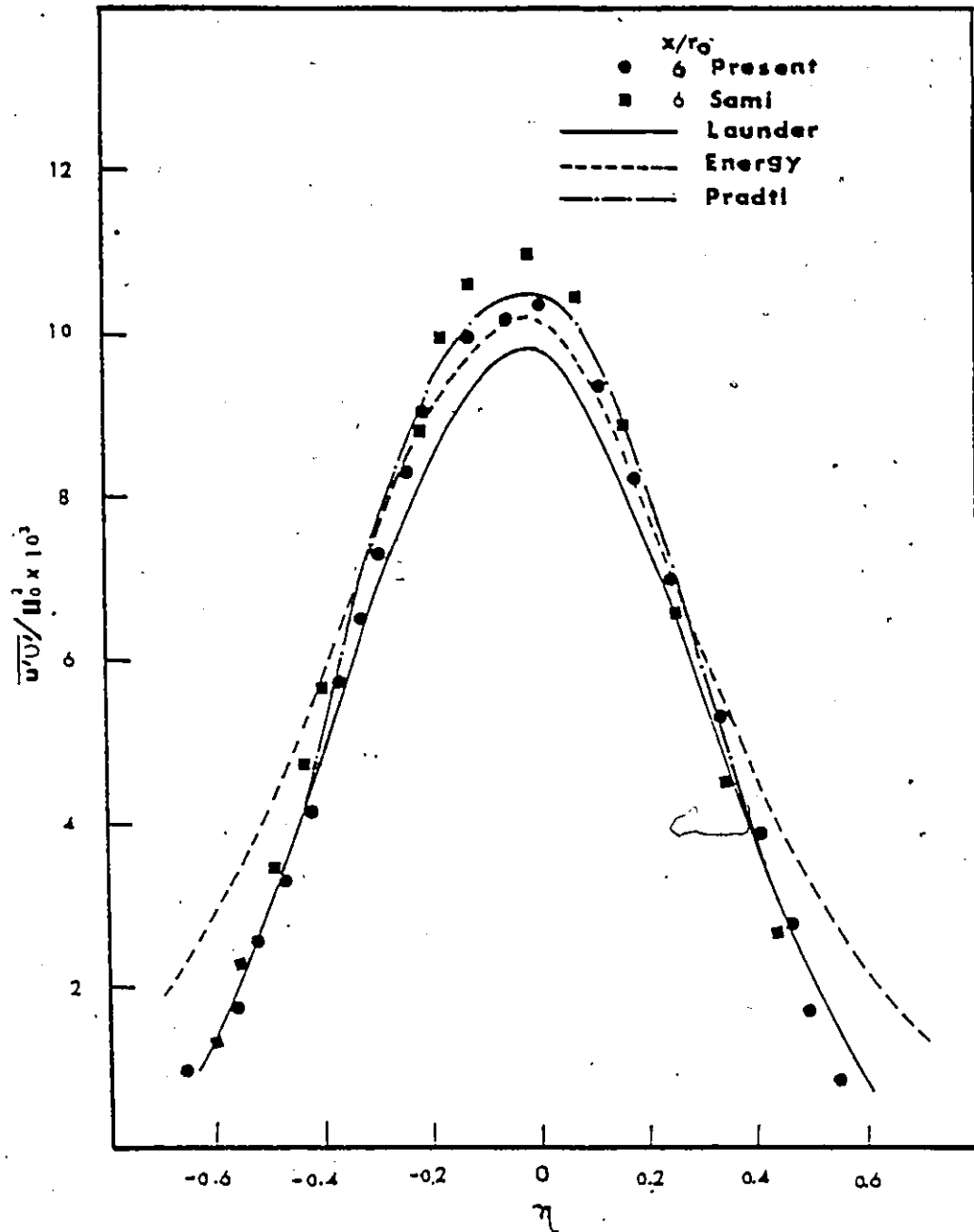


Fig.5.24.

Comparison of Shear Stress Models and  
Measurements, Thin Boundary Layer,  $x/r_0 = 6$ .

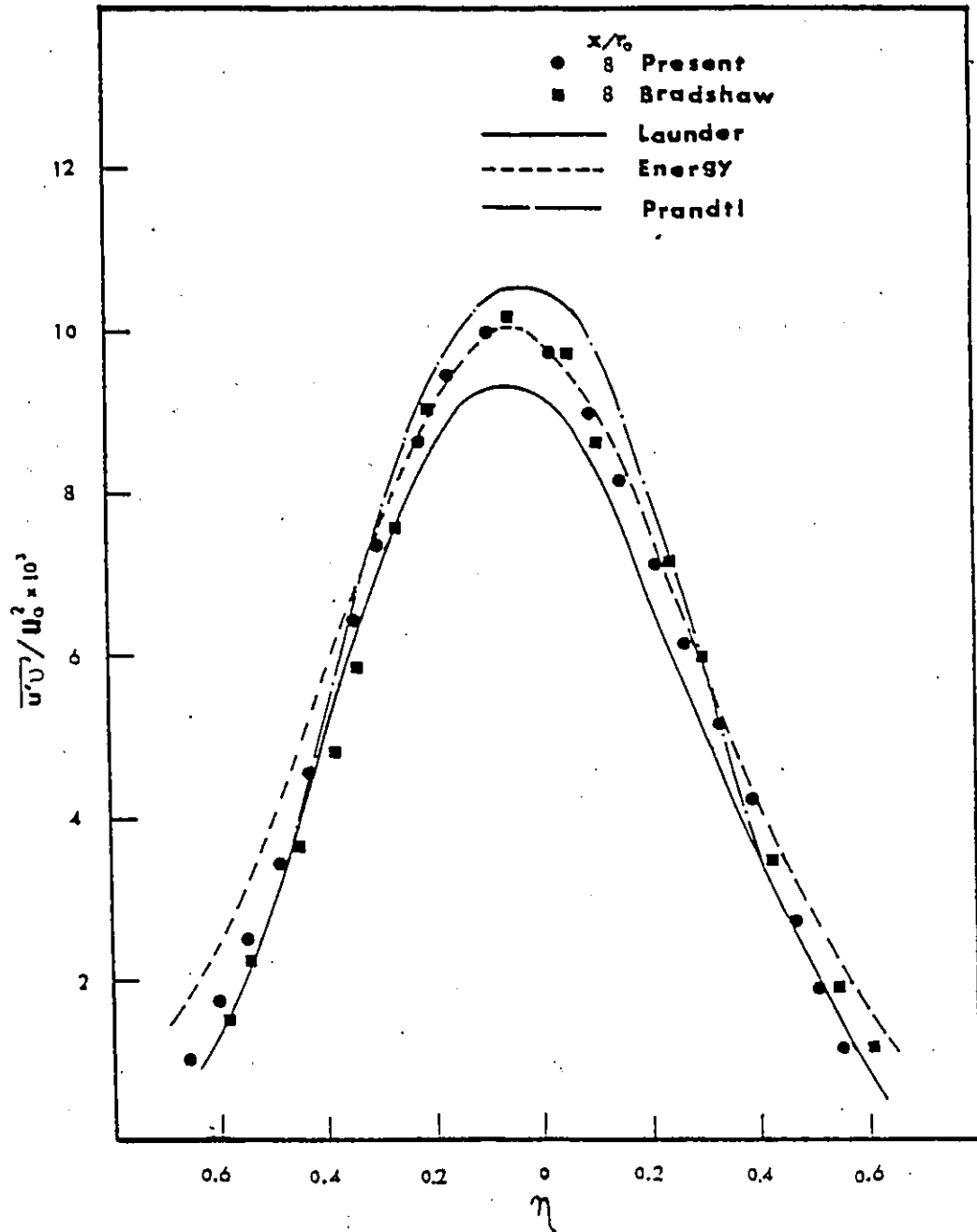


Fig.5.25.

Comparison of Shear Stress Models and Measurements, Thin Boundary Layer,  $x/r_0 = 8$ .

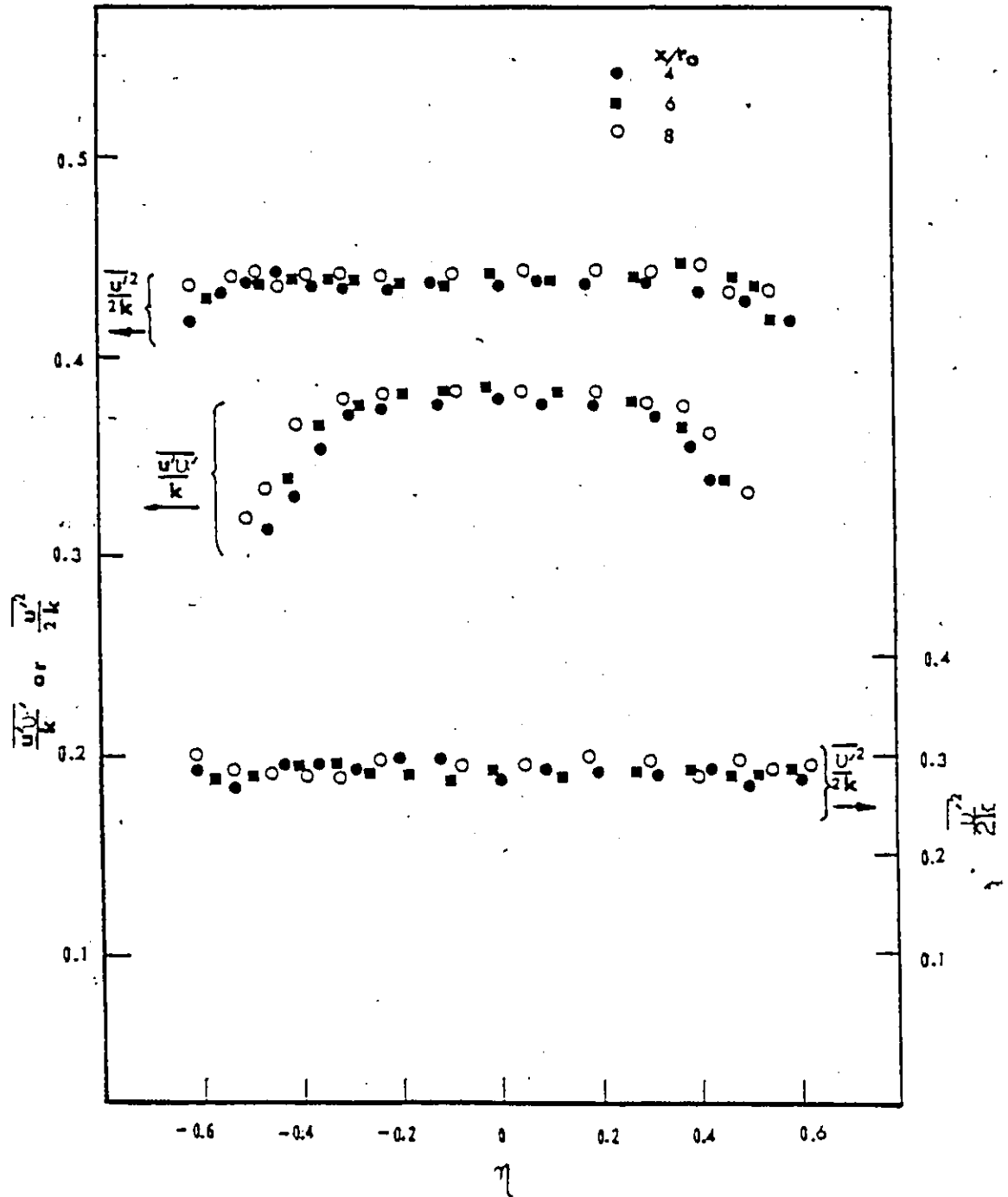


Fig.5.26.

Experimental Values of  $\frac{u'^2}{2k}$ ,  $\frac{u^2}{2k}$  and  $\frac{u'u'}{k}$  in the Initial Region.

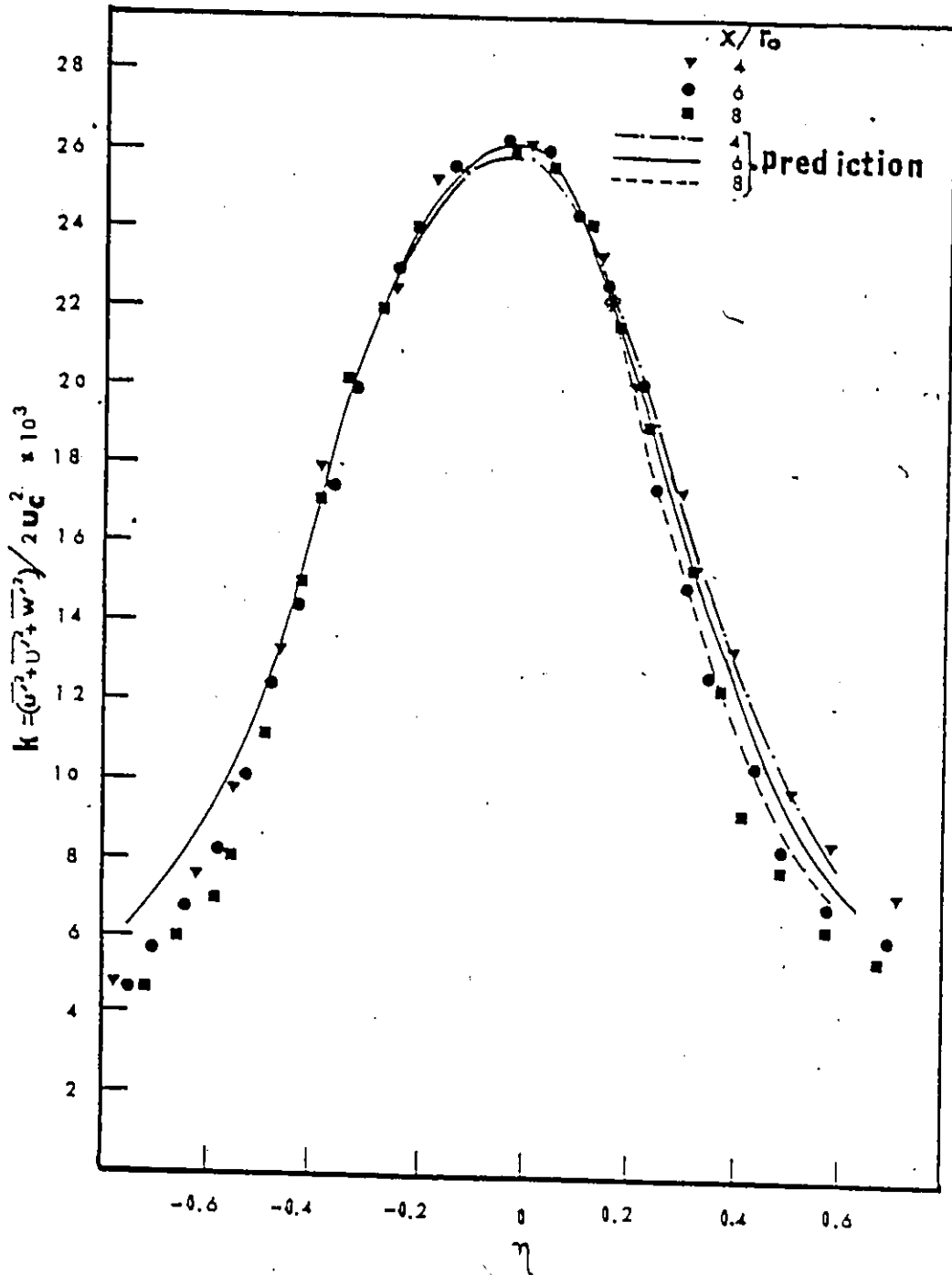


Fig.5.27.

Calculated and Experimental Turbulent Kinetic Energy Distributions, Thin Boundary Layer.

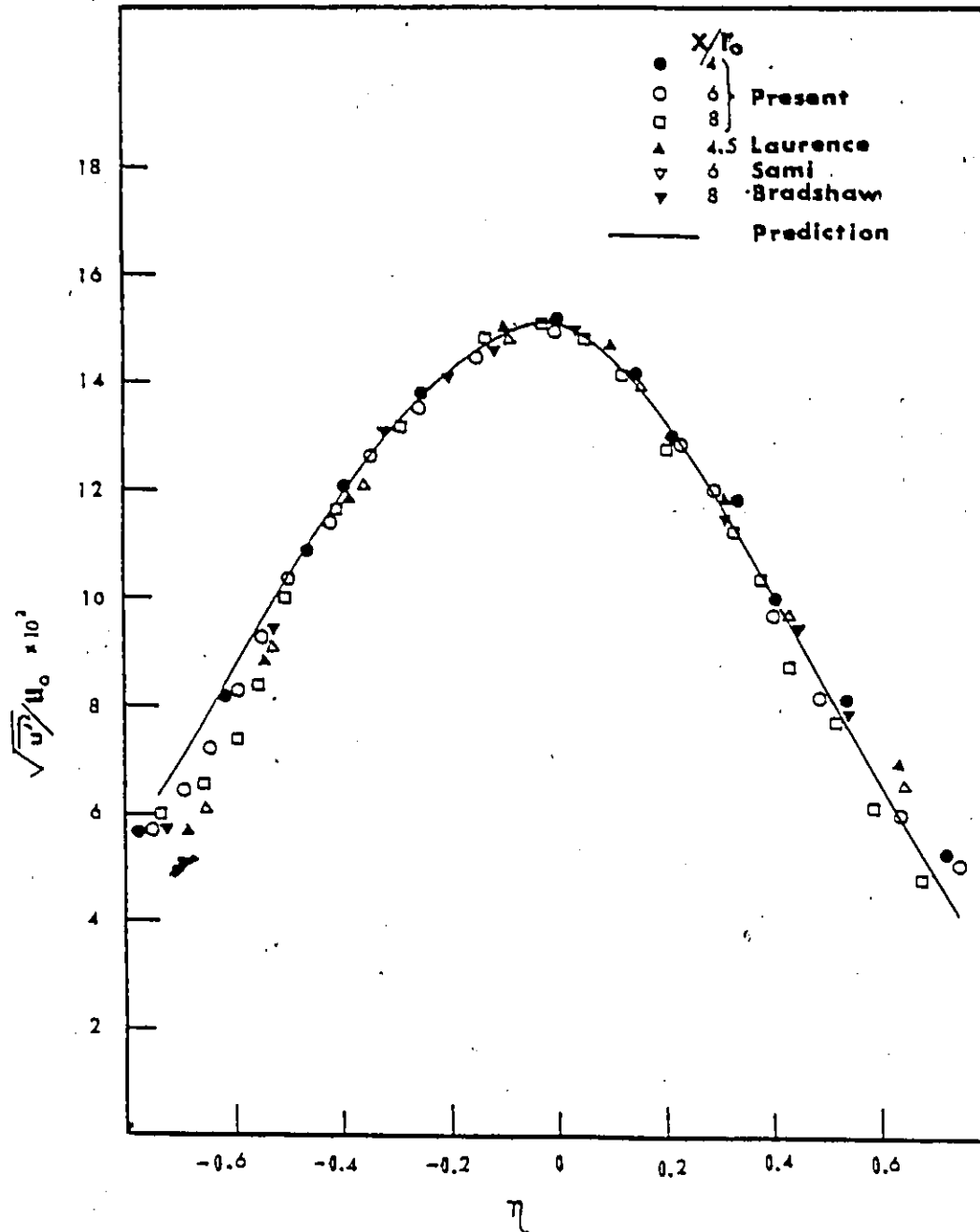


Fig.5.28.

Calculated and Experimental Turbulent Axial Intensity Distributions, Thin Boundary Layer.

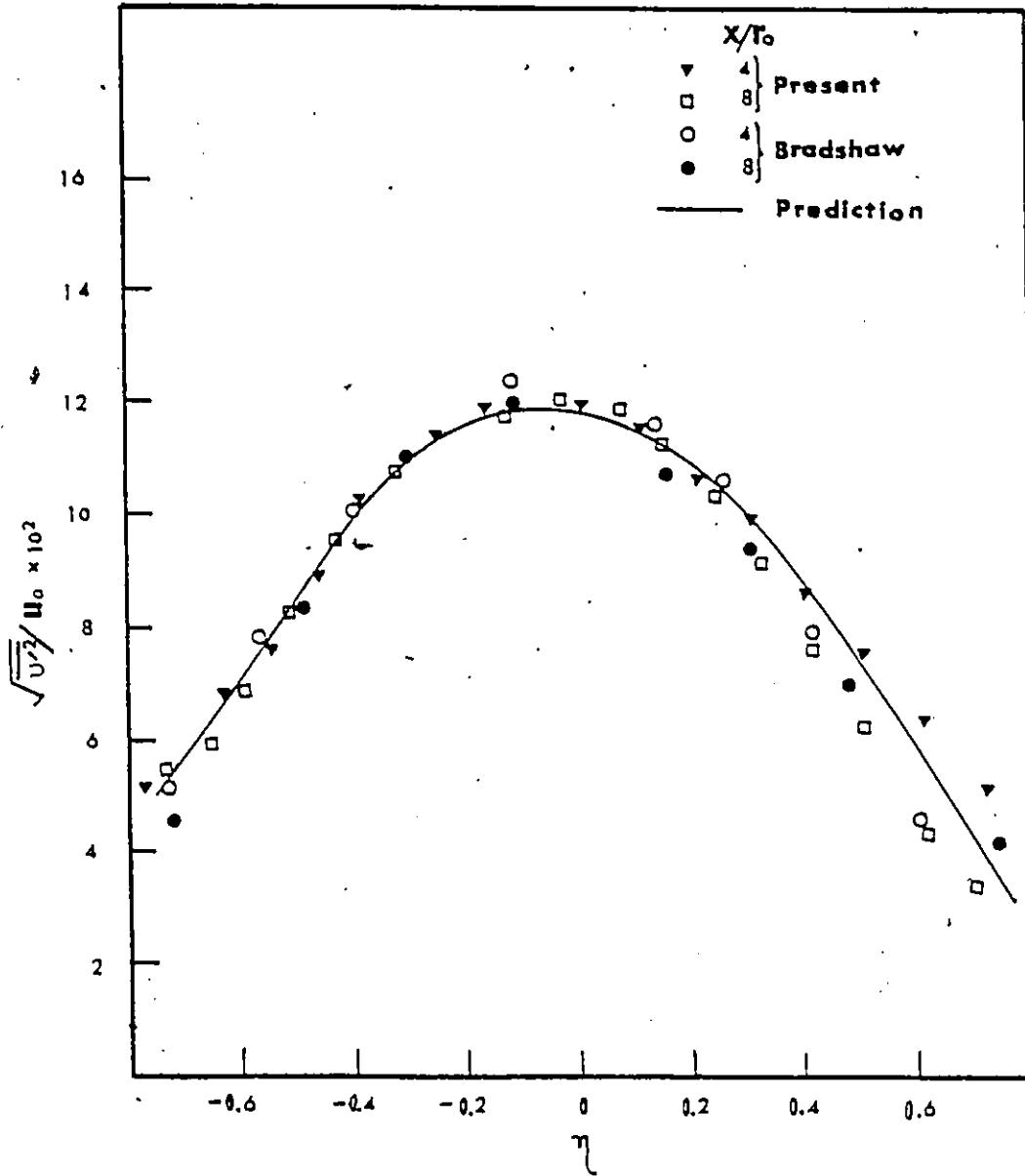


Fig.5.29.

Calculated and Experimental Turbulent Radial Intensity Distributions, Thin Boundary Layer.



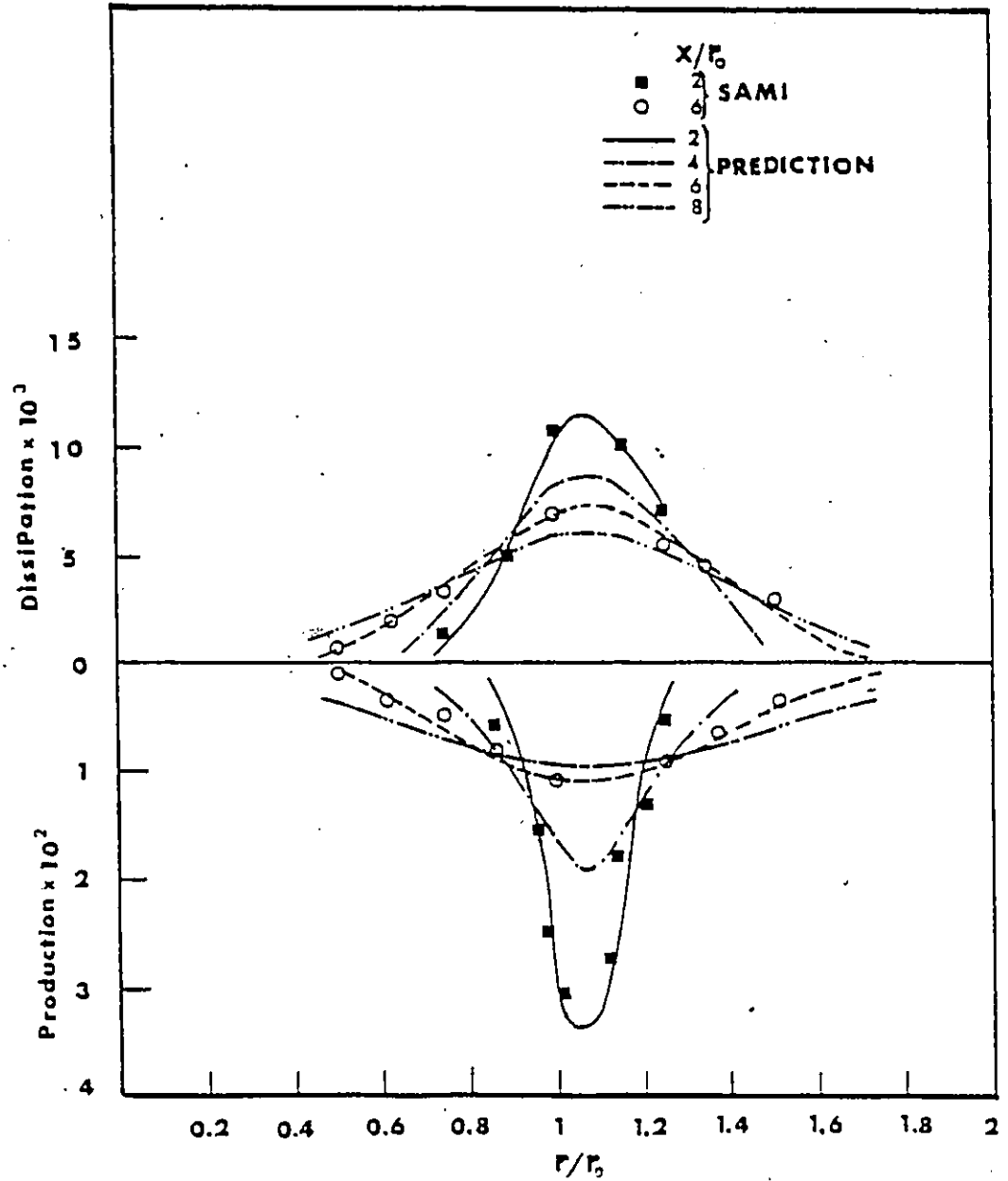


Fig.5.30.

Calculated and Experimental Production and Dissipation of Turbulent Energy Distributions, Thin Boundary Layer.

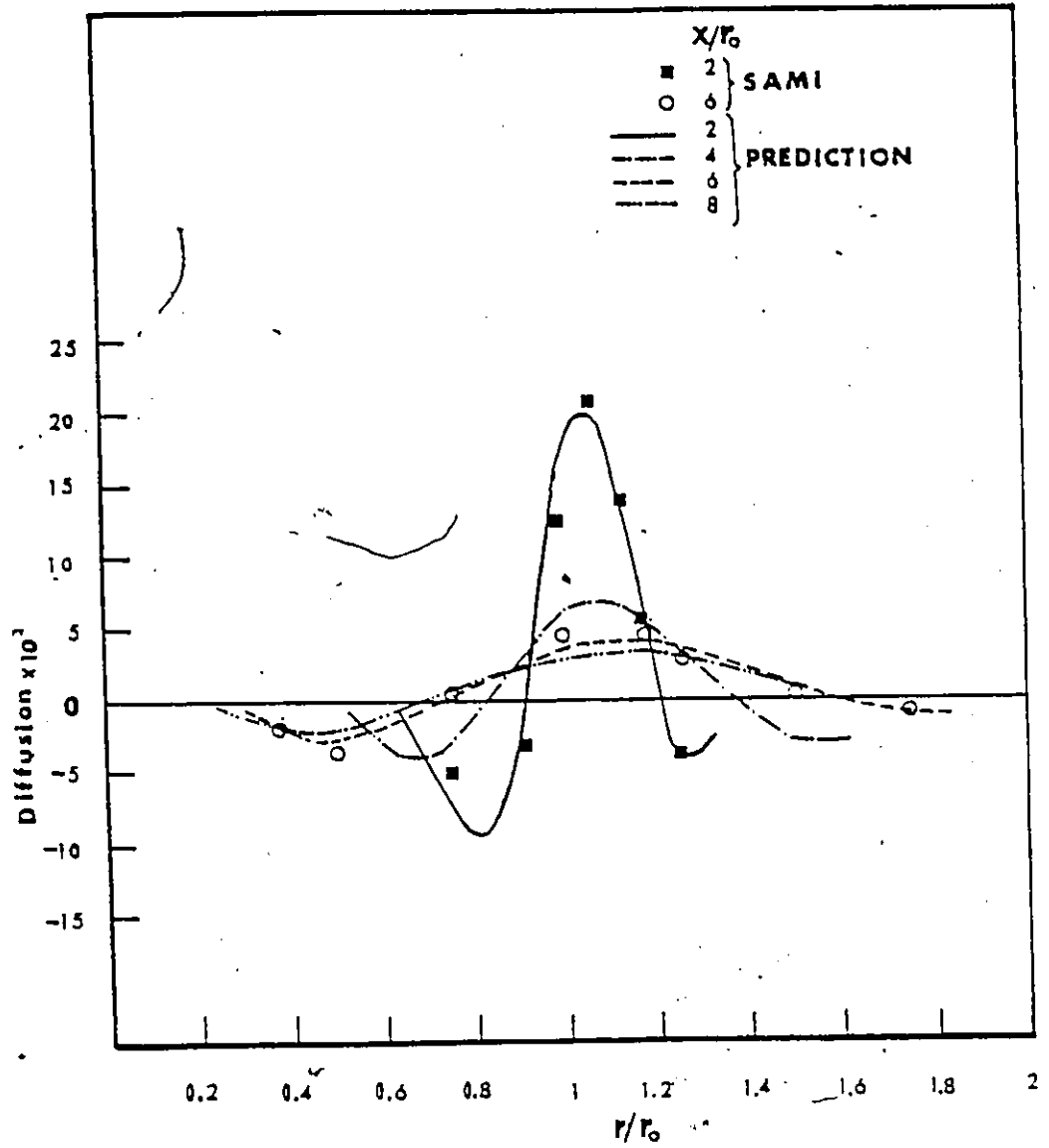


Fig.5.31.

Calculated and Experimental Diffusion of  
Turbulent Energy Distributions, Thin Boundary Layer.

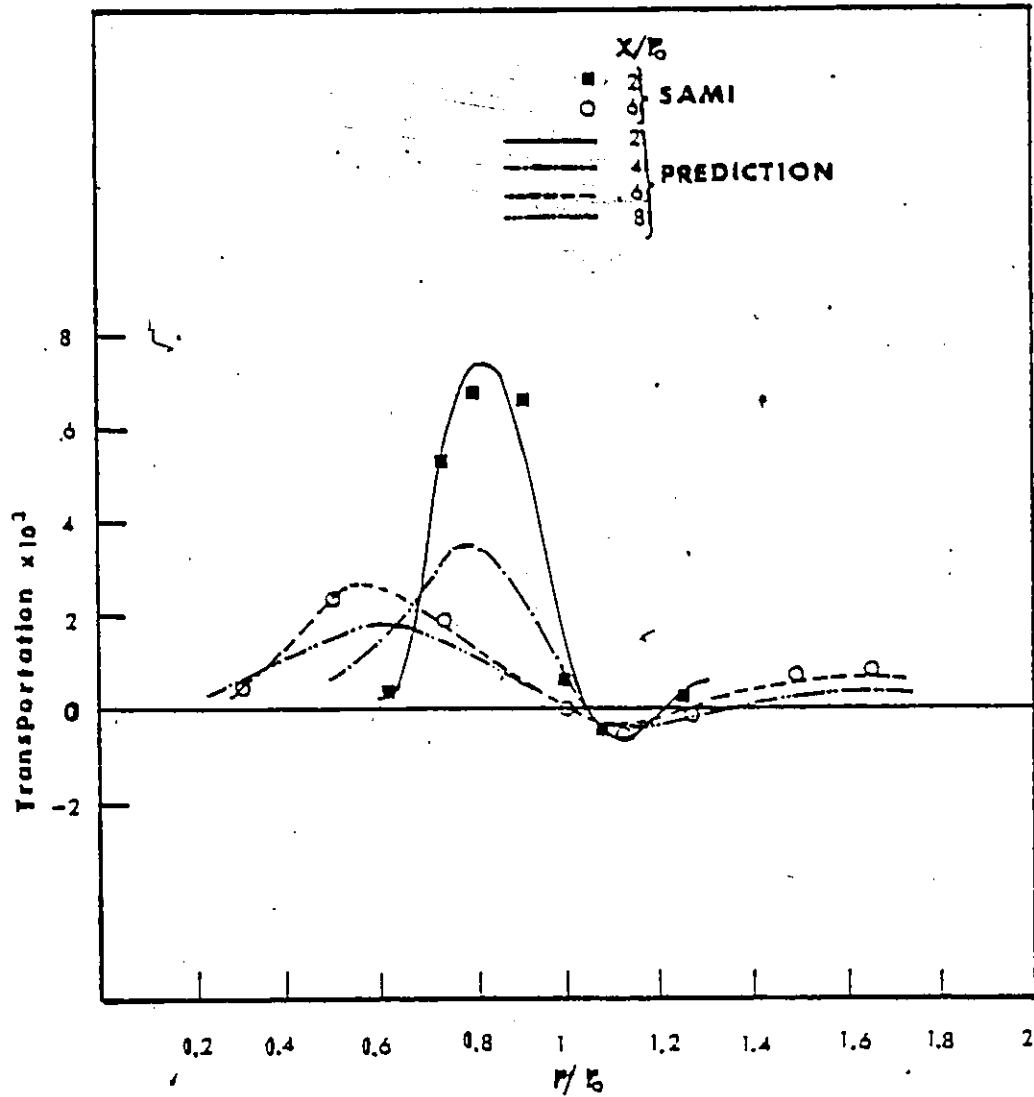


Fig.5.32.

Calculated and Experimental Convective Transport  
of Turbulent Energy Distributions, Thin Boundary Layer.

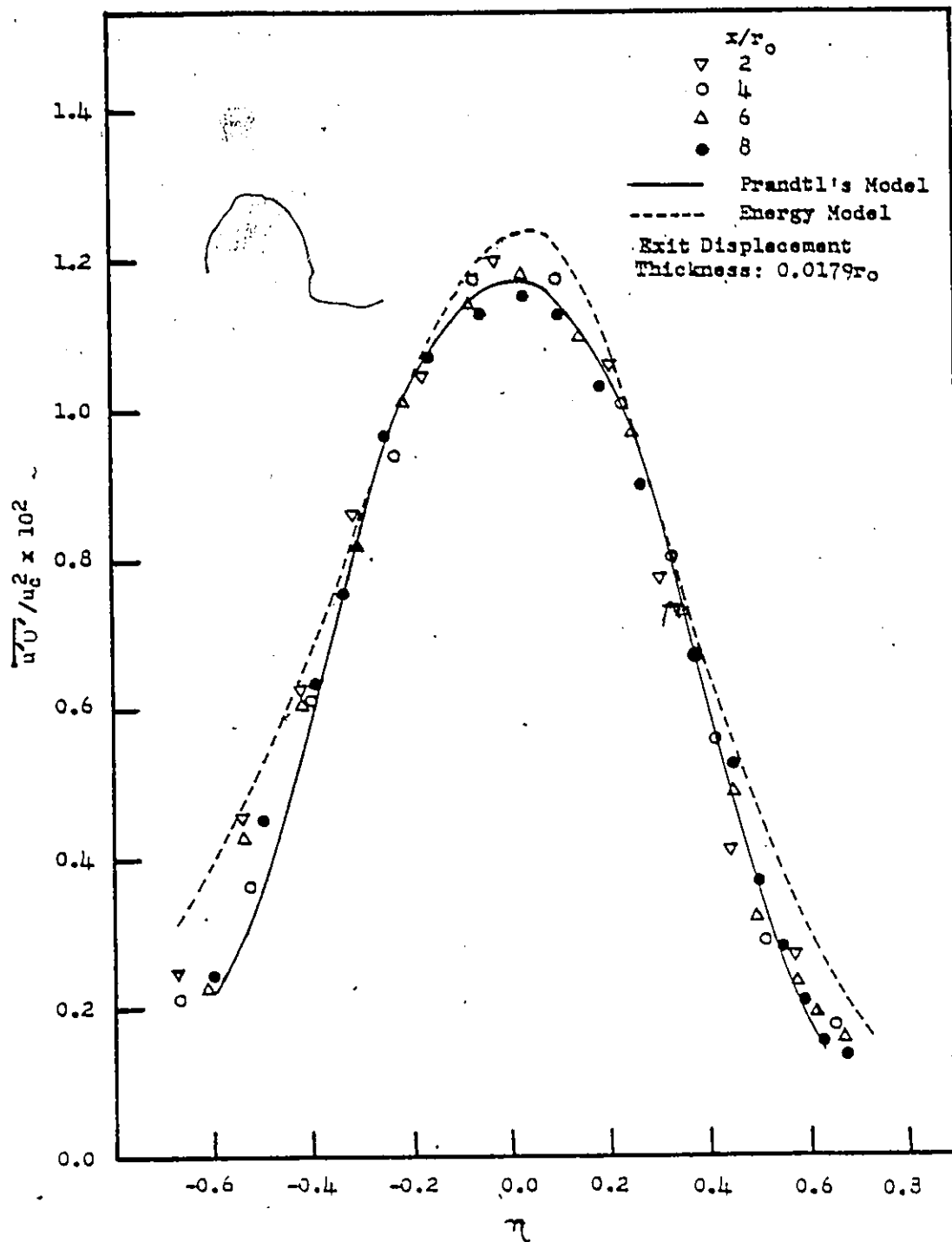


Fig.5.33

Calculated and Experimental Shear Stress Distributions, Intermediate Boundary Layer.

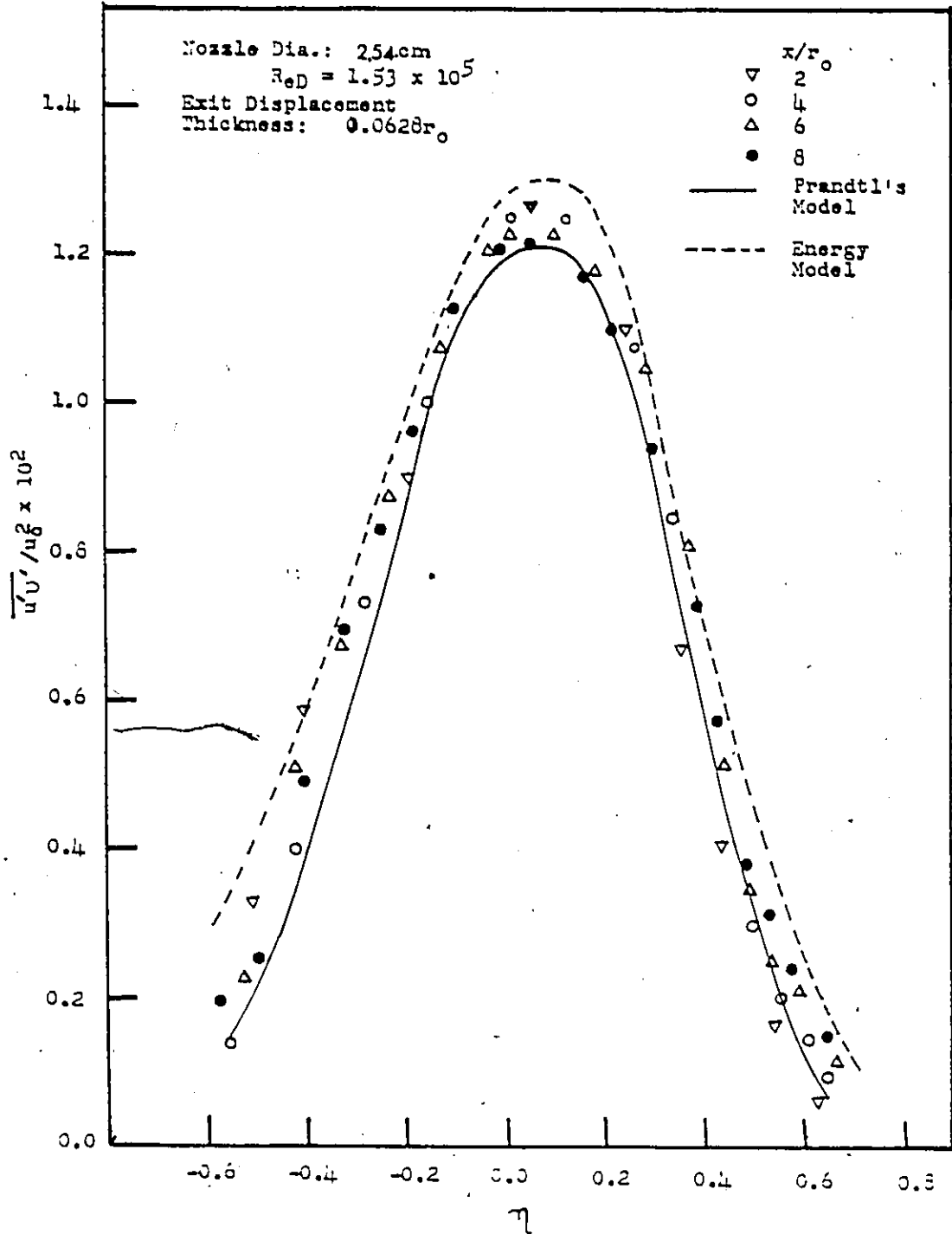


Fig. 5.34

Calculated and Experimental Shear Stress Distributions,  
 Thick Boundary Layer.

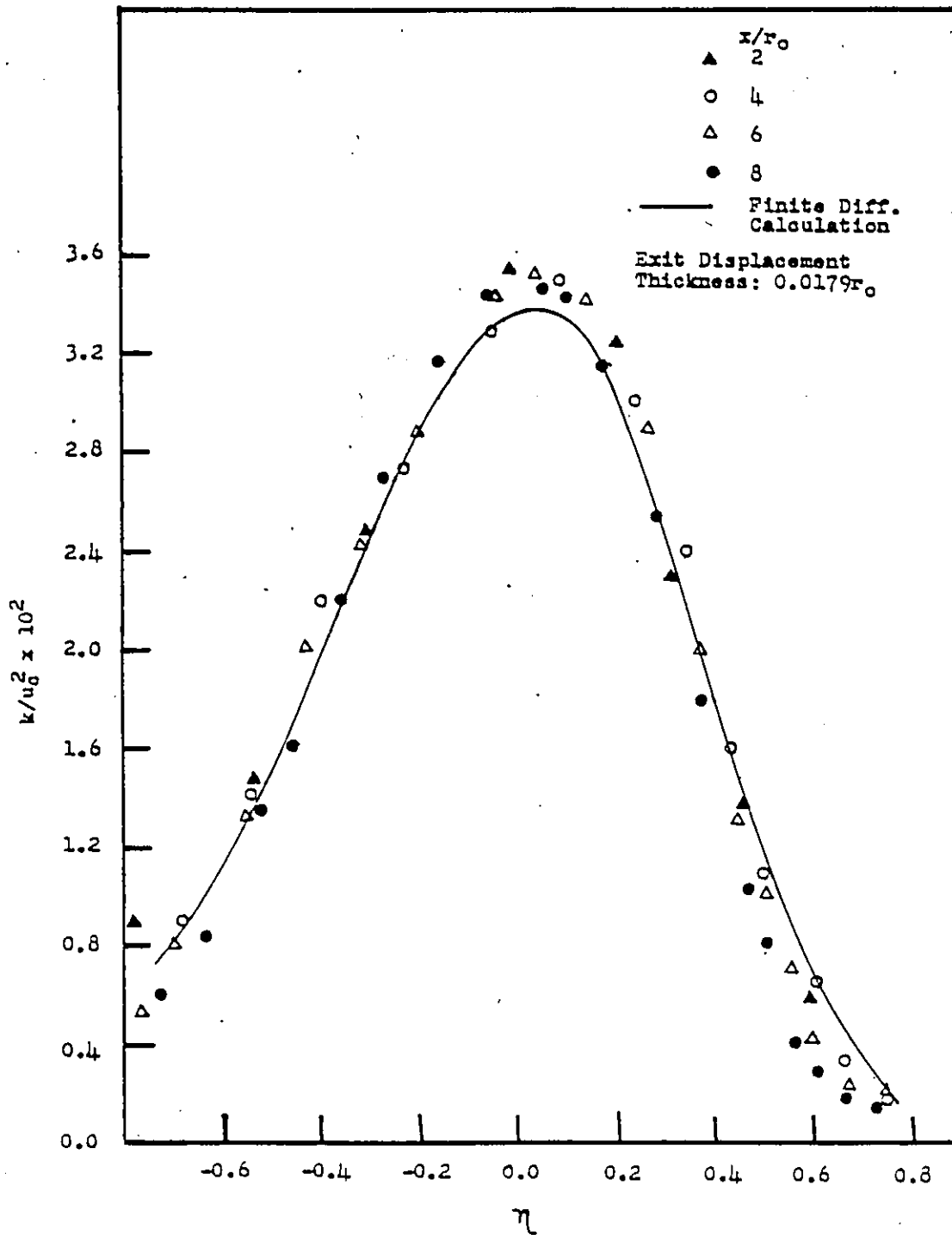


Fig.5.35

Calculated and Experimental Turbulent Kinetic Energy Distributions, Intermediate Boundary Layer.

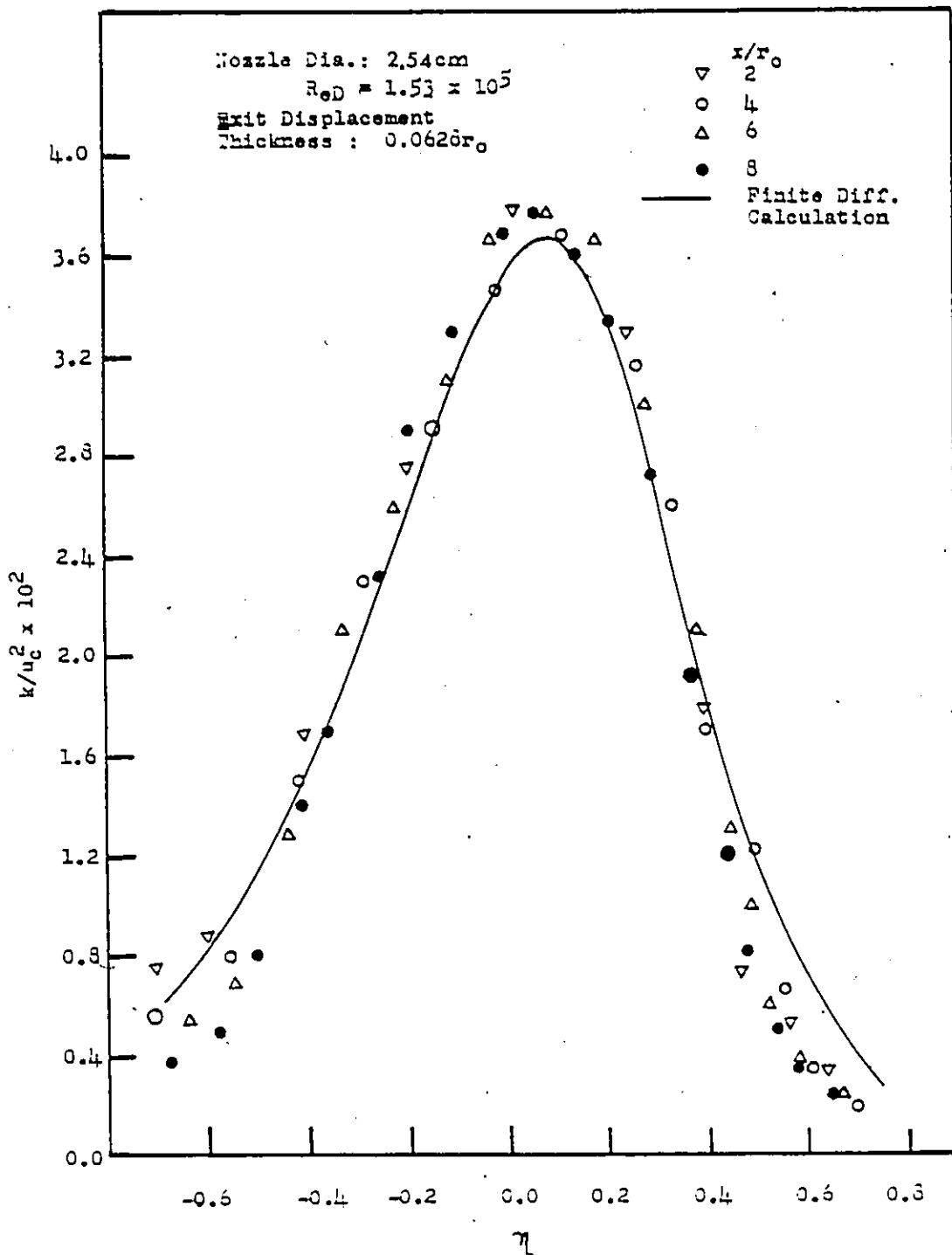


Fig.5.36

Calculated and Experimental Turbulent Kinetic Energy

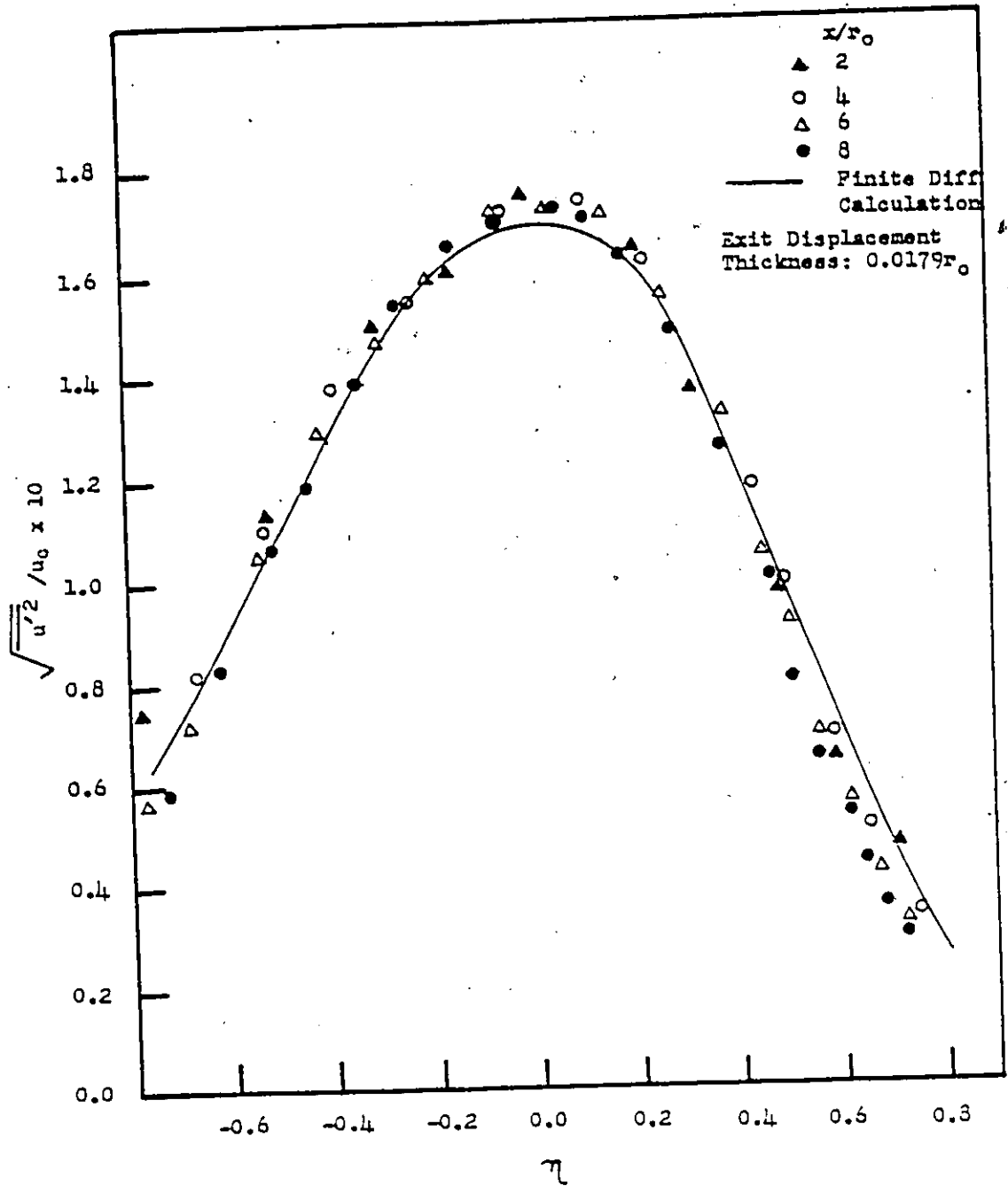


Fig.5.37

Calculated and Experimental Turbulent Axial Intensity Distributions, Intermediate Boundary Layer.



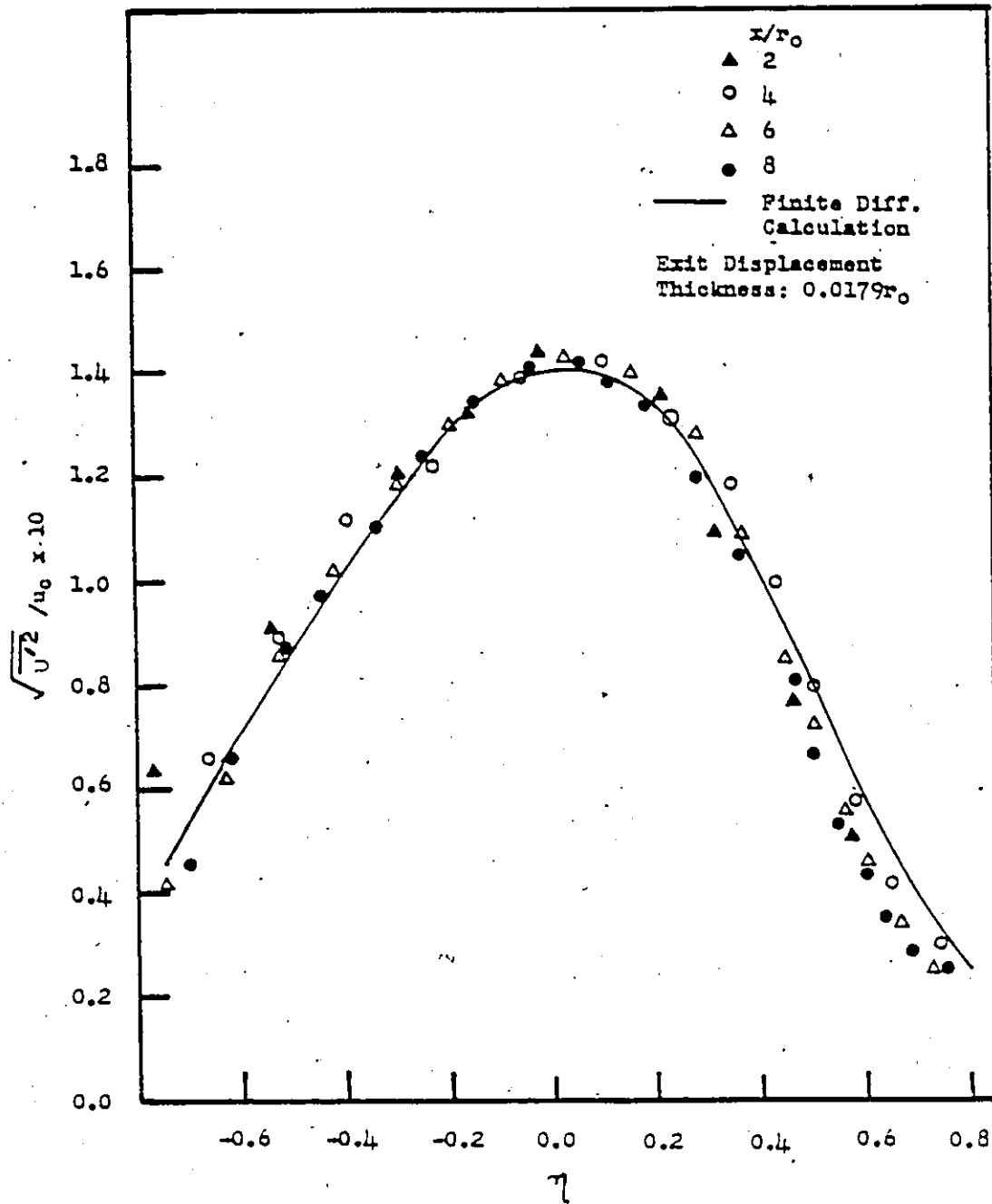


Fig.5.38

Calculated and Experimental Turbulent Radial Intensity Distributions, Intermediate Boundary Layer.

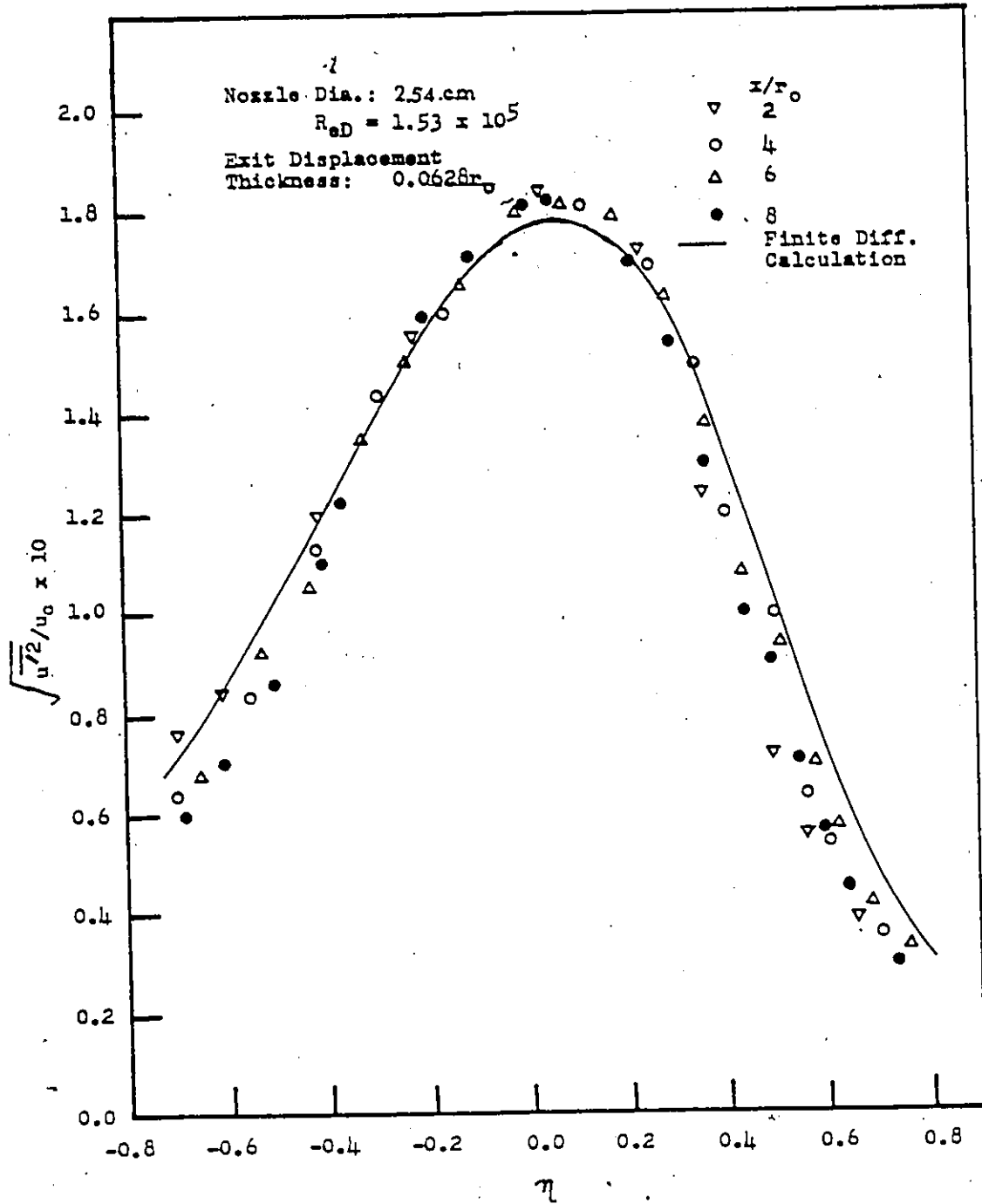


Fig.5.39

Calculated and Experimental Turbulent Axial Intensity Distributions, Thick Boundary Layer.

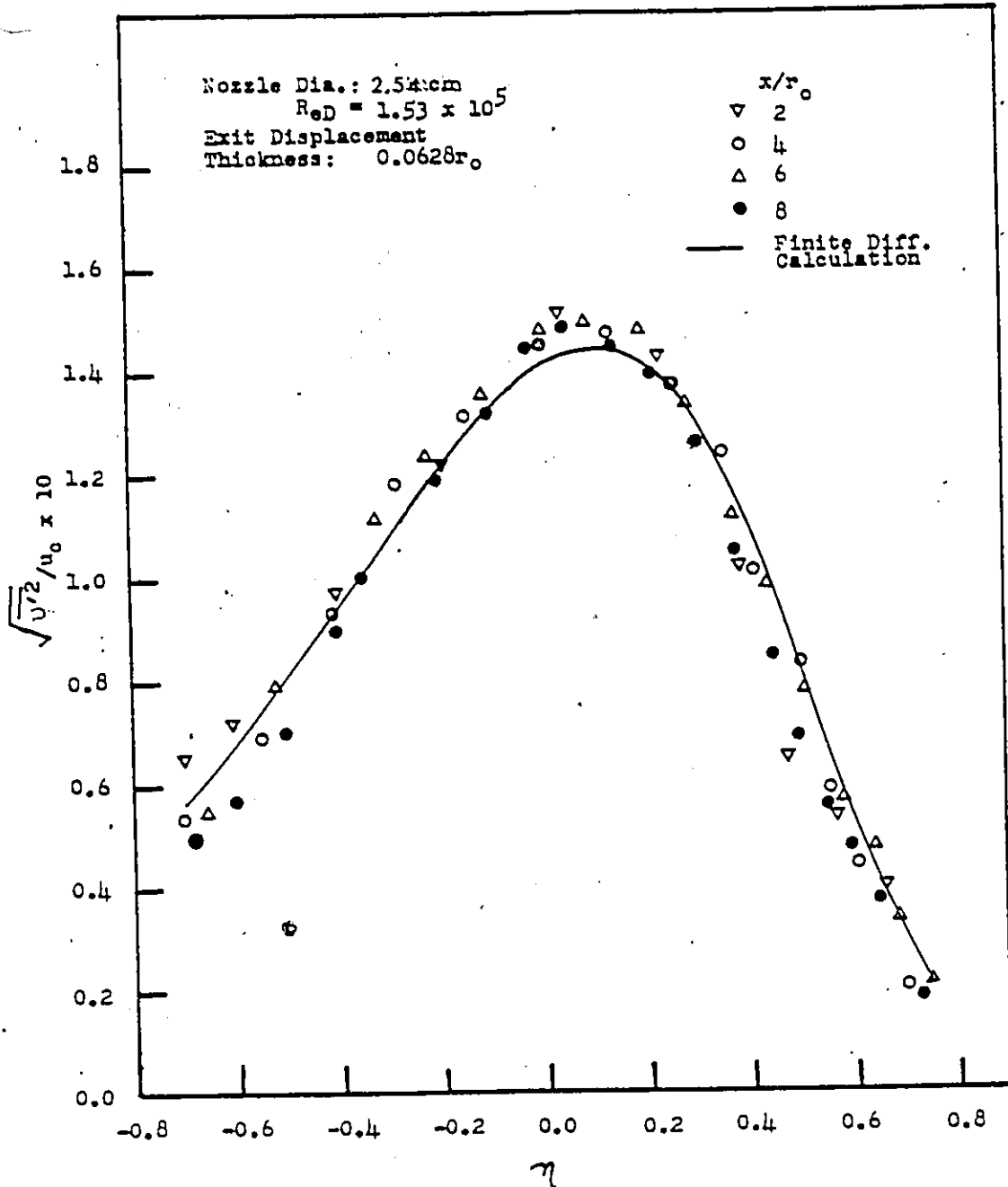


Fig. 5.40

Calculated and Experimental Turbulent Radial  
 Intensity Distributions, Thick Boundary Layer.

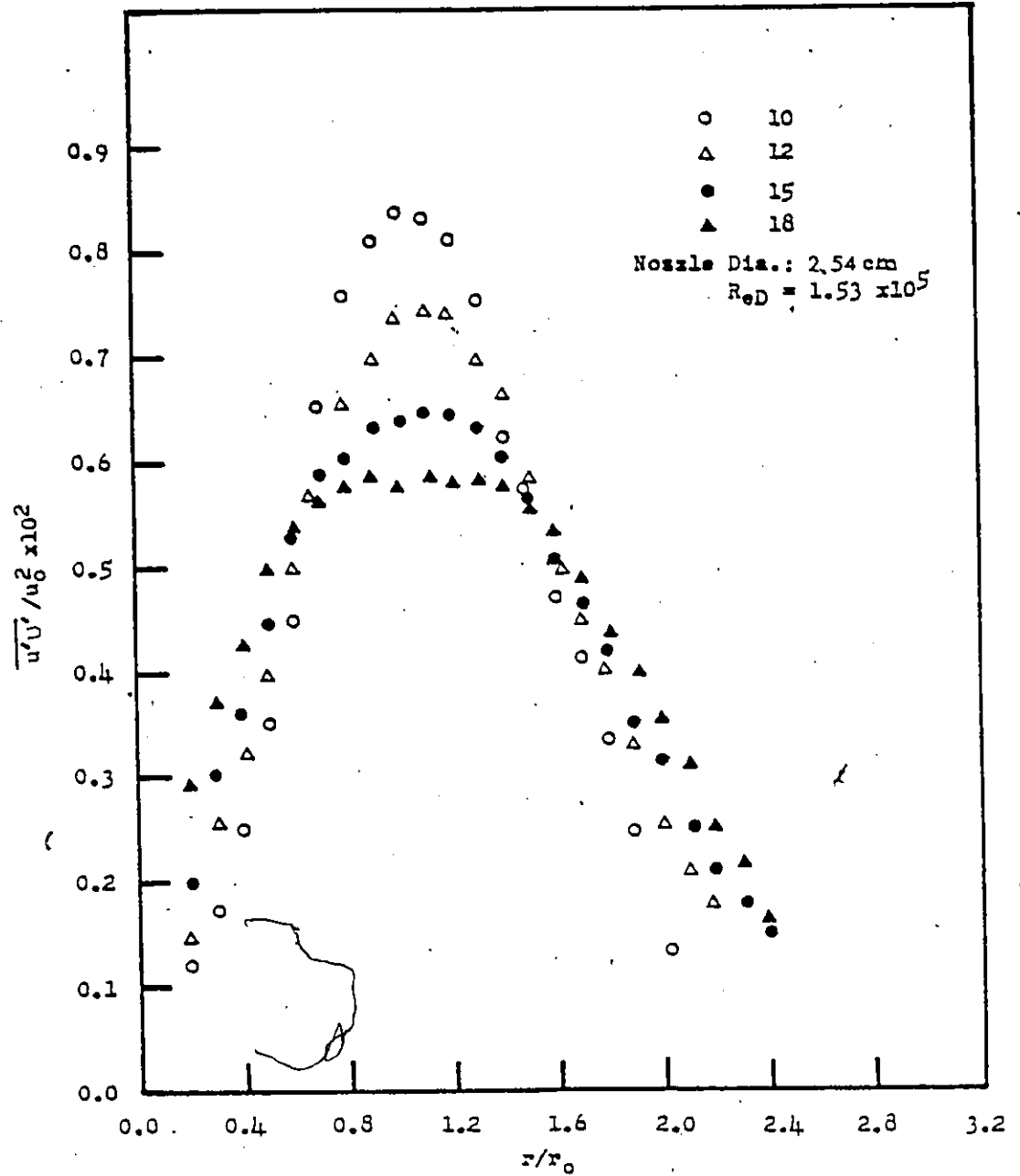


Fig.5.41

Experimental Turbulent Shear-Stress Distributions  
in the Transition Region.

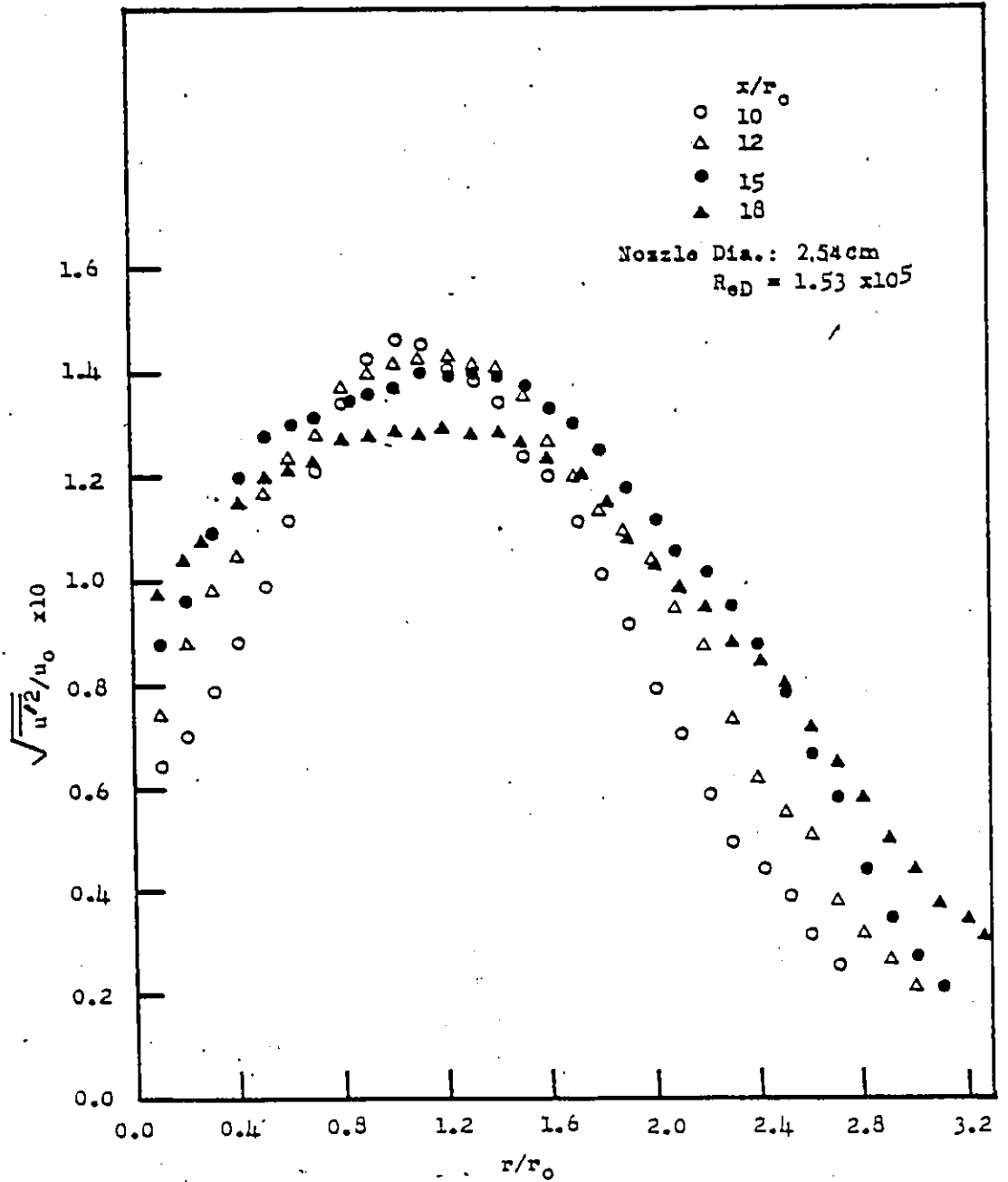


Fig.5.42

Experimental Turbulent  $x$ -Intensity Distributions  
in the Transition Region.

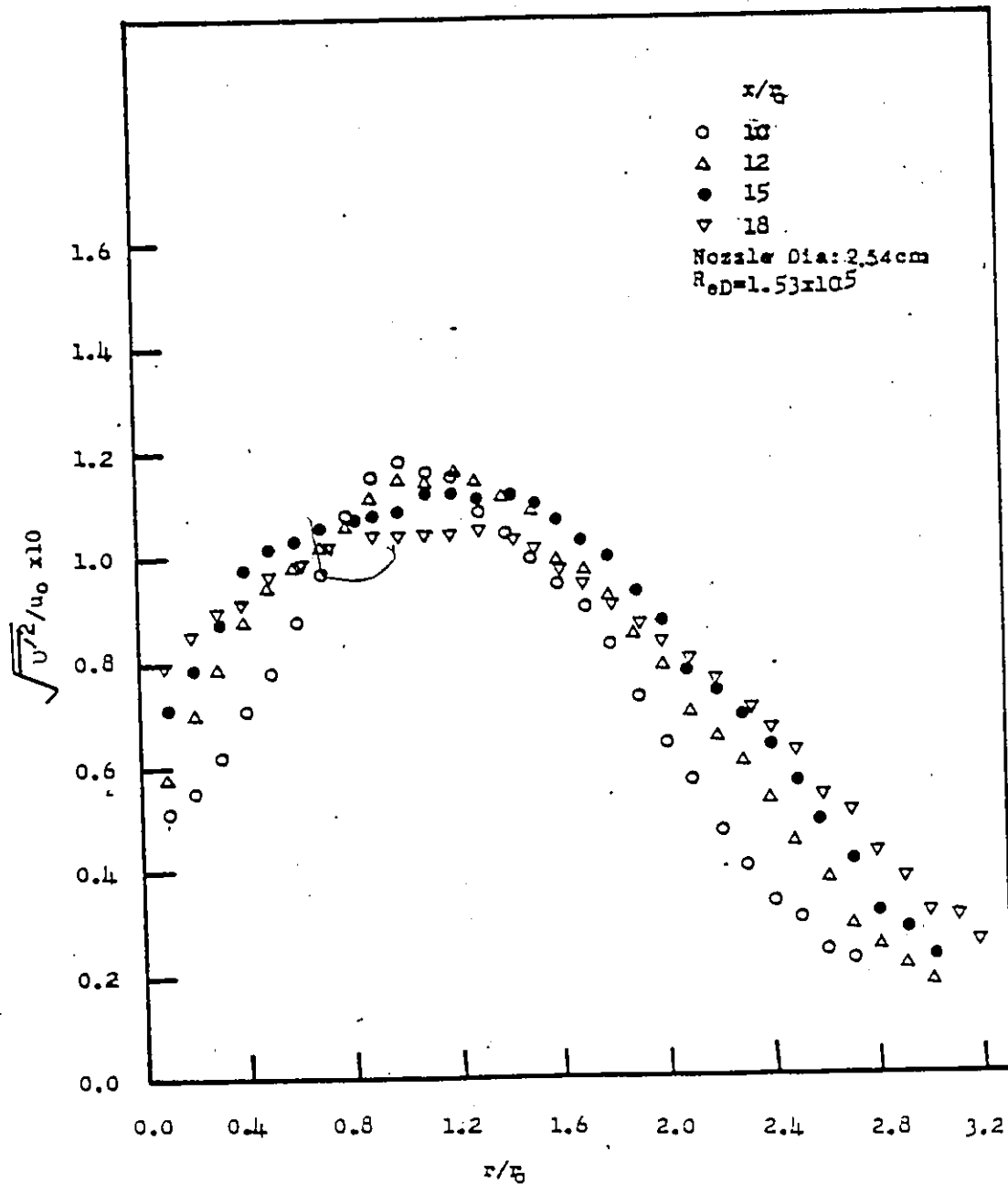


Fig.5.43

Experimental Turbulent  $r$ -Intensity Distributions  
in the Transition Region.

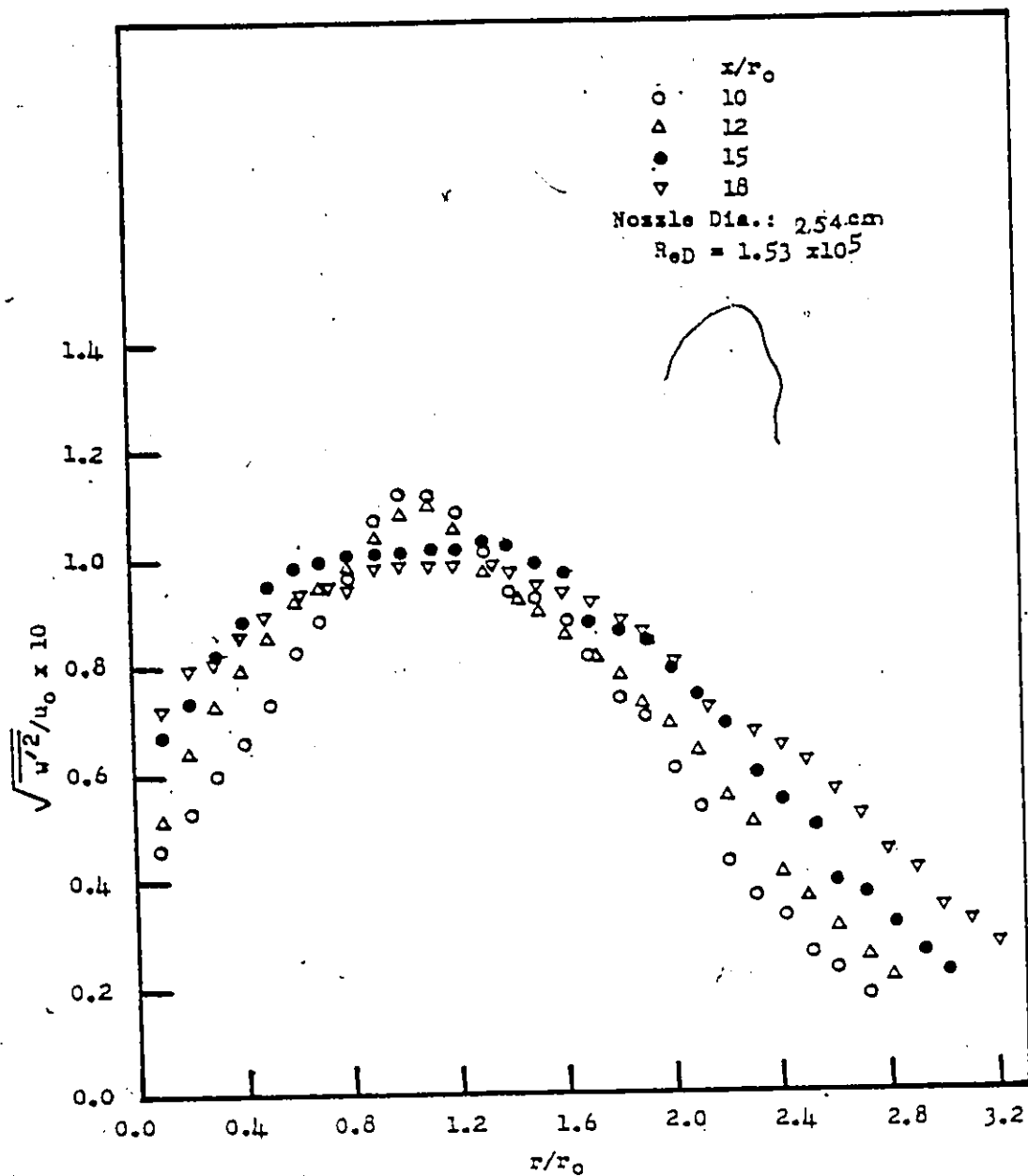


Fig.5.44

Experimental Turbulent 3-Intensity Distributions  
in the Transition Region.

APPENDICES



## APPENDIX A

### DERIVATION OF EQUATIONS

#### A.1 Differential Equations

Turbulent flow is governed by the continuity equation and the Navier-Stokes equations. In cylindrical co-ordinates the mass conservation equation for incompressible flow field is:

$$\frac{\partial u^{\circ}}{\partial x} + \frac{1}{r} \frac{\partial}{\partial r} (r v^{\circ}) + \frac{1}{r} \frac{\partial w^{\circ}}{\partial \theta} = 0 \quad (\text{A.1})$$

The co-ordinate system is given in Figure 1.1 and  $u^{\circ}$ ,  $v^{\circ}$  and  $w^{\circ}$  are instantaneous velocity components in x, r and  $\theta$  directions respectively. Splitting instantaneous variables into mean and fluctuating components:

$$\left. \begin{aligned} u^{\circ} &= u + u' \\ v^{\circ} &= v + v' \\ w^{\circ} &= w' \\ p^{\circ} &= p + p' \end{aligned} \right\} \quad (\text{A.2})$$

where  $u$  and  $v$  are mean components and  $u'$ ,  $v'$  and  $w'$  are the fluctuating components of the instantaneous velocity. The instantaneous pressure  $p^{\circ}$  has a mean and a fluctuating component,  $p$  and  $p'$ , respectively.

Introducing Equation (A.2) in Equation (A.1):

$$\frac{\partial}{\partial x} (u+u') + \frac{1}{r} \frac{\partial}{\partial r} [r(v+v')] + \frac{1}{r} \frac{\partial w'}{\partial \theta} = 0 \quad (\text{A.3})$$

taking a time average,

$$\frac{\partial u}{\partial x} + \frac{1}{r} \frac{\partial}{\partial r} (ur) = 0 \quad (\text{A.4})$$

Subtracting Equation (A.4) from Equation (A.3),

$$\frac{\partial u'}{\partial x} + \frac{1}{r} \frac{\partial}{\partial r} (ru') + \frac{1}{r} \frac{\partial w'}{\partial \theta} = 0 \quad (\text{A.5})$$

Writing the Navier-Stokes equations in cylindrical co-ordinates for incompressible flow in absence of body forces [89],

$$\left. \begin{aligned} \text{x-component:} \quad & \rho \frac{Du^0}{Dt} = -\frac{\partial p^0}{\partial x} - \left[ \frac{1}{r} \frac{\partial}{\partial r} (r\tau_{rx}) + \frac{1}{r} \frac{\partial \tau_{r\theta}}{\partial \theta} + \frac{\partial \tau_{xx}}{\partial x} \right] \\ \text{r-component:} \quad & \rho \left( \frac{Du^0}{Dt} - \frac{w^{02}}{r} \right) = -\frac{\partial p^0}{\partial r} - \left[ \frac{1}{r} \frac{\partial}{\partial r} (r\tau_{rr}) + \frac{1}{r} \frac{\partial \tau_{r\theta}}{\partial \theta} \right. \\ & \left. - \frac{\tau_{\theta\theta}}{r} + \frac{\partial \tau_{rx}}{\partial x} \right] \\ \theta\text{-component:} \quad & \rho \left( \frac{Dw^0}{Dt} + \frac{u^0 w^0}{r} \right) = -\frac{1}{r} \frac{\partial p^0}{\partial \theta} - \left[ \frac{1}{r^2} \frac{\partial}{\partial r} (r^2 \tau_{r\theta}) + \frac{1}{r} \frac{\partial \tau_{\theta\theta}}{\partial \theta} \right. \\ & \left. + \frac{\partial \tau_{\theta x}}{\partial x} \right] \end{aligned} \right\} \quad (\text{A.6})$$

All  $\tau$ 's are stresses on fluid elements and their expressions for incompressible flow with constant viscosity,  $\mu$ , are:

$$\left. \begin{aligned} \tau_{xx} = -2\mu \frac{\partial u^0}{\partial x} ; \quad \tau_{rr} = -2\mu \frac{\partial u^0}{\partial r} ; \quad \tau_{\theta\theta} = -\mu \left[ \frac{2}{r} \frac{\partial w^0}{\partial \theta} + \frac{u^0}{r} \right] \\ \tau_{xr} = \tau_{rx} = -\mu \left[ \frac{\partial u^0}{\partial r} + \frac{\partial u^0}{\partial x} \right] ; \quad \tau_{r\theta} = \tau_{\theta r} = -\mu \left[ r \frac{\partial}{\partial r} \left( \frac{w^0}{r} \right) + \frac{1}{r} \frac{\partial u^0}{\partial \theta} \right] \\ \text{and} \quad \tau_{\theta z} = \tau_{z\theta} = -\mu \left[ \frac{\partial w^0}{\partial x} + \frac{1}{r} \frac{\partial u^0}{\partial \theta} \right] \end{aligned} \right\} \quad (\text{A.7})$$

Using Equation (A.7) in Equation (A.6):

$$\rho \frac{Du^0}{Dt} = -\frac{\partial p^0}{\partial x} + \mu \left[ \frac{1}{r} \frac{\partial}{\partial r} \left( r \frac{\partial u^0}{\partial r} \right) + \frac{1}{r^2} \frac{\partial^2 u^0}{\partial \theta^2} + \frac{\partial^2 u^0}{\partial x^2} \right] \quad (A.8)$$

$$\rho \left( \frac{Du^0}{Dt} - \frac{w^{02}}{r} \right) = -\frac{\partial p^0}{\partial r} + \mu \left[ \frac{\partial}{\partial r} \left( \frac{1}{r} \frac{\partial}{\partial r} (r v^0) \right) + \frac{1}{r^2} \frac{\partial^2 v^0}{\partial \theta^2} - \frac{2}{r^2} \frac{\partial w^0}{\partial \theta} + \frac{\partial^2 v^0}{\partial x^2} \right] \quad (A.9)$$

$$\rho \left( \frac{Dw^0}{Dt} + \frac{v^0 w^0}{r} \right) = -\frac{1}{r} \frac{\partial p^0}{\partial \theta} + \mu \left[ \frac{\partial}{\partial r} \left( \frac{1}{r} \frac{\partial}{\partial r} (r w^0) \right) + \frac{1}{r^2} \frac{\partial^2 w^0}{\partial \theta^2} + \frac{2}{r^2} \frac{\partial v^0}{\partial \theta} + \frac{\partial^2 w^0}{\partial x^2} \right] \quad (A.10)$$

Using Equation (A.2) in Equation (A.8)

$$\begin{aligned} \frac{\partial(u+u')}{\partial t} + (u+u') \frac{\partial}{\partial x} (u+u') + (v+v') \frac{\partial}{\partial r} (u+u') + \frac{w'}{r} \frac{\partial}{\partial \theta} (u+u') \\ = -\frac{1}{\rho} \frac{\partial}{\partial x} (p+p') + \nu \left[ \frac{\partial^2}{\partial r^2} (u+u') + \frac{1}{r} \frac{\partial}{\partial r} (u+u') \right. \\ \left. + \frac{1}{r^2} \frac{\partial^2}{\partial \theta^2} (u+u') + \frac{\partial^2}{\partial x^2} (u+u') \right] \end{aligned} \quad (A.11)$$

Time Averaging Equation (A.11)

$$\begin{aligned} \frac{\partial u}{\partial t} + u \frac{\partial u}{\partial x} + \overline{u' \frac{\partial u'}{\partial x}} + v \frac{\partial u}{\partial r} + \overline{v' \frac{\partial u'}{\partial r}} + \frac{w'}{r} \frac{\partial u'}{\partial \theta} \\ = -\frac{1}{\rho} \frac{\partial p}{\partial x} + \nu \left[ \frac{\partial^2 u}{\partial r^2} + \frac{1}{r} \frac{\partial u}{\partial r} + \frac{1}{r^2} \frac{\partial^2 u}{\partial \theta^2} + \frac{\partial^2 u}{\partial x^2} \right] \end{aligned} \quad (A.12)$$

Multiplying Equation (A.5) by  $u'$ , and time averaging:

$$\overline{u' \frac{\partial u'}{\partial x}} + \overline{\frac{1}{r} \frac{\partial}{\partial r} (ru'u')} - \overline{u' \frac{\partial u'}{\partial r}} + \overline{\frac{1}{r} \frac{\partial}{\partial \theta} (w'u')} - \overline{\frac{w'}{r} \frac{\partial u'}{\partial \theta}} = 0 \quad (\text{A.13})$$

Adding Equation (A.13) and Equation (A.12), and rearranging:

$$\begin{aligned} \frac{\partial u}{\partial t} + u \frac{\partial u}{\partial x} + v \frac{\partial u}{\partial r} = & - \frac{\partial}{\partial x} \left( \frac{p}{\rho} + \overline{u'^2} \right) - \frac{1}{r} \frac{\partial}{\partial r} (r \overline{u'u'}) - \frac{1}{r} \frac{\partial}{\partial \theta} (\overline{w'u'}) \\ & + v \left[ \frac{\partial^2 u}{\partial r^2} + \frac{1}{r} \frac{\partial u}{\partial r} + \frac{1}{r^2} \frac{\partial^2 u}{\partial \theta^2} + \frac{\partial^2 u}{\partial x^2} \right] \end{aligned} \quad (\text{A.14})$$

$\overline{u'^2}$ ,  $\overline{u'u'}$  and  $\overline{w'u'}$  are the Reynolds stresses. Miller and Comings [19] experimentally showed that  $\overline{u'^2}$  and  $p/\rho$  are approximately equal and opposite for jet flow, i.e.,

$$(p/\rho + \overline{u'^2}) \approx 0. \quad \text{For axisymmetry, } \frac{\partial}{\partial \theta} (\overline{w'u'}) = 0, \text{ and } \frac{\partial^2 u}{\partial \theta^2} = 0.$$

Applying the boundary layer approximations,  $\frac{\partial^2 u}{\partial x^2}$  has been neglected. For steady flow, Equation (A.14) becomes:

$$u \frac{\partial u}{\partial x} + v \frac{\partial u}{\partial r} = \frac{1}{r} \frac{\partial}{\partial r} \left[ r \left( v \frac{\partial u}{\partial r} - \overline{u'u'} \right) \right],$$

$$\text{or, } u \frac{\partial u}{\partial x} + v \frac{\partial u}{\partial r} = \frac{1}{r} \frac{\partial}{\partial r} \left[ r \frac{\tau}{\rho} \right] \quad (\text{A.15})$$

$$\text{where } \frac{\tau}{\rho} = v \frac{\partial u}{\partial r} - \overline{u'u'} \quad (\text{A.16})$$

Subtracting Equation (A.12) from Equation (A.11):

$$\begin{aligned} & \frac{\partial u'}{\partial t} + u \frac{\partial u'}{\partial x} + u' \frac{\partial u}{\partial x} + u' \frac{\partial u'}{\partial x} - \overline{u' \frac{\partial u'}{\partial x}} + u \frac{\partial u'}{\partial r} + u' \frac{\partial u}{\partial r} + u' \frac{\partial u'}{\partial r} \\ & - \overline{u' \frac{\partial u'}{\partial r}} + \frac{w'}{r} \frac{\partial u}{\partial \theta} + \frac{w'}{r} \frac{\partial u'}{\partial \theta} - \frac{w'}{r} \frac{\partial u'}{\partial \theta} = -\frac{1}{\rho} \frac{\partial p'}{\partial x} \\ & + \nu \left[ \frac{\partial^2 u'}{\partial r^2} + \frac{1}{r} \frac{\partial u'}{\partial r} + \frac{1}{r^2} \frac{\partial^2 u'}{\partial \theta^2} + \frac{\partial^2 u'}{\partial x^2} \right] \end{aligned}$$

Multiplying by  $u'$ , time averaging and rearranging:

$$\begin{aligned} & \frac{\partial}{\partial t} \left( \frac{\overline{u'^2}}{2} \right) + u \frac{\partial}{\partial x} \left( \frac{\overline{u'^2}}{2} \right) + u \frac{\partial}{\partial r} \left( \frac{\overline{u'^2}}{2} \right) + \overline{u'^2} \frac{\partial u}{\partial x} + \overline{u' u'} \frac{\partial u}{\partial r} \\ & + \frac{\overline{u' w'}}{r} \frac{\partial u}{\partial \theta} + \overline{u'^2} \frac{\partial u'}{\partial x} + \overline{u' u'} \frac{\partial u'}{\partial r} + \frac{\overline{u' w'}}{r} \frac{\partial u'}{\partial \theta} \\ & = -\frac{1}{\rho} \frac{\partial p'}{\partial x} + \nu \left[ \overline{u'^2} \frac{\partial^2 u'}{\partial r^2} + \frac{1}{r} \overline{u' u'} \frac{\partial u'}{\partial r} + \frac{\overline{u' u'}}{r^2} \frac{\partial^2 u'}{\partial \theta^2} + \overline{u' u'} \frac{\partial^2 u'}{\partial x^2} \right] \end{aligned}$$

(A.17)

Multiplying Equation (A.5) by  $u'^2$ , time averaging and arranging:

$$\begin{aligned} & \overline{u'^2} \frac{\partial u'}{\partial x} + \frac{\overline{u' u'}}{r} \frac{\partial}{\partial r} (r u' u') - \overline{u' u'} \frac{\partial u'}{\partial r} \\ & + \frac{\overline{u' u'}}{r} \frac{\partial}{\partial \theta} (u' w') - \frac{\overline{w' u'}}{r} \frac{\partial u'}{\partial \theta} = 0 \end{aligned} \quad (\text{A.18})$$

Adding Equation (A.18) and Equation (A.17) and rearranging:

$$\begin{aligned}
 \frac{\partial}{\partial t} \left( \frac{\overline{u'^2}}{2} \right) + u \frac{\partial}{\partial x} \left( \frac{\overline{u'^2}}{2} \right) + v \frac{\partial}{\partial r} \left( \frac{\overline{u'^2}}{2} \right) &= - \left[ \overline{u'^2} \frac{\partial u}{\partial x} + \overline{u'v'} \frac{\partial u}{\partial r} \right. \\
 &+ \left. \frac{\overline{u'w'}}{r} \frac{\partial u}{\partial \theta} \right] - \overline{u' \frac{\partial}{\partial x} \left( \frac{p'}{\rho} + \frac{u'^2}{2} \right)} - \overline{v' \frac{\partial}{\partial r} \left( \frac{u'^2}{2} \right)} - \overline{w' \frac{\partial}{\partial \theta} \left( \frac{u'^2}{2} \right)} \\
 &- \overline{u'^2 \left\{ \frac{\partial u'}{\partial x} + \frac{1}{r} \frac{\partial}{\partial r} (ru') + \frac{1}{r} \frac{\partial w'}{\partial \theta} \right\}} + v \left[ \frac{\partial^2}{\partial r^2} \left( \frac{\overline{u'^2}}{2} \right) + \frac{1}{r} \frac{\partial}{\partial r} \left( \frac{\overline{u'^2}}{2} \right) \right. \\
 &+ \left. \frac{1}{r^2} \frac{\partial^2}{\partial \theta^2} \left( \frac{\overline{u'^2}}{2} \right) + \frac{\partial^2}{\partial x^2} \left( \frac{\overline{u'^2}}{2} \right) - \left( \frac{\partial u'}{\partial r} \right)^2 - \left( \frac{1}{r} \frac{\partial u'}{\partial \theta} \right)^2 - \left( \frac{\partial u'}{\partial x} \right)^2 \right]
 \end{aligned} \tag{A.19}$$

Using continuity Equation (A.5), and rearranging:

$$\begin{aligned}
 \frac{D}{Dt} \left( \frac{\overline{u'^2}}{2} \right) &= - \left[ \overline{u'^2} \frac{\partial u}{\partial x} + \overline{u'v'} \frac{\partial u}{\partial r} + \frac{\overline{u'w'}}{r} \frac{\partial u}{\partial \theta} \right] - \overline{u' \frac{\partial}{\partial x} \left( \frac{p'}{\rho} + \frac{u'^2}{2} \right)} \\
 &- \overline{v' \frac{\partial}{\partial r} \left( \frac{u'^2}{2} \right)} - \overline{w' \frac{\partial}{\partial \theta} \left( \frac{u'^2}{2} \right)} + v \left[ \frac{\partial^2}{\partial r^2} \left( \frac{\overline{u'^2}}{2} \right) + \frac{1}{r} \frac{\partial}{\partial r} \left( \frac{\overline{u'^2}}{2} \right) \right. \\
 &+ \left. \frac{1}{r^2} \frac{\partial^2}{\partial \theta^2} \left( \frac{\overline{u'^2}}{2} \right) + \frac{\partial^2}{\partial x^2} \left( \frac{\overline{u'^2}}{2} \right) \right] - v \left[ \overline{\left( \frac{\partial u'}{\partial r} \right)^2} + \overline{\left( \frac{1}{r} \frac{\partial u'}{\partial \theta} \right)^2} + \overline{\left( \frac{\partial u'}{\partial x} \right)^2} \right]
 \end{aligned} \tag{A.20}$$

Similar mathematical operations in Equations (A.9) and (A.10) yield:

$$\begin{aligned}
\frac{D}{Dt} \left( \frac{\overline{u'^2}}{2} \right) &= - \left[ \overline{u'u'} \frac{\partial u}{\partial x} + \overline{u'^2} \frac{\partial u}{\partial r} + \frac{\overline{w'u'}}{r} \frac{\partial u}{\partial \theta} \right] - \overline{u' \frac{\partial}{\partial r} \left( \frac{p'}{\rho} + \frac{u'^2}{2} \right)} \\
&+ \frac{\overline{w'^2 u'}}{r} - \overline{u' \frac{\partial}{\partial x} \left( \frac{u'^2}{2} \right)} - \frac{\overline{w'} \frac{\partial}{\partial \theta} \left( \frac{u'^2}{2} \right)}{r} + \nu \left[ \frac{\partial^2}{\partial r^2} \left( \frac{u'^2}{2} \right) \right] + \frac{1}{r} \frac{\partial}{\partial r} \left( \frac{u'^2}{2} \right) \\
&+ \frac{1}{r^2} \frac{\partial^2}{\partial \theta^2} \left( \frac{u'^2}{2} \right) + \frac{\partial^2}{\partial x^2} \left( \frac{u'^2}{2} \right) - \nu \left[ \left( \frac{\partial u'}{\partial r} \right)^2 + \left( \frac{1}{r} \frac{\partial u'}{\partial \theta} \right)^2 + \left( \frac{\partial u'}{\partial x} \right)^2 \right] \\
&+ \left[ \frac{\overline{u'^2}}{r^2} + \frac{2\overline{u'} \frac{\partial w'}{\partial \theta}}{r^2} \right] \quad (A.21)
\end{aligned}$$

and,

$$\begin{aligned}
\frac{D}{Dt} \left( \frac{\overline{w'^2}}{2} \right) &= - \overline{w'^2} \frac{u}{r} - \frac{\overline{w'} \frac{\partial}{\partial \theta} \left( \frac{p'}{\rho} + \frac{w'^2}{2} \right)}{r} - \frac{\overline{u' w'^2}}{r} - \overline{u' \frac{\partial}{\partial x} \left( \frac{w'^2}{2} \right)} \\
&- \overline{u' \frac{\partial}{\partial r} \left( \frac{w'^2}{2} \right)} + \nu \left[ \frac{\partial^2}{\partial r^2} \left( \frac{w'^2}{2} \right) + \frac{1}{r} \frac{\partial}{\partial r} \left( \frac{w'^2}{2} \right) + \frac{1}{r^2} \frac{\partial^2}{\partial \theta^2} \left( \frac{w'^2}{2} \right) \right] \\
&+ \frac{\partial^2}{\partial x^2} \left( \frac{w'^2}{2} \right) - \nu \left[ \left( \frac{\partial w'}{\partial r} \right)^2 + \left( \frac{1}{r} \frac{\partial w'}{\partial \theta} \right)^2 + \left( \frac{\partial w'}{\partial x} \right)^2 + \frac{\overline{w'^2}}{r} - \frac{2\overline{w'} \frac{\partial u'}{\partial \theta}}{r^2} \right] \quad (A.22)
\end{aligned}$$

Equations (A.20), (A.21) and (A.22) are Reynolds normal stress transport differential equations. The turbulent kinetic energy equation is formed by adding Equations (A.20), (A.21) and (A.22). For steady flow, the turbulent kinetic energy equation is:

$$\begin{aligned}
u \frac{\partial k}{\partial x} + v \frac{\partial k}{\partial r} &= - \left[ \overline{u'^2} \frac{\partial u}{\partial x} + \overline{u'v'} \left( \frac{\partial u}{\partial r} + \frac{\partial v}{\partial x} \right) + \frac{\overline{u'w'}}{r} \frac{\partial u}{\partial \theta} \right. \\
&+ \frac{\overline{w'u'}}{r} \frac{\partial v}{\partial \theta} + \overline{w'^2} \frac{v}{r} \left. \right] - v \left[ \left( \frac{\partial u'}{\partial x} \right)^2 + \left( \frac{\partial v'}{\partial x} \right)^2 + \left( \frac{\partial w'}{\partial x} \right)^2 + \left( \frac{\partial u'}{\partial r} \right)^2 \right. \\
&+ \left. \left( \frac{\partial v'}{\partial r} \right)^2 + \left( \frac{\partial w'}{\partial r} \right)^2 + \left( \frac{1}{r} \frac{\partial u'}{\partial \theta} \right)^2 + \left( \frac{1}{r} \frac{\partial v'}{\partial \theta} - \frac{w'}{r} \right)^2 + \left( \frac{1}{r} \frac{\partial w'}{\partial \theta} + \frac{v'}{r} \right)^2 \right] \\
&- \left[ \frac{\partial}{\partial x} \left\{ u' \left( \frac{p'}{\rho} + k \right) \right\} + \frac{1}{r} \frac{\partial}{\partial r} \left\{ u' r \left( \frac{p'}{\rho} + k \right) \right\} + \frac{1}{r} \frac{\partial}{\partial \theta} \left\{ w' \left( \frac{p'}{\rho} + k \right) \right\} \right. \\
&\left. - v \left\{ \frac{\partial^2 k}{\partial x^2} + \frac{1}{r} \frac{\partial}{\partial r} \left( r \frac{\partial k}{\partial r} \right) + \frac{1}{r^2} \frac{\partial^2 k}{\partial \theta^2} \right\} \right] \tag{A.23}
\end{aligned}$$

where  $k = (\overline{u'^2} + \overline{v'^2} + \overline{w'^2})/2$ .

## A.2 Integral Equations

Differential form of the mass and momentum conservation equations for the mean flow are given by Equations (A.4) and (A.15). Integral equations may be formed by taking integrals of Equation (A.15) over a control volume and using mass conservation Equation (A.4).

### A.2.1 Momentum Integral Equation

Multiplying Equation (A.4) by  $u$  and rearranging,

$$u \frac{\partial u}{\partial x} + \frac{1}{r} \frac{\partial}{\partial r} (ruv) - v \frac{\partial u}{\partial r} = 0 \tag{A.24}$$

Adding Equation (A.24) and Equation (A.15) and arranging,

$$\frac{\partial}{\partial x} (ru^2) + \frac{\partial}{\partial r} (ruv) = \frac{\partial}{\partial r} (r \tau / \rho) \tag{A.25}$$



For axisymmetric jet  $u$  and  $\tau$  are equal to zero at  $r=0$  and  $\infty$ . Integrating Equation (A.25) over a control volume with  $r=0$  to  $\infty$ ,

$$\frac{\partial}{\partial x} \int_0^{\infty} ru^2 \partial r = 0 \quad (\text{A.26})$$

### A.2.2 Mean Energy Integral Equation

Multiplying Equation (A.15) by  $u$ ,

$$u^2 \frac{\partial u}{\partial x} + uv \frac{\partial u}{\partial r} = \frac{u}{r} \frac{\partial}{\partial r} (r \tau / \rho) \quad (\text{A.27})$$

Multiplying Equation (A.4) by  $u^2$ , and arranging,

$$\frac{u^2 \partial u}{2 \partial x} + \frac{1}{2r} \frac{\partial}{\partial r} (u^2 ur) - uv \frac{\partial u}{\partial r} = 0 \quad (\text{A.28})$$

Adding Equation (A.27) and Equation (A.28) and arranging,

$$\frac{1}{2} \frac{\partial}{\partial x} (ru^3) + \frac{1}{2} \frac{\partial}{\partial r} (u^2 ur) = \frac{\partial}{\partial r} (ur \tau / \rho) - \tau / \rho (r \frac{\partial u}{\partial r}) \quad (\text{A.29})$$

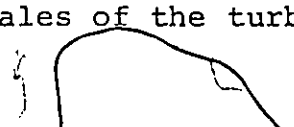
For axisymmetric jets,  $u$  and  $\tau$  are equal to zero at  $r=0$  and  $\infty$ . Integrating Equation (A.29) over a control volume in the limit  $r=0$  to  $\infty$ ,

$$\frac{1}{2} \frac{\partial}{\partial x} \int_0^{\infty} ru^3 \partial r = - \int_0^{\infty} (r \frac{\partial u}{\partial r}) \tau / \rho \partial r \quad (\text{A.30})$$

Using Equation (A.16) for  $\tau/\rho$  in Equation (A.30),

$$\frac{1}{2} \frac{\partial}{\partial x} \int_0^{\infty} ru^3 \partial r = - \int_0^{\infty} (r \frac{\partial u}{\partial r}) (v \frac{\partial u}{\partial r} - \overline{u'u'}) \partial r \quad (\text{A.31})$$

$-\rho \overline{u'u'}$  is turbulent shear stress and  $\rho v \frac{\partial u}{\partial r}$  represents shear stress due to molecular motion. Using  $\sqrt{k}$  and  $L^1$  as the velocity and length scales of the turbulence, the shear stress



magnitude may be represented by:

$$\left. \begin{array}{l} \overline{u'u'} \sim \sqrt{k} \sqrt{k} \\ \text{or} \\ \overline{u'u'} \sim k \end{array} \right\} \quad (\text{A.32})$$

$$\left. \begin{array}{l} \nu \frac{\partial u}{\partial r} \sim \nu \frac{\sqrt{k}}{L^1} \\ \text{or} \\ \nu \frac{\partial u}{\partial r} \sim \frac{k}{(\sqrt{k}L^1)/\nu} \end{array} \right\} \quad (\text{A.33})$$

Comparing Equation (A.32) and Equation (A.33),  $\overline{u'u'}$  is  $(kL^1/\nu)$  times greater than  $\nu(\partial u/\partial r)$ . For high turbulence Reynolds numbers,  $(\sqrt{k}L/\nu)$ , the viscous-shear stress is negligible. Expressing turbulent shear stress  $-\rho \overline{u'u'}$  by Prandtl's mixing length model:

$$-\rho \overline{u'u'} = \rho \nu_t \frac{\partial u}{\partial r} \quad (\text{A.34})$$

where,

$$\nu_t = L^2 \left| \frac{\partial u}{\partial r} \right| \quad (\text{A.35})$$

Neglecting molecular shear stress and using Equation (A.34) in Equation (A.31), the energy integral equation becomes:

$$\frac{1}{2} \frac{\partial}{\partial x} \int_0^\infty u^3 r \partial r = - \int_0^\infty \nu_t r \left( \frac{\partial u}{\partial r} \right)^2 \partial r \quad (\text{A.36})$$

APPENDIX B

CALCULATION BY THE INTEGRAL METHOD

B.1 Integral Calculations

The empirical velocity profile obtained by fitting a curve to the experimental measurements is:

$$\left. \begin{aligned} \frac{u}{u_c} &= 1.0 & ; & \eta \leq -0.736 \\ \frac{u}{u_c} &= 0.5 - \eta + 0.05\eta^2 + 0.66\eta^3 & ; & -0.736 \leq \eta \leq 0.5 \\ \frac{u}{u_c} &= 0.095 \left[ 1.0 - \tanh 4.79(\eta - 0.5) \right] & ; & \eta \geq 0.5 \end{aligned} \right\} \quad (B.1)$$

The momentum integral equation is obtained using the boundary layer approximation:

$$\frac{\partial}{\partial x} \int_0^{\infty} u^2 r \partial r = 0$$

where  $x$  is axial coordinate and  $r$  is radial coordinate as shown in Figure 1.1.

The momentum equation can be written as:

$$\frac{\partial}{\partial x} \left[ \int_0^{r_1} u^2 r \partial r + \int_{r_1}^{\infty} u^2 r \partial r \right] = 0$$

In the potential core  $0 \leq r \leq r_1$ ,  $u = u_c = \text{constant}$ , so the above equation becomes:

$$\frac{\partial}{\partial x} \left[ \frac{r_1^2}{2} + \int_{r_1}^{\infty} \left( \frac{u}{u_c} \right)^2 r \partial r \right] = 0 \quad (B.2)$$

A new variable,  $\eta$ , is defined as:

$$\eta = \frac{r-r_{1/2}}{b}$$

where  $r_{1/2}$  is the radial distance for  $u/u_c = 0.5$ , and

$$b/r_0 = \left[ \frac{\partial r/r_0}{\partial u/u_c} \right]_{r=r_{1/2}}$$

Transforming Equation (B.2) into variable  $\eta$ :

$$\frac{\partial}{\partial x} \left[ \frac{r_1^2}{2} + \int_{\eta_1}^{\eta_2} (r_{1/2} + \eta b) b (u/u_c)^2 \partial \eta \right] = 0 \quad (B.3)$$

where,

$$\eta_1 = \frac{r_1 - r_{1/2}}{b} \text{ and } \eta_2 = \frac{r_2 - r_{1/2}}{b}$$

The energy equation in integral form is also obtained by using boundary layer approximation; it is:

$$\frac{1}{2} \frac{\partial}{\partial x} \int_0^{\infty} r u^3 \partial r - L^2 \int_0^{\infty} r \left( \frac{\partial u}{\partial r} \right)^3 \partial r = 0$$

where  $L$  is Prandtl's mixing length,

$$\frac{1}{2} \frac{\partial}{\partial x} \left[ \int_0^{r_1} r u^3 \partial r + \int_{r_1}^{r_2} r u^3 \partial r \right]$$

$$\text{or, } - L^2 \left[ \int_0^{r_1} r \left( \frac{\partial u}{\partial r} \right)^3 \partial r + \int_{r_1}^{r_2} r \left( \frac{\partial u}{\partial r} \right)^3 \partial r \right] = 0$$

In core  $0 \leq r \leq r_1$ ,  $u = u_c$  and  $\partial u / \partial r = 0$ , so the above equation becomes:

$$\frac{1}{2} \frac{\partial}{\partial x} \left[ \frac{r_1^2}{2} + \int_{r_1}^{r_2} r (u/u_c)^3 \partial r \right] - L^2 \int_{r_1}^{r_2} r \left( \frac{\partial u/u_c}{\partial r} \right)^3 \partial r = 0$$

Transforming into the variable,  $\eta = \frac{r-r_{1/2}}{b}$  :

$$\frac{1}{2} \frac{\partial}{\partial x} \left[ \frac{r_1^2}{2} + \int_{\eta_1}^{\eta_2} (r_{1/2} b + \eta b^2) (u/u_c)^3 \partial \eta \right]$$

$$\therefore \left( \frac{L}{b} \right)^2 \int_{\eta_1}^{\eta_2} \eta^2 (r_{1/2} + \eta b) \left( \frac{\partial (u/u_c)}{\partial \eta} \right)^3 \partial \eta = 0 \quad (\text{B.4})$$

$\eta_1 = -0.736$  which represents the edge of the core, and  $\eta_2$  is chosen to be 0.8 where  $u/u_c = 0.01$ . This choice is made only to have easy access to the integration of higher powers of the product of  $\eta$  and  $\tanh 4.79(\eta - \eta_0)$ .

## B.2 Momentum Integral Equation

Using velocity profile (B.1) in Equation (B.3) and using the limits for  $\eta$ ,

$$\frac{\partial}{\partial x} \left[ \frac{r_1^2}{2} + \int_{-0.736}^{0.5} (r_{1/2} b + \eta b^2) (0.5 - \eta + 0.5\eta^2 + .66\eta^3)^2 \partial \eta \right. \\ \left. + \int_{0.5}^{0.8} (r_{1/2} b + \eta b^2) \{ .095(1.0 - \tanh 4.79(\eta - 0.5)) \}^2 \partial \eta \right] = 0$$

or,

$$\frac{\partial}{\partial x} \left[ \frac{r_1^2}{2} + r_{1/2} b \underbrace{\int_{-0.736}^{0.5} (.5 - \eta + 0.5\eta^2 + .66\eta^3)^2 \partial \eta}_{\text{1st Integral}} \right. \\ \left. + b^2 \underbrace{\int_{-0.736}^{0.5} \eta (.5 - \eta + .05\eta^2 + .66\eta^3)^2 \partial \eta}_{\text{2nd Integral}} \right. \\ \left. + r_{1/2} b \underbrace{\int_{0.5}^{0.8} \{ .095(1 - \tanh 4.79(\eta - .5)) \}^2 \partial \eta}_{\text{3rd Integral}} \right. \\ \left. + b^2 \underbrace{\int_{0.5}^{0.8} \eta \{ .095(1 - \tanh 4.79(\eta - .5)) \}^2 \partial \eta}_{\text{4th Integral}} \right] = 0 \quad (\text{B.5})$$

### B.2.1 Calculation of Integrals of Equation (B.5)

$$\begin{aligned}
 \text{1st Integral} &= \int_{-.736}^{0.5} (.5 - \eta + .05\eta^2 + .66\eta^3) \partial\eta \\
 &= \int_{-.736}^{0.5} [.25 - \eta + 1.05\eta^2 + .56\eta^3 - 1.3175\eta^4 \\
 &\quad + .066\eta^5 + .4356\eta^6] \partial\eta \\
 &= 0.54685577
 \end{aligned}$$

$$\begin{aligned}
 \text{2nd Integral} &= \int_{-.736}^{0.5} \eta(0.5 - \eta + .05\eta^2 + .66\eta^3) \partial\eta \\
 &= \int_{-.736}^{0.5} [0.25\eta - \eta^2 + 1.05\eta^3 + .56\eta^4 + 1.37175\eta^5 \\
 &\quad + .066\eta^6 + .4356\eta^7] \partial\eta \\
 &= -0.21578334
 \end{aligned}$$

$$\begin{aligned}
 \text{3rd Integral} &= \int_{0.5}^{0.8} [.095(1 - \tanh 4.79(\eta - .5))]^2 \partial\eta \\
 &= (.095)^2 \int_{0.5}^{0.8} [1 - 2 \tanh 4.79(\eta - .5) \\
 &\quad + \tanh^2 4.79(\eta - .5)] \partial\eta \\
 &= (.095)^2 \int_{0.5}^{0.8} [2 - 2 \tanh 4.79(\eta - .5) \\
 &\quad - \operatorname{sech}^2 4.79(\eta - .5)] \partial\eta \\
 &= (.095)^2 \left[ 2\eta - \frac{2}{4.79} \ln \cosh 4.79(\eta - .5) \right. \\
 &\quad \left. - \frac{1}{4.79} \tanh 4.79(\eta - .5) \right]_{.5}^{.8} \\
 &= 0.00072225
 \end{aligned}$$

$$\begin{aligned}
\text{4th Integral} &= \int_{0.5}^{0.8} \eta \left[ .095(1 - \tanh 4.79(\eta - .5)) \right]^2 d\eta \\
&= (.095)^2 \int_{0.5}^{0.8} \left[ \eta - 2\eta \tanh 4.79(\eta - .5) \right. \\
&\quad \left. + \eta \tanh^2 4.79(\eta - .5) \right] d\eta \\
&= (.095)^2 \left[ \frac{\eta^2}{2} - 2 \int \eta \tanh 4.79(\eta - .5) d\eta \right. \\
&\quad \left. + \int (\eta - \eta \operatorname{sech}^2 4.79(\eta - .5)) d\eta \right]_{0.5}^{0.8} \\
&= (.095)^2 \left[ \eta^2 - 2 \int \eta \tanh 4.79(\eta - .5) d\eta \right. \\
&\quad \left. - \int \eta \operatorname{sech}^2 4.79(\eta - .5) d\eta \right]_{0.5}^{0.8} \\
&= (.095)^2 \left[ \eta^2 - 2 \int \eta \tanh 4.79(\eta - .5) d\eta \right. \\
&\quad \left. - \frac{\eta}{4.79} \tanh 4.79(\eta - .5) \right. \\
&\quad \left. + \frac{1}{4.79} \int \tanh 4.79(\eta - .5) d\eta \right]_{0.5}^{0.8} \\
&= (.095)^2 \left[ \eta^2 - 2 \int \eta \tanh 4.79(\eta - .5) d\eta \right. \\
&\quad \left. - \frac{\eta}{4.79} \tanh 4.79(\eta - .5) \right. \\
&\quad \left. + \left( \frac{1}{4.79} \right)^2 \ln \cosh 4.79(\eta - .5) \right]_{0.5}^{0.8} \\
&= (.095)^2 \left[ \eta^2 - \frac{2}{4.79} \int 4.79(\eta - .5) \tanh 4.79(\eta - .5) d\eta \right. \\
&\quad \left. - 2 \cdot 0.5 \int \tanh 4.79(\eta - .5) d\eta \right. \\
&\quad \left. - \frac{\eta}{4.79} \tanh 4.79(\eta - .5) \right. \\
&\quad \left. + \left( \frac{1}{4.79} \right)^2 \ln \cosh 4.79(\eta - .5) \right]_{0.5}^{0.8}
\end{aligned}$$

$$\begin{aligned}
\text{4th Integral} &= (.095)^2 \left[ \eta^2 - \frac{2}{(4.79)^2} \int \left\{ (4.79(\eta-.5))^2 - \frac{(4.79(\eta-.5))^4}{3} \right. \right. \\
&\quad + \frac{2}{15} (4.79(\eta-.5))^6 - \frac{17}{315} (4.79(\eta-.5))^8 \\
&\quad + \left. \frac{62}{2835} (4.79(\eta-.5))^{10} - \dots \right\} \partial \{ 4.79(\eta-\eta_0) \} \\
&\quad - \frac{1}{4.79} \ell n \cosh 4.79(\eta-.5) - \frac{\eta}{4.79} \tanh 4.79(\eta-.5) \\
&\quad + \left. \left( \frac{1}{(4.79)^2} \ell n \cosh 4.79(\eta-.5) \right) \right]_{0.5}^{0.8} \\
&= (.095)^2 \left[ \eta^2 - \frac{2}{(4.79)^2} \left\{ \frac{(4.79(\eta-.5))^3}{3} - \frac{(4.79(\eta-.5))^5}{15} \right. \right. \\
&\quad + \frac{2}{105} (4.79(\eta-.5))^7 - \frac{17}{2835} (4.79(\eta-.5))^9 \\
&\quad + \left. \frac{62}{31185} (4.79(\eta-.5))^{11} - \dots \right\} \\
&\quad - \frac{1}{4.79} \ell n \cosh 4.79(\eta-.5) \\
&\quad - \frac{\eta}{4.79} \tanh 4.79(\eta-.5) \\
&\quad + \left. \left( \frac{1}{(4.79)^2} \ell n \cosh 4.79(\eta-.5) \right) \right]_{0.5}^{0.8} \\
&= 0.00037526
\end{aligned}$$

Substituting the values of the integrals into Equation (B.5):

$$\frac{\partial}{\partial x} \left[ \frac{r^2}{2} + 0.547578 r_{\frac{1}{2}} b - 0.215408 b^2 \right] = 0 \quad (\text{B.6})$$

This is a first order differential equation with starting condition at  $x=0$  is  $r_1=r_0$  and  $b=0$ ; integrating:

$$\frac{r_1^2}{2} + .547578 r_{\frac{1}{2}} b - .215408 b^2 = \frac{r_0^2}{2} \quad (\text{B.7})$$



Since,

$$\eta_1 = -.736 = \frac{r_1 - r_{1/2}}{b}$$

$$r_1 = r_{1/2} - 0.736b \quad (B.8)$$

Substituting (B.8) into Equation (B.7):

$$\frac{(r_{1/2} - .736b)^2}{2} + .547578 r_{1/2} b - .215408b^2 = \frac{r_0^2}{2}$$

or

$$r_{1/2}^2 - 0.37684397 r_{1/2} b + 0.05544 b^2 = \frac{r_0^2}{2}$$

or

$$r_{1/2} = 0.18842198b \pm \sqrt{r_0^2 - .075377b^2}$$

Since at  $b=0$ ,  $r_{1/2}$  can never be negative, the positive sign is included with the following relationship:

$$\frac{r_{1/2}}{r_0} = 0.18842198 b/r_0 + \sqrt{1.0 - 0.075377(b/r_0)^2} \quad (B.9)$$

### B.3 Energy Integral Equations

Using velocity profile (B.1) in Equation (B.4), we get:

$$\begin{aligned} & \frac{1}{2} \frac{\partial}{\partial x} \left[ \frac{r_1^2}{2} + \int_{-.736}^{0.5} (r_{\frac{1}{2}} + nb^2) (0.5 - \eta + 0.5\eta^2 + .66\eta^3)^3 \partial\eta \right. \\ & \left. + \int_{0.5}^{0.8} (r_{\frac{1}{2}}b + nb) \{ .095(1 - \tanh 4.79(\eta - .5)) \}^3 \partial\eta \right] \\ & - \left( \frac{L}{b} \right)^2 \left[ \int_{-.736}^{0.5} (r_{\frac{1}{2}} + nb) (-1 + 0.1\eta + 1.98\eta^2)^3 \partial\eta \right. \\ & \left. + \int_{0.5}^{0.8} (r_{\frac{1}{2}} + nb) \{ -0.455 \operatorname{sech}^2 4.79(\eta - 0.5) \}^3 \partial\eta \right] = 0 \end{aligned}$$

or,

$$\begin{aligned} & \frac{1}{2} \frac{\partial}{\partial x} \left[ \frac{r_1^2}{2} + r_{\frac{1}{2}}b \underbrace{\int_{-.736}^{0.5} (0.5 - \eta + 0.05\eta^2 + 0.66\eta^3)^3 \partial\eta}_{\text{1st Integral}} \right. \\ & \left. + b^2 \underbrace{\int_{-.736}^{0.5} (0.5 - \eta + 0.05\eta^2 + .66\eta^3)^3 \partial\eta}_{\text{2nd Integral}} \right. \\ & \left. + r_{\frac{1}{2}}b(0.095)^3 \underbrace{\int_{0.5}^{0.8} \{ 1 - \tanh 4.79(\eta - .5) \}^3 \partial\eta}_{\text{3rd Integral}} \right. \\ & \left. + b^2(0.095)^3 \underbrace{\int_{0.5}^{0.8} \eta \{ 1 - \tanh 4.79(\eta - .5) \}^3 \partial\eta}_{\text{4th Integral}} \right] \end{aligned}$$

$$- \left(\frac{1}{b}\right)^2 \left[ r_{\frac{1}{2}} \int_{-.736}^{0.5} (-1 + 0.1\eta + 1.98\eta^2)^3 \partial\eta \right]$$

5th Integral

$$+ b \int_{-.736}^{0.5} \eta (-1 + 0.1\eta + 1.98\eta^2)^3 \partial\eta$$

6th Integral

$$- r_{\frac{1}{2}} (0.455)^3 \int_{0.5}^{0.8} \{\operatorname{sech}^2 4.79(\eta-.5)\}^3 \partial\eta$$

7th Integral

$$- b(0.455)^3 \int_{0.5}^{0.8} \eta \{\operatorname{sech}^2 4.79(\eta-.5)\}^3 \partial\eta = 0$$

8th Integral

(B.10)

### B.3.1 Calculation of Integrals in Equation (B.10)

$$\begin{aligned} \text{1st Integral} &= \int_{-.736}^{0.5} (0.5 - \eta + 0.05\eta^2 + 0.66\eta^3)^3 \partial\eta \\ &= \int_{-.736}^{0.5} \{0.125 - 0.75\eta + 1.5375\eta^2 - 0.655\eta^3 \\ &\quad - 1.82623\eta^4 + 2.0715\eta^5 + 0.455525\eta^6 \\ &\quad - 1.30165\eta^7 + 0.06534\eta^8 + 0.287496\eta^9\} \partial\eta \\ &= 0.45097066 \end{aligned}$$

$$\begin{aligned} \text{2nd Integral} &= \int_{-.736}^{0.5} \eta (0.5 - \eta + 0.05\eta^2 + 0.66\eta^3)^3 \partial\eta \\ &= \int_{-.736}^{0.5} \{0.125\eta - 0.75\eta^2 + 1.5375\eta^3 - 0.655\eta^4 \\ &\quad - 1.82625\eta^5 + 2.0715\eta^6 + 0.455525\eta^7 \\ &\quad - 1.30185\eta^8 + 0.06534\eta^9 + 0.287496\eta^{10}\} \partial\eta \end{aligned}$$

$$\text{2nd Integral} = -0.20326464$$

$$\begin{aligned} \text{3rd Integral} &= (0.095)^3 \int_{0.5}^{0.8} \{1 - \tanh 4.79(\eta - .5)\}^3 \partial \eta \\ &= (0.095)^3 \int_{0.5}^{0.8} \left[ 1 - 3 \tanh 4.79(\eta - .5) \right. \\ &\quad \left. + 3 \tanh 4.79(\eta - .5) - \tanh^3 4.79(\eta - .5) \right] \partial \eta \\ &= (0.095)^3 \int_{0.5}^{0.8} \left[ 4 - 4 \tanh 4.79(\eta - .5) \right. \\ &\quad \left. - 3 \operatorname{sech}^2 4.79(\eta - .5) \right. \\ &\quad \left. + \tanh 4.79(\eta - .5) \operatorname{sech}^2 4.79(\eta - .5) \right] \partial \eta \\ &= (.095)^3 \left[ 4\eta - \frac{4}{4.79} \ln \cosh 4.79(\eta - .5) \right. \\ &\quad \left. - \frac{3}{4.79} \tanh 4.79(\eta - .5) \right. \\ &\quad \left. + \frac{1}{4.79} \int \tanh 4.79(\eta - .5) \partial \{ \tanh 4.79(\eta - .5) \} \right]_{0.5}^{0.8} \\ &= (.095)^3 \left[ 4\eta - \frac{4}{4.79} \ln \cosh 4.79(\eta - .5) \right. \\ &\quad \left. - \frac{3}{4.79} \tanh 4.79(\eta - .5) \right. \\ &\quad \left. + \frac{1}{4.79} \frac{\tanh^2 4.79(\eta - .5)}{2} \right]_{0.5}^{0.8} \\ &= 0.00004875 \end{aligned}$$

$$\text{4th Integral} = (.095)^3 \int_{0.5}^{0.8} \eta \{1 - \tanh 4.79(\eta - .5)\}^3 \partial \eta$$

$$4^{\text{th}} \text{ Integral} = (.095)^3 \int_{0.5}^{0.8} [4\eta - 4\eta \tanh 4.79(\eta - .5)$$

$$- 3\eta \operatorname{sech}^2 4.79(\eta - .5)$$

$$+ \eta \tanh 4.79(\eta - .5) \operatorname{sech}^2 4.79(\eta - .5)] \partial \eta$$

$$= (.095)^3 [2\eta^2 - 4 \int \eta \tanh 4.79(\eta - .5) \partial \eta$$

$$- 3 \int \eta \operatorname{sech}^2 4.79(\eta - .5) \partial \eta$$

$$+ \int \eta \tanh 4.79(\eta - .5) * \operatorname{sech}^2 4.79(\eta - .5) \partial \eta]_{0.5}^{0.8}$$

$$= (.095)^3 [2\eta^2 - \frac{4}{4.79} \int \{4.79(\eta - .5) \tanh 4.79(\eta - .5)$$

$$+ 4.79 * 0.5 \tanh 4.79(\eta - .5)\} \partial \eta$$

$$- \frac{3\eta}{4.79} * \tanh 4.79(\eta - .5)$$

$$+ \frac{3}{(4.79)^2} \eta \cosh 4.79(\eta - .5)$$

$$+ \frac{\eta}{4.79} \frac{\tanh^2 4.79(\eta - .5)}{2}$$

$$- \frac{1}{9.58} \tanh^2 4.79(\eta - .5) \partial \eta]_{0.5}^{0.8}$$

$$= (.095)^3 [2\eta^2 - \frac{4}{4.79} \int \{ \frac{(4.79(\eta - .5))^2}{1} - \frac{(4.79(\eta - .5))^4}{3}$$

$$+ \frac{2}{15} (4.79(\eta - .5))^6 - \frac{17}{315} (4.79(\eta - .5))^8$$

$$+ \frac{62}{2835} (4.79(\eta - .5))^{10} - \dots \} \partial \eta$$

$$- \frac{2}{4.79} \eta \cosh 4.79(\eta - .5) - \frac{3\eta}{4.79} \tanh 4.79(\eta - .5)$$

$$\begin{aligned}
& + \frac{3}{(4.79)^2} \ln \cosh 4.79(\eta-.5) \\
& + \frac{\eta}{4.79} \frac{\tanh^2 4.79(\eta-.5)}{2} \\
& - \frac{1}{9.58} \int_{0.5}^{0.8} \{1 - \operatorname{sech}^2 4.79(\eta-.5)\} \partial \eta \\
= & (.095)^3 \left[ 2\eta^2 - \frac{4}{(4.79)^2} \left\{ \frac{(4.79(\eta-.5))^3}{3} \right. \right. \\
& - \frac{(4.79(\eta-.5))^5}{15} + \frac{2(4.79(\eta-.5))^7}{105} - \frac{17(4.79(\eta-.5))^9}{315 \cdot 9} \\
& \left. \left. + \frac{62(4.79(\eta-.5))^{11}}{2835 \cdot 11} - \dots \dots \dots \right\} \right. \\
& - \frac{2}{4.79} \ln \cosh 4.79(\eta-.5) - \frac{3\eta}{4.79} \tanh 4.79(\eta-.5) \\
& + \frac{3}{(4.79)^2} \ln \cosh 4.79(\eta-.5) + \frac{\eta}{4.79} \frac{\tanh^2 4.79(\eta-.5)}{2} \\
& \left. - \frac{\eta}{9.58} + \frac{1}{9.58 \cdot 4.79} \tanh 4.79(\eta-.5) \right]_{0.5}^{0.8}
\end{aligned}$$

$$4\text{th Integral} = 0.00002021$$

$$\begin{aligned}
5\text{th Integral} &= \int_{-.736}^{0.5} \{-1 + 0.1\eta + 1.98\eta^2\}^3 \partial \eta \\
&= \int_{-.736}^{0.5} \{-1 + 0.3\eta + 5.91\eta^2 - 1.187\eta^3 - 11.7018\eta^4 \\
&\quad + 1.17604\eta^5 + 7.762392\eta^6\} \partial \eta \\
&= -0.64783662
\end{aligned}$$

$$\begin{aligned}
\text{6th Integral} &= \int_{-.736}^{0.5} \eta \{-1 + 0.1\eta + 1.98\eta^2\}^3 \partial \eta \\
&= \int_{-.736}^{0.5} \{-\eta + 0.3\eta^2 + 5.91\eta^3 - 1.187\eta^4 - 11.7018\eta^5 \\
&\quad + 1.17604\eta^6 + 7.762392\eta^7\} \partial \eta \\
&= 0.01906390
\end{aligned}$$

$$\begin{aligned}
\text{7th Integral} &= (0.455)^3 \int_{0.5}^{0.8} \text{sech}^6 4.79(\eta-.5) \partial \eta \\
&= \frac{(0.455)^3}{4.79} \int_{0.5}^{0.8} \{1 - \tanh^2 4.79(\eta-.5)\}^2 \\
&\quad * 6 \{ \tanh 4.79(\eta-.5) \\
&= \frac{(0.455)^3}{4.79} \int_{0.5}^{0.8} \left[ 1 - 2 \tanh^2 4.79(\eta-.5) \right. \\
&\quad \left. + \tanh^4 4.79(\eta-.5) \right] \partial \tanh 4.79(\eta-.5) \\
&= \frac{(0.455)^3}{4.79} \left[ \tanh 4.79(\eta-.5) - \frac{2}{3} \tanh^3 4.79(\eta-.5) \right. \\
&\quad \left. + \frac{1}{5} \tanh^5 4.79(\eta-.5) \right]_{0.5}^{0.8} \\
&= 0.01045859
\end{aligned}$$

$$\begin{aligned}
\text{8th Integral} &= (0.455)^3 \int_{0.5}^{0.8} \eta \text{sech}^6 4.79(\eta-.5) \partial \eta \\
&= (0.455)^3 \left[ \int \eta \text{sech}^6 4.79(\eta-.5) \partial \eta \right. \\
&\quad \left. - \int \{ \int \text{sech}^6 4.79(\eta-.5) \partial \eta \} \partial \eta \right]_{0.5}^{0.8}
\end{aligned}$$

Using 7th Integral,

$$\begin{aligned}
\text{8th Integral} &= \frac{(0.455)^3}{4.79} \left[ \eta \{ \tanh 4.79(\eta-.5) - \frac{2}{3} \tanh^3 4.79(\eta-.5) \right. \\
&\quad \left. + \frac{1}{5} \tanh^5 4.79(\eta-.5) \} - \int \{ \tanh 4.79(\eta-.5) \right. \\
&\quad \left. - \frac{2}{3} \tanh^3 4.79(\eta-.5) + \frac{1}{5} \tanh^5 4.79(\eta-.5) \} \partial \eta \right]_{0.5}^{0.8} \\
&= \frac{(0.455)^3}{4.79} \left[ \eta \{ \tanh 4.79(\eta-.5) - \frac{2}{3} \tanh^3 4.79(\eta-.5) \right. \\
&\quad \left. + \frac{1}{5} \tanh^5 4.79(\eta-.5) \} - \int \left\{ \frac{8}{15} \tanh 4.79(\eta-.5) \right. \right. \\
&\quad \left. \left. + \frac{7}{5} \tanh 4.79(\eta-.5) \operatorname{sech}^2 4.79(\eta-.5) \right. \right. \\
&\quad \left. \left. - \frac{1}{5} \tanh^3 4.79(\eta-.5) \operatorname{sech}^2 4.79(\eta-.5) \right\} \partial \eta \right]_{0.5}^{0.8} \\
&= \frac{(0.455)^3}{4.79} \left[ \eta \{ \tanh 4.79(\eta-.5) - \frac{2}{3} \tanh^3 4.79(\eta-.5) \right. \\
&\quad \left. + \frac{1}{5} \tanh^5 4.79(\eta-.5) \} - \frac{1}{4.79} \left\{ \frac{8}{15} \operatorname{ncosh} 4.79(\eta-.5) \right. \right. \\
&\quad \left. \left. + \frac{7}{30} \tanh^2 4.79(\eta-.5) - \frac{1}{20} \tanh^4 4.79(\eta-.5) \right\} \right]_{0.5}^{0.8} \\
&= 0.00598443
\end{aligned}$$

Substituting the values of integrals in Equation (B.10):

$$\frac{1}{2} \frac{\partial}{\partial x} \left[ \frac{r^2}{2} + 0.45101941 r_{\frac{1}{2}} b - 0.20326464 b^2 \right] - \left( \frac{L}{b} \right)^2$$

$$* \left[ -0.65829521 r_{\frac{1}{2}} + 0.01311954 b \right] = 0$$



or,

$$\begin{aligned} \frac{1}{2} \frac{\partial}{\partial x} \left[ \left( -\frac{r_1^2}{2} + 0.547578r_{\frac{1}{2}}b - 0.215408b^2 \right) - 0.9655859r_{\frac{1}{2}}b \right. \\ \left. + 0.01214336b^2 \right] - \frac{L^2}{b^2} \left[ -0.65829521r_{\frac{1}{2}} + 0.01311954b \right] \\ = 0 \end{aligned}$$

Using Equation (B.6):

$$\begin{aligned} \frac{1}{2} \frac{\partial}{\partial x} \left[ 0.09655859r_{\frac{1}{2}}b - 0.01214336b^2 \right] \\ = + \frac{L^2}{b^2} \left[ 0.65829521r_{\frac{1}{2}} - 0.01311954b \right] \end{aligned}$$

Substituting the expression for  $r_{\frac{1}{2}}$  from Equation (B.9):

$$\begin{aligned} \frac{1}{2} \frac{\partial}{\partial x} \left[ 0.09655859b \{ 0.18842198b + \sqrt{r_0^2 - 0.075377b^2} \} \right. \\ \left. - 0.01214336b^2 \right] = \left( \frac{L}{b} \right)^2 \left[ 0.65829521 \cdot 0.18842198b \right. \\ \left. + \sqrt{r_0^2 - 0.075377b^2} \right] - 0.01311954b \end{aligned}$$

or

$$\begin{aligned} \frac{1}{2} \frac{\partial}{\partial x} \left[ 0.09655859b \sqrt{r_0^2 - 0.075377b^2} + 0.0060504b^2 \right] \\ = \frac{L^2}{b^2} \left[ 0.65829521 \sqrt{r_0^2 - 0.075377b^2} + 0.11019775b \right] \end{aligned}$$

Differentiating,

$$\begin{aligned} \frac{1}{2} \frac{\partial b}{\partial x} & \left[ 0.09655859 \sqrt{r_o^2 - 0.075377b^2} \right. \\ & \left. - \frac{.09655859 * 0.075377b^2}{\sqrt{r_o^2 - .075377b^2}} + 0.121008b \right] \\ & = \left(\frac{L}{b}\right)^2 \left[ 0.65829521 \sqrt{r_o^2 - 0.075377b^2} + 0.11091775b \right] \end{aligned}$$

or,

$$\begin{aligned} \frac{1}{2} \frac{\partial b}{\partial x} & \left[ .09655859 (r_o^2 - 0.075377b^2) - .09655859 * 0.075377b^2 \right. \\ & \left. + 0.0121008b \sqrt{r_o^2 - 0.075377b^2} \right] \\ & = \frac{L^2}{b^2} \left[ 0.65829521 (r_o^2 - 0.075377b^2) \right. \\ & \left. + 0.11091775b \sqrt{r_o^2 - 0.075377b^2} \right] \end{aligned}$$

or,

$$\begin{aligned} \frac{\partial b}{\partial x} & = 2 \left(\frac{L}{b}\right)^2 \left[ 0.65829521 r_o^2 - 0.04962032b^2 + \right. \\ & \left. + 0.11091775b \sqrt{r_o^2 - 0.075377b^2} \right] / \\ & \left[ 0.09655859 r_o^2 - 0.01455659b^2 \right. \\ & \left. + 0.0121008 \sqrt{r_o^2 - 0.075377b^2} \right] \end{aligned}$$

(B.11)

## APPENDIX C

### HOT-WIRE EQUATIONS AND CALIBRATION

#### C.1 Hot-Wire Equations

##### C.1.1 Without A Linearizer

For a hot-wire anemometer without linearizer,

$$E^2 = A + BU_E^C \quad (C.1)$$

where  $E$  is the output voltage,  $U_E$  is the effective cooling velocity and  $A, B, C$  are constants. The effective cooling velocity is given by the following empirical equation [22]:

$$U_E^2 = U_N^2 + k_2^2 U_T^2 \quad (C.2)$$

where  $U_N$  is the velocity component normal to the wire and  $U_T$  is the tangential velocity component. Webster [90] and Champagne [91] determined  $k_2$  to be 0.20, with no dependence on the wire  $\ell/d$  ratio, and only a weak dependence on velocity.

Considering the wire in x-y plane; Figure C.1.

$$\left. \begin{aligned} U_N^2 &= \{(u+u')\cos\alpha + v'\sin\alpha\}^2 + w'^2 \\ \text{and} \\ U_T^2 &= \{(u+u')\sin\alpha - v'\cos\alpha\}^2 \end{aligned} \right\} \quad (C.3)$$

Assuming weak turbulence, so that:

$$u \gg u', \quad u \gg v', \quad u \gg w'$$

Neglecting terms containing quadratic and higher powers of fluctuating velocities, Equation (C.3) becomes:

$$\left. \begin{aligned} U_N &= u\cos\alpha \left[ \left(1 + \frac{u'}{u}\right) + \frac{v'}{u}\tan\alpha \right] \\ U_T &= u\cos\alpha \left[ \left(1 + \frac{u'}{u}\right)\tan\alpha - \frac{v'}{u} \right] \end{aligned} \right\} \quad (C.4)$$

Using Equation (C.4) in Equation (C.2):

$$\begin{aligned}
 U_E^2 &= u^2 \cos^2 \alpha \left[ 1 + 2 \frac{u'}{u} + \frac{u'^2}{u^2} + 2 \tan \alpha \left( \frac{u'}{u} + \frac{u' u'}{u^2} \right) \right. \\
 &+ \frac{u'^2}{u^2} \tan^2 \alpha + k_2^2 \left\{ \frac{u'^2}{u^2} - 2 \tan \alpha \left( \frac{u'}{u} + \frac{u' u'}{u^2} \right) \right. \\
 &\left. \left. + \tan^2 \alpha \left( 1 + 2 \frac{u'}{u} + \frac{u'^2}{u^2} \right) \right\} \right]
 \end{aligned}$$

or

$$\begin{aligned}
 U_E^c &= u^c \cos^c \alpha \left[ 1 + 2 \frac{u'}{u} + \frac{u'^2}{u^2} + 2 \tan \alpha \left( \frac{u'}{u} + \frac{u' u'}{u^2} \right) \right. \\
 &+ \frac{u'^2}{u^2} \tan^2 \alpha + k_2^2 \left\{ \frac{u'^2}{u^2} - 2 \tan \alpha \left( \frac{u'}{u} + \frac{u' u'}{u^2} \right) \right. \\
 &\left. \left. + \tan^2 \alpha \left( 1 + 2 \frac{u'}{u} + \frac{u'^2}{u^2} \right) \right\} \right]^{c/2} \quad (C.5)
 \end{aligned}$$

Expanding Equation (C.5) in power series and retaining the first power terms of fluctuating components:

$$U_E^c = s_1 u^c \cos^c \alpha \left[ 1 + c \frac{u'}{u} + c \frac{s_1}{s_2} \frac{u'}{u} \right] \quad (C.6)$$

where,

$$s_1 = 1 + \frac{c}{2} k_2^2 \tan^2 \alpha + \frac{c(c-2)}{8} k_2^4 \tan^4 \alpha$$

$$s_2 = \tan \alpha \left[ 1 - k_2^2 \left( 1 - \frac{c-2}{2} \tan^2 \alpha \right) + \frac{k_2^4}{2} \tan^2 \alpha \right]$$

$$* \left( 2 - c + \frac{(c-2)(c^2-4)}{4} \tan^2 \alpha \right) \quad (C.7)$$

The hot-wire anemometer output voltage, E, has mean and fluctuating components:

$$E = \bar{E} + e \quad (C.8)$$

Using Equations (C.6) and (C.8) in Equation (C.1) and assuming  $\bar{E} \gg e$ :

$$\bar{E}^2 + 2\bar{E}e = A + Bs_1 u^c \cos^c \alpha \left[ 1 + c \frac{u'}{u} + c \frac{s_2}{s_1} \frac{u'}{u} \right] \quad (C.9)$$

Taking average of Equation (C.9):

$$\bar{E}^2 = A + (Bs_1 \cos^c \alpha) u^c \quad (C.10)$$

$(Bs_1 \cos^c \alpha)$  is the slope in the plane  $\bar{E}^2$  vs.  $u^c$ . Using experimental values of  $\bar{E}$  and  $u$ , a series of curves can be drawn in the plane with different values of  $c$ . The best fit curve designates the best value of  $c$ , and it is represented by calibration curves in Figures C.4 and C.5 for normal and slanting wires respectively.

To linearize a signal it is necessary to set the value of  $c$  on the linearizer. The determined value of  $c$  does not always give the best linearization, but it can be adjusted by trial.

### C.1.2 With a Linearizer

For a hot-wire anemometer with a linearizer:

$$E_L = B_L U_E \quad (C.11)$$

where  $E_L$  is the linearizer output and  $B_L$  is a constant. The expression for cooling velocity,  $U_E$  for this case is obtained by using  $c=1$  in Equation (C.6):

$$U_E = s_1 u \cos \alpha \left[ 1 + \frac{u'}{u} + \frac{s_1}{s_2} \frac{u'}{u} \right] \quad (C.12)$$

For  $c=1$ ,  $s_1$  and  $s_2$  from Equation (C.7):

$$\left. \begin{aligned} s_1 &= 1 + \frac{1}{2}k_2^2 \tan^2 \alpha - \frac{1}{8}k_2^4 \tan^4 \alpha \\ s_2 &= \tan \alpha \left[ 1 - k_2^2 \left( 1 + \frac{1}{2} \tan^2 \alpha \right) + \frac{k_2^4}{2} \tan^4 \alpha \left( 1 + \frac{3}{4} \tan^2 \alpha \right) \right] \end{aligned} \right\} \text{(C.13)}$$

The output voltage,  $E_L$ , has two components:

$$E_L = \bar{E}_L + e_L \quad \text{(C.14)}$$

Using Equations (C.14) and (C.12) in Equation (C.11):

$$\bar{E}_L + e_L = B_L s_1 u \cos \alpha \left[ 1 + \frac{u'}{u} + \frac{s_2}{s_1} \frac{u'}{u} \right] \quad \text{(C.15)}$$

Taking mean of Equation (C.15):

$$\bar{E}_L = (B_L s_1 \cos \alpha) u \quad \text{(C.16)}$$

$$\bar{E}_L = (\text{slope}) u \quad \text{(C.17)}$$

where,

$$(\text{slope}) = B_L s_1 \cos \alpha$$

For normal wire,  $\alpha=0$  and  $s_1=1$ , so, the slope,  $n_1$  for normal wire becomes,  $n_1=B_L$ , and the slope,  $n_2$  for slanting wire is;  $n_2=B_L s_1 \cos \alpha$ . The best values  $n_1$  and  $n_2$  for normal and slanting wires are determined by calibration presented later:

Subtracting Equation (C.16) from Equation (C.15):

$$e_L = (B_L s_1 \cos \alpha) \left[ u' + \frac{s_2}{s_1} u' \right] \quad \text{(C.18)}$$

If a wire is located normal to the flow in Position I, and a single slanting wire is placed alternately in Positions II and III, as shown in Figure C.2, Equation (C.18) can be written as:

$$\left. \begin{aligned}
 e_{L1} &= n_1 u_1, \text{ since } s_2=0 \\
 e_{L2} &= n_2 \left( u' + \frac{s_2}{s_1} u' \right) \\
 e_{L3} &= n_2 \left( u' - \frac{s_2}{s_1} u' \right)
 \end{aligned} \right\} \quad (C.19)$$

If Position III is obtained by rotating the wire  $180^\circ$  about the axis of the wire support, then  $n_2=n_3$ .

Equation (C.19) can be written as:

$$\overline{u'^2} = \overline{e_{L1}^2} / n_1^2$$

$$\overline{u'^2} = (s_1/s_2)^2 \left[ (\overline{e_{L2}^2} + \overline{e_{L3}^2}) / 2n_2^2 - \overline{u'^2} \right] \quad (C.20)$$

$$\overline{u' u'} = s_1/s_2 (\overline{e_{L2}^2} - \overline{e_{L3}^2}) / 4n_2^2$$

The values of  $\overline{e_{L1}^2}$ ,  $\overline{e_{L2}^2}$  and  $\overline{e_{L3}^2}$  were obtained by squaring the voltage which were read from the RMS meter to the hot-wire anemometer, and with the wires in Positions I, II and III. The constant  $(s_1/s_2)$  was determined by calibration in a developed pipe flow as in ref. [3]. As a check,  $s_1$  and  $s_2$  were also calculated from Equation (C.13) knowing  $\alpha$  from measurement and  $k_2=0.2$  for wires ( $l/d=200$ ) used here.

## C.2 Calibration

### C.2.1 Determination of c

The hot-wire Equation (C.10) for an anemometer without a linearizer contains three empirical constants. For calibration purpose  $\overline{E^2}$  and  $u$  were measured by increasing the main flow, in steps, to give the nozzle exit velocities

from 2.5 m/s to 100 m/s. The measured values of  $\bar{E}^2$  and  $u^2$  were plotted by least square principle varying the values of  $c$  between 0.4 and 0.5. The least RMS deviation designates the best value of  $c$ , and typical plottings for normal and slanting wires are shown in Figures C.4 and C.5, respectively.

### C.2.2 Anemometer with a Linearizer

The hot-wire anemometer signal is nonlinear. At higher degrees of turbulence, the distortion caused by the curvature of the calibration curve becomes noticeable; also, measurements at varying degrees of mean flow velocity are rendered difficult by consequent sensitivity variations. This problem is overcome by linearizing the signal through an electronic circuit. The hot-wire Equation (C.17) for this case contains one empirical constant.

For calibrating the hot-wire anemometer, the hot-wire and the pitot tube were placed side by side in a core of uniform velocity. A suitable value of the exponent,  $c$ , is necessary to set to the linearizer to produce a linearized signal. The best value of  $c$  obtained by curve fitting principle described in Section C.2.1 does not always produce the best linearization. By trial,  $c$  was adjusted to the linearizer to achieve the best linear output. The values of  $c$  for the best linear output and that obtained in Section C.2.1 for a number of wires ( $5\mu$ ,  $l/d = 200$ ) are shown in Table C.1. Adjusting the value of  $c$  to the linearizer,  $\bar{E}$  and  $u$  were measured. Typical calibration curves for both normal and slanting wire are shown in Figure C.6. The calibration was



TABLE C.1: Best Values of Exponent  $c$  in Hot-Wire Equation

Wire	Velocity Range (m/s)	Points of Calibration	Best Fit Without Linearizer		Best Fit With Linearizer	
			$c$	RMS Dev.	$c$	RMS Dev.
N-1	1.5-100	12	0.46	0.128	0.47	0.078
N-2	1.5-100	12	0.44	0.095	0.48	0.101
N-3	1.5-100	12	0.40	0.132	0.48	0.121
N-4	1.5-100	12	0.45	0.115	0.46	0.098
S-1	1.5-100	12	0.49	0.085	0.50	0.131
S-1	1.5-100	12	0.50	0.068	0.48	0.110
S-2	1.5-100	12	0.50	0.099	0.50	0.115

checked by measuring shear stress and turbulent intensities in a fully developed pipe flow and comparing these with the measurements of Tucker [3] and Laufer [92] as shown in Figures C.8 and C.9.

A straight commercial aluminum pipe of 10.8 cm inside diameter and 15.24 m long was connected to a wooden settling chamber of length 1.65 m and cross-section 0.91 m x 0.91 m square. The settling chamber, having flow straighteners and screens inside, received air from a blower through a flexible pipe. The turbulent intensities and shear stress were measured by a hot-wire anemometer (type 55M10) with a linearizer (type 55D10) at the exit of the pipe. The inside surface of the pipe was polished by glasswool. The hot-wire probe was traversed over a scale of precision 0.0254 mm.

The low velocity calibration was performed following the procedure given in the instruction manual for the linearizer type 55D10. A typical low velocity calibration curve is shown in Figure C.7. The calibration of the pitot tube with the micromanometer is shown in Figure C.3.

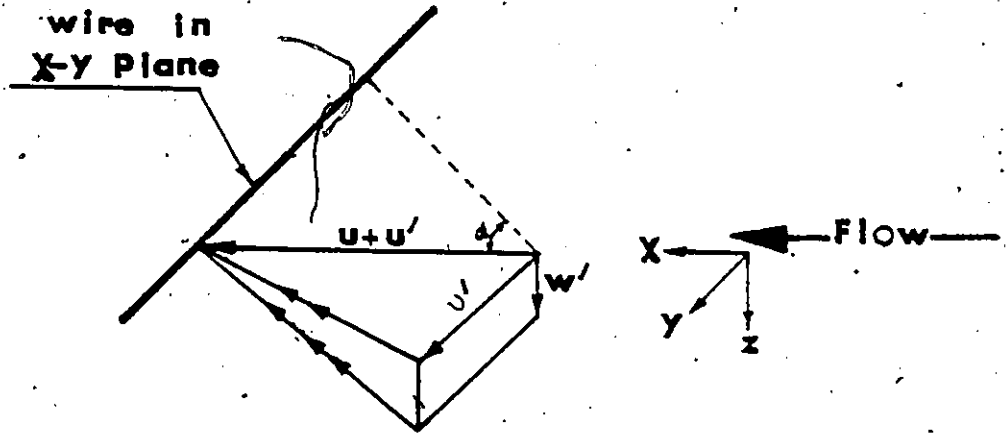


Fig.C.1

Wire Configuration in 3-Dimensional Velocity Field.

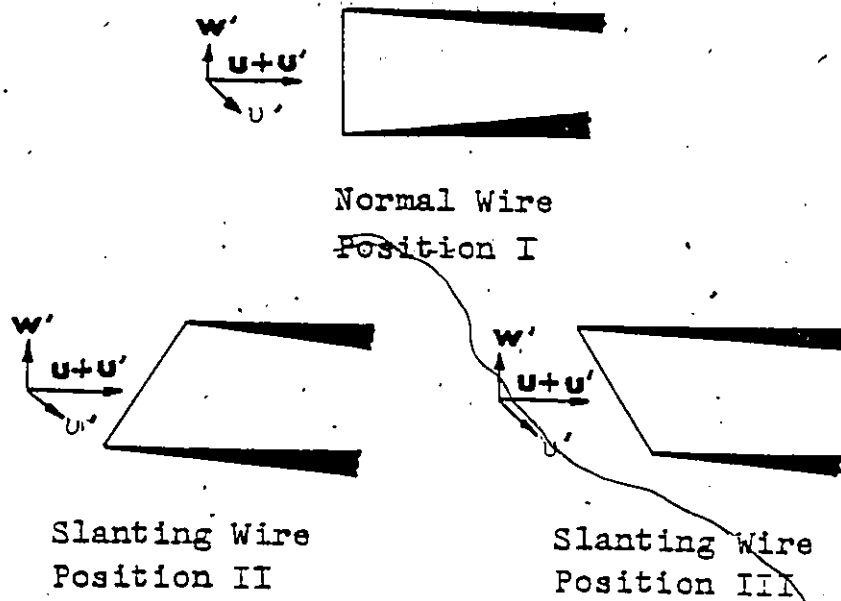


Fig.C.2

Hot-Wire Configuration for Measurements of  $\overline{u'^2}$ ,  $\overline{u'w'}$  and  $\overline{u'u'}$ .

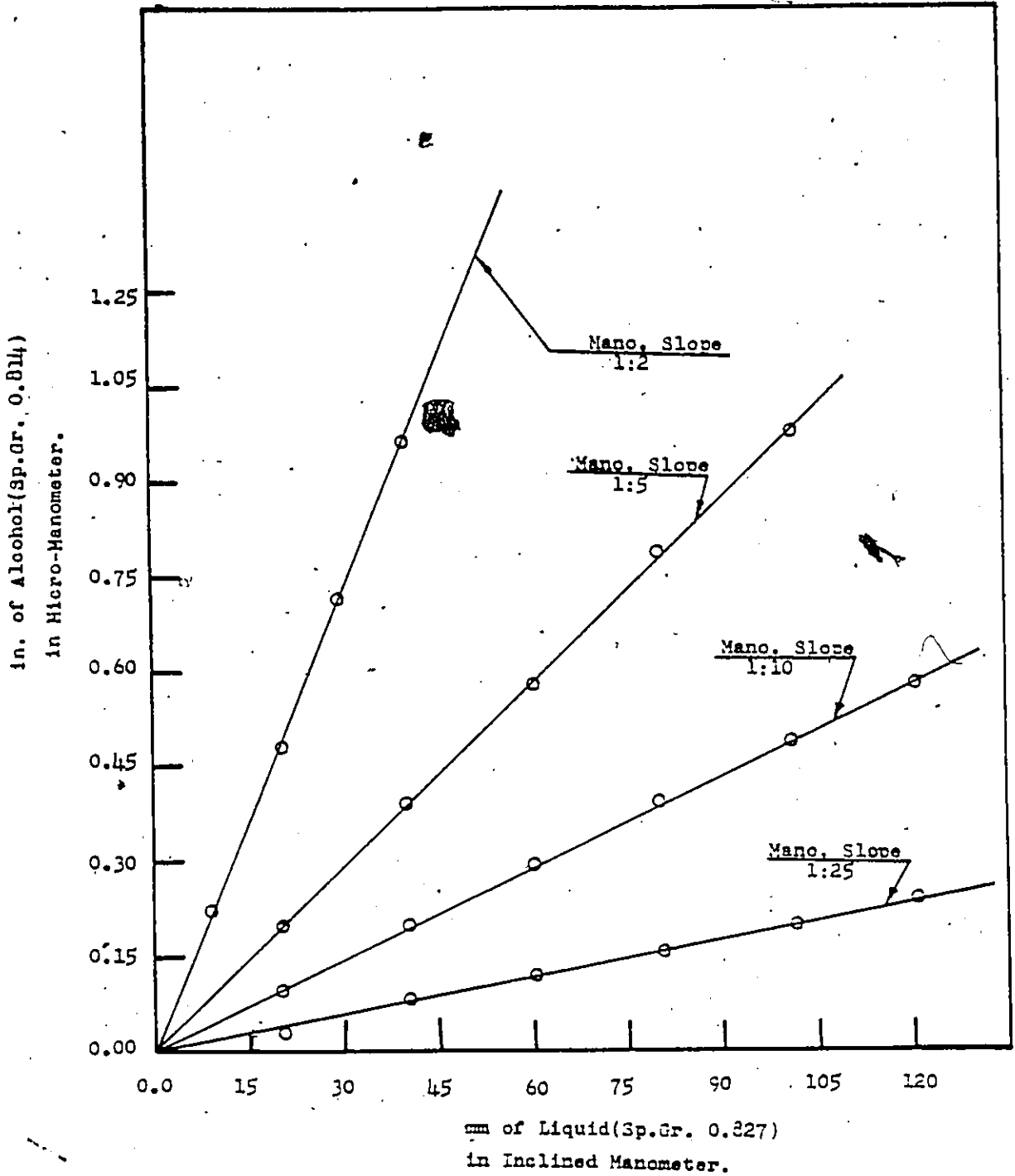


Fig.C.3

Calibration of a Pitot Tube Against a Micro-Manometer.

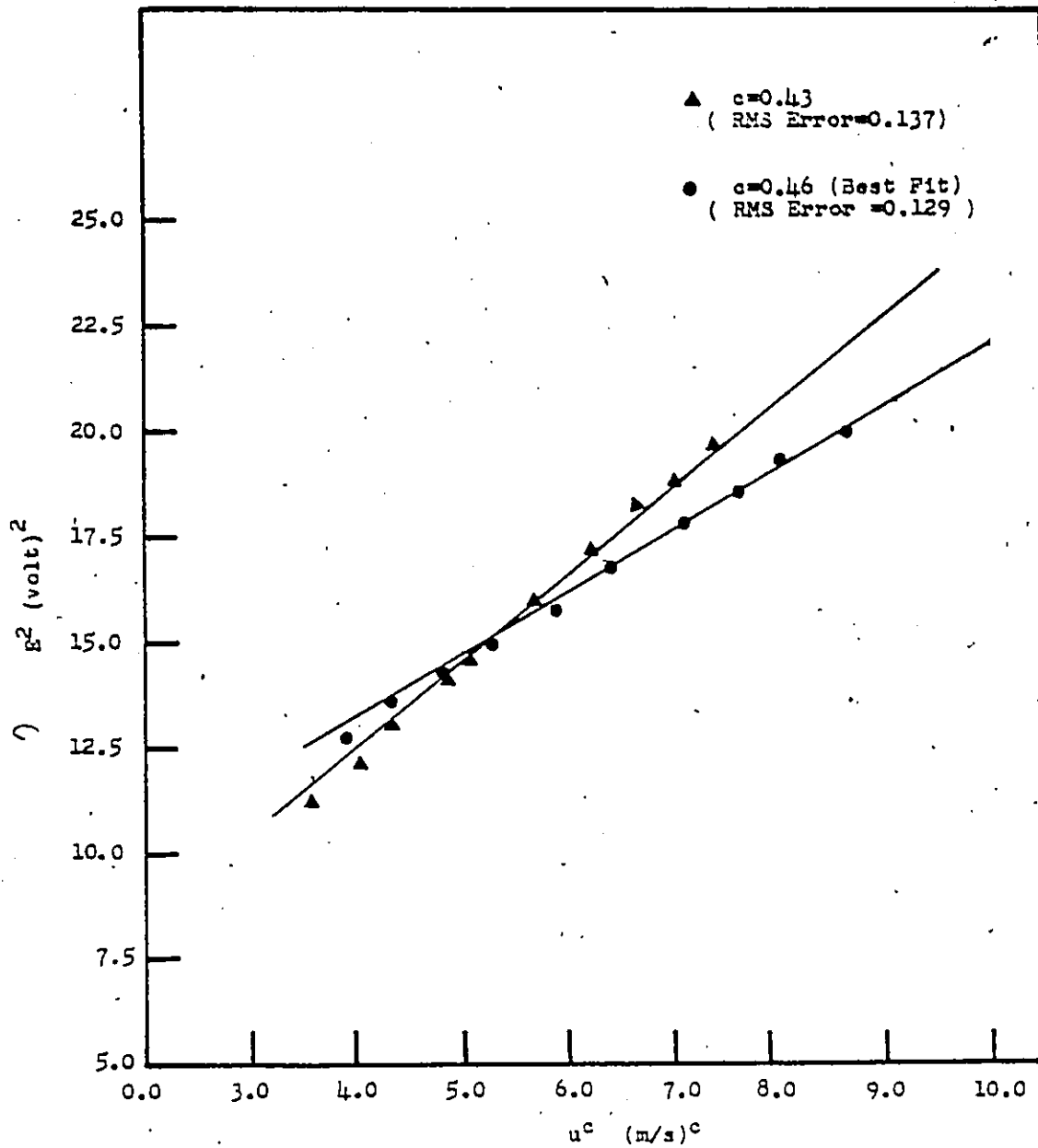


Fig.C.4

A Typical Calibration Curve for a Normal Wire  
Without a Linearizer.

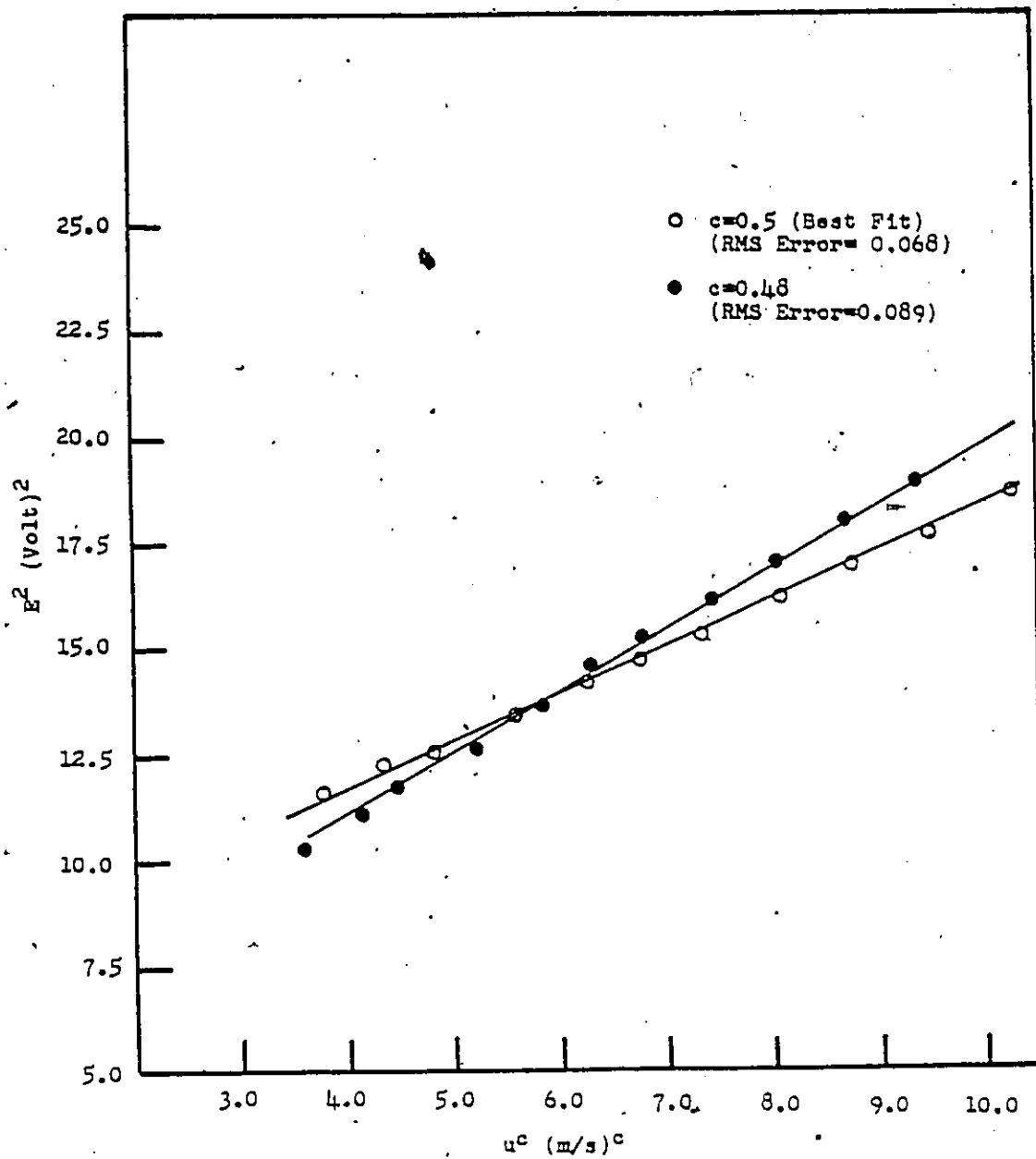


Fig.C.5

Typical Calibration Curves for a Slanting Wire Without a Linearizer.

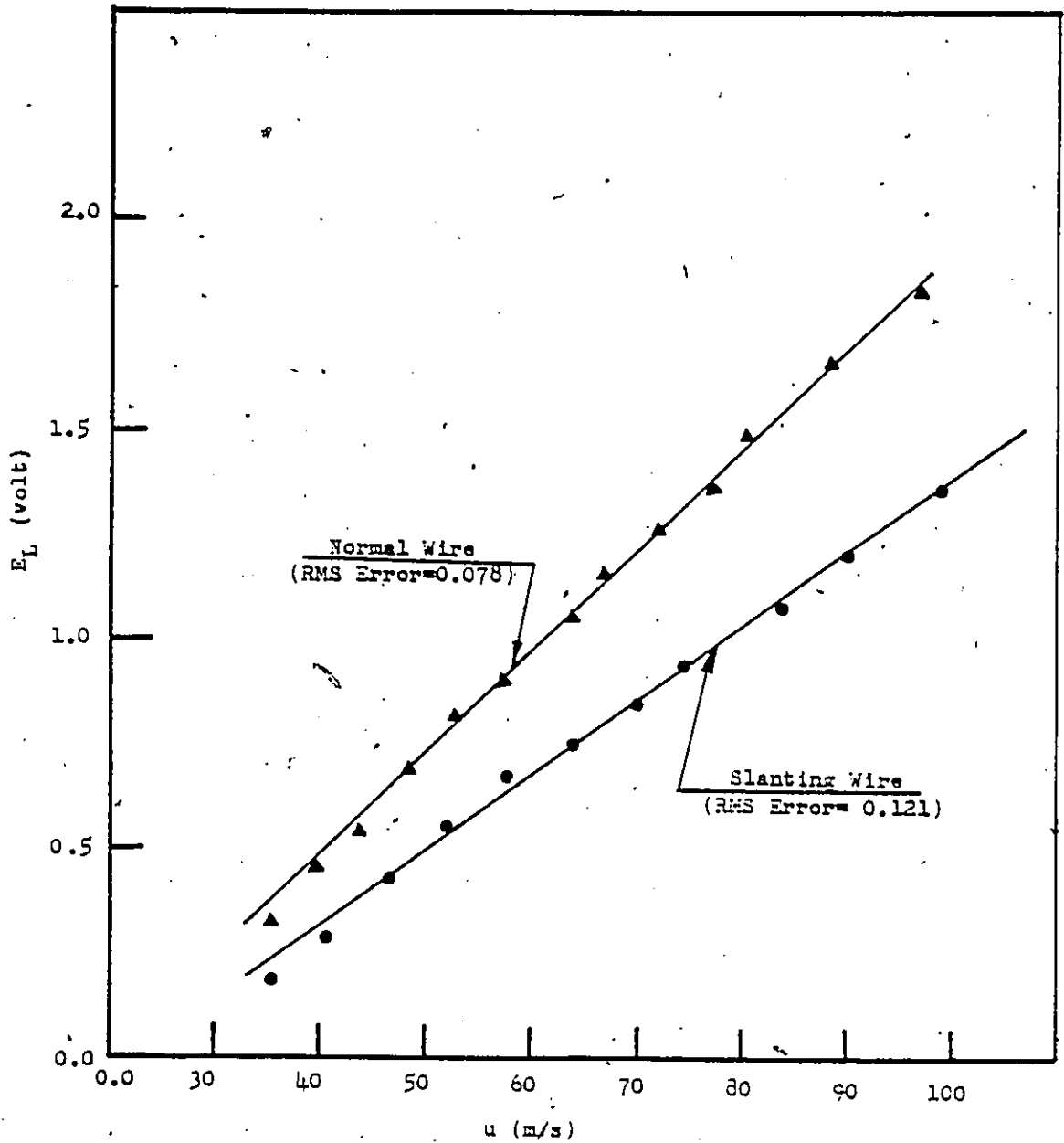


Fig.C.6

Typical Calibration Curves for Normal and Slanting Wires with a Linearizer.

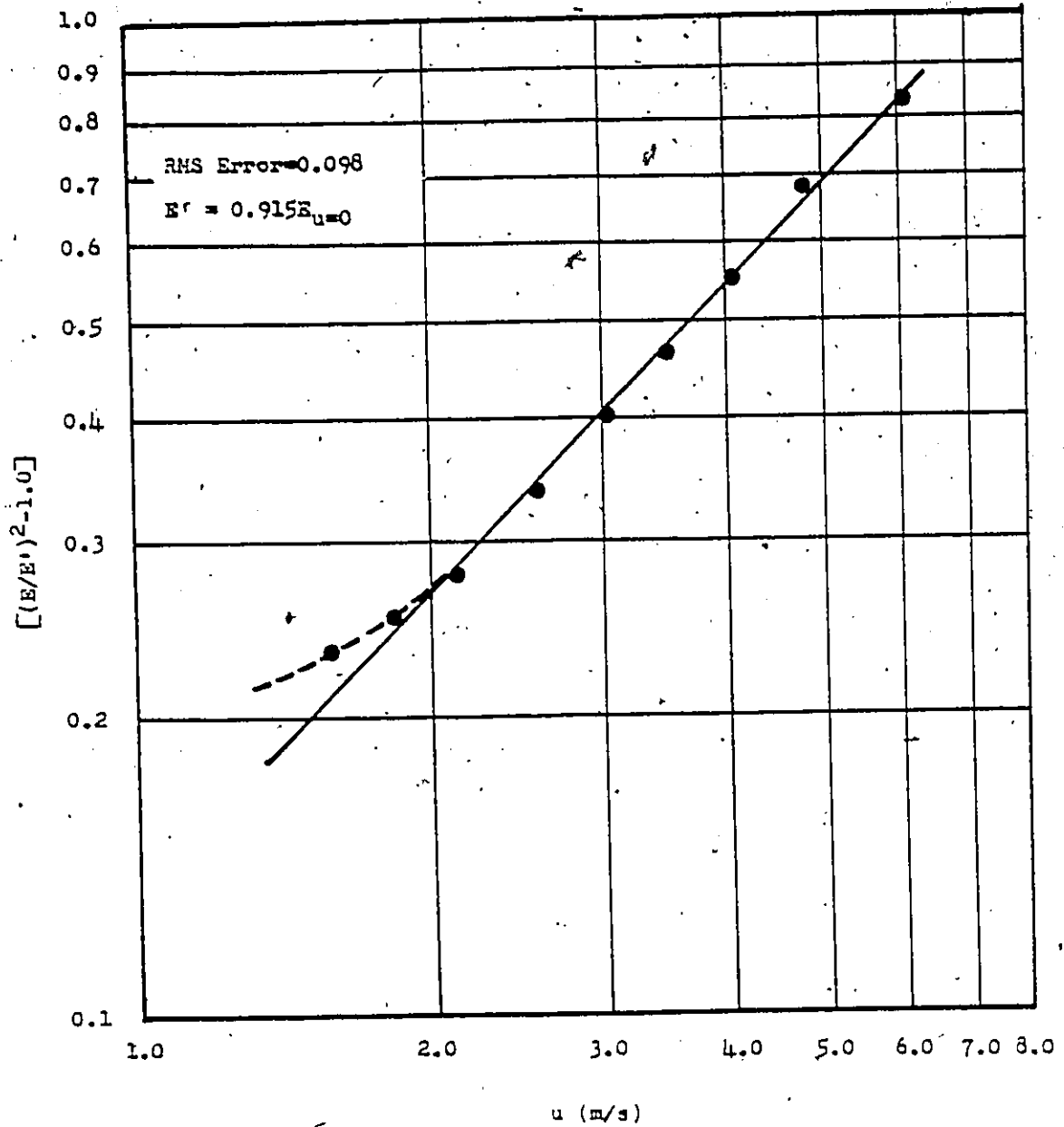


Fig.C.7

Typical Calibration Curve for Normal Wire at  
Low Velocity.



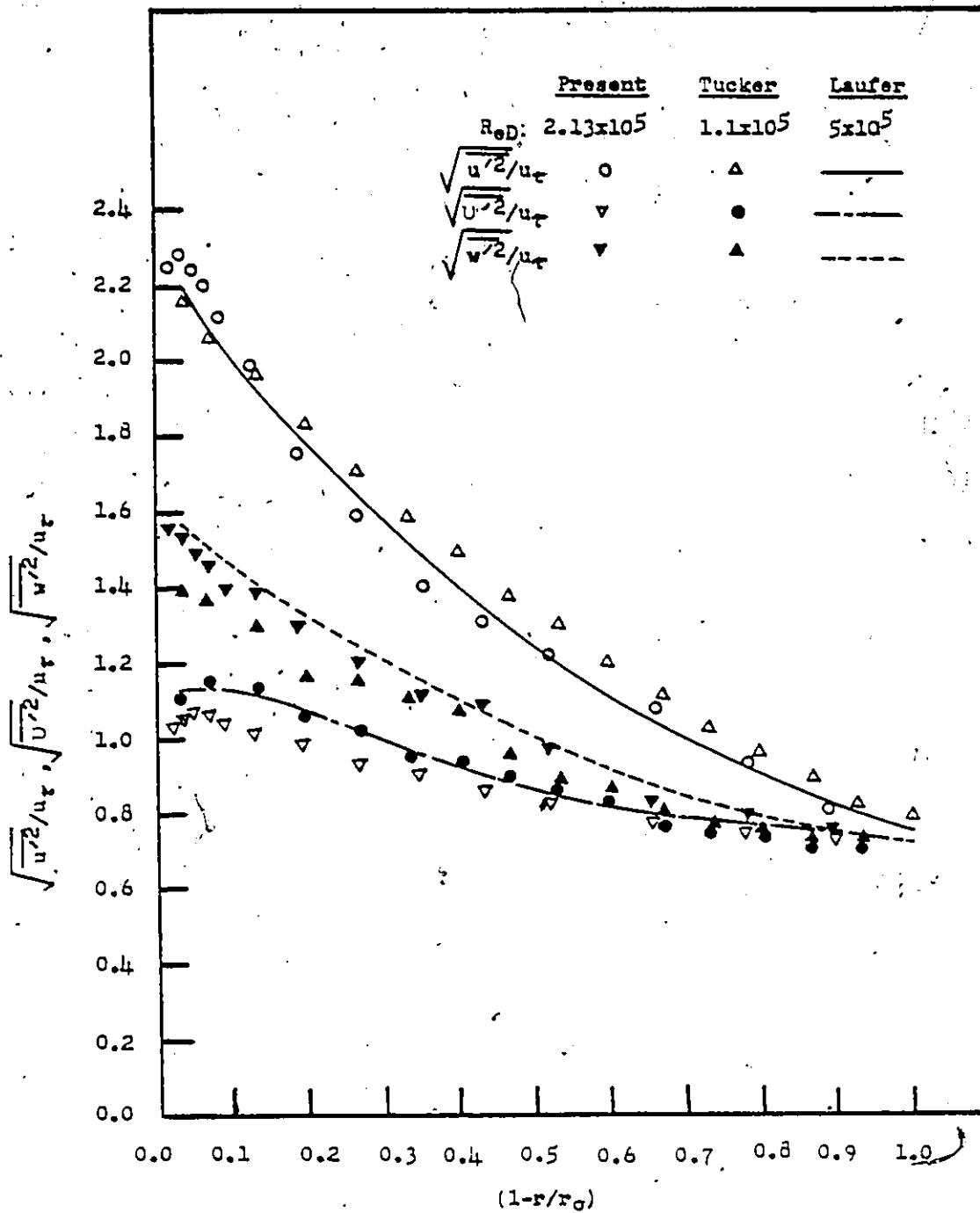


Fig.C.8

Distributions of Turbulent Intensities in a Fully Developed Pipe Flow.

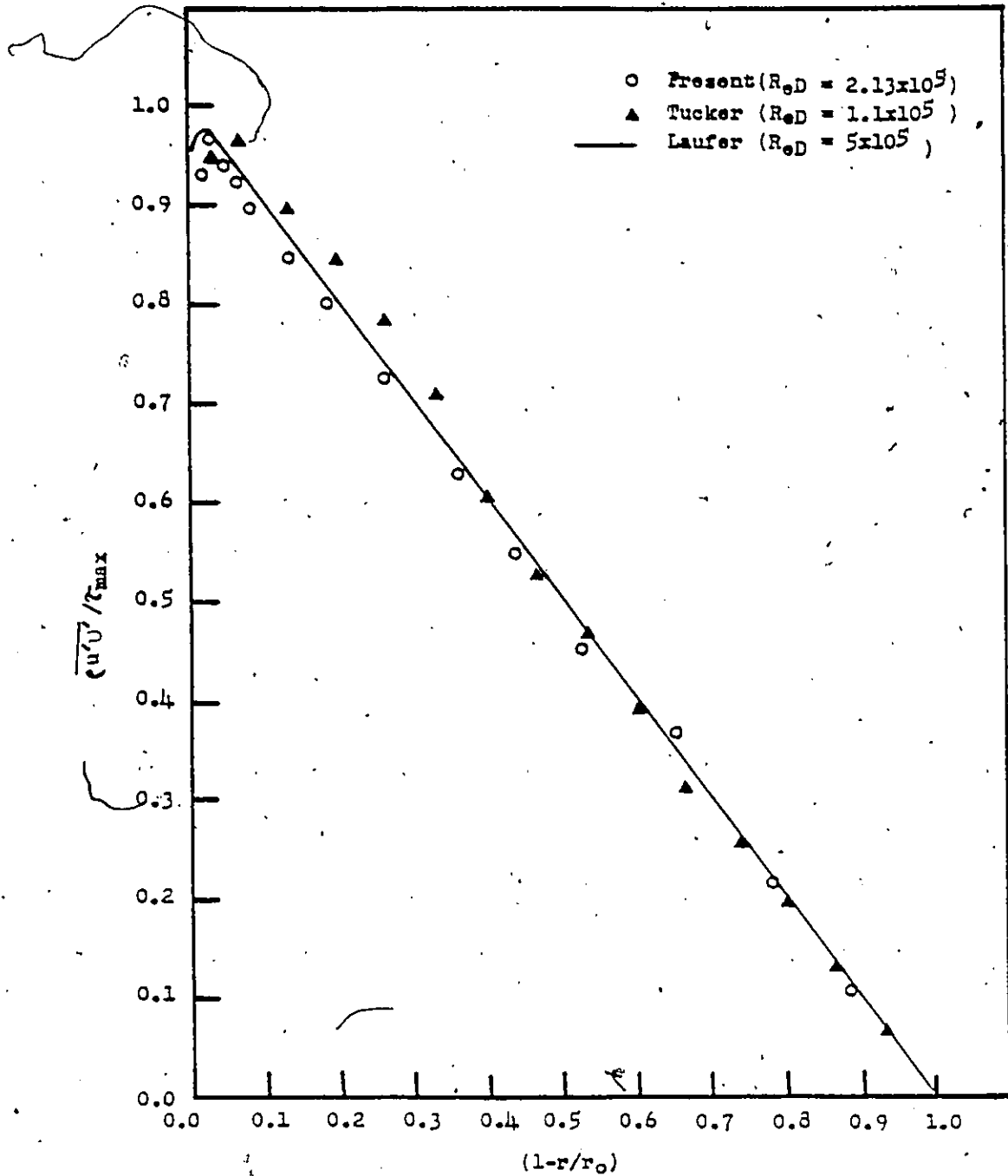


Fig.0.9

Reynold's Shear Stress Distributions in a Fully Developed Pipe Flow.

## APPENDIX D

### THE FINITE-DIFFERENCE FORMULATION

#### D.1 General

A standard explicit finite-difference technique requires very small streamwise steps [93] to satisfy the stability criterion. The Dufort-Frankel [94] method was found to be stable for the varying step size that was used here. The standard explicit scheme was used as a starting method for the Dufort-Frankel procedure which requires information from the two previous streamwise stations.

The finite-difference problem domain is usually established by letting  $\Delta X$  and  $\Delta R$  be small increments of the coordinates  $X$  and  $R$  and the considering of all the variables as existing on the finite set of points  $X=i\Delta X$ ,  $R=j\Delta R$  (valid for fixed  $\Delta X$ ,  $\Delta R$ ) where  $i$  and  $j$  are integers. Here the finite-difference equations will be written in a form that will be applicable for uneven grid spacing with  $x$  and  $r$  directions. For this purpose, the notation  $\Delta R_+ = (R_{j+1} - R_j)$ ,  $\Delta R_- = (R_j - R_{j-1})$ ,  $\Delta X_+ = (X_{i+1} - X_i)$  and  $\Delta X_- = (X_i - X_{i-1})$  will be introduced. The dependent variables are expanded in Taylor series [95].

The basic variables are made non-dimensional by using the following transformation.

$$\begin{aligned}
 X &= \frac{xu_0}{v}, & R &= \frac{ru_0}{v}, & L^* &= \frac{Lu_0}{v}, & N &= \frac{v+v_t}{v}, \\
 U &= \frac{u}{u_0}, & V &= \frac{v}{u_0}, & K^* &= \frac{k}{u_0^2}
 \end{aligned}
 \tag{D.1}$$

Replacing shear stress,  $\tau/\rho$  by  $(\nu + \nu_t) \partial u / \partial r$  and introducing the above transformation (D.1) in the continuity Equation (3.1), the momentum Equation (3.2) and the turbulent kinetic energy Equation (3.13):

the continuity equation is:

$$\frac{\partial (UR)}{\partial X} + \frac{\partial (VR)}{\partial R} = 0 \quad (D.2)$$

the momentum equation is:

$$U \frac{\partial U}{\partial X} + V \frac{\partial U}{\partial R} = \frac{1}{R} \frac{\partial}{\partial R} (RN \frac{\partial U}{\partial R}) \quad (D.3)$$

and the turbulent kinetic energy equation is:

$$U \frac{\partial K^*}{\partial X} + V \frac{\partial K^*}{\partial R} = P - \epsilon + \frac{1}{R} \frac{\partial}{\partial R} [k_q L^* K^* R \frac{\partial K^*}{\partial R}] \quad (D.4)$$

In all calculations  $L^1 = L$ .

## D.2 Finite Difference Equations for Dufort-Frankel Method

### D.2.1 Continuity Equation

Taylor's expansions about half a grid in r-direction and one grid in x-direction.

$$U(i+1, j+1) = U(i, j+\frac{1}{2}) + \Delta X_+ U_x + \frac{\Delta R_+}{2} U_r + \frac{1}{2} \{ (\Delta X_+)^2 U_{xx} + \Delta X_+ \Delta R_+ U_{xr} + (\frac{\Delta R_+}{2})^2 U_{rr} \} + O(\Delta^3) \quad (D.5)$$

$$U(i-1, j+1) = U(i, j+\frac{1}{2}) - \Delta X_- U_x + \frac{\Delta R_+}{2} U_r + \frac{1}{2} \{ (\Delta X_-)^2 U_{xx} - \Delta X_- \Delta R_+ U_{xr} + (\frac{\Delta R_+}{2})^2 U_{rr} \} + O(\Delta^3) \quad (D.6)$$

$$U(i+1, j) = U(i, j+\frac{1}{2}) + \Delta X_+ U_x - \frac{\Delta R_-}{2} U_r + \frac{1}{2} \{ (\Delta X_+)^2 U_{xx} - \Delta X_+ \Delta R_- U_{xr} + (\frac{\Delta R_-}{2})^2 U_{rr} \} + 0(\Delta^3) \quad (D.7)$$

$$U(i-1, j) = U(i, j+\frac{1}{2}) - \Delta X_- U_x - \frac{\Delta R_-}{2} U_r + \frac{1}{2} \{ (\Delta X_-)^2 U_{xx} + \Delta X_- \Delta R_- U_{xr} + (\frac{\Delta R_-}{2})^2 U_{rr} \} + 0(\Delta^3) \quad (D.8)$$

Subtracting (D.8) from (D.5), (D.7) from (D.6), and adding,

$$\left( \frac{\partial U}{\partial X} \right)_{i, j+\frac{1}{2}} = \frac{U(i+1, j+1) + U(i+1, j) - U(i-1, j+1) - U(i-1, j)}{2(\Delta X_+ + \Delta X_-)} + 0(\Delta) \quad (D.9)$$

Subtracting expansions for  $V$  as in Equation (D.5) and Equation (D.7):

$$\left( \frac{\partial V}{\partial R} \right)_{i, j+\frac{1}{2}} = \frac{V(i+1, j+1) - V(i+1, j)}{(\Delta R_+ + \Delta R_-)/2} \quad (D.10)$$

Using approximations (D.9) and (D.10) in the continuity Equation (D.1), the finite difference equation becomes:

$$\frac{R(j) + R(j+1)}{2} \frac{U(i+1, j+1) + U(i+1, j) - U(i-1, j+1) - U(i-1, j)}{2(\Delta X_+ + \Delta X_-)} + \frac{R(j+1)V(i+1, j+1) - R(j)V(i+1, j)}{(\Delta R_+ + \Delta R_-)/2} = 0 \quad (D.11)$$

### D.2.2 Momentum Equation

Taylor's expansion of  $U$  about one grid in  $r$ -direction,

$$U(i, j+1) = U(i, j) + \Delta R_+ U_r + \frac{(\Delta R_+)^2}{2} U_{rr} + 0(\Delta^3) \quad (D.12)$$

$$U(i, j-1) = U(i, j) - \Delta R_- U_r + \frac{(\Delta R_-)^2}{2} U_{rr} + O(\Delta^3) \quad (D.13)$$

Subtracting Equation (D.13) from Equation (D.12),

$$\left(\frac{\partial U}{\partial R}\right)_{i,j} = \frac{U(i, j+1) - U(i, j-1)}{\Delta R_+ + \Delta R_-} + O(\Delta^2) \quad (D.14)$$

Similarly, expanding U about one grid distance in x-direction it is obtained,

$$\left(\frac{\partial U}{\partial X}\right)_{i,j} = \frac{U(i+1, j) - U(i-1, j)}{(\Delta X_+ + \Delta X_-)} + O(\Delta^2) \quad (D.15)$$

Taylor's expansion of U about half a grid spacing in r-direction:

$$U(i, j+\frac{1}{2}) = U(i, j) + \frac{\Delta R_+}{2} U_r + \frac{1}{2} \left(\frac{\Delta R_+}{2}\right)^2 U_{rr} + O(\Delta^3) \quad (D.16)$$

$$U(i, j-\frac{1}{2}) = U(i, j) - \frac{\Delta R_-}{2} U_r + \frac{1}{2} \left(\frac{\Delta R_-}{2}\right)^2 U_{rr} + O(\Delta^3) \quad (D.17)$$

Subtracting Equation (D.17) from Equation (D.16),

$$\left(\frac{\partial U}{\partial R}\right)_{i,j} = \frac{2}{\Delta R_+ + \Delta R_-} [U(i, j+\frac{1}{2}) - U(i, j-\frac{1}{2})] \quad (D.18)$$

Similarly, it is written:

$$\left[\frac{\partial}{\partial R} \left\{ RN \frac{\partial U}{\partial R} \right\}\right]_{i,j} = \frac{2}{\Delta R_+ + \Delta R_-} \left[ \left( RN \frac{\partial U}{\partial R} \right)_{i, j+\frac{1}{2}} - \left( RN \frac{\partial U}{\partial R} \right)_{i, j-\frac{1}{2}} \right]$$

or,

$$\left[\frac{\partial}{\partial R} \left\{ RN \frac{\partial U}{\partial R} \right\}\right]_{i,j} = \frac{2}{\Delta R_+ + \Delta R_-} \left[ \frac{R(j)+R(j+1)}{2} \cdot \frac{N(i, j)+N(i, j+1)}{2} \right.$$

$$\left. * \left(\frac{\partial U}{\partial R}\right)_{i, j-\frac{1}{2}} - \frac{R(j)+R(j-1)}{2} \right.$$

$$\left. * \frac{N(i, j)+N(i, j-1)}{2} \left(\frac{\partial U}{\partial R}\right)_{i, j-\frac{1}{2}} \right] \quad (D.19)$$

Using expansions similar to Equations (D.16) and (D.17), it is written:

$$\left(\frac{\partial U}{\partial R}\right)_{i,j+\frac{1}{2}} = \frac{U(i,j+1)-U(i,j)}{\Delta R_+} + O(\Delta^2) \quad (D.20)$$

$$\left(\frac{\partial U}{\partial R}\right)_{i,j-\frac{1}{2}} = \frac{U(i,j)-U(i,j-1)}{\Delta R_-} + O(\Delta^2)$$

Writing the following expansions for U:

$$U(i+1,j) = U(i,j) + \Delta X_+ U_x + \frac{\Delta X_+^2}{2} U_{xx} + O(\Delta^3) \quad (D.21)$$

$$U(i-1,j) = U(i,j) - \Delta X_- U_x + \frac{\Delta X_-^2}{2} U_{xx} + O(\Delta^3) \quad (D.22)$$

Adding Equation (D.21) and Equation (D.22):

$$U(i,j) = 0.5[U(i+1,j) + U(i-1,j)] - \frac{\Delta X_+^2 + \Delta X_-^2}{2} U_{xx} + O(\Delta^4) \quad (D.23)$$

The differential equation is for a thin shear layer where  $U_{xx}$  is negligibly small compared to  $U_{rr}$ . Using Equations (D.23) and (D.20) in Equation (D.19):

$$\begin{aligned} \frac{\partial}{\partial R} \left\{ RN \frac{\partial U}{\partial R} \right\}_{i,j} &= \frac{2}{\Delta R_+ + \Delta R_-} \left[ \frac{R(j)+R(j+1)}{2} \cdot \frac{N(i,j)+N(i,j+1)}{2} \right. \\ &\quad * \frac{U(i,j+1) - 0.5\{U(i+1,j)+U(i-1,j)\}}{\Delta R_+} \\ &\quad - \frac{R(j)+R(j-1)}{2} \cdot \frac{N(i,j)+N(i,j+1)}{2} \\ &\quad \left. * \frac{0.5\{U(i+1,j)+U(i-1,j) - U(i,j-1)\}}{\Delta R_-} \right] + O(\Delta) \end{aligned} \quad (D.24)$$

Using Equations (D.24), (D.15) and (D.14) in Equation (D.3), the finite-difference equation for the momentum equation is:

$$\begin{aligned}
 U(i,j) & \frac{U(i+1,j)-U(i-1,j)}{\Delta X_+ + \Delta X_-} + v(i,j) \frac{U(i,j+1)-U(i,j-1)}{\Delta R_+ + \Delta R_-} \\
 & = \frac{1}{R(j)} \frac{2}{\Delta R_+ + \Delta R_-} \left[ \frac{R(j)+R(j+1)}{2} \cdot \frac{N(i,j)+N(i,j+1)}{2} \right. \\
 & \quad * \frac{U(i,j+1)-0.5\{U(i+1,j)-U(i-1,j)\}}{\Delta R_+} - \frac{R(j)+R(j-1)}{\Delta 2} \\
 & \quad \left. * \frac{N(i,j)+N(i,j-1)}{2} \cdot \frac{0.5\{U(i+1,j)+U(i-1,j)\}-U(i,j-1)}{\Delta R_-} \right]
 \end{aligned} \tag{D.25}$$

### D.2.3 Turbulent Energy Equation

Using the similar approximation as for the momentum equation, the finite-difference equation for the turbulent energy equation (D.4) is:

$$\begin{aligned}
 U(i,j) & \frac{K^*(i+1,j)-K^*(i-1,j)}{\Delta X_+ + \Delta X_-} + v(i,j) \frac{K^*(i,j+1)-K^*(i,j-1)}{\Delta R_+ + \Delta R_-} \\
 & = P(i,j) - \epsilon(i,j) + \frac{k_q}{R(j)} \frac{L^*(i)}{\Delta R_+ + \Delta R_-} \\
 & \quad * \left[ \frac{R(j)+R(j+1)}{2} \cdot \frac{K^*(i,j)+K^*(i,j+1)}{2} \right. \\
 & \quad * \frac{K^*(i,j+1)-0.5\{K^*(i+1,j)+K^*(i-1,j)\}}{\Delta R_+} \\
 & \quad - \frac{R(j)+R(j-1)}{2} \cdot \frac{K^*(i,j)+K^*(i,j-1)}{2} \\
 & \quad \left. * \frac{0.5\{K^*(i+1,j)+K^*(i-1,j)\}-K^*(i,j-1)}{\Delta R_-} \right]
 \end{aligned}$$

(D.26)



and,

$$P(i, j) = a_1 \text{TAU}(i, j) \cdot \frac{U(i, j+1) - U(i, j-1)}{\Delta R_+ + \Delta R_-} \quad (\text{D.27})$$

$$c(i, j) = c_r \frac{[K^*(i, j)]^{3/2}}{L^*(i)} \quad (\text{D.28})$$

$$\text{TAU}(i, j) = L^{*2}(i) \left| \frac{U(i, j+1) - U(i, j-1)}{\Delta R_+ + \Delta R_-} \right| \left( \frac{U(i, j+1) - U(i, j-1)}{\Delta R_+ + \Delta R_-} \right) \quad (\text{D.29})$$

### D.3 Direct Explicit Scheme

The finite-difference equations for this scheme were used to start the Dufort-Frankel method. These equations can be derived by standard method [95].

the continuity equation is:

$$\begin{aligned} & \frac{R(j+1)}{4\Delta X} [U(i+1, j) - U(i, j) + U(i+1, j+1) - U(i, j+1)] \\ & + \frac{1}{\Delta R} [R(j+1)V(i+1, j+1) - R(j)V(i+1, j)] = 0 \end{aligned} \quad (\text{D.30})$$

the momentum equation is:

$$\begin{aligned} U(i, j) & \frac{U(i+1, j) - U(i, j)}{\Delta X} + V(i, j) \frac{U(i, j) - U(i, j-1)}{\Delta R_-} \\ & = \frac{1}{R(j)} \frac{2}{\Delta R_+ + \Delta R_-} \left[ \frac{R(j) + R(j+1)}{2} \cdot \frac{N(i, j) + N(i, j+1)}{2} \right. \\ & * \frac{U(i, j+1) - U(i, j)}{\Delta R_+} - \frac{R(j) + R(j-1)}{2} \\ & * \left. \frac{N(i, j) + N(i, j-1)}{2} \cdot \frac{U(i, j) - U(i, j-1)}{\Delta R_-} \right] \end{aligned} \quad (\text{D.31})$$

the turbulent energy equation is:

$$\begin{aligned}
 U(i,j) & \frac{K^*(i+1,j)-K^*(i,j)}{\Delta X} + V(i,j) \frac{K^*(i,j)-K^*(i,j-1)}{\Delta R_-} \\
 & = P(i,j) - \epsilon(i,j) + \frac{1}{R(j)} \frac{2k_o L^*(i)}{\Delta R_+ + \Delta R_-} \left[ \frac{R(j)+R(j+1)}{2} \right. \\
 & * \frac{K^*(i,j)+K^*(i,j+1)}{2} \frac{K^*(i,j+1)-K^*(i,j)}{\Delta R_+} - \frac{R(j)+R(j-1)}{2} \\
 & * \left. \frac{K^*(i,j)+K^*(i,j-1)}{2} \frac{K^*(i,j)-K^*(i,j-1)}{\Delta R_-} \right] \quad (D.32)
 \end{aligned}$$

where,

$$P(i,j) = a_1 \text{TAU}(i,j) \frac{U(i,j+1)-U(i,j)}{\Delta R_+} \quad (D.33)$$

$$\epsilon(i,j) = c_r \frac{[K^*(i,j)]^{3/2}}{L^*(i)} \quad (D.34)$$

$$\text{TAU}(i,j) = L^{*2}(i) \left| \frac{U(i,j+1)-U(i,j)}{\Delta R_+} \right| \frac{U(i,j+1)-U(i,j)}{\Delta R_+} \quad (D.35)$$

TAU(i,j) is the shear stress, P(i,j) is the production of turbulent energy and  $\epsilon(i,j)$  is the dissipation of energy.

## APPENDIX E

### STABILITY ANALYSIS OF THE MOMENTUM EQUATION

The finite-difference solution should ensure:

1) the solution being obtained is that corresponding to the partial differential equations, at least if the mesh were to be refined in a particular manner.

2) due to the particular method of solution, round off errors or errors from any source are not amplified or allowed to grow in subsequent steps in the solution.

The first point is called the consistency condition [96] which can be studied by expanding the dependent variables in Taylor series expansions in a manner such that the difference between the partial differential equations and the finite difference representation can be observed [96,97]. This difference is known as truncation error of the equations, and if it vanishes in the limit as the mesh size is shrunk, the finite difference representation is said to be consistent.

The second point is called the stability condition. In dealing with stability and convergence, the ideas of Von Neumann [79] were used.

Let the error growth in  $U$  be  $\delta$ , and according to Neumann [79], it was expressed in first harmonic by:

$$\delta = Ae^{\beta_1 R} e^{i\beta_2 X} \quad (E.1)$$

With the error, the velocities change to:

$$\left. \begin{aligned} \dot{U}(i, j+1) &\sim U(i, j+1) + \delta(i, j+1) \\ U(i, j-1) &\sim U(i, j-1) - \delta(i, j-1) \\ U(i+1, j) &\sim U(i+1, j) + \delta(i+1, j) \end{aligned} \right\} \quad (E.2)$$

and

$$\left. \begin{aligned} \delta(i, j+1) &= Ae^{\beta_1(R+\Delta R)} e^{i\beta_2 X} \\ \delta(i, j-1) &= Ae^{\beta_1(R-\Delta R)} e^{i\beta_2 X} \end{aligned} \right\} \quad (E.3)$$

etcetera

Substituting Equation (E.2) in Equation (D.25) and then subtracting Equation (D.25) and using  $\Delta R_+ = \Delta R_- = \Delta R$ :

$$\begin{aligned} U(i, j) & \frac{\delta(i+1, j) - \delta(i-1, j)}{\Delta X_+ + \Delta X_-} + V(i, j) \frac{\delta(i, j+1) - \delta(i, j-1)}{\Delta R} \\ &= \frac{1}{2(\Delta R)^2} \left[ \left( 1 + \frac{\Delta R}{2R(j)} \right) (N(i, j) + N(i, j+1)) \right. \\ & * \{ \delta(i, j+1) - 0.5(\delta(i+1, j) + \delta(i-1, j)) \} - \left( 1 - \frac{\Delta R}{2R(j)} \right) \\ & * \left. (N(i, j) + N(i, j-1)) \{ 0.5(\delta(i+1, j) + \delta(i-1, j)) - \delta(i, j-1) \} \right] \end{aligned} \quad (E.4)$$

Substituting Equation (E.3) in Equation (E.4), using  $\xi = e^{\beta_1 \Delta R}$  and rearranging:

$$\xi^2 + A_0 \xi + B_0 = 0 \quad (E.5)$$

where,

$$A_0 = \frac{-U(i, j) / (\Delta X_+ + \Delta X_-)}{\frac{V(i, j)}{2\Delta R} - \frac{1}{2(\Delta R)^2} \left( 1 + \frac{\Delta R}{2R(j)} \right) (N(i, j) + N(i, j+1))}$$

$$B_0 = \frac{V(i,j)/2\Delta R + \frac{1}{2(\Delta R)^2} \left(1 - \frac{\Delta R}{R(j)}\right) (N(i,j) + N(i,j-1))}{\frac{V(i,j)}{2\Delta R} - \frac{1}{2(\Delta R)^2} \left(1 + \frac{\Delta R}{2R(j)}\right) (N(i,j) + N(i,j+1))}$$

The roots of Equation (E.5) is:

$$\xi = -\frac{A_0}{2} \pm \sqrt{\left(\frac{A_0}{2}\right)^2 - B_0} \quad (E.6)$$

According to Von Neumann [79] stability condition,

$$|\xi| \leq 1 \quad (E.7)$$

For real roots, inequality (E.7) are:

$$-\frac{A_0}{2} + \left(\frac{A_0}{2}\right)^2 - B_0 \leq 1 \quad (E.8)$$

$$-\frac{A_0}{2} - \left(\frac{A_0}{2}\right)^2 - B_0 \geq -1 \quad (E.9)$$

For  $A_0 > 0$ , Equation (E.9), and for  $A_0 < 0$ , Equation (E.8) yield:

$$(A_0 - B_0) \leq 1 \quad (E.10)$$

Using expressions for  $A_0$  and  $B_0$  in Equation (E.10) and rearranging,

$$-\frac{U(i,j)}{\Delta X_+ + \Delta X_-} \leq \left[ \frac{V(i,j)}{\Delta R} + \frac{1}{2\Delta R} \left( \frac{N(i,j-1) + N(i,j+1)}{\Delta R} \right) \left( 1 - \frac{\Delta R}{2R(j)} \right) \right] \quad (E.11)$$

Since  $U(i,j)/(\Delta X_+ + \Delta X_-)$  is always positive,

$$\frac{U(i,j)}{\Delta X_+ + \Delta X_-} \geq \left| \frac{V(i,j)}{\Delta R} + \frac{1}{2\Delta R} \left( \frac{N(i,j-1) + N(i,j+1)}{\Delta R} \right) \left( 1 - \frac{\Delta R}{2R(j)} \right) \right|$$

or,

$$(\Delta X_+ + \Delta X_-) \leq \frac{U(i,j)\Delta R}{\left| \frac{V(i,j)}{\Delta R} + \frac{(N(i,j-1) + N(i,j+1))}{2\Delta R} \left( 1 - \frac{\Delta R}{2R(j)} \right) \right|}$$

For complex roots,

$$\zeta = -\frac{A_0}{2} \pm i \sqrt{B_0 - (A_0/2)^2}$$

and Inequality (E.7) becomes:

$$\left(\frac{A_0}{2}\right)^2 + B_0 - \left(\frac{A_0}{2}\right)^2 \leq 1$$

or,

$$B_0 \leq 1$$

(E.13)

The stability constraint given by Equation (E.12) determines the grid spacings in x-direction with uniform grid spacings in r-direction. As the radial velocity on the outside is negative, the condition (E.13) satisfies automatically, but it is not satisfied in the inner side where instability did not show at all.







PROGRAM IN G LEVEL 11 1111 DATE = 11/17/74 11/12/74

```

1134 F=JL*VARI*(V(I,J)/C(J)*DELTA*E(1111)
1135 A=PI*E*AA*V(I)*V(J)*R(1111)
1136 C=PI*J*E
1137 DELTA=PI*1.5708*(C1-DELTA)
1138 IF(DELTA*AL2>0) DELTA=PI*1.5708
1139 DELTA=DELTA*(C1)
1140 DELTA=DELTA*(C1)
1141 CALL VVEL
1142 CALL VVEL
1143 DO 73 J=1,200
1144 JX(J)=X(J)
1145 JY(J)=Y(J)
1146 V(J)=V(J)
1147 V(J)=V(J)
1148 V(J)=V(J)
1149 CALL SPVISC
1150 I=I+NS
1151 I1=IOUT*4
1152 IF(I1*E7.1111) GO TO 75
1153 GO TO 76
1154 CALL OUTPUT
1155 75 I=I+1
1156 IF(I1*E0.1) JX=JX*MAX(0.5)*CXFMAX
1157 IF(I1*E0.25) JY=JY*MAX(0.75)*CXFMAX
1158 DELX=DELX*CXF
1159 DXF=INCR*DXF
1160 IF(1)*X*SE*DXF IAX) GO TO 76
1161 GO TO 75
1162 76 WRITE(A,72) JX
1163 F=J*AT(1) * JYF HAS REACHED THE VALUE 1.01433
1164 C=J*DXFMAX
1165 I=I+1
1166 95 IF(I1*E7.1) ENDIT TO 100
1167 GO TO 97
1168 100 STOP
1169 END

```

```

1101 SUBROUTINE SDELX
C .....
C ..... USING THE STABILITY CONSTRAINTS DERIVED BY VAN DIJAN'S METHOD, THE AXIAL
C ..... AND TORSIONAL SPACINGS ARE CALCULATED. THE AXIAL CHAINS ARE SHOWN.
C .....
1102 C=J*MM*VAREAL/11(3) * JX(200) * JY(200) * V(200) * VP(200) * V(200)
1103 I=TEST*J*E * JX(1) * JSTART * AL1 * AL2
1104 C=J*MM*VAREAL/DELXP * DELX * DELTA * Y(200) * I * NS * NY * EV(200)
1105 I=CC*J*V * UC*J * CC*V * J * DELX * I * X
1106 C=J*MM*VAREAL/COEFF(200) * COEFF(200) * S*JX(200) * S*JY(200)
1107 C=J*MM*VAREAL/CONST1 * CONST2 * FAC * DXF * I * X
1108 V(I)=0
1109 S=JX(1) * EV(1) + EV(2)
1110 D=1 * J*2.194
1111 V(J)=I * J-1 * DELX
1112 Y=JY(J)
1113 Y=JY * J * DELX
1114 Y=JY * (J-1)
1115 CC1=J * J * (J) * Y * DELX
1116 S=JX(J) * EV(J) + EV(J+1)
1117 S=JX(J) * EV(J) + EV(J+1)
1118 IF(J(J) * C2 * J) GO TO 4
1119 C=J*E * J * (YJ + YJ) / (CC1 * DELX)
1120 C=J*E * J * (YJ + YJ) / (CC1 * DELX)
1121 4 CONTINUE
1122 IF(C1 * E * J * J) GO TO 10
1123 GO TO 10
1124 10 DELXP=10 * J * DELX
1125 GO TO 10
1126 10 CC2=J * J
1127 CC2=J * J
1128 C1=J * J * NY
1129 AL1=S*JX(J)
1130 AL2=S*JY(J)
1131 S=MAX(A * AXI * (AL1 * CC2))
1132 S=MAX(A * AXI * (AL2 * CC2))
1133 IF(C1 * E * J * J) GO TO 5
1134 CC2=(A * J * V(I)) / (J * J * DELX) * COEFF(J) * S * MAX * COEFF(J) * S * MAX
1135 CC2=J * AXI * (CC2 * CC2)
1136 5 CONTINUE
1137 25 DELXP=10 * S / CC2
1138 IF(I1 * E * J * J) GO TO 7
1139 GO TO 7
1140 7 DELXP=DXF * I * X * DELX * I * X
1141 IF(DELXP > 10 * J * DELXP) GO TO 4
1142 DELXP=DELXP
1143 9 IF(DELXP > 10 * J * DELXP) GO TO 10
1144 3 DELXP=DELXP
1145 10 DELXP=DELXP * FAC * DELXP
1146 12 RETURN
1147 END

```

VERY POOR PRINT

FORTRAN IV G.LEVEL 21

UVEL

DATE = 79179

11/10/66

```

0001 SUBROUTINE JVEL
0002 DIMENSION DER(200)
0003 COMMON/AREA1/J(200),UP(200),UJ(200),V(200),VP(200),VM(200),
0004 UTEST,UE,UF,VAXIS,USTART,AL1,AL2
0005 COMMON/AREA2/DELXP,DELXM,DELXT,DELY,DELTA,Y(200),I,NS,NY,EV(200)
0006 COMMON/AREA3/COEFP(200),CCEFN(200),SMUP(200),SMUM(200)
0007 COMMON/AREA7/YUHALF
0008 COMMON/AREA9/JCORE,JJ,JINFL
0009 L=1
0010 K=1
0011 M=1
0012 I=1
0013 [F(I,GT,NS)GO TO 20
0014 DJ 19 J=2,199
0015 UJ=U(J)
0016 UJP=U(J+1)
0017 UJM=U(J-1)
0018 YJ=Y(J)
0019 VJ=V(J)
0020 AL1=SMUP(J)
0021 AL2=SMUM(J)
0022 VT=VJ*DELY
0023 SMUP(J)=0.5*(AL1+ABS(VT)+ABS(AL1-ABS(VT)))
0024 SMUM(J)=0.5*(AL2+ABS(VT)+ABS(AL2-ABS(VT)))
0025 IF(VJ,GT,0)GO TO 11
0026 JP(J)=UJ-DELXP*VJ*(UJP-UJM)/(DELY*JJ)+DELXP*(CCEFP(J)*SMUP(J)+
0027 (UJP-UJM)-COEFN(J)*SMUM(J)*(UJ-UJM))
0028 GJ TO 34
0029 11 JP(J)=UJ-DELXP*VJ*(UJ-UJM)/(DELY*JJ)+DELXP*(CCEFP(J)*SMUP(J)+
0030 (UJP-UJM)-COEFN(J)*SMUM(J)*(UJ-UJM))
0031 34 UJP=UP(J)
0032 IF(K,GT,1)GO TO 30
0033 GO TO 12
0034 30 IF(K,GT,2)GO TO 31
0035 JP(1)=(4.0*UP(2)-JP(3))/3.0
0036 31 IF(N,GT,1)GO TO 12
0037 JPMEAN=(JP(1)+UE)/2.0
0038 IF(UPJ,LE,UPMEAN)GO TO 32
0039 GO TO 12
0040 32 JJ=J
0041 JMJ=J-1
0042 UPJJ=UP(JJ)
0043 UPMJ=UP(JMJ)
0044 YJJ=Y(JJ)*DELY
0045 YJM=Y(JMJ)*DELY
0046 YHALF=YJM+((YJJ-YJM)/(UPJJ-UPJM))*(UPMEAN-UPJM)
0047 M=M+1
0048 12 K=K+1
0049 IF(L,GT,1)GO TO 13
0050 IF(JPJ,LT,(0.99*LSTART))GC TO 14
0051 GO TO 13
0052 14 YCORE=(J-1)*DELY
0053 JCORE=J
0054 L=L+1
0055 13 IF(K,LT,3)GO TO 19
0056 UTEST=(UP(1)-UPJ)/(JP(1)-UE)
0057 IF(UTEST,GT,0.99)GO TO 27
0058 19 CONTINUE
0059 GJ TO 29
0060 20 SMUP(1)=EV(1)+EV(2)
0061 DJ 26 J=2,199
0062 YJ=Y(J)
0063 UJ=U(J)
0064 UJP=U(J+1)
0065 UJM=U(J-1)
0066 SMUP(J)=EV(J)+EV(J+1)
0067 SMUM(J)=EV(J)+EV(J-1)
0068 AL1=SMUP(J)
0069 AL2=SMUM(J)
0070 VT=VJ*DELY
0071 SMUP(J)=0.5*(AL1+ABS(VT)+ABS(AL1-ABS(VT)))
0072 SMUM(J)=0.5*(AL2+ABS(VT)+ABS(AL2-ABS(VT)))
0073 UA=UJ/DELXT
0074 JH=(Y(J+1)+YJ)*SMUP(J)/(3.0*YJ*DELY*DELY)
0075 JC=(YJ+Y(J-1))*SMUM(J)/(3.0*YJ*DELY*DELY)
0076 UJ=UJ+UA

```

```

FORTRAN IV G LEVEL 21          UVEL          DATE = 79179          11/10/76

0075      VJ=V(J)
0076      UM=-VJ*(UJP-UJM)/(2.0*DELY)
0077      JI=(UJP-0.5*UMJ)*UB*2.0
0078      JU=(UJM-0.5*UMJ)*UC*2.0
0079      JP(J)=(UJ+UM+UI+UJ)/(UA+UB+UC)
0080      J=JP(J)
0081      IF(UJP.GE.UE)GO TO 125
0082      JP(J)=UE
0083      125 IF(K.GT.1)GO TO 40
0084      GO TO 33
0085      40 IF(K.GT.2)GO TO 41
0086      UP(1)=(4.0*UP(2)-UP(3))/3.0
0087      41 IF(4.GT.1)GO TO 33
0088      UPMEAN=(UP(1)+UE)/2.0
0089      IF(UJP.LE.UPMEAN)GO TO 42
0090      GO TO 33
0091      42 JJ=J
0092      JM=J-1
0093      JPJJ=UP(JJ)
0094      UPJM=UP(JM)
0095      YJJ=(JJ-1)*DELY
0096      YJM=(JM-1)*DELY
0097      YUMALF=YJM+((YJJ-YJM)/(UPJJ-UPJM))*(UPMEAN-UPJM)
0098      Y=UM+Y
0099      33 K=K+1
0100      IF(K.LT.3)GO TO 21
0101      IF(UP(1).LT.(0.99*UJSTART))GO TO 23
0102      21 IF(L.GT.1)GO TO 22
0103      IF(UJP.LT.0.99*UJSTART)GO TO 24
0104      GO TO 22
0105      24 YCORE=(J-1)*DELY
0106      JCORE=J
0107      L=L+1
0108      GO TO 22
0109      23 YCORE=0.0
0110      JCORE=1
0111      22 IF(K.LT.4)GO TO 26
0112      UTEST=(UP(1)-UPJ)/(UP(1)-UE)
0113      DER(J-1)*ABS(UPJ-UP(J-2))
0114      DER(J-2)*ABS(UP(J-1)-UP(J-3))
0115      IF(IM.GT.1)GO TO 100
0116      IF(DER(J-1).LT.DER(J-2))GO TO 105
0117      GO TO 100
0118      105 JINFL=J-2
0119      IN=IN+1
0120      100 IF(UTEST.GE.0.99)GO TO 27
0121      26 CONTINUE
0122      27 DELTA=(J-1)*DELY
0123      DELMIX=DELTA-YCORE
0124      NY=J
0125      NNY=J+1
0126      DO 29 J=NNY,200
0127      29 VP(J)=UF
0128      VP(1)=VAXIS
0129      29 RETURN
0130      END
    
```

```

FORTRAN IV G LEVEL 21          VVEL          DATE = 79179          11/10/76

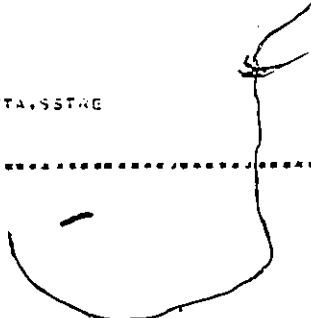
0001      SUBROUTINE VVEL
0002      CJMMUN/AREA1/J(200),JP(200),J4(200),V(200),VP(200),VM(200),
0003      UTEST,UE,UF,VAXIS,UJSTART,ALI,AL2
0004      CJMMUN/AREA2/DELXP,DELXN,DELXT,DELY,DELTA,Y(200),[NS,NY,CV(200)]
0005      1,ECONV,UCONV,XCONV,N,DELMIX
0006      IF(1.GT.NS)GO TO 20
0007      DO 10 J=1,199
0008      YJ=Y(J)
0009      YJP=YJ+DELY
0010      VP(J+1)=YJ*VP(J)/YJP-(DELY/(4.0*DELXP*YJP))*(YJP+YJ)*(JP(J+1)
0011      +JP(J))-U(J+1)-U(J)
0012      IF(ABS(VP(J+1)).GT.0.8) VP(J+1)=VP(J)
0013      10 CONTINUE
0014      GO TO 25
0015      20 DO 21 J=1,199
0016      YJ=Y(J)
0017      YJP=YJ+DELY
0018      VP(J+1)=YJ*VP(J)/YJP-(DELY/(4.0*DELXT*YJP))*(YJP+YJ)*(JP(J+1)
0019      +JP(J))-UM(J+1)-UM(J)
0020      IF(ABS(VP(J+1)).GT.0.8) VP(J+1)=VP(J)
0021      21 CONTINUE
0022      25 RETURN
0023      END
    
```



```

FOURTH IV G LEVEL          OUTPUT          DATE = 1917-          11/1/76
0001      SUBROUTINE OUTPUT
0002      CUMIGN/AREAL/J(200),JP(200),J4(200),V(200),VP(200),V4(200),
0003      JTEST,JE,JP,AXIS,USTART,ALL,AL2
0004      CUMGN/AREAL/DELX,DELX2,DELX3,DELX4,DELTA,Y(200),I,NS,NY,EV(200)
0005      I=CCNV/JCINV,CCNV=N,DELX=DELX*57,C_2P
0006      CUMGN/AREAS/X,AD,RAD,LE
0007      CUMGN/AREAT/YUHALF
0008      NNN=1
0009      NNY=NY+1
0010      NUN=NY
0011      DIST=X*CCNV
0012      DELTA=DELTA/PA
0013      DCJDE=(DELTA-DELX)/RAD
0014      KAP=X/RAD
0015      SLB=SB/RAD
0016      RUMALF=YUHALF/RAD
0017      UCL=(J(1)-JE)/(USTART-JE)
0018      JPI=DELX*CCNV*12.5
0019      JYP=DELX*CCNV*12.5
0020      JAX=DELX*CCNV*12.5
0021      WRITE(6,13)
0022      13 FORMAT('1',*)
0023      WRITE(6,15) DIST,DCJDE
0024      15 FORMAT('1,5X','1',I2,5X,'X_DISTANCE=',G12.5,5X,'HALF_IDTH=',
0025      |G12.5,5X,'CUPE_RADIUS=',G12.5)
0026      WRITE(6,16) KAP,RUMALF,UCL
0027      16 FORMAT('1,15X','X/RD=',G12.5,5X,'HALF_RAD=',G12.5,5X,'CENTRE_VELUC
0028      |ITY=',G12.5)
0029      WRITE(6,17) JPI,JXP,JXM,SLB
0030      17 FORMAT('1,15X','JPI=',G12.5,5X,'JXP=',G12.5,5X,'JXM=',G12.5,5X,'SL
0031      |B=',G12.5)
0032      WRITE(6,20)
0033      20 FORMAT('1,2X','J',5X,'YBARU',5X,'YBARU',5X,'V_VEL',5X,'VIRCOSITY',
0034      |5X,'(4-2N)/3')
0035      DO 30 J=1,40
0036      Z/JREV(J)*CCNV
0037      YJ=J
0038      Y17J=YJ/PA
0039      YETA=(YBARU-RUMALF)/SLB
0040      JREV(J)
0041      IF(J=3,1)GO TO 1
0042      JREV(J)=J-(J-1)/(2.5*DELX)
0043      SSTR=REV(J)*JUP
0044      JREV(J)=JUP
0045      1 GO TO 2
0046      2 JREV(J)
0047      SSTR=REV(J)*JUP
0048      2 *-ITE(6,25) J,YPA,U,JJ,VJ,E/J,YETA,SSTR
0049      25 FORMAT('1,13.7(2X,G12.5)')
0050      3) CONTINUE
0051      WRITE(6,31)
0052      31 FORMAT('1',*)
0053      41 RETURN
0054      END

```





FORTRAN IV G LEVEL 31

MAIN

DATE = 79179

13/05/73

```

0057      60 J=J+1
0058      S(J-1)=7(J)+.3
0059      T4(J-1)=R(J+1)/70
0060      IF(1-4(J).LE.A1(1))GO TO 60
0061      70 E(1,J)=(44(J)-R(1))/4(1)
0062      IF(E(1,J).GT.3.5)GO TO 75
0063      U(1,J)=3.5-E(1,J)+.35*E(1,J)**2+.008*E(1,J)**3
0064      GJR(1,J)=1.0-0.13*E(1,J)+1.77*E(1,J)**2
0065      GJR(1,J)=GJR(1,J)
0066      GO TO 70
0067
0068      75 EKE=4.7*(U(1,J)-0.5)
0069      J(1,J)=J.395*(1.7-EXP(EKE)-EXP(-EAL))/ (EXP(EKE)+EXP(-EAL))
0070      T4=(EXP(EKE)-EXP(-EKE))/ (EXP(EKE)+EXP(-EKE))
0071      GJR(1,J)=3.045*.7/*(1.0-T**2)
0072      GJR(1,J)=GJR(1,J)
0073      79 GJXR(1,J)=-(E(1,J)*GJX+GJX)/4(1)*GUR(1,J)
0074      GJXR(1,J)=GJXR(1,J)*K(J)/.0
0075      S1=5+GJXR(1,J)
0076      V(1,J)=3+0.7/R(J)
0077      IF(1(J(1,J)-.))J1=-5.0J+.0
0078
0079      80 J(1,J)=1.
0080      E(1,J)=-.750
0081      V(1,J)=3.0
0082      GJR(1,J)=0.
0083      GO TO 60
0084
0085      85 N2=J+5
0086      J14=41+J.42
0087      J(1,41)=J(1,J-1)
0088      V(1,41)=V(1,J-1)
0089      89 GUR(1,41)=GUR(1,J-1)
0090      IF(1.0E-21GO TO 100
0091      JE=5
0092      DO 15 L=1,J
0093      95 J(1,L)=S2(I,L)**0.5
0094      J1=0
0095      99 J2=J2+1
0096      IF(J(1,J2).GT.3.5)GO TO 95
0097      J1=U(1,J2)-0.5
0098      IF(A*3(DU1).GT.3.00)GO TO 97
0099      R(1)=R(J2)
0100      GO TO 99
0101      97 R(1)=(R(J2-1)+R(J2))/2.0
0102      98 IF(1.0E-1)GO TO 99
0103      H=H*(1)/.0
0104      A=1.0
0105      J=1.0-.15*(4H-R(1))
0106      K=0
0107
0108      105 K=K+1
0109      IF(1.0T.2)GO TO 106
0110      AL1=(P(K)-R(1-1))/X(1-1)**2
0111      AL1=EXP(-AL1)
0112      G(1-1,K)=XL(1-1)
0113      106 AL1=(R(K)-R(1))/X(1)**2
0114      AL1=EXP(-AL1)
0115      X(1,K)=XL(1)
0116      IF(1.0T.2)GO TO 109
0117      J.SS(1-1,K)=3*(1-1,K)*Q(1-1,K)/X(1-1,K)+C7
0118      TAJ(1-1,K)=(XK*GUR(1-1,K)**2
0119      P.CD(1-1,K)=A*TAG(1-1,K)*GUR(1-1,K)/(E(1-1)+.1.50)
0120      J=J-1
0121      109 IF(K.LE.J)GO TO 110
0122      T(K+1)=T(K)+OH
0123      T(K+1)=R(K+1)/4
0124      110 IF(J(K)/R(1)-.50)15.25+.25
0125      Z=(JH-0(K)/PH(1))**2.5*5.J=(1.0+EXP(-X(1)/1.5))
0126      GO TO 11
0127      25 IF(R(K)/PH(1)-AA)120.120.20
0128      3) Z=(Z(K)/PH(1)-AA)**2.5*3.5
0129      31 XI=NT(1,K)+0.5**2
0130      GO TO 105
0131      120 XI=NT(1,K)+1.
0132      100 C=1.0J
0133      IF(1.0T.2)GO TO 102
0134      XI=NT(1-1,K)+XI(1,K)
0135      XI=NT(1,K)+1)=XI(1,K)
0136      IF(K.L.7)105 TO 105
0137      IF(1.0T.2)GO TO 105
0138      AN=30(1-1,K)-30(1-1,K-1)

```

VERY POOR PRINT

FORTRAN IV G LEVEL 21

MAIN

DATE = 72177

13/06/33



```

2139 A=SQ(I-1,K+1)-SC(I-1,K)
2140 A7=A9
2141 I=(V(I-1,K).LT.3.)A7=A9
2142 C1=(R(K+1)+R(K))*(S(I-1,K+1)+S(I-1,K))*XS(I-1,K)*BK/
2143 I=(A.*R(K)+U(I-1,K))*DP21
2144 C2=(R(K+1)+R(K))*(S(I-1,K+1)+S(I-1,K))*XS(I-1,K)*BK/
2145 I=(A.*R(K)+U(I-1,K))*DP21
2146 S(I,K)=SQ(I-1,K)-(V(I-1,K)*DX+A7)/(U(I-1,K)+CR)+DX*(DP20(I-1,K)
2147 -)ISS(I-1,K)/U(I-1,K)+2.*DX*(C1*(SQ(I-1,K+1)-SC(I-1,K))-
2148 C2*(SQ(I-1,K)-SC(I-1,K-1)))/(CR+DP21)
2149 I=(SQ(I,K).LT.3.)S(I,K)=0.00001
2150 S(I,K)=SQ(I,K)**.5
2151 IF(I.EQ.2)GU TO 155
2152 C1=(R(K+1)+R(K))*XS(I-1,K+1)+XS(I-1,K)*(S(I-1,K+1)+S(I-1,K))/C.
2153 I*(R(K+1)+R(K))*XS(I-1,K+1)+XS(I-1,K)*(S(I-1,K+1)+S(I-1,K))/C.
2154 C2=(R(K+1)+R(K))*XS(I-1,K+1)+XS(I-1,K)*(S(I-1,K+1)+S(I-1,K))/C.
2155 I*(R(K+1)+R(K))*XS(I-1,K+1)+XS(I-1,K)*(S(I-1,K+1)+S(I-1,K))/C.
2156 C1=SQ(I-1,K)/(CR+DXN)+BK*(C1+C2)/(R(K)*(CR+DP21))
2157 S=SQ(I-1,K)-SC(I-1,K-1)
2158 D=(U(I-1,K)+S(I-1,K))/(DXC+X.)-V(I-1,K)*B
2159 I=(D+DP21)*DP20(I-1,K)-0.155*(S(I-1,K)+S(I-1,K-1))/(C1*(SQ(I-1,K+1)-
2160 S(I-1,K))-C2*(SQ(I-1,K)-S(I-1,K-1)))/(R(K)*(CR+DP21))
2161 S(I,K)=D/C
2162 IF(S(I,K).LT.3.)S(I,K)=0.00001
2163 S(I,K)=SQ(I,K)**.5
2164 155 TAU(I,K)=(XK*QJR(I,K))*2
2165 S(I,K)=S(I,K)*Q(I,K)/XS(I,K)*C7
2166 TV(I,K)=(2.*DP7*S(I,K))*0.5
2167 TV(I,K)=(2.*DP7*S(I,K))*0.5
2168 T(I,K)=(2.*DP7*S(I,K))*0.5
2169 P20(I,K)=A*TAU(I,K)*QUR(I,K)/(S(I)*Q=1.50)
2170 IF(P2(K).LE.-2(I))GU TO 155
2171 44(I)=R4(I)/2
2172 TAU(I,1)=TAU(I,2)
2173 TV(I,1)=TV(I,2)
2174 TV(I,1)=TV(I,2)
2175 T(I,1)=T(I,2)
2176 S(I,1)=S(I,2)
2177 DP20(I,1)=DP20(I,2)
2178 S(I,1)=S(I,2)
2179 S(I,1)=S(I,2)**0.5
2180 J=150 44(I,K)
2181 S(I,4)=C5*S(I,1)*Q(I,4)*Q/XJ(I,1)
2182 P=C(I,4)*A*TAU(I,4)*QUR(I,4)/R(I)
2183 LI=K+5
2184 J=150 L2=K+LI
2185 S(I,L2)=SQ(I,K)
2186 DP20(I,L2)=DP20(I,K)
2187 DIS(I,L2)=DIS(I,K)
2188 E(I,L2)=E(I,K)
2189 TAU(I,L2)=TAU(I,K)
2190 XI(I,L2)=XI(I,K)
2191 XI(I,L2)=XI(I,K)
2192 XI(I,L2)=XI(I,K)
2193 TV(I,L2)=TV(I,K)
2194 TV(I,L2)=TV(I,K)
2195 T(I,L2)=T(I,K)
2196 XS(I,L2)=XS(I,K)
2197 DIS(I,L2)=DIS(I,K)
2198 DP20(I,L2)=DP20(I,K)
2199 DP20(I,L2)=DP20(I,K)
2200 J(I,L2)=J(I,K)
2201 IF(I.LT.2)GU TO 240
2202 I=I-1
2203 C1=SQ(I-1,K)
2204 P1=(SQ(I-1,K)-SC(I-1,K))/(CR+DXN)
2205 I=(P1.LT.3.)AND.(R5(K).LT.1.3))P1=-21
2206 IF((P1.EQ.0.3).AND.(R4(K).GT.1.3))GU TO 245
2207 GU TO 240
2208 IF((SQ(I-1,K).LE.SQ(I,J2)).AND.(V(I,4).GT.0.3))P1=-21
2209 IF(4.EQ.1)P2=(SQ(I,4+1)-SC(I,4))/CR
2210 I=(4.EQ.1)P2=(SQ(I,4+1)-SC(I,4-1))/(CR+DP21)
2211 I=(I.EQ.4).LT.3.)P2=-21
2212 J=J(I,4)+R4(I,4)*XI(I,4)**2
2213 S(I,4)=S(I,4)*XI(I,4)**2
2214 S(I,4)=S(I,4)*XI(I,4)**2
2215 DIS(I,4)=DIS(I,4)*XI(I,4)**2
2216 TAU(I,4)=0.5*DP20(I,4)
2217 XS(I,4)=XS(I,4)/2

```



CONTRAN IV G LEVEL 11 MAIN DATE = 79170 13/06/73

```

0205 TAU(I,M)=TAU(I,N)*XINT(I,I)**2
0206 TUI(I,M)=TUI(I,N)*XINT(I,I)
0207 TV(I,M)=TV(I,N)*XINT(I,I)
0208 TAI(I,M)=TAI(I,N)*XINT(I,I)
0209 TAI(I,M)=TUI(I,N)*XINT(I,I)
0210 I=(ABS(X4(I)-2.0).LE.0.001)GO TO 3
0211 IF(ABS(X4(I)-1.0).LE.0.001)GO TO 3
0212 IF(ABS(X4(I)-0.0).LE.0.001)GO TO 3
0213 IF(ABS(X4(I)-3.0).LE.0.001)GO TO 3
0214 GO TO 190
0215 2 AS(1)=TUI(I,I)**2
0216 3 AS(2)=TAI(I,I)**2
0217 AS(3)=TV(I,I)**2
0218 AS(4)=0.0
0219 AS(5)=0.0
0220 AS(5)=TAI(I,I)**2
0221 N=M
0222 N=M
0223 I=(ABS(AS(1)-4.0).LE.0.001) GO TO 7
0224 2 I=(ABS(AS(2)-15.0).LE.0.001) GO TO 7
0225 7 CALL TIME(AS,2,2,4,4)
0226 AS(1)=AS(1)/3.0
0227 AS(2)=AS(2)/3.0
0228 AS(3)=AS(3)/3.0
0229 AS(5)=AS(5)/50.0
0230 AS(5)=AS(5)/50.0
0231 TAU(I,M)=TAU(I,N)
0232 TUI(I,M)=TUI(I,N)
0233 TV(I,M)=TV(I,N)
0234 TAI(I,M)=TAI(I,N)
0235 TUI(I,M)=TUI(I,N)
0236 5 3(1)=ARCOS(AS(1))=180.0/3.141593
0237 THETA=AS(1)
0238 THETA=TAI(THETA)
0239 R=AS(2)*0.51*(3.02+).45*THETA+.071*THETA**2
0240 3 INT 3 AS(1),AS(3),AS(5),R,TAU(I,M),TUI(I,M)
0241 4 3(1)=R
0242 3 4(1)=R
0243 4 3(1)=R
0244 3(1)=R
0245 3(1)=R
0246 3(1)=R
0247 3(1)=R
0248 3(1)=R
0249 3(1)=R
0250 3(1)=R
0251 3(1)=R
0252 3(1)=R
0253 3(1)=R
0254 3(1)=R
0255 3(1)=R
0256 3(1)=R
0257 3(1)=R
0258 3(1)=R
0259 3(1)=R
0260 3(1)=R
0261 3(1)=R
0262 3(1)=R
0263 3(1)=R
0264 3(1)=R
0265 3(1)=R
0266 3(1)=R
0267 3(1)=R
0268 3(1)=R
0269 3(1)=R
0270 3(1)=R
0271 3(1)=R
0272 3(1)=R
0273 3(1)=R
0274 3(1)=R
0275 3(1)=R
0276 3(1)=R
0277 3(1)=R

```

VERY POOR PRINT

FORTRAN IV G LEVEL 31

MAIN

DATE \* 79173

13/06/73

```

3277   SUR(1-2,4)=GUR(1-1,4)
3278   SU(1-2,4)=SU(1-1,4)
3279   SI(1-2,4)=SI(1-1,4)
3280   SE(1-2,4)=SE(1-1,4)
3281   DO 295 N=1,K
3282   SI(1-1,4)=SI(1,4)
3283   VI(1-1,4)=VI(1,4)
3284   TAU(1-1,4)=TAU(1,4)
3285   XLNT(1-1,4)=XLNT(1,4)
3286   T(1-1,4)=T(1,4)
3287   TV(1-1,4)=TV(1,4)
3288   T-(1-1,4)=T-(1,4)
3289   S(1-1,4)=S(1,4)
3290   PU(1-1,4)=PU(1,4)
3291   XU(1-1,4)=XU(1,4)
3292   DIS(1-1,4)=DIS(1,4)
3293   PUC(1-1,4)=PUC(1,4)
3294   SUR(1-1,4)=SUR(1,4)
3295   S-(1-1,4)=S-(1,4)
3296   S(1-1,4)=S(1,4)
3297   E(1-1,4)=E(1,4)
3298   X(1-2)=X(1-1)
3299   X(1-1)=X(1)
3300   X4(1-2)=X4(1-1)
3301   X4(1-1)=X4(1)
3302   XL(1-2)=XL(1-1)
3303   XL(1-1)=XL(1)
3304   PM(1-2)=PM(1-1)
3305   PM(1-1)=PM(1)
3306   PM(1)=PM(1+1)
3307   B(1-2)=B(1-1)
3308   B(1-1)=B(1)
3309   Q(1)=Q(1+1)
3310   Q(1-2)=Q(1-1)
3311   P(1-1)=P(1)
3312   P(1)=P(1+1)
3313   R2(1-2)=R2(1-1)
3314   R2(1-1)=R2(1)
3315   R2(1)=R2(1+1)
3316   R4(1-2)=R4(1-1)
3317   R4(1-1)=R4(1)
3318   R4(1)=R4(1+1)
3319   I=1-1
3320   DO 298 N=1,K
3321   TR4(1-1,4)=TR4(1,4)
3322   298   DIFF(1-1,4)=DIFF(1,4)
3323   GO TO 40
3324   300   STOP
3325   END

```

VITA AUCTORIS

- 1948 Born at Hiran, Gopalganj, Bangladesh, on February 10.
- 1963 Completed Secondary School Certificate Education from Bagdha High School, Barisal, Bangladesh.
- 1965 Completed Higher Secondary Certificate Education from Jagannath College, Dacca, Bangladesh.
- 1969 Received the Degree of Bachelor of Science in Mechanical Engineering from University of Engineering and Technology, Dacca, Bangladesh.
- 1970 Joined the Department of Mechanical Engineering of University of Engineering and Technology, Dacca, Bangladesh, as a lecturer.
- 1975 Received the Degree of Master of Science in Mechanical Engineering from University of Engineering and Technology, Dacca, Bangladesh.
- 1975 Promoted to the Rank of Assistant Professor, University of Engineering and Technology, Dacca, Bangladesh.
- 1979 Currently a candidate for the Degree of Doctor of Philosophy in Mechanical Engineering at the University of Windsor, Windsor, Ontario, Canada.